

Improving Alpine Flood Prediction through Hydrological Process Characterization and Uncertainty Analysis

THÈSE N° 5416 (2012)

PRÉSENTÉE LE 5 JUILLET 2012

À LA FACULTÉ DE L'ENVIRONNEMENT NATUREL, ARCHITECTURAL ET CONSTRUIT
LABORATOIRE D'ÉCOHYDROLOGIE
PROGRAMME DOCTORAL EN ENVIRONNEMENT

ÉCOLE POLYTECHNIQUE FÉDÉRALE DE LAUSANNE

POUR L'OBTENTION DU GRADE DE DOCTEUR ÈS SCIENCES

PAR

Cara Christine TOBIN

acceptée sur proposition du jury:

Prof. F. Golay, président du jury
Prof. A. Rinaldo, Prof. B. Schaefli, directeurs de thèse
Dr D. Bérod, rapporteur
Prof. A. Montanari, rapporteur
Prof. M. Parlange, rapporteur



ÉCOLE POLYTECHNIQUE
FÉDÉRALE DE LAUSANNE

Suisse
2012

Creative study ... finds its largest applications in those subjects in which, while much is known, more remains to be known. Such are the fields which we, as naturalists, cultivate; and we are gathered for the purpose of developing improved methods lying largely in the creative phase of study, though not wholly so.

— T.C. Chamberlin, 1890, Science

To Cameron. . .

Acknowledgements

First and foremost I would like to thank my doctoral advisors, Andrea Rinaldo and Bettina Schaefli. Andrea has been extremely supportive in all my research endeavors and provided me continual guidance on thought-provoking topics in hydrology. He has been a great mentor and role model on how civil engineers can make a difference in the world. Bettina has also been a guiding light by greatly helping me to find interesting research avenues which are applicable to the operational aspects of this thesis. She was additionally extremely generous with assisting me on the cumbersome details of codes and publications. I would also like to thank my original host professor at EPFL, Marc Parlange, who enabled me to gain unique field experience in the Swiss Alps with weather station installations. Through this work I was able to build a knowledge-base in meteorology, which inspired me to return to obtain a PhD.

None of this doctoral work would have been possible if it were not for the financial support of the MINERVE project. I sincerely thank Dominique Bérod for supporting my research ideas and seeing their utility in the context of the MINERVE project. I also thank my two guides in the MINERVE project, Ion Iorgulescu and Fred Jordan for their invaluable knowledge which enabled me to find the most efficient pathways to improving the MINERVE model. Similarly, I thank my two colleagues in the MINERVE project, Javier García-Hernandez and Pascal Horton for our regular knowledge-sharing meetings over coffee and at conferences. Finally, I also thank Jean-Louis Boillat for his support on the MINERVE project, particularly in perfecting my French for presentations and reports.

I would also like to give a special thank you to Alberto Montanari for participating as an external expert on my jury. His evaluation of my work, particularly in the uncertainty discussions, has been invaluable to my thesis. I also thank Alexis Berne for assisting me with geostatistics topics and guiding me with the publication process for one of the chapters of this thesis.

I must also give a tremendous thanks to Ludovico Nicótina, a post-doctoral fellow in the Ecohydrology (ECHO) laboratory who was particularly helpful during the first half of my thesis when I was trying to find my way. I further thank my other colleagues in the ECHO laboratory: Enrico and Lorenzo Mari, thank you for your continual good programming advice, Serena,

Acknowledgements

thanks for being a great fellow teaching assistant and friend and Lorenzo Righetto, Samir, Francesco, Allyn and Andrea, thanks for making the lab an entertaining place, particularly with Italian desserts and laughter. Thank you also to Anna and Bernard for organizing just about everything. It made life in the lab easy and pleasant.

At EPFL, I have to thank my dearest friends for being supportive through all of these years. Thank you, Kristen, Alex, Jan, Megan, Sam, Natalie, Jessica and Pam! I enjoyed our regular lunches, walks and runs and appreciate all of you for being such great, fun confidants. Also, I must thank my close neighbors at Avenue Ruchonnet 15 for the fun apéros, entertaining stories and overall support, particularly Isabelle M., Audrey, Isabelle B., Maya and Barbara, who inspired me as strong female role models.

Most significantly, I have the sincerest gratitude to my parents who supported my quest to do environmental studies at the age of sixteen. My parent's and brother's endless support and prayers undoubtedly helped me reach this point of my career. Similarly, I thank my in-laws, or more appropriately termed in French, 'ma belle famille', Margareta, Andy and the Hausser Greene clan for their continual support, guidance and outdoor adventures. Lastly, but clearly not least, I would like to thank my husband and son for the happiness they provided me during this sometimes arduous journey. My son's smiles and laughter always put everything in perspective, while without my husband's support, guidance and inspiration I would not be where I am today.

Lausanne, 11 June 2012

C. T.

Abstract

Among the many challenges of Alpine flood prediction is describing complex, meteo-hydrological processes in a simplified, robust manner that can be easily integrated into operational forecasting. In this dissertation, improved methods to characterize these processes are developed and integrated into the hydrological modeling component of an operational flood forecasting system used in the Swiss Alps. Detailed studies are conducted to improve hydrological model inputs, processes and outputs. Improvements, detailed in four chapters of this thesis, address the overarching goal of this work – the reduction of flood forecasting uncertainty.

The accuracy of flood predictions in Alpine areas is contingent upon adequate interpolation of meteorological forcings, which has significant impacts on discharge volumes and flood peaks. This thesis demonstrates an improvement in the interpolation of temperature and precipitation inputs using a robust variogram which considers anisotropy and using a geostatistical interpolation method to distribute inputs in space and time. Results show that using elevation as the external drift factor better describes orographically-induced precipitation and temperature gradients. Also, the consideration of anisotropy is integral in detailing spatial patterns of precipitation induced by storm advection.

Hydrological flood forecasting in mountainous areas also requires accurate partitioning between rain and snowfall to properly estimate the extent of runoff contributing areas. Partitioning is improved in this work by using a new method to integrate Limited Area Model output. Unlike standard hydrological procedures in inferring snowfall limit estimates based on dry, ground temperature measurements, Limited Area Model output considers the vertical, humid, atmospheric structure in its snowfall limit calculations. In effect, this method provides good estimates of runoff contributing areas in the spring as evidenced by validation on discharge measurements and satellite images of snow coverage.

Accurately describing snowmelt processes on a sub-daily scale is also of critical importance in Alpine flood forecasting. However, the complex topography of the study region has limited observations available for validation. This thesis presents the development of a new physically-based snowmelt method applicable to regions with limited data. This method uses only daily minimum and maximum temperatures to mimic the effects of radiation. A comparative analysis of snowmelt methods is validated with snow lysimeter data and with a unique, distributed meteorological dataset collected by a wireless weather station network. Results

demonstrate that the new method is competitive with more complex snowmelt methods as shown by accurately reproducing diurnal snowmelt cycles.

Conveying limits of certainty on flood prediction outputs to users is critical because of epistemic and aleatory errors inherent to environmental modeling. Due to the presence of these errors, the GLUE methodology and multi-criteria performance ideas have been adapted with a fit-for-purpose uncertainty estimation technique in the final part of this thesis. With this method, hydrological model parameters are constrained based on hydrograph behavior, with a particular focus on flood peak response. A key component of the technique is a visualization tool which shows acceptable ensembles of discharge with respect to individual and combined criteria. By integrating the aforementioned input and process improvements into the hydrological model, calibration achieves model outputs that capture observed river discharge. Also, the uncertainty associated with hydrological modeling output error is reduced.

Findings of this thesis are applicable to operational flood forecasting in general and have proven utility in improving hydrological model predictions in mountainous regions. Due to the novelty of the developments in terms of new methods or the use of tools and data sources previously unexploited in flood forecasting, further testing of the improvements is recommended. Future research in quantifying the chain of uncertainty produced by combining probabilistic forecast inputs with the hydrological output ensembles is also critical when the improved flood forecasting model becomes fully operational.

Keywords: Flood modeling, geostatistics, Limited Area Models, snowfall limit, snowmelt, uncertainty, GLUE

Résumé

Parmi les nombreux défis de la prévision des inondations alpines se trouve la description des processus météo-hydrologiques complexes d'une manière simplifiée et robuste pouvant être facilement intégrée dans la prévision opérationnelle. Dans cette thèse, des méthodes améliorées pour caractériser ces processus sont mises au point et intégrées dans la composante hydrologique d'un système de prévision opérationnel des crues, utilisé dans les Alpes suisses. Des études détaillées sont menées pour améliorer à la fois le modèle hydrologique, les intrants, les processus et les résultats. Les améliorations détaillées au cours des quatre chapitres de cette thèse adressent l'objectif primordial de ce travail - la réduction de l'incertitude des prévisions de crues.

La précision des prédictions des inondations dans les régions alpines est contingente à une interpolation adéquate des forçages météorologiques, ce qui a des répercussions importantes sur les volumes de débits et des pics des crues. Cette thèse démontre une amélioration de l'interpolation des intrants de la température et de précipitation en utilisant un variogramme robuste qui prend en compte l'anisotropie ainsi qu'une méthode d'interpolation géostatistique permettant la distribution des intrants dans l'espace et dans le temps. Les résultats montrent que l'utilisation de l'élévation comme facteur de dérive externe décrit le mieux la précipitation induite orographiquement ainsi que les gradients de température. Aussi la prise en compte de l'anisotropie est cruciale dans la description de la répartition spatiale des précipitations induite par l'advection des orages.

La prévision des crues hydrologiques dans les régions montagneuses exige également un partitionnement précis entre pluie et neige, pour estimer correctement l'étendue des zones qui contribuent au ruissellement. Le partitionnement est amélioré dans ce travail en utilisant une nouvelle méthode pour intégrer les sorties de 'Limited Area Models'. Contrairement aux procédures hydrologiques standard qui estiment la limite des chutes de neige en fonction des mesures de température sèches au sol, les sorties de 'Limited Area Models' considère la structure de l'atmosphère verticale et humide dans ses calculs des limites pluie-neige. Cette méthode permet donc une bonne estimation des zones contribuant au ruissellement de printemps, ceci étant validé par les mesures de débit ainsi que des images satellite de la couverture

de neige.

Décrire précisément les processus de fonte des neiges à l'échelle horaire est également d'une importance cruciale dans la prévision des crues alpines. Cependant, la topographie complexe de la région d'étude limite les observations disponibles pour la validation. Cette thèse présente le développement d'une nouvelle méthode à base physique de la fonte des neiges, applicable aux régions ayant des données limitées. Cette méthode utilise seulement les températures journalières minimales et maximales pour mimer les effets des rayonnements solaires. Une analyse comparative des méthodes de fonte des neiges est validée par des données lysimétriques de neige avec une agrégation de données météorologiques distribuées, collectées par un réseau de stations météorologiques sans fil. Les résultats démontrent que la nouvelle méthode est compétitive avec des méthodes de fonte de neiges plus complexes ; cette méthode permet en effet une reproduction fidèle des mesures de débits réels ainsi que des images satellite de couverture neigeuse.

Il est également impératif de pouvoir communiquer aux utilisateurs les incertitudes sur les sorties de prévision des crues dues aux erreurs épistémiques et aléatoires inhérentes à la modélisation de l'environnement. En raison de la présence de ces erreurs, la méthodologie GLUE ainsi que d'autres idées de performance multicritères sont adaptées à une technique d'estimation de l'incertitude 'fit-for-purpose' dans la dernière partie de cette thèse. Dans cette méthode, les paramètres de modèles hydrologiques sont limités en fonction du comportement de l'hydrogramme, avec un accent particulier sur la réponse aux pics de crue. Un élément clé de la technique est un outil de visualisation qui montre les ensembles acceptables de débit vis-à-vis des critères individuels et combinés. En intégrant les intrants améliorées et l'amélioration des processus ci-dessus dans le modèle hydrologique, les résultats indiquent que le calage donne des résultats en accord avec le débit fluvial observé, et l'incertitude associée aux erreurs de sortie de la modélisation hydrologique est réduite.

Les résultats de cette thèse sont applicables à la prévision des crues opérationnelle en général et ont fait leurs preuves dans l'amélioration des prévisions des modèles hydrologiques de régions montagneuses. En raison de la nouveauté des développements en terme de nouvelles méthodes ou de l'utilisation d'outils et de sources de données inexploitées jusqu'alors dans la prévision des crues, des tests supplémentaires des améliorations sont recommandés. Lorsque le modèle amélioré de prévision des crues deviendra opérationnel, il sera également crucial d'effectuer des travaux supplémentaires dans le domaine de la quantification de la chaîne d'incertitude produite par la combinaison des intrants de prévisions probabilistes avec des ensembles de sorties hydrologiques.

Mots-clés : Simulations des crues, géostatistiques, limite pluie-neige, fonte des neiges, incertitude, GLUE

Contents

Acknowledgements	iii
Abstract	v
Abstract (Français)	vii
1 Introduction	1
1.1 Complexities in characterizing mountain floods	1
1.1.1 Unique meteo-hydrological characteristics	1
1.1.2 Hydraulic influences	3
1.1.3 Climate change impacts on mountain floods	4
1.2 Challenges for Alpine flood forecasting models	4
1.2.1 Numerical Weather Prediction forecasts as inputs	5
1.2.2 Hydrological modeling inputs	6
1.2.3 Snow processes	8
1.3 Uncertainty of flood forecasting models	9
1.4 Research objectives and thesis organization	11
2 MINERVE and hydrological modeling	15
2.1 Background	15
2.2 Study catchments	17
2.2.1 Analysis of catchment geomorphology	17
2.3 Inputs	19
2.3.1 Meteorological forcing inputs	19
2.3.2 COSMO Forecasts	19
2.4 MINERVE model - Routing System, RSII	20
2.4.1 Inputs	21
2.4.2 Snow model production	21
2.4.3 Glacier model production	23
2.4.4 Infiltration model production	25
2.4.5 Overland flow model	26
	ix

Contents

2.4.6	Channel routing	27
2.5	Spatially-explicit model of the hydrological response	28
2.6	Conclusions	45
3	Improved interpolation of meteorological forcings	47
3.1	Introduction	47
3.2	Materials and methods	50
3.2.1	Study region and data	50
3.2.2	Spatial interpolation methods	53
3.2.3	Hydrological model	54
3.2.4	Interpolation details	54
3.3	Results and discussion	57
3.3.1	Variogram estimates	57
3.3.2	Precipitation interpolation	57
3.3.3	Temperature interpolation	62
3.3.4	Effect of interpolation techniques on runoff predictions	66
3.4	Conclusions	68
4	Snowfall limits and hydrological modeling	71
4.1	Introduction	71
4.2	Materials and methods	73
4.2.1	Study site and meteorological data	73
4.2.2	COSMO models and output	73
4.2.3	Hydrological model	74
4.2.4	Snowfall limit methods	74
4.2.5	Hydrological model calibration and validation	76
4.2.6	Snow cover validation	77
4.3	Results	78
4.3.1	COSMO and ground station data comparison	78
4.3.2	Hydrological modeling	80
4.4	Conclusions	85
5	Improving the degree-day method for sub-daily melt simulations	87
5.1	Introduction	87
5.2	Data and study catchment	90
5.2.1	Point scale analysis	90
5.2.2	Distributed point and catchment analysis	90
5.3	Modeling approaches	93
5.3.1	Aggregation state of precipitation	93
5.3.2	Snowmelt and refreezing	95
5.3.3	Spatially-explicit hydrological model	98
5.4	Experimental set-up	98
5.4.1	Point scale analysis	98

5.4.2	Distributed point analysis	99
5.4.3	Catchment-scale analysis	99
5.4.4	Hydrological model set-up	101
5.5	Results and discussion	105
5.5.1	Point analysis of melt methods	105
5.5.2	Distributed point melt analysis	106
5.5.3	Catchment-scale analysis	108
5.6	Conclusions	113
6	A fit-for-purpose uncertainty approach for Alpine hydrological model calibration	115
6.1	Introduction	115
6.1.1	Background: Uncertainty approaches	116
6.1.2	Formal Bayesian methods	117
6.1.3	Informal methods	118
6.1.4	Likelihood measures and multi-criteria performances	119
6.1.5	Uncertainty estimation technique and tool	120
6.2	Materials and methods	121
6.2.1	Zones for parameter space exploration	122
6.2.2	Constraining prior parameter ranges	123
6.2.3	Inputs and processes	128
6.3	Results	132
6.3.1	Round 1 MC simulations: Input and process improvement analysis	132
6.3.2	Round 2 MC simulations: Sensitivity analysis	134
6.3.3	Visualization Tool	136
6.3.4	Round 3 MC simulations: Application of weighted criterion	137
6.4	Conclusions	141
7	Conclusions and Perspectives	143
	Bibliography	165
	Curriculum Vitae	167

Introduction

Flood prediction in Alpine regions is a challenging task due to complex, physical interactions, including spatially and temporally variable meteorological processes as well as varied runoff contributions from rain and snowmelt. Aggregating such processes into a forecasting model brings uncertainties to all components of the flood forecasting chain (e.g., inputs, model structure). The nonlinear nature of models and the correlation of errors makes uncertainty quantification and disaggregation a difficult task in hydrology (Gupta et al., 2005; Vrugt et al., 2009). Despite much research, proper means of characterizing mountain floods is still poorly understood (de Jong et al., 2005), and as a result, significant, comprehensive efforts have been made to quantify uncertainties of flood predictions in Alpine areas (Zappa et al., 2008). This dissertation aims to improve an operational flood forecasting model in the Upper Rhone River basin located in the Swiss Alps by accurately characterizing hydrological processes and by associating an uncertainty with flood forecasting model outputs. The model was originally created to simulate preventative hydropower operations for flood mitigation measures (e.g., reservoir releases, gate and turbine operations). This research intends to improve the hydrology component of the existing model so that more confidence is instilled in the rainfall-melt-runoff transformations which dictate the extent of hydropower management necessary. All research endeavors herein have the particular goal of being easily integrated into the operational flood forecasting model whose uncertainty estimates must be easily understood by end-users.

1.1 Complexities in characterizing mountain floods

1.1.1 Unique meteo-hydrological characteristics

Mountain floods can be attributed to a unique set of physical, dynamic processes that lead to spatially heterogeneous snow accumulation and runoff-generation. One of the most influential processes is orography whose effects are characterized by a rapid decrease of atmospheric

Chapter 1. Introduction

moisture with altitude combined with a rain shadow effect on the leeward side of mountains (Figure 1.1). These effects are produced by the forced mechanical lifting of air over mountains, resulting in cooling of the air column, condensation and increasing precipitation with altitude while progressive warming and drying occurs on leeward sides. Such processes must be considered in flood modeling because the effective terrain elevation combined with synoptic scale meteorological processes have been proven to be highly correlated with the high precipitation intensities associated with mountain floods (Roe, 2005). Weather patterns are also highly influential during flood periods and in Alpine contexts (Sevruk, 1997). The direction of synoptic-scale flow often dictates patterns of precipitation accumulation (Molini et al., 2011). Similarly, strong wind effects result in high spatial variability of snow accumulation (Weingartner et al., 2003; Loffler and Rossler, 2005).

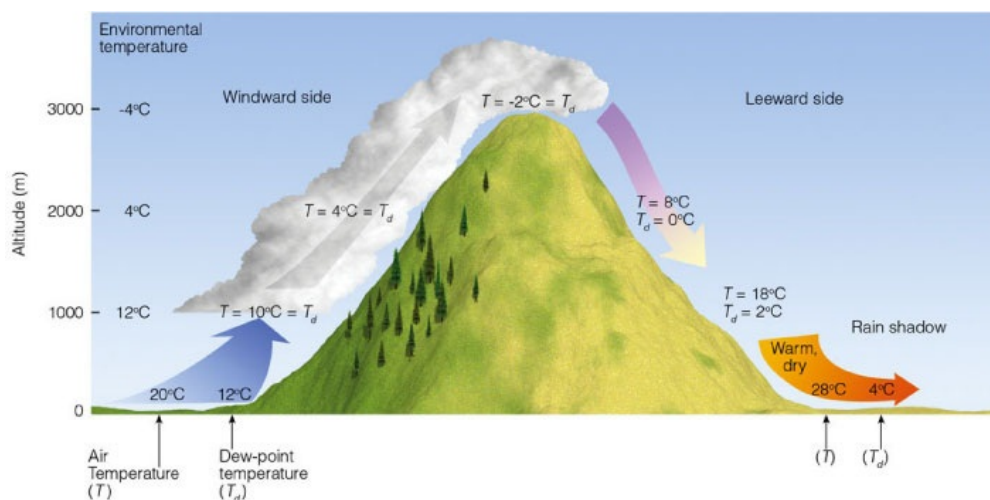


Figure 1.1: The orographic effect demonstrating the increase of precipitation and decrease of temperature with elevation on windward sides of mountains and the analog effect on leeward sides (Source: Thomson Higher Education)

There are also various hydrological processes which contribute to flood producing mechanisms in Alpine areas. Merz and Bloschl (2003) proposed a framework for identifying the causative mechanisms of floods. Their research demonstrated that long-rain or intense short-rain periods, snow-on-rain events and snowmelt processes are the most influential mechanisms affecting runoff response (in this order of influence). In the particular case of mountain watersheds, analysis of flood discharge indicates that rising and falling limbs of stormflow hydrographs are steep (de Jong et al., 2005). This behavior is related to the fact that surface runoff represents a large portion of the total runoff and that baseflow recession is rapid in mountain areas. On the order of hours to days, depending on the size of the basin, surface and near-surface paths can become significant contributors to flood volumes. In particular, the size of flood peaks is determined by the combination of antecedent baseflow and surface stormflow conditions (Dunne, 1978).

An ever-present challenge in mountain watersheds is how to accurately describe the partition-

1.1. Complexities in characterizing mountain floods

ing between surface and subsurface runoff. Key factors defining flow partitioning include the infiltration capacity of the upper soil layers and the soil hydraulic properties (de Jong et al., 2005). For instance, if rainfall intensity exceeds infiltration capacity during a storm, Hortonian-overland flow will develop. In mountain areas, field experiments have demonstrated that flood-producing rainfall intensities of 10 mm h^{-1} or more on soils with low saturated hydraulic conductivity (e.g., $10^{-6} \text{ mm h}^{-1}$) leads to Hortonian-overland flow (Dunne, 1978). A particularly challenging hillslope process to model is return flow, which is created when shallow subsurface paths emerge from the soil surface and return to channels as overland flow, thereby contributing to storm hydrographs as saturation overland flow. Furthermore, the sources of saturated contributing area over which return flow and direct precipitation are generated vary seasonally and throughout a storm. Fluctuations of saturated areas are related to topography, soils, antecedent moisture and rainfall characteristics (Beven, 2004).

Moreover, snow cover in Alpine regions produces particular hydrologic situations; snow pack densities evolve due to freezing (re-freezing) and thawing or melting mechanisms. The dynamics of glacier retreat and re-freezing greatly impacts the accumulation of snow on glaciers and the melting of snow and ice (Huss, 2011). Antecedent snowmelt can saturate soils to the extent that overland flow is produced during rain events (Merz and Blöschl, 2003). In addition, the input of latent heat into the snowpack during rainfall events causes rain-on-snow events to exacerbate flood damage (Sui and Koehler, 2001).

1.1.2 Hydraulic influences

Hydraulic structures in Alpine regions also add to the complexity of modeling hydrologic processes for flood prediction. Reservoir storage and turbine schemes for hydropower management dramatically re-distribute runoff. Particular to Alpine regions in Europe, runoff regimes are dominated by water capture for hydropower operations. For example, in the Swiss Alps, water is commonly captured at the headwaters, capitalizing on snow and ice melt and placed in storage lakes. Discharge from the lakes is passed through hydropower turbines where it is either returned to lower parts of the rivers or pumped back up to feed hydropower plants. Levels of the storage lakes depend on the economic incentive to store or produce energy; lakes serve as a means to shift electricity production from times of high water availability to times of peak electricity demand. In the Upper Rhone River basin (the region this research concerns), which generates 50% of Swiss electricity, 38% of the rivers are affected by hydropower (Weingartner and Pearson, 1999; OFEN, 2012). To add to the challenge of modeling runoff flows, hydropower discharge data is typically daily (thereby not evident for flood modeling on hourly timescales) and day to day reservoir management is generally unknown due to confidential hydropower operations by private companies (Hingray et al., 2010).

1.1.3 Climate change impacts on mountain floods

In the context of current and future climate change, flood risks in mountainous areas are increasing due to overall Alpine temperature increases. Large floods in mountain basins are likely to become more frequent with climate change (Allamano et al., 2009). Analysis of climate change scenarios indicates that snowmelt periods will begin earlier in the spring for Alpine regions, leading to a shift of hydrological regimes and maximum monthly discharges (Messerli et al., 2004; Horton et al., 2006). Climate change has also been proven to result in complex non-linear changes in temperature gradients; in the European Alps, minimum and mean maximum temperatures have shown variable increases (in some cases have remained constant) depending on the altitude range considered (Pepin, 2000). Such changes in temperature gradients highly impact flood runoff responses (Tobin et al., 2011). Furthermore, variations in cloudiness and atmospheric transmission are altering quantities of incoming solar radiation. Snowmelt models which commonly link temperature to incoming radiation to produce the equivalent precipitation component of hydrological models are impacted as a result (Huss et al., 2008). Moreover, the resulting changes in radiation are not aligned with changes in air temperature caused by climate change indicating that snowmelt models calibrated in the past must be scrutinized in order to ensure that they still provide valid melt calibrations in today's models.

1.2 Challenges for Alpine flood forecasting models

Integrating the aforementioned meteo-hydrological physical processes and hydraulic influences into a flood forecasting model which is robust to changes from one flood event to the next is a challenge for hydrological modelers (Beven, 2009), particularly in Alpine contexts. The flood forecasting chain (as depicted in Figure 1.2) must aggregate and estimate these modeling difficulties along each step of the forecasting cascade (Pappenberger et al., 2005). The cascade includes the following components: Input to flood forecasting models comes from numerical weather prediction (NWP) models or measured data. Post treatment is generally required for inputs from NWP models in order to remove biases and use data assimilation for model correction. Data assimilation is also used with input measurements to correct hydrograph predictions (Alfieri et al., 2011). Input is fed into a hydrologic/hydraulic model which provides river discharge predictions that are compared against measured responses. If the simulated responses differ from the measured, parameters are calibrated to provide results similar to those measured. At times, however, hydrologic/hydraulic models can be ill-defined so that it becomes necessary to re-identify more appropriate model processes. The following discussion details the inherent difficulties in defining and calibrating each part of this cascade, with a particular emphasis on the complexities of Alpine flood forecasting.

1.2. Challenges for Alpine flood forecasting models

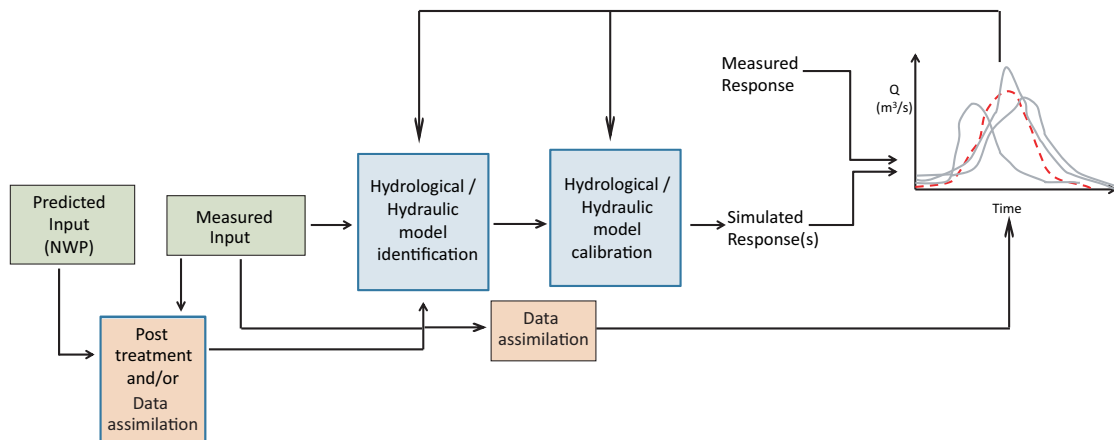


Figure 1.2: The flood forecasting chain

1.2.1 Numerical Weather Prediction forecasts as inputs

Flood forecasting models are typically fed by down-scaled Global Climate Models via Numerical Weather Prediction (NWP) which provide forecasts as deterministic or probabilistic inputs to hydrological models. The input uncertainty associated with such meteorological forecasts typically represents the largest source of uncertainty in the prediction of floods due to the non-linear nature of the atmosphere (Cloke and Pappenberger, 2009). Weather forecasts are limited by not only the numerical representation of the atmosphere's physical processes, but by the resolution of the simulated atmospheric dynamics and the sensitivity of the solutions to the initial conditions and sub-grid parameterization (Buizza et al., 1999). One of the biggest challenges in improving forecasts remains to increase the resolution of the representation of physical processes. Limited Area Models have been generated from NWP models to characterize more fine scale dynamics. The resolution of Limited Area Model grid cells generally ranges between 1-10 km². In spite of advances in resolving finer physical phenomena, the time/space scale of the hydrological model is typically 100 to 1,000 times finer than that of a Limited Area Model forecast model (Cloke and Pappenberger, 2009). As a result, disaggregation of meteorological processes is required for input into hydrological modeling. However, associated uncertainties in downscaling must be propagated throughout the flood forecasting model. Furthermore, generally Limited Area Models require some kind of initial bias correction (i.e., post-treatment of inputs as in Figure 1.2) through data assimilation in order to correspond with statistics of related observations. However, bias correction has not systematically provided an increase in forecast skill (Hagedorn et al., 2007). Uncertainties also arise due to the rarity of flood events which makes a limited dataset difficult to condition or train forecasting models (Pappenberger et al., 2011). Floods are also seasonal so relevant data becomes even more limited for determining relationships between rainfall and flood

discharge (a spring flood can not necessarily be characterized in the same manner as an autumn flood) Merz and Blöschl (2003).

In the context of this thesis, the Limited Area Models utilized in flood forecasting for Switzerland are Consortium for small Scale MOdeling (COSMO) products. Such products are geared to improving early and medium-range predictability for extreme and localized weather events taking into account orographic effects. A probabilistic meteorological-hydrological ensemble prediction chain has shown much success in providing guidance for extreme flood forecasting of 72 to 120 hours for the August 2005 flood in the Upper Rhine catchment in Switzerland (Juan et al., 2008). Details of the COSMO products are provided in Chapter 2 of this thesis.

1.2.2 Hydrological modeling inputs

For calibration and data assimilation purposes, measured data are used to update hydrological models. A primary challenge in mountainous regions is the lack of measurement stations, particularly above 2000 m (Frei and Schär, 1998). Because gauged networks are relatively sparse at high altitudes, it is necessary to interpolate (extrapolate) between (from) meteorological stations to extend the limited measurement data to vast unmeasured, spatial areas. Interpolation is generally implemented at a resolution where physical hydrological processes are valid and not overly generalized. The difficulty of interpolation is how to maintain spatial and temporal correlations with minimum error while considering the influential effects of altitude and orography (Guan et al., 2005).

Proper precipitation interpolation is quite important because the areal volumes induced by rainfall provide the runoff and infiltration in hydrological models (where infiltration impacts antecedent soil conditions). Smith et al. (2004) and Woods and Sivapalan (1999) have demonstrated that the distance-averaged rainfall excess needs to be considered in understanding the response of different catchments. The variability of the rainfall pattern can exert a strong influence on the timing of the hydrograph peak at a downstream gauging station (Gupta et al., 2005). However, the sensitivity of the flow hydrograph to the uncertainty in rainfall decreases with catchment scale (Rodríguez-Iturbe and Mejía, 1998). Gabellini et al. (2007) showed significant changes (up to 25 percent in peak discharge) in the hydrologic response for storm events with different space-time structures depending on catchment size. The variability of the precipitation inputs is also generally dampened in larger catchments due to smoothing effects of the modeled catchment (Beven and Wood, 1993). In these cases, it is only vital to have accurate information on catchment average precipitation (Obled et al., 1994). Mesoscale studies, in particular, by Nicótina et al. (2008) indicated that the spatial variability of rainfall does not have a significant effect on catchment aggregated flood response if the spatial scales that characterize precipitation processes are comparable to the average dimension of the hydrologic model units (i.e., subcatchments). In such a case, it is most critical to correctly estimate rainfall volumes at each time interval. Overall, the most difficult aspect of interpolating precipitation is the fact that rainfall is highly non-linear with an asymmetric probability

1.2. Challenges for Alpine flood forecasting models

distribution (Blöschl and Montanari, 2010), making it difficult to make rainfall predictions temporally and spatially.

The interpolation of input temperature is also particularly critical in Alpine areas. To produce correct snowmelt volumes it is necessary to accurately estimate non-stationary temperature distributions with elevation. According to Garen et al., (2005), in order to accurately reproduce the processes of snow and ice accumulation and ablation, temperature spatial interpolation with reference to altitude is the driving force which enables a good representation of real runoff conditions. Temperature interpolation also has an impact on long-term simulations because what is stored in the snowpack will be eventually released in the melting season. In the case of the study region, dynamic changes in temperature have been attributed to large over and underestimations of discharge for floods in Switzerland (Hingray et al., 2010).

For Alpine contexts, the reduction, or lapse of air temperature with increasing altitude, i.e., lapse rate, is highly influential in snowmelt and hydrological models. Lapse rates are complex in that they are influenced by moisture level, cloudiness/solar radiation and wind speed (Pepin et al., 1999). A shallower lapse rate is typically associated with colder, moister atmospheric conditions whereas steeper lapse rates are generally associated with warmer, drier conditions that occur with increased solar radiation. On a seasonal scale, lapse rates are steeper in the summer months and shallower in winter months whereas on a daily scale lapse rates typically change diurnally (Blandford et al., 2008). Most hydrological and snow melt models currently use the constant, dry adiabatic lapse rate in an observed standard atmospheric profile, $-0.0065\text{ }^{\circ}\text{C m}^{-1}$ or lapse rates determined by annual mean temperatures (Braithwaite, 2008; Brubaker et al., 1996; Hebel and Purves, 2008; Konz et al., 2007; Koboltschnig et al., 2009). However, because the meteorological processes in complex terrain change rapidly on a sub-daily scale, constant lapse rates have been indicated to be highly inappropriate in mountainous regions (Rolland, 2003; Blandford et al., 2008; Minder et al., 2010).

Another complexity for Alpine hydrological models is the partitioning between rain and snow (Tobin et al., 2012) (Figure 1.3). The so-called snowfall limit dictates non-stationary snow cover; it is integral in hydrological models in detailing the source areas receiving rain which directly contribute to runoff and infiltration. However, the spatial variability of snow cover can be very high due to the orientation of winds, different climatic situations and continental versus oceanic forcings (Messerli et al., 2004). Moreover, the observed precipitation type defining the snow limit is influenced by complex, physical processes which are practically impossible to integrate into a simplified hydrological model used for flood forecasting; a comprehensive account of precipitation type would include, among other factors, the incorporation of latent heat (Unterstrasser and Zaengl, 2006), relative humidity (Matsuo and Sasyo, 1981), and thermal and moisture distributions (Bourgouin, 2000).

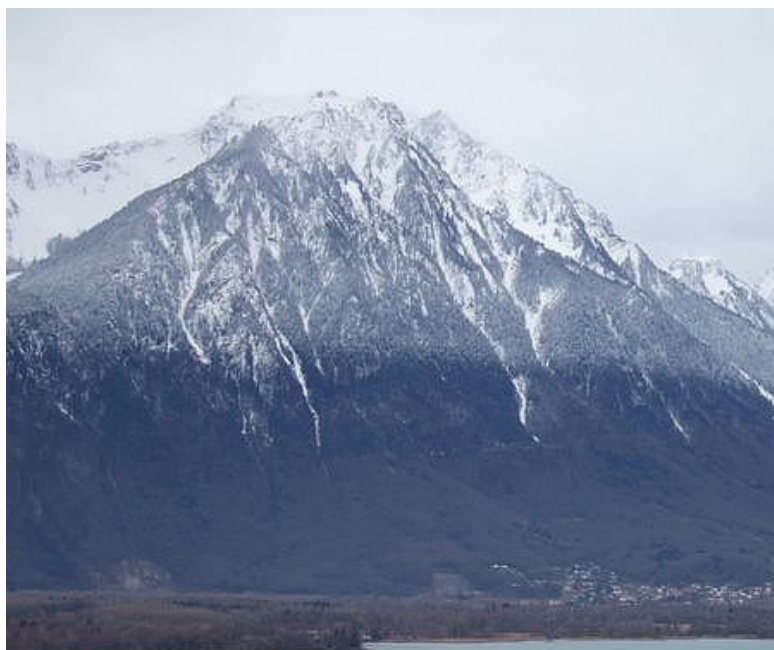


Figure 1.3: Snowfall limit at the outlet of the Upper Rhone River basin into Lake Geneva

1.2.3 Snow processes

In mountain contexts, snow melt estimations are a great source of uncertainty for flood forecasting (Heilig et al., 2010). The rate of snow cover depletion highly impacts snow melt runoff at the catchment-scale (Anderton et al., 2002). One of the most common and simplest means of estimating snow or glacier melt, particularly in data constrained mountainous areas, is to use temperature index methods which define melt rates on the basis of a well-known relationship between melt and air temperature (Finsterwalder and Schunk, 1887; WMO, 1986). In contrast, more comprehensive, full energy balance methods define melt on the basis of local turbulent fluxes of sensible and latent heat (Braithwaite, 1995) and warm-air advection (Sicart et al., 2008). These methods are based upon the most important variables affecting melt including incoming shortwave radiation, reflected shortwave radiation, air temperature, vapor pressure and wind speed (Anderson, 1973; Rohrer and Braun, 1994; Pellicciotti et al., 2005; Lehning et al., 2006).

It is not trivial to model energy and mass balance processes related to snowmelt because they are coupled with evolving heterogenous states of snow-covered and non-snow covered surfaces (Pomeroy et al., 2003). In fact, snowmelt energy balances with flat plane conceptions require corrections because varying slopes and aspects cause notable differences in net radiation and surface temperatures (e.g., a 30% reduction in turbulent and conductive fluxes was noted when changing from a flat to a 45° slope) (Pomeroy et al., 2003). Furthermore, as snow progressively melts, net radiation and melt energetics are magnified due to exposure of vegetation and bare ground (Pomeroy et al., 2003). Practically, due to these complexities and with limited measurements available in Alpine regions, it is difficult to close the energy

balance on a catchment-scale. Also, in the context of real-time flood forecasting, limited point measurements available preclude generalized model calibration and validation for the quantifications of snow covered area and snow water equivalent (Jonas et al., 2009; Dozier, 2011).

1.3 Uncertainty of flood forecasting models

Due to the complexities in modeling complex, Alpine physical processes along the flood forecasting chain, sources of uncertainty can be assumed to stem from an interaction of input, model structure, parameter choice and operational use errors. Understanding all of these model uncertainties is a prerequisite for making decisions based on flood forecast outputs (Cloke and Pappenberger, 2009). In mountain areas, uncertainties are typically higher due to sparse measurements at higher elevations and heterogeneities in meteo-hydrological patterns (Viviroli et al., 2007). For general contexts, input forcing error has been shown to have a strong effect on hydrological model parameter values and output uncertainty and has been indicated to be one of the major sources of uncertainty in rainfall-runoff modeling (Ajami et al., 2007). Parameter uncertainty is also significant due to a lack of comprehensive databases and the inability to measure certain parameters in the field (Fleming et al., 2010; Montanari, 2011). Model structure uncertainty can be common due to a misrepresentation of complex, flow dynamics in simplified, rainfall-runoff models (Hostache et al., 2010; Montanari, 2011). In fact, due to the impact of model uncertainty, recent research advances have explored using multiple model structures to represent hydrological processes (Hoeting et al., 1999).

Formal uncertainty approaches have been developed to use statistical methods to quantify the various sources of uncertainty in hydrological modeling (Vrugt et al., 2009). It is generally assumed that individual errors are additive and the resulting total error has a Gaussian distribution, zero bias and constant variance (Beven, 2009). Note that if this is not the case, it is still possible to transform non-Gaussian distributions to the equivalent density value of a Gaussian distribution using the meta-Gaussian approach (Montanari and Brath, 2004) or to use autoregressive models to reformulate the errors (Schaepli et al., 2007; Yang et al., 2007). Effectively, formal approaches have enabled the improvement of individual hydrological modeling components in specific cases (Krzysztofowicz, 1999; Kavetski et al., 2006).

However, practically, with most hydrological models, it is difficult to disentangle the various sources of error because one type of error can compensate for another during the calibration process (Ajami et al., 2007). As a result, it is believed that a satisfactory approach to separate the various sources of hydrological modeling error has yet to be proposed (Gupta et al., 2005), and, in some cases, entangling error sources is thought to be impossible (Beven, 2005). Fortunately, as in the case of this research, the users of operational flood forecasting systems are concerned solely with reducing the total or global output uncertainty (Montanari, 2011). In this respect, both formal and informal approaches have shown success in providing global uncertainty estimates (Vrugt et al., 2003; Brath et al., 2004; Beven, 2006).

Chapter 1. Introduction

Formal approaches are based on Bayesian inference which maintains that model parameters are in themselves random variables with unknown distributions. In formal methods, the posterior distribution of a parameter is updated sequentially as evidence becomes available thereby becoming the prior distribution with each time step. Such an approach assumes that enough information in measurements/observations is present to define distributions, and the likelihood (or probability) of defining a model is directly proportional to the prior probability density of observations (Mantovan and Todini, 2006). An advantage of formal methods is that the likelihood function leads to reduced uncertainty in the estimated parameter values as more data become available (Beven, 2009). A possible limitation of formal methods is their assumption that the error model is stationary and ergodic (Montanari, 2007), which is often not the case in hydrological modeling (Vrugt et al., 2009). Nonetheless, using this assumption enables Bayesian inference to extend information, collected from observations, to unknown events rather than neglecting the information (Montanari, 2007). (A more in-depth analysis of formal methods is provided in Chapter 6 of this thesis.)

In situations where data is scarce, however, a full treatment of all uncertainties with formal approaches can be prohibited by the ability to define prior probability distributions due to epistemic error (i.e., lack of knowledge or evidence). Moreover, informal theory maintains that it is not possible to define an appropriate likelihood function by ignoring the effects of epistemic uncertainty; assuming all errors are inherently aleatory, as in formal methods, can lead to over-fitting (Beven et al., 2011).

Currently, the most utilized informal method to address the issue of epistemic uncertainty in data-sparse regions is the GLUE Monte Carlo approach (Beven and Binley, 1992), inspired by the generalized sensitivity analysis methodology proposed by Spear and Hornberger (1980). GLUE adheres to the concept of equifinality where more than one parameter set is feasible and thereby multiple likely models, or working hypotheses (Beven et al., 2012), are possible. This method assumes that epistemic uncertainties exist in environmental modeling because observations do not contain enough information and can contain disinformation (Beven and Westerberg, 2011). As a result, even if many simulations are conducted, it is still not possible to know the entire distribution of a random variable; it is only possible to know a few values that a random variable can express. Thus, an assumption for GLUE is that prior to the input of data into a model, all models and parameter sets have an equal likelihood of being acceptable (if there is no previous information provided on parameter distributions). Then, one generates multiple model runs by randomly sampling the parameter space to derive statistics of the output. Based on the results of numerous model runs, a subset of the parameter space is provided which can plausibly assert whether parameter sets which perform well are contained in the sample space. The output is weighted through a formal likelihood measure in order to define acceptable solutions.

Some issues of the GLUE approach include that it samples the space of the model structure inefficiently with its random approach. Also, the formal likelihood measures employed in GLUE have been found to provide inconsistent estimates of the probability density of the model

1.4. Research objectives and thesis organization

output (Montanari, 2007), although solutions have been proposed (Beven and Freer, 2001). As a result, with the classical GLUE methodology, it is not possible to obtain confidence limits in the probabilistic sense with a given frequency (Montanari, 2005); GLUE confidence limits are more accurately described as plausibility intervals (Montanari, 2011). Most significantly, a primary disadvantage of GLUE is that its output can be dependent on subjective, formal likelihood measures which are inherently not probabilistic.

To address these issues, integration of different types of information (soft and hard) can be made (within an unavoidably subjective framework (Montanari, 2011)) which can attempt to use both formal statistical and informal treatments for some part of the forecasting cascade. Winsemius et al., (2009) deals with data limitation constraints by defining quasi-objective limits of acceptability based on estimations of targets defined by interannual variability. These targets are based on statistical and hydrological signatures of available river discharge data and soft data (e.g., monthly water balances). Most recently, headway has been made in defining limits of acceptability for non-stationary biases with informal approaches. Liu et al. (2009) have allowed for a combination of input and model structure error based on uncertainty in the rating curve with dynamic limits which provide over- or under-predictions with every time step.

1.4 Research objectives and thesis organization

Considering an evaluation of uncertainty assessment methodologies aforementioned, along with the sources of complexity for the hydrological component of the flood forecasting model, this research has the aim of reducing model output uncertainty by providing a plausible range of good performing models. In practice this will be achieved by matching the observed, dynamic behavior of the catchment with the hydrological model. The operational flood forecasting model in question is RSII, a semi-distributed conceptual model which describes a vast and complex 4,000 km² catchment area characterized by significant hydropower schemes which drains into the Upper Rhone River in the Valais region of the Swiss Alps. Although this model has been in operation since 2005, it has been unable to accurately simulate measured hydrologic responses in two problematic catchments. (The study catchments and hydrological model are fully detailed in Chapter 2 of this thesis.) This dissertation will test the proposed improvements on the concerned catchments and will focus on improving specific hydrograph behaviors with the thesis work flow process depicted in Figure 1.4.

Objective 1: Inputs, Thesis Chapters 3 and 4

The first objective of this dissertation will be to improve the representation of inputs by estimating accurate instantaneous rainfall volumes and temperature gradients given all available point observations and reanalysis outputs. COSMO forecast reanalyses will be used as additional input due to the limited number of gauges at high altitudes and due to the fact that COSMO reanalyses (corrected with data assimilation) are based on integrating meteorological variables over the vertical atmospheric profile, not solely measured variables at the ground.

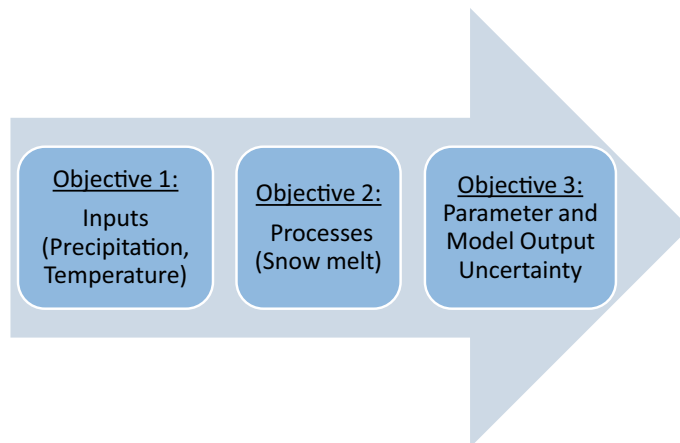


Figure 1.4: Work flow of thesis. Objective 1 is dealt with in Chapters 3 and 4, Objective 2 in Chapter 5 and Objective 3 in Chapter 6

Input uncertainty will be assumed to decrease when the variability of the spatial and temporal distribution of the observed hydrological variables (rainfall and temperature) is better represented. Supporting this hypothesis is a recent analysis of the study region with a similar hydrological model (Hingray et al., 2010). In this analysis, uncertainty was identified as stemming from the precipitation and temperature inputs (Objective 1) as well as the parameters and processes influencing effective liquid water for runoff (Objectives 2 and 3).

Objective 2: Processes, Thesis Chapter 5

The second objective of this research will focus on improving the snowmelt model process. It is assumed here that an overly simplified snowmelt model is included in the current hydrological model and a new formulation of mathematical equations is expected to better represent melting so that it is more physically-based. Epistemic model structural uncertainty will be addressed by better emulating measured radiation effects on melt rather than using a constant degree-day melt factor. By developing a more physically-based, minimalist snowmelt estimation model which requires minimal data inputs, this development will be expected to be useful for a broad range of hydrological models (lumped, distributed, etc) utilized in flood forecasting schemes.

Objective 3: Parameter and model uncertainty, Thesis Chapter 6

The third objective of this research will be to create a tool for managers to identify plausibility intervals defined by acceptable parameter sets so that operators can easily handle decision-

making for preventive hydropower management. In the presence of limited and uncertain information typical of Alpine contexts where not all measured data have the required time step and/or data is scarce or missing, a probabilistic framework is not straightforward (Winsemius et al., 2009). The basis of the proposed method is GLUE (Beven and Binley, 1992) because of its adaptability to data sparse regions and its demonstrated competitiveness with formal methods (Vrugt et al., 2009). In Chapter 6 of this thesis, the GLUE methodology is adapted to constrain plausible model outputs with strict limits of acceptability based on peak flows. Multi-criteria analysis and a customized visualization interface are designed to aid water resource managers in understanding the limits of hydrological modeling certainty. Through the use of these tools and the integration of input and process improvements, an improved calibrated hydrological model leads to the reduction of flood forecasting uncertainty.

The subsequent chapter of this thesis introduces the input data and hydrological models used in this work. It should be noted that both hydrological models were originally developed under previous research projects. As a result, a comprehensive description of both models is given based on previous studies. Further details of the hydrological models and results from previous applications can be found in the references provided.

In addition, Chapters 3-5 represent a collection of papers that have either been published in scientific journals or are in the process of final review before publication. These chapters describe work developed principally by the author of this thesis with the guidance of the other authors listed below:

Chapter 3: Tobin, C and L. Nicotina and M.B. Parlange and A. Berne and A. Rinaldo 2011. *Improved interpolation of meteorological forcings in a Swiss Alpine region*, J. Hydrol. 401, 77-89.

Chapter 4: Tobin, C. and A. Rinaldo and B. Schaefli 2012. *Snowfall limits and hydrological modeling*. In press. J. Hydrometeor.

Chapter 5: Tobin, C. and B. Schaefli and L. Nicotina and S. Simoni and G. Barrenetxea and R. Smith and M.B. Parlange and A. Rinaldo 2012. *Improving the degree-day method for sub-daily melt simulations with physically-based diurnal variations*. Minor revisions finalized, Advance. Water Resour. Special Issue Snow and Atmosphere.

MINERVE and hydrological modeling

2.1 Background

This thesis has been supported by the MINERVE project, a joint venture funded by the Swiss Federal Office on the Environment (OFEV) and the governments of the Valais and Vaud cantons in Switzerland. The goal of this project is to manage floods by using the retention capacity of existing dams and reservoirs in the Upper Rhone River basin in the Valais region of Switzerland (see Figure 2.1). The project complements the Third Rhone Correction plan, currently in progress, which involves physically changing the Upper Rhone River banks and adapting channel roughness properties so that both measures can provide protection against flooding in the Upper Rhone River valley region.

The first phase of the MINERVE project was initiated in 1999. At this time, a hydraulic-hydrological model, Routing System II (hereafter referred to as RSII) was developed at the Swiss Federal Institute of Technology (EPFL), Lausanne. This tool combines a hydrological forecasting model with a decision optimization tool for hydraulic structures (Garcia Hernández et al., 2011). Based on the discharge forecast, the optimization tool can recommend preventive turbine and gate operations for hydropower reservoirs to enable an increase in reservoir capacity in sight of an incoming strong storm event (Garcia Hernández et al., 2009a).

The hydrological model within RSII is based on the Glacier-SnowMelt-SOil CONTRIBUTION (GSM-SOCONT) model (Schaepli et al., 2005; Hamdi et al., 2005; Hingray et al., 2006). In its RSII version, the GSM-SOCONT model has been adapted to run on an hourly timestep for dynamic flood forecasting purposes (see Jordan, 2007, for model details and calibration parameters). It is used operationally with CONSORTIUM for small Scale MODELing (COSMO) forecast inputs.

The RSII model was successful in generating appropriate flood responses in twenty-three of the twenty-five catchments (defined by hydrology and hydraulic works) of the Valais. However, for two particular catchments, the Visp and the Dranse (Figure 2.1), the complex, hydrological

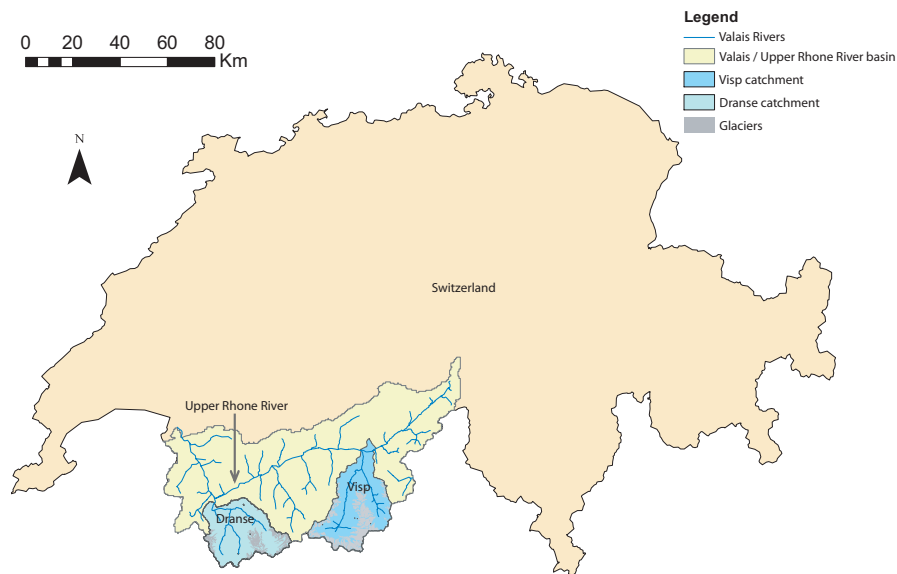


Figure 2.1: Map of the Dranse and Visp catchments in Switzerland with the Valais river network. Glaciers within the Visp and Dranse catchments are indicated in grey.

processes, including precipitation and temperature space/time distributions and rainfall-runoff partitioning, were not able to be accurately characterized in the model. Modeling the Visp and the Dranse catchments is complicated due to several factors: The catchments have a complex topography, ranging in altitude between approximately 650 and 4500 m asl and have significant glacier coverage (approximately 33 % in the Visp and 13 % in the Dranse). The catchments are relatively ungauged, particularly at higher elevations, where most snow and rain is deposited due to orographic effects and synoptic weather patterns. Calibrating the model to measured discharge is an additional challenge because the majority of discharge measurements are perturbed by hydropower operations.

A manual calibration of the RSII model was conducted between 2004 and 2007 (Jordan, 2007). However, due to the difficulties aforementioned, all hydrograph peaks were underestimated with the RSII model at the outlets of the Visp and Dranse catchments for the major flood events of 1987, 1993, 1994, and 2000. Simulated initial saturation varied significantly from measured antecedent conditions in these catchments while recession hydrographs did not show bi-modal, slow and fast responses characteristic of measured discharge.

The overarching goal of this thesis is to further develop the RSII hydrological model to improve input and process characterizations and associate uncertainty to the model output so that the model can capture hydrograph responses. This is accomplished by analyzing meteorological processes in both the Visp and Dranse catchments (or within a subset of these catchments) and proposing methodologies for improvements in the subsequent chapters of this thesis. In a particular study on snowmelt processes in Chapter 5, a geomorphic model for the Dranse catchment was developed to test snowmelt methods. This spatially-explicit model provides a physically based, semi-distributed description of the hydrologic response

and incorporates geomorphologic information extracted from a thorough study of the digital terrain models (DTMs) of the study catchment. This model was chosen based on the results of a geomorphologic analysis indicating that hillslope processes dominate in the study catchments. Below, details on the study catchments and a geomorphologic analysis of the catchments are provided. The measured inputs, forecasts, and hydrological models are subsequently described.

2.2 Study catchments

The catchments analyzed in this thesis are the Visp and Dranse, located in the Swiss mountainous region of the Valais. The Valais is situated in the central part of the Alps. It is drained by the Rhone River that flows from East to West and is boarded by two high mountain ranges: the Penninic Alps in the South and the Bernese Alps in the North. Because of rain shadow effects, the climate is relatively dry at the bottom of the valley and annual rainfall at approximately 500 m asl is 600 mm and 800 mm at 1600 m asl respectively. Due to orographic effects, annual rainfall surrounding and near the ridges of the Visp catchment is generally greater than 2800 mm. Highest mean monthly discharges in the Valais occur during July and August due to snow and ice melting. Due to intense rainfall, high discharge events are common between September and October. These events induce critical situations because reservoirs are typically filled and cannot be used to mitigate floods (Schaepli et al., 2005). Detailed topography of the Valais is available from a 25 m × 25 m resolution digital elevation model developed by Swisstopo. The Visp and Dranse catchments (800 km² and 650 km² respectively) show similar characteristics with steep slopes, high peaks (Matterhorn, 4500 m, in the Visp) and high passes (Saas, 1800 m, in the Visp and Grand St. Bernard, 2500 m, in the Dranse). Soil cover in the Visp and in the Dranse is predominantly sandy-loam.

2.2.1 Analysis of catchment geomorphology

The digital terrain models (DTMs) for the Visp and Dranse catchments were processed through the TAUDEM package to define the channel network based on drainage directions and to derive objective information that defines the hydrologic processes in the hillslopes (Tarboton, 1997). The river networks and unchanneled flow paths were analyzed to define invariant morphologic properties of the river basin (Rodriguez-Iturbe and Rinaldo, 1997) which are controlling factors on the hydrologic response.

Defining a catchment and its drainage network with a fixed threshold on accumulated area produces a distribution of unchanneled lengths, $P(L \geq l)$. The experimental cumulative density function can be estimated by means of the plotting position technique:

$$P = m/(n + 1) \tag{2.1}$$

where m is the ranking from longest to shortest unchanneled length and n is the number of

unchanneled segments in the sample.

The unchanneled lengths define how long a water particle must travel prior to entering the stream network. The greater the unchanneled length, the longer the water particles must travel on the hillslopes before reaching the river network. This analysis thereby defines the relative travel times for runoff over hillslopes within a catchment.

For the Visp and Dranse catchments, the distribution of unchanneled lengths, $P(L \geq l)$, is shown in Figure 2.2.

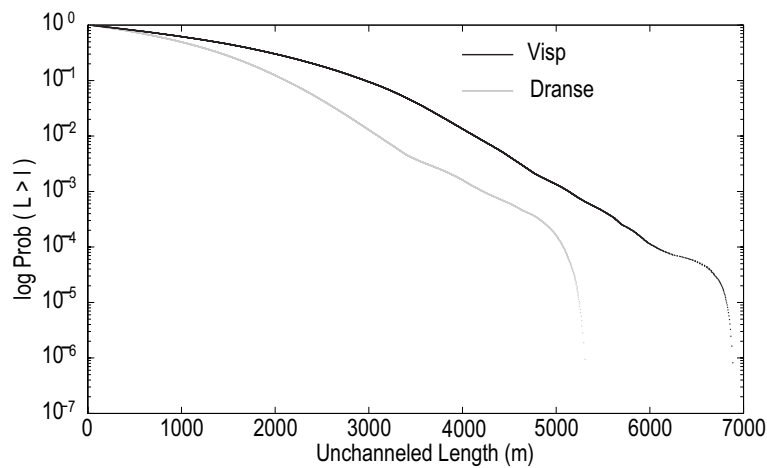


Figure 2.2: Probability of exceedance for unchanneled lengths in the Dranse and the Visp.

This figure shows that the drainage density is different in the Visp and the Dranse. The Visp flow is unchanneled for longer distances. However, in both cases, the drainage density is very large. In other words, a water particle in the Visp basin may have to travel 7 kilometers before reaching a channel. Similarly, the furthest unchanneled length in the Dranse is 5.5 kilometers.

This study demonstrates that flow pathways are predominantly controlled by the topography of the catchments; the basic travel timescales are chiefly defined by travel times within unchanneled areas. This is due to high velocities and relatively short channeled lengths associated with the steep topography of the catchments. The particular morphology of the catchments requires a proper accounting of the structure of the residence time distributions in the hillslope states. Although existing geomorphologically-based hydrological models have demonstrated effectiveness in flood prediction (Bérod et al., 1995), a generalized, spatially-explicit model of the hydrological response has been developed to be representative of hydrologic models which are lumped in some nature. It thereby serves as a good reference for the RSII model due to its use of physically-based descriptions for hydrologic processes. With this model, a subset of the Dranse catchment which is unperturbed by hydraulic controls is analyzed in Chapter 5 of this thesis. This model enables a comprehensive analysis of snowmelt schemes based on an accurate identification of natural, unperturbed flow paths across the catchment.

2.3 Inputs

2.3.1 Meteorological forcing inputs

Precipitation and temperature inputs are obtained from a network of meteorological stations managed by the national weather service, MeteoSwiss (Gutermann, 1986). Data from the automatic ANETZ meteorological network is used in all studies in the subsequent chapters (Figure 3.1). Although the network has a mean next-neighbor distance of 7 km, these stations are more limited in the high elevation regions of the study catchments as discussed in Chapter 4 of this thesis.

2.3.2 COSMO Forecasts

Operationally, the RSII model is driven by Consortium for small Scale MOdeling (COSMO) forecasts. Studies in this thesis concern the two most utilized deterministic COSMO models, COSMO2 and COSMO7. Both models are non-hydrostatic limited-area models integrated at horizontal resolutions of $2 \times 2 \text{ km}^2$ and $6.8 \times 6.8 \text{ km}^2$ respectively (Addor et al., 2011). They use a generalized terrain-following height coordinate with user-defined grid stretching in the vertical. Data assimilation is performed using nudging to update model states based on observations from radio soundings and pilots, conventional surface station data (such as MeteoSwiss ANETZ temperature and precipitation data), AMDARs (i.e., airplane data), data from ships and buoys, wind profilers, and radar data (for COSMO2 only). The forecast ranges for COSMO2 and COSMO7 are 24 and 72 hours respectively.

Grid-scale clouds are resolved in the COSMO models by using a scheme including ice clouds as a prognostic variable, which leads to a function describing the fraction of cloudiness. The partitioning of water into water vapor, the non-precipitating categories of cloud water and cloud ice, and the precipitating categories, i.e. rain, snow, and graupel (graupel, in the case of COSMO2 only) is performed by a prognostic scheme where the full hydrological budget equations for precipitating hydrometeors are solved (including 3-d advective transport). Further details on the parameterization of cloud and precipitation physics, boundary layer turbulence and surface fluxes are detailed in COSMO (2011).

The differences between COSMO2 and COSMO7 relate to their driving forces, their configurations, their reinitialization frequencies and their treatment of convection. The initial and lateral boundary conditions, i.e., the driving models, for COSMO7 and COSMO2 are the Integrated Forecasting System (IFS) from ECMWF and COSMO7, respectively. COSMO7 has 45 vertical layers while COSMO2 has 60 layers, both with model tops set at 20 hPa. Below 3 km in the atmospheric profile where melting typically takes place, the COSMO model's vertical grid spacing becomes progressively finer closer to the ground. Vertical differences range from approximately 1200 m between the top layers at 3 km to a difference of approximately 20 m at the ground. The frequency of reinitialization of COSMO2 is every 3 hours (i.e., 8 runs per day) whereas the COSMO7 model is re-initialized twice per day. The COSMO7 model parameterizes

both deep and shallow convection while COSMO2 considers only shallow convection because its high resolution enables the explicit resolution of deep convection, which reduces model uncertainty (Weusthoff et al., 2010). COSMO-7 deep convection is parameterized by the mass flux scheme of Tiedtke (1989).

Numerous research endeavors have demonstrated the success of these COSMO products in the MAP D-Phase project (Mesoscale Alpine Programme Demonstration of Probabilistic Hydrological and Atmospheric Simulation of flood Events in the Alpine region). Bauer et al. (2011) showed that the COSMO models are capable of forecasting correct distributions of precipitation, particularly for low precipitation thresholds. In complex terrain, COSMO2 has been shown to yield better precipitation forecasting performance than coarser COSMO products due to its more frequent initialization and its explicit calculation of deep convection (Weusthoff et al., 2010; Ament et al., 2011). Similarly, flood peaks have been proven to be accurately captured with short-term COSMO2 forecasts (Zappa et al., 2008).

Although, this research will not use the COSMO forecasts real time, since the goal of this thesis is to improve and calibrate the hydrological model, this dissertation will take advantage of COSMO reanalyses to provide a greater meteorological context to the flood event analyses. In using COSMO as input, each elevation band of the hydrological model (details of the hydrological model are provided in the next section of this Chapter) is assigned the closest COSMO grid point using MeteoSwiss procedures where the Euclidian distance in the horizontal is summed with the vertical difference multiplied by a correction factor. The correction factor is used to make the vertical and horizontal differences have relatively equal importance in spite of the vertical distance being typically an order of magnitude less (Kaufmann, 2008).

2.4 MINERVE model - Routing System, RSII

RSII is a semi-distributed, reservoir-based model that has been implemented for operational flood forecasting (see Jordan, 2007; Hingray et al., 2010, for model details and calibration parameters). Catchment limits are defined according to topography described by a 25 m resolution DTM. Hydraulic works (i.e. water diversions due to pumping and piping configurations) act as physical constraints in the model.

Each subbasin is discretized on two levels: 1) the separation of ice-covered and non ice-covered portions based on DTM data; and 2) the division of each subbasin into a set of elevation bands, set at approximately every 300 m. The Visp and Dranse catchments are subdivided into 32 and 35 subbasins respectively. Each subbasin is represented as a set of spatial units, each of which is assumed to have a homogenous hydrological behavior.

The RSII runoff model depends on whether the elevation band forms part of the ice-covered area. According to Schaepli et al. (2005), the total runoff from the entire catchment can be

defined as

$$Q = \sum_{i=1}^2 \sum_{j=1}^{n_j} a_{i,j} \times Q_{i,j} \quad (2.2)$$

Where i is an index for either the snow-covered or ice-free part of the catchment and j is an index for each of the n_j elevation bands in part i . $a_{i,j}$ (km²) is the area of an elevation band j belonging to the catchment part i and the $Q_{i,j}$ (mm h⁻¹) is the mean hourly specific runoff from this spatial unit, rather than daily as in Schaefli et al. (2005).

Details of the RSII hydrological modeling components are listed below.

2.4.1 Inputs

Temperature and precipitation inputs are interpolated with Inverse Distance Weighting, IDW (Isaaks and Srivastava, 1989), to the centroid of each elevation band in the x,y,z space and are assumed to be representative of the whole band. Temperature interpolation is based on an altitude dependent regression of the observations at meteorological measurement stations located in or nearby the study catchments. Temperature interpolations are carried out on normalized measured data, detrended for elevation. Vertical distributions are then extrapolated using a constant lapse rate of -6.5 °C per 1000 m. Temperature time series are computed separately for each elevation band. Precipitation is assumed to be uniform over each subbasin, i.e. all elevation bands within a subbasin have the same quantity of precipitation.

As discussed previously in Chapter 1, Section 1.2.2, accurate precipitation and temperature interpolations are critical in Alpine environments. It should be noted that temperature interpolations have significant impacts in the Dranse and Visp catchments. As shown by the hypsometric curves in Figure 2.3, if temperatures are not correctly interpolated with altitude spatially (i.e., assigning improper lapse rates), the contributions of snow and rainfall to runoff can be highly inaccurate. In fact, an error of 2 °C or approximately 300 m (as indicated by the horizontal lines on Figure 2.3) can account for approximately 15 % of the relative surface area (indicated by the vertical lines) in the watersheds which does not contribute correctly to the rainfall-meltwater-runoff transformation. Therefore, temperature errors can provide inaccurate productions of runoff by all components of the hydrological model described hereafter.

2.4.2 Snow model production

For each elevation band, the temporal evolution of the snowpack is computed based on an accumulation and melt model. This model is a function of temperature T and precipitation P . Snowmelt contributes to the equivalent precipitation (P_{eq}) which is used as an input variable

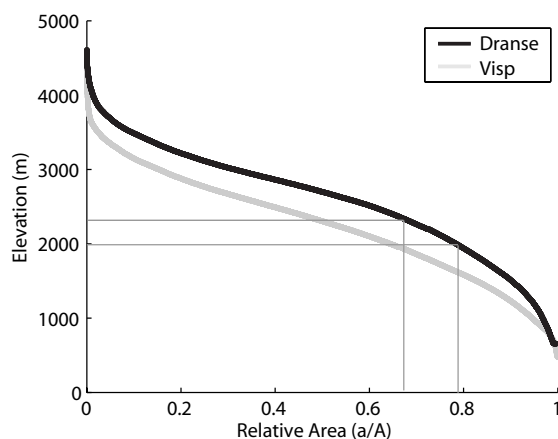


Figure 2.3: Hypsometric curves for the Visp and Dranse catchments in the Upper Rhone River basin of the Valais region in Switzerland. Lines indicate an incorrect lapse rate of 2 °C (i.e., 300 m) which produces a miscalculation of surface area contributing to runoff (approximately 15%).

by the infiltration or glacier model.

The RSII model uses the degree-day method to define the melt as defined by M_N in Figure 2.4 and Equation 2.3. This approach has been justified on physical grounds in other hydrological models (Rango and Martinec, 1995). According to Schaepli et al. (2005), the snow and glacier degree-day factors have a major influence on the simulation quality during summer months.

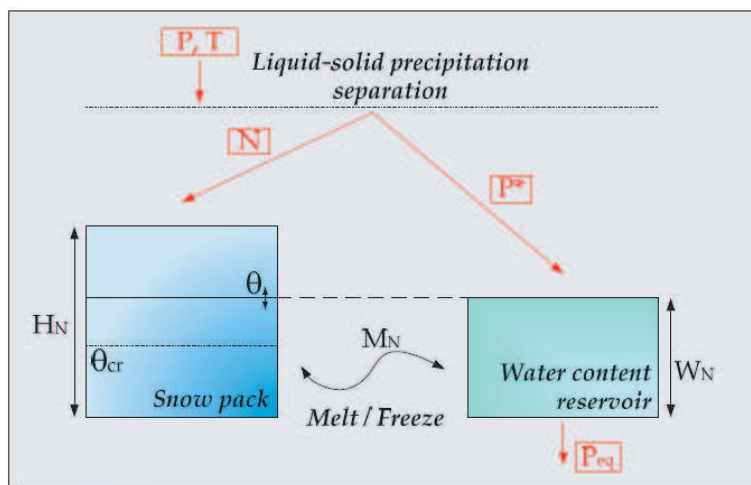


Figure 2.4: RSII snow melt production (Garcia Hernández et al., 2007).

In the first step of the snow model, precipitation is partitioned per elevation band into snow- and rainfall using a linear transition between 0°C and 2°C based on sensitivity tests with the hydrological model, other studies (Zappa et al., 2003; Schaepli et al., 2005; Kienzle, 2008) and other observations from the Swiss Alps (Rohrer and Braun, 1994). Below 0°C all precipitation is

considered to fall as snow and above 2°C only rainfall occurs. In between these two thresholds, a mixture of rainfall and snowfall occurs.

The total discharge of the snow module depends on the snow height, temperature and partitioning between rain and snow. Snowmelt or freezing is calculated based on the degree-day method (Rango and Martinec, 1995) as follows:

$$Mn = \begin{cases} a_c(1 + b_p P_l)(T - T_{cr}) & \text{if } T \geq T_{cr} \text{ and } Mn \leq N + \frac{H_n}{dt} \\ a_c(T - T_{cr}) & \text{if } T \leq T_{cr} \text{ and } Mn \geq \frac{-W_n}{dt} \end{cases} \quad (2.3)$$

where P_l is the liquid precipitation (m s^{-1}), N is the solid precipitation (m s^{-1}), T_{cr} is the critical temperature 0°C, b_p is the precipitation coefficient due to snowmelt fixed at 0.0125 (s m^{-1}), a_c is the degree-day factor ($\text{mm day}^{-1} \text{ }^\circ\text{C}^{-1}$), $\frac{-W_n}{dt}$ is the dynamic water content (m s^{-1}) and $\frac{H_n}{dt}$ is the dynamic snow height (m s^{-1}).

Refreezing is calculated analog to melting and assumes that the melt and refreezing rates are the same, similar to Bergstrom (1975). The water content of the snowpack evolves every time step when the ratio of the liquid to solid water store in the snowpack (the snowpack's relative liquid water content) is computed. Water outflow of the liquid store (called snowpack outflow) only occurs if this relative liquid water content is above a critical retention capacity θ_r , which is fixed to 0.09 in the analyses with the RSII model.

2.4.3 Glacier model production

The total discharge of the glacier depends on the transfer processes within the linear snow on glacier and glacier reservoirs R_N and R_{GL} (Figure 2.5).

Equivalent precipitation P_{eq} for the snow on glacier model is provided by the snowmelt model previously described and is transferred to the linear snow on glacier reservoir R_N according to Figure 2.5.

Equivalent precipitation P_{eqGL} for the glacier model is dependent on the critical temperature T_{cr} and snow height H_N . It is defined as follows:

$$P_{eqGL} = \begin{cases} 0 & \text{if } T \leq T_{cr} \text{ or } H_N > 0 \\ A_{GL}(T - T_{cr}) & \text{if } T > T_{cr} \text{ and } H_N = 0 \end{cases} \quad (2.4)$$

where P_{eqGL} is the glacier melt (m s^{-1}) and A_{GL} is the degree-day glacier melt coefficient ($\text{mm day}^{-1} \text{ }^\circ\text{C}^{-1}$).

The change in storage of the linear snow on glacier reservoir is defined as:

$$\frac{dH_{NGL}}{dt} = P_{eq} - K_N H_{NGL} \quad (2.5)$$

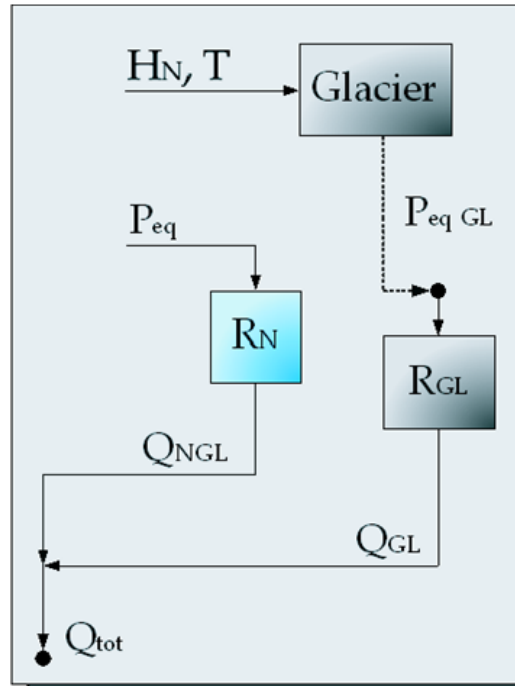


Figure 2.5: RSII snow and glacier reservoirs (Garcia Hernández et al., 2007).

where H_{NGL} is the level in the linear snow on glacier reservoir (m) and K_N is the release coefficient of the linear snow reservoir (s^{-1}).

The outflow of the linear snow on glacier reservoir Q_{NGL} is:

$$Q_{NGL} = K_N H_{NGL} S_{GL} \quad (2.6)$$

where Q_{NGL} is in ($m^3 s^{-1}$) and S_{GL} is the surface area of the glacier (m^2). The snow on glacier model produces discharge when snow is present on the glacier.

Similarly, the change in storage of the linear glacier reservoir is defined as:

$$\frac{dH_{GL}}{dt} = P_{eqGL} - K_{GL} H_{GL} \quad (2.7)$$

where P_{eqGL} is the glacier melt ($m s^{-1}$), H_{GL} is the level of the glacier melt reservoir (m) and K_{GL} is the coefficient of the linear glacier reservoir (s^{-1}).

The outflow of the linear glacier reservoir is:

$$Q_{GL} = K_{GL} H_{GL} S_{GL} \quad (2.8)$$

where Q_{GL} is in ($\text{m}^3 \text{s}^{-1}$) and S_{GL} is the surface area of the glacier (m^2).

The glacier model only provides the discharge when the snow level is zero, $H_N = 0$.

The discharge produced by the glacier melt P_{eqGL} is transferred to the linear glacier reservoir R_{GL} and the resulting glacier discharge Q_{GL} is summed with the snow on glacier discharge Q_{NGL} at the outlet of the subcatchment to produce the total discharge Q_{tot} .

2.4.4 Infiltration model production

The infiltration or groundwater reservoir model is the next reservoir used to define rainfall-meltwater-runoff transformation (Figure 2.6). The infiltration reservoir has a slow and fast component.

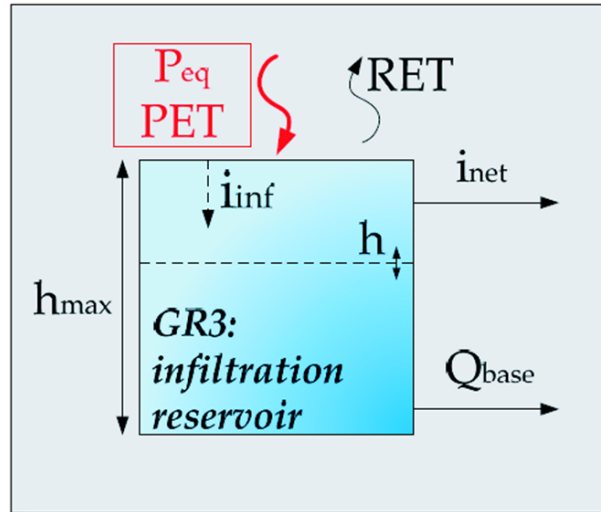


Figure 2.6: RSII infiltration reservoir (Garcia Hernández et al., 2007).

Infiltration, i_{inf} (m s^{-1}), is defined with a non-linear relation and is a function of the water level in the groundwater reservoir h , the maximum height of groundwater reservoir h_{max} (m) and the equivalent precipitation Peq .

$$i_{inf} = \begin{cases} Peq(1 - (\frac{h}{h_{max}})^2) & \text{if } h \leq h_{max} \\ 0 & \text{if } h > h_{max} \end{cases} \quad (2.9)$$

Real evapotranspiration RET (m s^{-1}) is also described as a non-linear process as a function h and h_{max} . It is based on the potential evapotranspiration PET (m s^{-1}).

$$RET = \begin{cases} PET\sqrt{h \setminus h_{max}} & \text{if } h \leq h_{max} \\ PET & \text{if } h > h_{max} \end{cases} \quad (2.10)$$

Base flow is defined by a linear relation:

$$Q_{base} = \begin{cases} khS & \text{if } h \leq h_{max} \\ kh_{max}S & \text{if } h > h_{max} \end{cases} \quad (2.11)$$

where Q_{base} is the base discharge ($\text{m}^3 \text{s}^{-1}$), k is the release coefficient of the groundwater reservoir (s^{-1}) and S is the surface area (m^2).

With the fluxes previously defined, the dynamic height of the water level in the groundwater reservoir is defined as follows:

$$\frac{dh}{dt} = i_{inf} - RET - \frac{Q_{base}}{S} \quad (2.12)$$

2.4.5 Overland flow model

The transfer of the net intensity to an impermeable surface is carried out by the help of a non-linear transfer reservoir.

The net intensity (m s^{-1}) is defined by the infiltration component of the model previously described.

$$i_{net} = P_{eq} - i_{inf} \quad (2.13)$$

The description of this reservoir is based on the SWMM model (Metacalf, Eddy, 1971), where overland flow is modeled with the Manning-Strickler equation. This is a standard flow resistance relation linking velocity, slope and hydraulic features for open channel flows (Chanson, 2004).

Runoff intensity, i_r (m s^{-1}), is defined as:

$$i_r = K_s \sqrt{J_o} (h_r)^{5/3} \frac{B}{S} \quad (2.14)$$

where h_r is the runoff water level downstream of the surface (m), K_s is the Strickler coefficient ($\text{m}^{1/3} \text{s}^{-1}$), J_o is the average slope of the plane, B is the width of the plane (m) and S is the surface area (m^2).

The runoff discharge for overland flow is defined as:

$$Q_r = \frac{i_r}{S} \quad (2.15)$$

2.4.6 Channel routing

Overland flow is routed based on three flow routing schemes for channel flow: 1) St. Venant routing for a trapezoidal section, 2) Muskingum-Cunge (diffusive wave with celerity and diffusion coefficients) or 3) the kinematic wave (where the terms of inertia and pressure of the St. Venant equations are assumed negligible).

The parameters used for calibration from the components of the RSII hydrological model are summarized in Table 2.1. No channel routing parameters were calibrated because they were defined by physical cross-section features assumed to be constant.

Table 2.1: RSII calibrated hydrological model parameters

Snow model	
Parameter	(unit)
Snow degree-day factor	(mm day ⁻¹ °C ⁻¹)
Critical retention capacity	(-)
Infiltration model	
Release coefficient of groundwater reservoir	(s ⁻¹)
Maximum height of groundwater reservoir	(m)
Glacier model	
Coefficient of linear snow reservoir	(s ⁻¹)
Coefficient of linear glacier reservoir	(s ⁻¹)
Glacier degree-day factor	(mm day ⁻¹ °C ⁻¹)
Overland flow model	
Strickler coefficient	(m ^{1/3} s ⁻¹)

2.5 Spatially-explicit model of the hydrological response

If water flow within natural formations (the whole catchment, composed of geomorphological states objectively connected through channeled or unchanneled pathways) can be seen as a conservative process, water particles are described as moving within control volumes towards an absorbing barrier (the catchment outlet) without significant variations of their mass. This, of course, entails a suitable partitioning of total snow/rainfall into effective components, as described in the previous sections. In this section we focus of the basic scheme that allows a model of the hydrologic response to become spatially-explicit i.e., capable of describing arbitrary geometrical attributes in an exact manner without discretizing differential balance equations. The formulation of transport by travel time distributions, neither Eulerian nor fully Lagrangian in nature but mathematically equivalent, serves as an ideal model for complex terrain (Rodriguez-Iturbe and Valdés, 1979; Gupta et al., 1980; Dagan, 1989; Rodriguez-Iturbe and Rinaldo, 1997; Rinaldo and Rodriguez-Iturbe, 1996) by employing in full, the large-scale collection and objective manipulation of geomorphic, hydrologic and/or land use data which are commonplace in science and engineering practice today. This section therefore describes the theoretical framework for a class of general continuous models of the hydrologic response. The approach consolidates and gives order to theoretical results from other fields in a coherent theoretical framework for both hydrologic flow and transport.

Let m be the (time-independent) water mass transported by a single particle injected at time $t_0=0$ in the initial position \mathbf{x}_0 . Each ensuing trajectory is defined by its Lagrangian coordinate $\mathbf{X}(t) = \mathbf{x}_0 + \int_0^t \mathbf{v}(\mathbf{X}(\tau), \tau) d\tau$, where $\mathbf{v}(\mathbf{x}, t)$ is the point value of the advective velocity vector. Note that a precise definition of the momentum balance that yields the field $\mathbf{v}(\mathbf{x}, t)$ is immaterial in this context, owing to the kinematic (and general) nature of the analysis. Indeed \mathbf{v} may in turn describe Darcian or Richards-like flows in variably saturated, gravity-driven flows appropriate for describing unchanneled pathways, or open-channel flow velocities can be noted in riverine branches. The spatial distribution of water concentration c in the transport volume \mathcal{V} as a result of the injection of a single particle is given by (Taylor, 1921):

$$c(\mathbf{x}, t) \propto m \delta(\mathbf{x} - \mathbf{X}(t)), \quad (2.16)$$

where $\delta(\cdot)$ is Dirac's delta distribution and, without loss of generality, we have assumed unit porosity within the whole control volume (i.e. $\int_{\mathcal{V}} c_w d\mathbf{x} = m_w$). Note that the proportionality in Equation (2.16) stems from the assumption of constant porosity of the transport volume along the flow paths, which proves feasible for a variety of cases of interest (Dagan, 1989). Equation (2.16) states that, in the one-particle one-realization case, volumetric water concentration (water mass per unit transport volume) is nonzero only at the site where the particle is instantaneously residing (i.e. at its trajectory). Thus uncertainty in the dynamical specification of the particle (i.e. the evolution in time and space of the trajectory $\mathbf{X}(t)$ of the labeled, traveling 'water particle') is reflected in the transport process.

Owing to the heterogeneity which characterizes transport processes and environments at

2.5. Spatially-explicit model of the hydrological response

basin scale, the trajectory is seen as a random function. Let therefore $g(\mathbf{X})d\mathbf{X}$ be the probability that the particle is found within the infinitesimal volume $d\mathbf{X}$ located around the position \mathbf{X} at time t (notice that the functional dependence $g(\mathbf{X})$ implies $g(\mathbf{x}, t)$ in terms of Cartesian coordinates because of the evolution of the trajectory with time). The ensemble average concentration $\langle c(\mathbf{x}, t) \rangle$ is given by the classic relation (Taylor, 1921; Dagan, 1989):

$$\langle c(\mathbf{x}, t) \rangle = \int_{-\infty}^{\infty} m\delta(\mathbf{x} - \mathbf{X})g(\mathbf{X})d\mathbf{X} = m g(\mathbf{x}, t) \quad (2.17)$$

The distribution $g(\mathbf{x}, t)$ is usually called displacement probability density function. Important models describing displacement distributions, g , or $\langle c_w \rangle$ (from Eq. (2.17) $g \propto \langle c_w \rangle$), notably the cases deriving from the Fokker-Planck equation, are reported in the literature (Rinaldo et al., 1991). Note that the above theoretical link between displacement distributions and mean concentrations allows the equivalence of the rate of change of displacement covariances (heuristically, the moments of inertia of the displaced particles) with half the dispersion coefficient of the Eulerian problem, originating from the definition of shear-flow, hydrodynamic or geomorphologic dispersion (Rodriguez-Iturbe and Rinaldo, 1997).

The displacement pdf $g(\mathbf{x}, t)$ due to the kinematics of the carrier flow determines the travel time distribution $f(t)$ of the water carrier within the control volume. The definition of a travel time distribution relies on the identification of a suitable control section for the transport process considered. We thus assume that the time t at which a particle crosses the control section is unique and, most importantly, that all particles injected in \mathcal{V} ensuing from $\mathbf{x}_0 \in \mathcal{V}$ must transit to the outlet control. The probability density of travel times is proportional to the instantaneous mass flux at the absorbing barrier of the control volume (Dagan, 1989). In fact water mass in storage within the control volume $M(t)$ is expressed by:

$$\begin{aligned} M(t) &= \int_{\mathcal{V}} \langle c \rangle d\mathbf{x} = m \int_{\mathcal{V}} g(\mathbf{x}, t) d\mathbf{x} = \\ &= mP(T \geq t) \end{aligned} \quad (2.18)$$

where $P(T \geq t)$ is the probability that the residence time is larger than current time t . Thus, by continuity, one has

$$\frac{dM(t)}{dt} = I - Q \quad (2.19)$$

(where $I [M][T]^{-1}$ is the mass water input and $Q(t) [M][T]^{-1}$ is the mass flux at the outlet of \mathcal{V}), and therefore, for an instantaneous water pulse, i.e., $I(t) = m\delta(t)$:

$$Q(t) = -m_w \frac{dP(T \geq t)}{dt} = m_w f(t) \text{ for } t > 0 \quad (2.20)$$

where $f(t)$ is the probability density function (pdf) of travel times for the water carrier. In

Chapter 2. MINERVE and hydrological modeling

surface hydrology, when the input is a unit of net rainfall, such a pdf is usually termed the instantaneous unit hydrograph (IUH).

In using the travel time formulation of transport in surface hydrology, two courses have been pursued: one course assumes the form of the pdf, and characterizes it by some parameters of clear physical meaning like mean travel times. An example of this are the exponential pdf's used to describe travel times of water particles in the seminal paper by (Rodriguez-Iturbe and Valdés, 1979) to derive the geomorphologic unit hydrograph. The second course exploits the equivalence of water fluxes and pdf's to deduce travel times from the equations of motion. Eulerian, Lagrangian or travel time approaches therefore may be derived strictly from the same assumptions (the common prejudice of considering one approach in principle superior to the other is therefore incorrect).

We now turn to hydrologic transport phenomena within the same framework which is deemed particularly suitable to tackle nonstationary process in runoff formation (Botter and Rinaldo, 2003; Rinaldo and Marani, 1987). Within such a domain, a given amount of tracer (of mass m_s) is injected within the control volume through an instantaneous release of water, and is thus allowed to move within the transport volume driven by the hydrologic carrier flow and to exchange mass within the surrounding environment. The reactive character of the transport is described by the (spatial and/or temporal) variability of the solute mass associated with the water particles moving within the control volume, that is, the function $m_s = m_s(\mathbf{X}, t; t_0)$ which embeds physical, chemical or biological exchanges with immobile phases in some contact with the carrier flow. Note that the so-called active transport framework (that is where the presence of the tracer provides a feedback on the velocity field, e.g. for non-aqueous phase liquids) is not considered herein.

One-particle, one-realization concentration fields resulting from the injection of a single reactive particle are given by the following equation:

$$c_s(\mathbf{x}, t; \mathbf{x}_0, t_0) \propto m_s(\mathbf{X}, t; t_0) \delta(\mathbf{x} - \mathbf{X}(t)), \quad (2.21)$$

The reactive components involved define the instantaneous solute mass m_s attached to the moving particle without affecting the trajectory \mathbf{X} of the particle itself which is determined by the usual kinematic relationship. The mass transfer occurring between the carrier and immobile phases (e.g. chemical or physical sorption, ion exchange, precipitation) leads in general to variability for m both in time and space. We assume, however, that the injection area is much larger than any correlation scale of heterogeneous transport properties and/or that the temporal scales relevant for the undergoing advective processes are smaller than (or, at most, comparable with) the characteristic timescales for the reaction processes. This suggests (Rinaldo et al., 1989; Rinaldo and Rodriguez-Iturbe, 1996; Botter et al., 2005) that the spatial gradients of mass exchange become negligible and that, therefore, contact time among fixed and mobile phases alone drives mass transfer between phases (i.e. the well-mixed approximation (Botter and Rinaldo, 2003)). The injection of identical particles labeled by

2.5. Spatially-explicit model of the hydrological response

carrier and solute masses m_w, m_s at different initial locations \mathbf{x}_0 at time t_0 produces, at time $t > t_0$, the sampling of different trajectories $\mathbf{X}(t)$ but yields roughly the same temporal evolution of the mass of solute transported $m_s(t-t_0, t_0)$, which thus depends (for a given injection time t_0) solely on the time available for the reaction processes, $t-t_0$. The expected value of the volumetric concentration $\langle c_s(\mathbf{x}, t) \rangle$ (solute mass for unit transport volume) is then given, from Eq. (3), by the relation (Rinaldo and Rodriguez-Iturbe, 1996):

$$\langle c_s(\mathbf{x}, t; t_0) \rangle = m_s(t-t_0, t_0) g(\mathbf{x}, t-t_0) \quad (2.22)$$

where the similarity of structure with respect to passive transport stems from the fact that m_s is unaffected by ensemble averaging. Thus a generalization of Taylor's theorem for reactive transport problems is defined (Rinaldo and Marani, 1987). The displacement distribution g defines the structure of the carrier residence time distribution within the control volume and thus epitomizes the complex chain of events determining the hydrologic flow. The mass function $m_s(t-t_0, t_0)$ accounts for all sorption/desorption processes which determine the temporal variability of the solute mass transported by the moving water particles.

The solute mass instantaneously stored in the water carrier within the transport volume \mathcal{V} (as a result of a solute injection occurring at $t=t_0$) may be thus expressed by the usage of Eq. (2.22) as:

$$\begin{aligned} M_s(t) &= \int_{\mathcal{V}} \langle c_s(\mathbf{x}, t; t_0) \rangle d\mathbf{x} \\ &= m_s(t-t_0, t_0) P(T \geq t-t_0) \end{aligned} \quad (2.23)$$

where $P(T \geq t)$ is the probability that the residence time is larger than the current time t . Thus, deriving Eq. (2.23) with respect to t , one has:

$$\frac{dM_s(t)}{dt} = -m_s(t-t_0, t_0) f(t-t_0) + \frac{dm_s}{dt} P(T \geq t-t_0) \quad (2.24)$$

where the last term of the right-hand side of the above equation represents the rate of solute, say R ($[M][T]^{-1}$), transferred from the immobile phase to the water carrier due to the active reaction processes. Since for $t > t_0$ by continuity one has $dM_s/dt = -Q_s + R$ (where Q_s $[M][T]^{-1}$ is the solute flux at the outlet of \mathcal{V}), by comparison with Eq. (2.24) we obtain:

$$Q_s(t; t_0) = m_s(t-t_0, t_0) f(t-t_0) \text{ for } t > t_0 \quad (2.25)$$

Equation (2.25) expresses the solute flux at the outlet due to the injection within the control volume at $t=t_0$ of an instantaneous water pulse carrying a solute mass m_s which is time-dependent owing to mass exchange processes.

One example of application deals with nonpoint source pollution. Therein, one assumes that the solutes transported by the carrier entertain mass exchange phenomena with immobile phases in contact with the water flow (e.g. soil grains, bed sediment, dead-end zones). The mass transfer between phases is therefore driven by the difference between the solute concentration sorbed in the immobile phase and the solute concentration, say C , characterizing the water particles moving along the control volume (solute mass for unit water volume) (Van Genuchten, 1981). The latter may be straightforwardly derived by use of Eqs. (2.17) and (2.22) as:

$$C(t - t_0, t_0) = \rho \frac{\langle c_s(\mathbf{x}, t; t_0) \rangle}{\langle c_w(\mathbf{x}, t; t_0) \rangle} = \rho \frac{m_s(t - t_0, t_0)}{m_w} \quad (2.26)$$

where ρ is the (constant) water density ($[M][L]^{-3}$). Notice that in Eq. (2.26) the capital letter C is employed for the solute concentration of the water particles (solute mass for unit water volume), so as to highlight the difference with respect to the volumetric concentration of solute c_s (mass for unit transport volume). Notice that at a given time t , the water particles injected into the system at the same injection time t_0 are all marked by the same resident concentration $C(t - t_0, t_0)$, independently from their trajectory. This is, of course, an important assumption which nonetheless seems applicable to most cases where rainfall is the driving factor (Botter et al., 2005; Botter and Rinaldo, 2003).

Note that it is appropriate to state clearly the mathematical analogies that stem from the relation

$$\tau = t - t_0 \quad (2.27)$$

where τ is the travel time of a single particle within the control volume after injection at time t_0 , thereby the contact time between phases, and t is chronological time. Thus, one may easily express the solute concentration of the water carrier as a function of only two of the above timescales (e.g. $C=C(\tau, t_0)$, or $C=C(\tau, t)$).

Within the above framework, solute mass transported by the water carrier, m_s , is defined by the rate of change of the scalar property $C(t - t_0, t_0)$ attached to the mobile phase. Incidentally, when the scalar is simply the density of the carrier i.e. $C(t - t_0, t_0) = \text{const} = \rho$, the above derivation reduces to the description of flowrates. In the general case, instead, the temporal variability of the function C (which retains all sorption/desorption processes determining the temporal variability of the mass transported by the moving particles) is related to the active reaction processes between the phases. For example, linear rate-limited kinetics have been assumed to drive the temporal evolution of the concentration function $C(t - t_0, t_0)$ (Rinaldo and Marani, 1987) like e.g.

$$\frac{\partial C(\tau, t_0)}{\partial \tau} = k \left(\frac{N(t)}{k_D} - C(\tau, t_0) \right) \quad (2.28)$$

2.5. Spatially-explicit model of the hydrological response

where N ($[MM^{-1}]$) is the concentration in the immobile phase (properly transformed by k_D ($[L^3M^{-1}]$), the equivalent of a partition coefficient) and k ($[T^{-1}]$) is the overall rate coefficient of the reaction kinetics between mobile and immobile phases. According to the well-mixed assumption, the concentration in the immobile phase N is assumed to solely depend on time and not on the position \mathbf{x} . The temporal evolution of the function $N(t)$ may be thus described on the basis of a global (rather than local) mass balance, applicable to each 'state' which is physically meaningful to identify. This is not the case, for instance, in the other approaches well known from the literature (Cvetkovic and Dagan, 1994).

An important indicator of the validity of the above assumptions comes from an application where the carrier flow is in steady state, which is a particular case of the above framework for constant input flowrates (Botter et al., 2005). Consider a steady-state flow through a generic heterogeneous medium and assume that the underlying Eulerian velocity field is a stationary random vectorial function $\mathbf{v}(\mathbf{x})$. The ensemble mean of the local velocity \mathbf{v} is assumed to be positive (i.e. a mean flow direction is determined) and – without loss of generality – aligned with one axis. Under the above assumptions, the transport domain may be thought of as a collection of independent and stationary streamlines, which are characterized by different residence times owing to the heterogeneity of the transport properties involved. Solute particles injected within the flow field, or released from the soil, are simultaneously advected by the carrier and affected by sorption-desorption processes with immobile phases in contact with the water flow.

In this context, a notable simplification of the transport problem may be achieved by projecting the transport equation along a single streamline and embedding all the heterogeneities of the transport properties within a single variable, the travel time τ (Cvetkovic and Dagan, 1994). If we assume that linear and reversible sorption processes occur between the mobile and the immobile phases, mass conservation yields:

$$\frac{\partial C(\tau, t)}{\partial t} + \frac{\partial C(\tau, t)}{\partial \tau} = R = k_2 N(\tau, t) - k_1 C(\tau, t) \quad (2.29)$$

and

$$\frac{\partial N(\tau, t)}{\partial t} = k_1 C(\tau, t) - k_2 N(\tau, t) \quad (2.30)$$

where C [ML^{-3}] represents the solute concentration in the mobile phase, N [ML^{-3}] is the solute concentration in the immobile phase (mass of solute per unit fluid volume), R [$ML^{-3}T^{-1}$] is the sink/source term due to chemical and/or physical reactions and k_1, k_2 [T^{-1}] are the forward and backward reaction coefficients, respectively. It is worth mentioning that τ is the time needed for a particle injected in \mathbf{x}_0 at $t=0$ (i.e. $\mathbf{X}(0)=\mathbf{x}_0$, with $\mathbf{X}(t)=(X(t), Y(t), Z(t))$ the trajectory of the particle) to reach a control plane, perpendicular to the mean flow direction, located at a distance x (measured along the mean flow direction) from the injection site

(Cvetkovic and Dagan, 1994):

$$\tau(x) = \int_0^x \frac{d\xi}{u(\xi, \eta(\xi), \zeta(\xi))} \quad (2.31)$$

The quantities η and ζ in Eq. (2.31) are the transversal displacements of the considered particle, i.e. $\eta(x)=Y(\tau(x))$ and $\zeta(x)=Z(\tau(x))$ (for a complete treatment, only sketched here, see (Cvetkovic and Dagan, 1994, 1996)). It should be noted that Eq. (2.29) is actually fully three dimensional, since the Lagrangian variable τ retains the 3D structure of the velocity field. Furthermore, in Eq. (2.29) we neglect pore-scale dispersion; in heterogeneous formations, in fact, pore scale dispersion may only affect the local values of resident concentrations but bears a negligible overall effect on global quantities, such as mass fluxes and the spatial/temporal plume moments (Dagan, 1989), particularly in the case of reactive solutes Botter et al. (see the discussion e.g. in 2005).

When considering basin scales, it has been shown that ensemble averaging over different injection points \mathbf{x}_0 embedding source areas larger than the scales characteristic of heterogeneous properties (thereby typically for particles injected by rainfall patterns) smooth out the dependence on the features of the single trajectory and that the above framework, forced to steady state, often gives negligible differences with respect to the full Lagrangian framework, and that in practice one has $N(t, \tau) \sim N(t)$ (Botter et al., 2005). This leads to the simplified formulation provided by Eq. (2.28), where the spatial gradients of immobile concentration are neglected (Botter et al., 2005).

The solute mass flux [M/T] due to an instantaneous injection of a water flux $J(t)=(m_w/\rho)\delta(t-t_0)$ ($[L]^3[T]^{-1}$) may be thus expressed by the use of Eqs. (2.25) and (2.26) as:

$$\begin{aligned} Q_s(t, t_0) &= \frac{m_w}{\rho} C(t-t_0, t_0) f(t-t_0) \\ &= J(t_0) \Delta t_0 C(t-t_0, t_0) f(t-t_0) \end{aligned} \quad (2.32)$$

where $J(t_0)\Delta t_0=m_w/\rho$ is the water volume injected in the system during the time interval Δt_0 . Equation (2.32) states the equality between the mass response function (i.e. the solute release corresponding to a unit water input) and the product between the carrier transfer function f (i.e. the travel time distribution for the water flow) and its solute concentration C .

Flowrates $[L^3/T]$ (constant m_w) and mass fluxes $[M/T]$ (variable m_s) generated by an arbitrary sequence of rainfall volumes $J(t) [L^3/T]$ (which we may treat as clean for $\tau=0$, i.e. $C(0, t_0)\equiv 0$) are thus derived, for a single transport volume, from Eqs. (2.20) and (2.32):

$$Q(t) = \int_0^t dt_0 J(t_0) f(t-t_0) [L^3/T] \quad (2.33)$$

2.5. Spatially-explicit model of the hydrological response

and

$$Q_s(t) = \int_0^t dt_0 J(t_0) C(t-t_0, t_0) f(t-t_0) \quad [M/T] \quad (2.34)$$

in the two respective cases.

It is important to notice that in the case of unsteady forcing one may also need to distinguish resident concentrations, $C(t-t_0, t_0)$, from flux concentrations, say $C^F(t)$, at the outlet of single transport volumes (thereby only a function of current time t):

$$C^F(t) = \frac{Q_s(t)}{Q(t)} \quad (2.35)$$

$C^F(t)$ being the solute concentration at the outlet resulting from the simultaneous arrival of water particles which have experienced different travel times and have come into contact with different immobile phases concentrations (Rinaldo and Marani, 1987).

In general, the determination of travel time distributions must be accomplished following an analysis of the detailed motion of water particles in space and time over a channel network. Indeed a complex catchment entails a nested structure of geomorphic states, quite different from one another, where hydrologic transport occurs. Typically one thinks of hillslopes (where solute generation within hydrologic runoff mostly occurs) and channel states (where usually routing occurs, though exchanges with hyporheic zones or riparian vegetation or biologic decays may be significant, especially if travel times therein become large). We thus need to define the collection Γ of all individual paths $\gamma \in \Gamma$ that a particle may follow up to the basin outlet. The collection of connected paths $\gamma = x_1, x_2, \dots, x_\Omega$ (where we define Ω as the closure of the catchment) consists of the set of all feasible routes to the outlet, that is $x_1 \rightarrow x_2 \rightarrow \dots \rightarrow x_\Omega$. A different notation clarifies the above geomorphic framework. If $A_i, i=1, N$ is the number of overland states whose total area covers the entire catchment (say, we neglect the actual surface of channelized patterns), and c_i defines any channel link of the catchment (N is the total number of links), all the paths are supposed to originate within hillslopes i.e. $A_i \rightarrow c_i \rightarrow \dots \rightarrow c_\Omega$, where Ω is the conventional notation for the outlet of the basin.

The above rules specify the spatial distribution of pathways available for hydrologic runoff through an arbitrary network of channel and overland regions. The travel time spent by a particle along any one of the above paths is composed by the sum of the residence times within each of the states actually composing the considered path. Nevertheless, the time T_x that a particle spends in state x ($x=A_i$ or $x=c_i$) is a random variable which can be described by probability density functions (pdf's) $f_x(t)$. Obviously, for different states x and y , T_x and T_y can have different pdf's $f_x(t) \neq f_y(t)$ and we assume that T_x and T_y are statistically independent for $x \neq y$. For a path $\gamma \in \Gamma$ defined by the collection of states $\gamma = \langle x_1, \dots, x_k \rangle$ (where, in turn, $x_1, \dots, x_k \in (A_1, \dots, A_\Omega, c_1, \dots, c_\Omega)$) we define a travel time T_γ through the path γ as:

$$T_\gamma = T_{x_1} + \dots + T_{x_k} \quad (2.36)$$

Chapter 2. MINERVE and hydrological modeling

From the statistical independence of the random variables T_{x_i} it follows that the derived distribution $f_\gamma(t)$ of the sum of the (independent) residence times T_{x_i} is the convolution of the individual pdf's:

$$f_\gamma(t) = f_{x_1} * \dots * f_{x_k} \quad (2.37)$$

where the asterisk $*$ denotes the convolution operator.

Travel time distributions $f(t)$ at the outlet of a system whose input mass is distributed over the entire domain are obtained by randomization over all possible paths (Rodriguez-Iturbe and Valdés, 1979; Gupta et al., 1980; Rodriguez-Iturbe and Rinaldo, 1997):

$$f(t) = \sum_{\gamma \in \Gamma} p(\gamma) f_\gamma(t) \quad (2.38)$$

where γ is the arbitrary path constituted of states $\langle x_1, \dots, x_k \rangle$, f_γ is the path travel time distribution as given by Eq. (2.37) and γ is the arbitrary path from source to outlet; furthermore, $p(\gamma)$ is the path probability, i.e. $\sum_{\gamma \in \Gamma} p(\gamma) = 1$, defining the relative proportion of particles in γ .

We now define (and generalize) different types of path probabilities. In the simplest case, the path probabilities may be simply defined as $p(\gamma) = A_\gamma / A$, where A_γ is the contributing area draining into the first channel state of any given path γ . In such a case $\sum_{\gamma \in \Gamma} A_\gamma = A$, where A is the total area drained by the channel network, and the path probability is solely determined by geomorphology. The above time-independent determination of the path probabilities is tantamount to assuming uniform rainfall in space, and this severely constrains the size of the catchment to be modeled, which is related to the basic scale of spatial heterogeneity of rainfall patterns.

Where rainfall patterns, say $j(\mathbf{x}, t)$, are distributed in space and time, the path probabilities would be simply dictated by the relative fraction of rainfall, i.e.

$$p(\gamma, t) = \frac{\int_{A_\gamma} j(\mathbf{x}, t) d\mathbf{x}}{\int_A j(\mathbf{x}, t) d\mathbf{x}} = \frac{J(\gamma, t)}{J(t)} \quad (2.39)$$

(where $J(\gamma, t) dt = dt \int_{A_\gamma} j(\mathbf{x}, t) d\mathbf{x}$ is the total quantity of rainfall entering the system in $(t-dt, t)$ through the path γ , and $J(t) dt$ is the total rainfall injected in the same period over the entire watershed) which enables any rainfall pattern in space and time to be routed through the catchment at each time interval. This capability is central to the innovation contained in our model, and constitutes a new and relevant extension of traditional GIUH approaches.

Whether a pattern in space and time of $j(\mathbf{x}, t)$ derives from the characters of rainfall or of runoff production will be seen elsewhere. Notice that we may derive arbitrary rainfall fields either by kriging of point rainfall measurements, or by assuming stochastic patterns derived

2.5. Spatially-explicit model of the hydrological response

from theoretical models. Hence one might derive the rainfall-weighted path probabilities in the general case by simple quadratures. A reliable operational procedure consists of isolating through suitable drainage directions on digital terrain maps a spanning set of subbasins of size considerably smaller than the macroscales of intense rainfall patterns, thereby defining spanning sets of landing areas γ where one can assume locally constant rainfall intensity $J(\gamma, t)$. This procedure is tantamount to a coarse-graining of the original rainfall patterns from the pixel size to that of a collection of thousands of them, with much improved computational efficiency at no cost of predictive loss. Moreover, any spatially distributed model of runoff production would result in distributions of input $j(\mathbf{x}, t)$ that are markedly heterogeneous in space.

Moreover, whether or not one needs to modify travel times depending on the intensity of the hydrologic events (e.g. geomorphoclimatically) depends by the modes of hydrologic transport, say when dominated by storage rather than kinematic effects, but the basic formal machinery remains unaffected. Many papers have addressed the characterization of travel times and the related hydrologic response. We will not review them here. Suffice it here to say that the description of hillslope transport is of great importance (e.g. Rinaldo et al., 1995; Botter and Rinaldo, 2003). In fact, hillslope residence times are responsible not only for key lags (and rather complex mechanisms like preferential pathways to runoff) in the overall routing, but are also important to the understanding of derived transport processes, chiefly solute generation and transport to runoff waters. The above matter, jointly with the physical problem of accurately characterizing where channels begin, still needs to be resolved satisfactorily.

In the framework previously depicted, flowrates are obtained by propagating spatially distributed, time-dependent net rainfall impulses by the use of linear invariant hydrologic responses. The basic formulation of the geomorphologic theory of the hydrologic response is thus given by the following convolution integral:

$$Q(t) = \int_0^t dt_0 J(t_0) \sum_{\gamma \in \Gamma} p(\gamma, t_0) f_\gamma(t - t_0) \quad (2.40)$$

In the occurrence of spatially uniform, time varying net rainfall intensity $J(t)$ one has

$$\begin{aligned} Q(t) &= \int_0^t dt_0 J(t_0) \sum_{\gamma \in \Gamma} p(\gamma) f_\gamma(t - t_0) \\ &= \int_0^t dt_0 J(t_0) f(t - t_0) \end{aligned} \quad (2.41)$$

because $f(t) = \sum_{\gamma \in \Gamma} p(\gamma) f_\gamma(t)$, and we recover the usual GIUH relationship (Gupta et al., 1980) which is employed in several practical cases. It should be stressed that the general formulation of Eq. (2.40) uses rainfall patterns in space and time both for determining the path probabilities $p(\gamma, t)$ and for filtering the net contribution $J(t)$.

Chapter 2. MINERVE and hydrological modeling

The convolution integrals in Eqs. (2.40) and (2.41) may be solved exactly for a number of cases (Rinaldo et al., 1991) where the dynamical parameters determining the propagation of the flood wave are assumed to be uniform. Alternatively, we may allow arbitrary variations in celerity and hydrodynamic dispersion, and thus numerical convolutions are often in order. In such cases, arbitrary travel time distributions may be used depending on the hydraulics and suitable numerical techniques (typically employing integral transforms) are used to accurately convolute in time. A strong control over the numerical machinery is obviously provided by continuity, given that $\int_0^\infty f_\gamma(\tau) d\tau \equiv 1 \quad \forall \gamma$.

We note that the key identification of the paths $\gamma \in \Gamma$ may be done directly from digital terrain maps, hence exploiting our capabilities of extracting useful geomorphic information from them and chiefly the extent of the channelized portion of the basin (see e.g. Rodriguez-Iturbe and Rinaldo, 1997).

From the results of the previous Section, solute mass discharge is given in the following form:

$$Q_s(t) = \int_0^t dt_0 J(t_0) \sum_{\gamma \in \Gamma} p(\gamma, t_0) C_\gamma(t - t_0, t_0) f_\gamma(t - t_0) \quad (2.42)$$

where C_γ is a "path" resident concentration. In the case of water flow one simply has $C_\gamma = \rho$, the density of water. In this case $Q_s(t)/\rho$ becomes a flowrate, $Q_w [L^3/T]$, and Eqs. (2.40) and (2.41) are straightforwardly recovered.

The particular formulation of a mass-response function (MRF) approach depends on the number and the arrangement of the reacting states. A (relatively) simple case is that of a path (say $\gamma = x_1 \rightarrow \dots \rightarrow x_\Omega$, where x_Ω denotes, as usual, the terminal reach of the catchment), where the state x_1 generates solute mass to the mobile phase (hence one has mobile and immobile concentrations in x_1 denoted by $C_{x_1}(t, \tau)$, $N_{x_1}(t)$), and all other states (from x_2 to x_Ω) route the transported matter without further exchanges. In this case one has in Eq. (2.42):

$$C_\gamma(t, 0) f_\gamma(t) = f_{x_1} C_{x_1}(t, 0) * f_{x_2} * \dots * f_{x_\Omega} \quad (2.43)$$

In the general case where x_1 is a "generation" state (wherein solutes are transferred from the immobile to the mobile phase) and $x_2, x_3, \dots, x_\Omega$ are reactive states where the solutes transported by the carrier may be retarded owing to chemical processes occurring with other immobile phases (e.g. bed sediment or dead zones that define chemical, biological or physical reactions), the mass response function may be expressed as:

$$C_\gamma(t, 0) f_\gamma(t) = f_{x_1} C_{x_1}(t, 0) * f_{x_2} \lambda_{x_2} * \dots * f_{x_\Omega} \lambda_{x_\Omega} \quad (2.44)$$

where λ_{x_i} ($i = 2, k$) represents the gain/loss function within each reactive state forced by a

2.5. Spatially-explicit model of the hydrological response

non-null input flux concentration of solute $C_{x_i}^{Fin}(t) \neq 0$:

$$\lambda_{x_i}(t - t_0, t_0) = \frac{C_{x_i}(t - t_0, t_0)}{C_{x_i}^{Fin}(t_0)} \quad (2.45)$$

Obviously when downstream states route the matter without sorption we have $\lambda_{x_i} \equiv 1$. The notation C_{x_i} and λ_{x_i} should not surprise, as we argued that for each state where gain/loss processes occur one needs to carry out a global mass balance to determine the instantaneous fraction of matter stored in immobile phases $N_{x_i}(t)$. We argue that Eq. (2.44) is the general form of Mass Response Function (MRF) which, in different forms that reduce to particular cases of Eq. (2.44), has been known for some time (Rinaldo and Marani, 1987).

On this basis alone one needs to weigh carefully the spatial and temporal scales relevant to a mathematical model of transport at catchment scales. All possible combinations of states generating, losing or simply routing solutes may thus be explored, thus straightforwardly extending the geomorphic theory of the hydrologic response to solute transport.

The linkage of travel times with the global, basin-scale contact times between phases controlling mass exchanges provides a quantum leap in our operational capabilities of describing large-scale transport processes. Indeed a complex catchment entails a nested structure of geomorphic states where the spatial pathways of any rain-driven particle moving through the network of channel and overland regions define the control volumes for which one needs to carry out mass balances and compute travel and lifetime distributions.

An example is now presented with the scope of clarifying the structure of spatially explicit models. The example is kept to a minimum of geomorphic and hydrologic complexity (rainfall is assumed constant in space, i.e. $p(\gamma, t) = p(\gamma)$). Figure 2.7 shows the chosen setup, composed of five source areas and five channels. Overall, the topological order is $\Omega = 2$.

The complete set Γ of paths to the outlet (see Fig. 2.7) is the following:

$$A_1 \rightarrow c_1 \rightarrow c_3 \rightarrow c_5$$

$$A_2 \rightarrow c_2 \rightarrow c_3 \rightarrow c_5$$

$$A_3 \rightarrow c_3 \rightarrow c_5$$

$$A_4 \rightarrow c_4 \rightarrow c_5$$

$$A_5 \rightarrow c_5$$

The states where paths originate are labeled by an area A_i , so that the total catchment area A obeys the relation $A = A_1 + \dots + A_5$ and path probabilities are defined by $p(1) = A_1/A$; ...; $p(5) = A_5/A$, thereby assuming that the rainfall is spatially uniform – this is tantamount to assuming that the watershed width is smaller than the correlation scale of rainfall events.

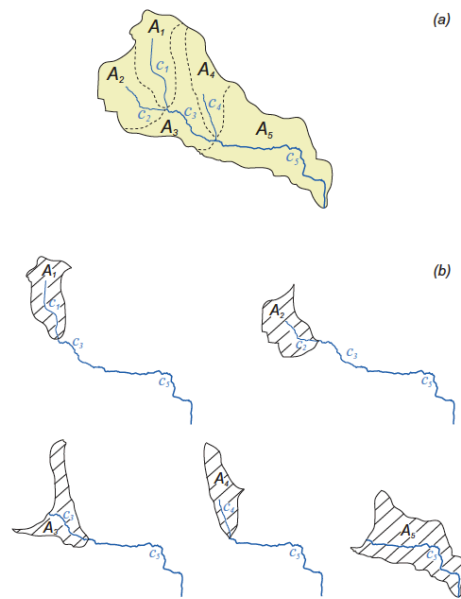


Figure 2.7: a) Parallel transport. Sample of a relatively simple geomorphological structure of a river basin and notation for the theoretical models. The basic elements of the MRF approach for basin scale solute transport are provided. Notice that the set Γ of all possible paths to the outlet defined by the geomorphic structure is made up by 10 states, five overland states and five channels (e.g. transitions to overland areas A_i to their outlet channel c_i and then to ensuing transitions ($c_i \rightarrow c_k \rightarrow \dots \rightarrow c_5$) towards the closure – the endpoint of the channel c_5). Notice the treatment of the i -th source area A_i as a well-mixed reactor. Here we assume that all sources areas A_1 to A_5 act as generators of solutes to the mobile phase, which emphasizes their independent roles; b) The set of independent paths available for hydrologic runoff is enumerated and shown (Rinaldo et al., 2006a).

2.5. Spatially-explicit model of the hydrological response

Under the circumstances shown in Fig. 2.7, Eqs. (2.38) and (2.43) apply with:

$$f(t) = \frac{A_1}{A} f_{A_1} * f_{c_1} * f_{c_3} * f_{c_5} +$$

$$\frac{A_2}{A} f_{A_2} * f_{c_2} * f_{c_3} * f_{c_5} + \frac{A_3}{A} f_{A_3} * f_{c_3} * f_{c_5} +$$

$$+ \frac{A_4}{A} f_{A_4} * f_{c_4} * f_{c_5} + \frac{A_5}{A} f_{A_5} * f_{c_5}$$

where we have neglected for the sake of simplicity the probability for a particle to land directly on a channel state).

Note that the transition $A_i \rightarrow c_i$ (i.e. hillslope to channel) entails a subtle issue. In fact, here it is assumed to describe the overall travel time distribution by a convolution of $f_{A_i}(t)$ and $f_{c_i}(t)$, where $f_{A_i}(t)$ is the hillslope travel time distribution, regardless of the point where the channel is reached, and $f_{c_i}(t)$ is the travel time distribution computed for the total length of the channel. In reality one should take into account the actual distribution of injections along the entire channel reach, rather than a fictitious headwater injection. The issue of the equivalence of the results has been studied (Rinaldo and Rodriguez-Iturbe, 1996).

Figure 2.8a shows the individual and compounded travel time distributions for the path γ_1 defined by the transitions: $A_1 \rightarrow c_1 \rightarrow c_3 \rightarrow c_5$. Also shown (Fig. 2.8b) is a comparison of the path, $f_\gamma(t)$, and the basin, $f(t)$, travel time distributions needed for the general definition of fluxes. The comparison shows the obvious blending of different arrivals that reflect the geomorphological complexity of the pathways to the outlet.

Mass response functions are easily determined when parallel generation states occur. If we assume that every hillslope A_i acts as a generator of solute matter to runoff (a usual assumption in nonpoint source pollution studies), we have, for the water pulse injected at $t_0=0$ (i.e. $\tau=t$):

$$\sum_{\gamma} p(\gamma) C_{\gamma}(t, 0) f_{\gamma}(t) = \frac{A_1}{A} f_{A_1} C_{A_1}(t, 0) * f_{c_1} * f_{c_3} * f_{c_5} +$$

$$+ \frac{A_2}{A} f_{A_2} C_{A_2}(t, 0) * f_{c_2} * f_{c_3} * f_{c_5} + \frac{A_3}{A} f_{A_3} C_{A_3}(t, 0) * f_{c_3} * f_{c_5}$$

$$+ \frac{A_4}{A} f_{A_4} C_{A_4}(t, 0) * f_{c_4} * f_{c_5} + \frac{A_5}{A} f_{A_5} C_{A_5}(t, 0) * f_{c_5}$$

which defines the mass-response function for the basin shown in Fig. 2.7. Note that for a unit pulse of rainfall one has $Q_s(t) = \sum_{\gamma} p(\gamma) C_{\gamma}(t, 0) f_{\gamma}(t)$ and the flux concentration is $C^F(t) = Q_s / Q_w$, while for compounded inputs of rainfall $J(t)$ one has to solve Eq. (2.42). Examples involving serial and parallel transport of passive or reactive solutes are elsewhere (Rinaldo et al., 2006b). Every possible combination is thus tackled, and a suitable extension of the geomorphic theory of the hydrologic response to transport at basin scales is therefore

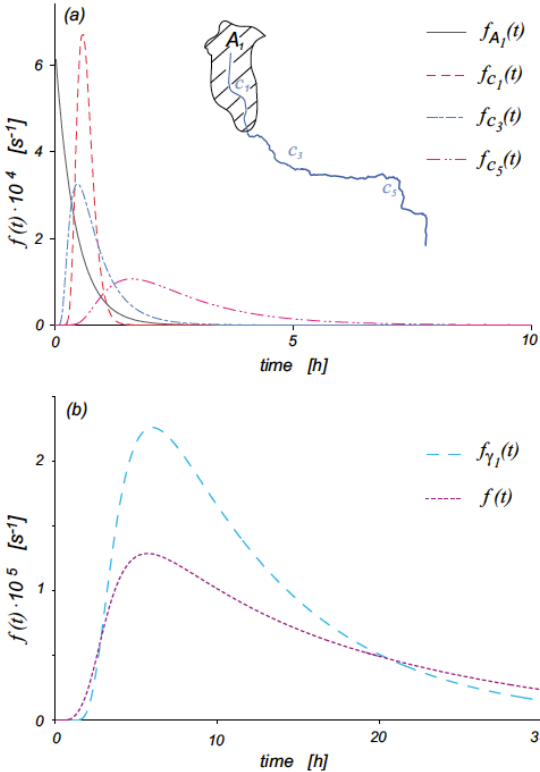


Figure 2.8: a) Individual travel time distributions along the path $A_1 \rightarrow \dots \rightarrow c_5$; b) Travel time distributions $f_{\gamma_1}(t)$ obtained by convolution of the individual pdfs, and catchment travel time distributions $f(t)$ (Rinaldo et al., 2006a).

2.5. Spatially-explicit model of the hydrological response

achieved.

In the context of the present thesis, the spatially-explicit model of the hydrologic response based on the formulation of transport by travel time distributions (Rodriguez-Iturbe and Valdés, 1979; Gupta et al., 1980; Rodriguez-Iturbe and Rinaldo, 1997) relies on catchment partitioning into a series of source areas according to the TAUDEM method mentioned previously in Section 2.2.1 (Tarboton, 1997). Source areas are delineated based on elevation, aspect and slope information in order to preserve relatively homogeneous hydrological conditions per area.

Runoff partitioning of the equivalent precipitation is performed via a minimalist approach that describes the dynamics of soil moisture at the source catchment scale (Laio et al., 2001; Rodriguez-Iturbe and Porporato, 2004; Rodriguez-Iturbe et al., 2001). Infiltrated water can either be transpired by vegetation, percolate towards deeper layers or exfiltrate towards the channel, producing with the latter mechanism the main contribution to hydrologic response at the event time-scale. Actual evapotranspiration fluxes at the subcatchment scale are assumed to be null for moisture levels below wilting point, increasing linearly with soil moisture until potential evapotranspiration is reached at 65 % of the field capacity. Potential evapotranspiration is evaluated with the Priestley-Taylor method (Maidment, 1993; Priestley and Taylor, 1972). The amount of mobilized water that travels toward the channel is modeled as a linear function of the soil moisture. Thus, the water balance for the soil depth can be written as:

$$\eta Z_r \frac{ds(t)}{dt} = F_I(t) - E(s(t)) - L(s(t)) \quad (2.46)$$

where η represents soil porosity (-), Z_r is the depth of the active soil layer during water redistribution processes (mm) and F_I is the infiltration flux (m s^{-1}). E and L represent the rate of evapotranspiration and mobilized water respectively and are functions of the catchment averaged soil moisture s (m s^{-1}).

Soil depth in the model is considered homogeneous for the source area. For the case study region (i.e., a subset of the Dranse catchment described in Chapter 5 of this thesis), preliminary results showed that including spatially variable soil depths in the model does not improve the hydrological model performance; this has several reasons: there is a limited range of soil depths in this region (generally between 0 for exposed rocks and about 20-30 cm for steep slopes), other factors of spatial variability dominate over soil depth heterogeneity (e.g., steep, complex topography) and the fact that, as in any conceptual model, the different model parameters can compensate for each other during model calibration (Nicótina et al., 2011). In general, this assumption would not fit other regions with more variable soil depths.

The rate of mobilized water in the soil moisture store is given by:

$$L(s(t)) = K_h s(t) \quad (2.47)$$

Chapter 2. MINERVE and hydrological modeling

where K_h is the hydraulic conductivity (mm h^{-1}). The soil reservoir is fed by the mobilized water L . Subsurface discharge from this reservoir as well as from the surface flow is defined by a linear relation with a residence time specific to the type of flow $K_{sb/sr}$:

$$Q(t)_{sb/sr} = K_{sb/sr} S_{sb/sr}(t) \quad (2.48)$$

where the subscript sb/sr refers respectively to subsurface or surface flows from the storage S .

The total discharge is obtained by convolution of each of the flows (subsurface, surface) from all subcatchments with a travel time distribution, which is obtained as follows:

1. For each source area A_γ , all possible flow paths to the outlet are identified. Given the tree-like structure of river networks, for any source area A_γ the transitions states are uniquely identified (Gupta et al., 1980; Rinaldo et al., 1991);
2. The probability of water entering the flowpath γ is defined proportionally to the relative rate of instantaneous inflow (Rinaldo et al., 2006a), whether by rain or melt;
3. A travel-time distribution for each flow path is determined through nested convolutions of the transition states' probability density functions (pdfs) (Rinaldo et al., 1991) under the general assumption of stationarity of the pdf (Botter et al., 2010; Rinaldo et al., 2011) which seems reasonably representative of snowmelt-dominated responses typical of the Visp and Dranse catchments. Unchanneled pathways are assumed to hold an exponential distribution in analogy with the geomorphic distribution of unchanneled lengths (Botter and Rinaldo, 2003), while open channel flow in mountain streams is assumed to be reasonably described by the parabolic model implying an inverse Gaussian distribution (Rinaldo et al., 1991, 2006a; Rodriguez-Iturbe and Rinaldo, 1997).

Mathematically, this translates into the following equations (see Nicótina et al., 2008, for more detail). The set of all possible paths leading to the outlet Γ reflects the spatial structure of the input forcing fields (i.e., the equivalent rainfall and/or snowmelt). This is tantamount to choosing a set of source areas A_γ constrained by continuity i.e. $\sum_{\gamma \in \Gamma} A_\gamma = A$ where A is the catchment area. The travel time distribution for the entire catchment, say $f(t)$, in Equation 2.49 (Gupta et al., 1980; Rinaldo et al., 1991) is given by:

$$f(t) = \sum_{\gamma \in \Gamma} p(\gamma, t) f_\gamma(t) \quad (2.49)$$

where: p_γ is the path probability; and $f_\gamma(t)$ is the probability density function of travel times (assumed statistically independent) in either hillslope or channel states, suitably convolved along any arbitrary path γ from source to outlet. As an example, if the path γ is made up by

transitions from the source area A_γ to downstream collecting channels $c_j \rightarrow c_k \rightarrow \dots \rightarrow c_\Omega$ (where Ω is the closure of the catchment), the related travel time distribution is:

$$f_\gamma(t) = f_{A_\gamma} * f_{c_j} * f_{c_k} * \dots * f_\Omega(t) \quad (2.50)$$

(where $*$ is the convolution operator) under the reasonable assumption of statistical independence of travel times in different states.

Path probabilities, $p(\gamma, t)$ define the relative proportion of particles injected into a particular path. They are defined by the spatial distribution of equivalent precipitation over the catchment according to the relation (Rinaldo et al., 2006a):

$$p(\gamma, t) = \frac{J(\gamma, t)}{J(t)}; \quad (2.51)$$

where $J(\gamma, t)$ is the total flux injected through path γ at time t (say, in $(t, t + \Delta t)$ where Δt is the time step) and $J(t)$ is the total instantaneous flux over the entire catchment. In practice, one discretizes time into intervals Δt as suited to the problem at hand, and computes the total inflow from snowmelt or rain, and those within each source area. Their relative proportions define the instantaneous path probabilities.

Flow rates at the basin outlet are evaluated by time convolution of the input flux (equivalent precipitation or snowmelt) with the residence time distribution related to the respective path, weighted by the respective path probabilities for the net forcing $J(\gamma, t)$:

$$Q(t) = \sum_{\gamma \in \Gamma} \int_0^t J(\gamma, \tau) f_\gamma(t - \tau) d\tau \quad (2.52)$$

Based on comparison with a measured discharge series containing a strong, snowmelt signal, the basin discharge, calculated in this manner, is used to validate the snowmelt methods in Chapter 5 of this thesis.

2.6 Conclusions

The RSII and spatially-explicit hydrological models as well as the measured and COSMO reanalysis inputs provide a means to confirm the suitability of the input and process improvements for the MINERVE operational flood forecasting model. This is accomplished in the subsequent chapters of this thesis as follows: In Chapter 3, both the measured and COSMO inputs along with the RSII hydrological model are used to test interpolation methods in terms of generating reliable, spatially distributed modeling inputs. In Chapter 4, using COSMO output as input, the RSII model tests an approach to re-define the snowfall limit. Chapter 5 of this thesis uses

Chapter 2. MINERVE and hydrological modeling

the spatially-explicit hydrological model described in Section 2.5 as an integrator to assess the performances of snowmelt models in terms of catchment-scale hydrology. By testing these methods in RSII or in the spatially-explicit model, input and process error is demonstrated to be reduced in the MINERVE model with the uncertainty analysis technique developed in Chapter 6.

Improved interpolation of meteorological forcings

Geostatistics is [...] used to model the uncertainty of unknown values through the generation of alternative images (realizations) that all honor the data and reproduce aspects of the patterns of spatial dependence [...].

Pierre Goovaerts, Author 'Geostatistics for Natural Resources Evaluation'

3.1 Introduction

To optimize water resources management for flood forecasting and hydropower operation purposes, it is crucial to have accurate estimates of meteorological forcings in space and time, particularly in Alpine terrain. However, within complex topography the characteristic spatial scales of hydrological forcings are typically, poorly captured even with a relatively dense network of measurements (Frei and Schär, 1998; Griffiths and McSaveny, 1983; Katzfey, 1995; Wratt et al., 2000, 1996). Moreover, topography impacts rainfall and snowfall patterns through the so-called orographic and shadowing effects as described in Chapter 1 of this thesis Section 1.1.1.

Due to orographic effects and weather patterns, there is on-going research as to whether precipitation, in general, increases with elevation. For instance, precipitation accumulation trends can show considerable scatter with altitude depending on the region's exposure to wind and synoptic situations (Sevruk, 1997). Also, unreliable data in complex terrain at high

Chapter 3. Improved interpolation of meteorological forcings

altitudes has also led to estimate biases as large as 25% where snow accumulates (Groisman and Legates, 1994). Furthermore, depending upon the predominant wind direction, rain shadows can be created when more precipitation is deposited at or near the crest and much less precipitation is deposited at lower elevations (Sinclair et al., 1997).

In the particular case of the European Alps, an analysis of long-term rainfall records demonstrated that maximum precipitation rates are observed on both the upper southern and northern faces (Frei and Schär, 1998). Regression analyses of corrected annual precipitation versus altitude in the Swiss Alps have also shown that in the upper reaches of the Rhone River valley (i.e., the Valais), between 90 and 100% of precipitation variability is explained by altitude with greater precipitation rates found at higher elevations (Sevruk, 1997). Furthermore, a climatological study (Attinger and Fallot, 2003) indicated that since 1975 over half of meteorological situations which have produced more than 100 mm/day of precipitation over three days in the upper Valais have originated in the south; these southerly events have deposited abundant precipitation on the upper windward and leeward sides of mountains. With southerly storms, precipitation in the Valais shows significant patterns on leeward sides where precipitation is effectively funneled into lower elevation areas due to shielding patterns created by adjacent high elevation mountains (e.g., the Matterhorn at 4500 m) (Petrascheck and Hegg, 2002).

In spite of a long-term knowledge on regional weather and precipitation accumulation patterns in the Swiss Alps, a non-exhaustive sampling of rainfall with few gauges located at high altitudes is unable to effectively capture short-term, catchment-scale, orographic effects during flood events (when the steep slopes and relatively shallow groundwater depths typical of Alpine areas generate short response times) (Petrascheck, 1996). A sparse rain gauge network at upper elevations necessitates a proper quantification of the local precipitation-elevation relationship using an extended description of topography (Frei and Schär, 1998). Moreover, the inability of correctly reproducing areal rainfall leads to notable failures of the ensuing models of the hydrologic response, which are sensitive to input volumes at the catchment scale (Nicótina et al., 2008). At reduced subcatchment scales, rainfall variability also has an important impact on peak flows (Mandapaka et al., 2009). Furthermore, a limited number of temperature stations in the region does not allow proper definitions of snow/rainfall partitioning during flood events. Accurate temperature fields are particularly important in mountainous regions because the combination of high temperatures producing snow/glacial melt or rain-on-snow processes can accelerate discharge production (Benestad and Haugen, 2007; Jasper et al., 2002; Sui and Koehler, 2001).

Several interpolation methods have been used in literature to reproduce the spatial distribution of temperature and rainfall fields based on sparse ground measurements (Goovaerts, 2000; Daly, 2006). Non-geostatistical techniques including IDW, splines and linear regression have been tested in numerous studies (e.g., Hancock and Hutchinson, 2006; Kurtzman and Kadmon, 1999). Although IDW is a relatively simple deterministic interpolation method which provides adaptable weights for sensible local interpolations, the choice of the weighting func-

tion is arbitrary and no measure of error is provided (Webster and Oliver, 2001). Particularly important to this study, IDW cannot explicitly account for climatic forcing particularly when elevation extrapolation is needed (Daly, 2006). Furthermore, single regression functions do not accurately represent spatially varying meteorological variables across large regions (Daly, 2006) and multiple regression models can become complicated and tend to over-extrapolate (Kurtzman and Kadmon, 1999).

To overcome such limitations, more studies are testing geostatistical tools to interpolate both rainfall and temperature data (Hudson and Wackernagel, 1994; Kravchenko, 1996; Dubois, 1997; Prudhomme and Reed, 1999; Goovaerts, 2000; Buytaert et al., 2006; Skoien and Bloschl, 2008). In the Swiss topographic context, previous studies have compared various precipitation interpolation schemes on a daily scale (e.g., kriging, splines, neural networks) (Dubois, 1997). With specific reference to flood events, KED with rainfall data and radar as an external drift factor has proven successful in interpolating hourly precipitation during a 2002 flood in Germany with improved rainfall predictions compared to IDW, Thiessen polygons, nearest neighbor, ordinary and indicator kriging estimations (Haberlandt, 2007). KED with radar was also successful in improving precipitation interpolations when automatically computing 2-D spatial correlograms for short term rainfall events (Velasco-Forero et al., 2008).

In this chapter, comparative analyses of various interpolators are addressed to test whether there exists a suitable procedure for interpolating hourly point measurements in the Valais region of the Swiss Alps which effectively captures orographic effects and accurately reproduces time-varying temperature lapse rates during flood events. With specific reference to the prediction of floods, emphasis is given on properly estimating total instantaneous volumes of rainfall on a catchment scale regardless of the rainfall-runoff tool employed. In specific catchments of this region, poor predictions with a hydrological model implementing IDW have resulted in gross underestimations of runoff volumes (Jordan et al., 2008). Unlike other kriging studies which have incorporated radar data (Krajewski, 1987; Haberlandt, 2007; Velasco-Forero et al., 2008; Sangati et al., 2009), this region cannot use radar estimates because the Valais mountains effectively block the radar beam at lower elevation angles (Germann et al., 2006) and only precipitation above the mountains can be seen by the radars. Due to the vertical variability of precipitation, this can lead to significant discrepancies with precipitation at ground level (Joss et al., 1997; Berne et al., 2004; Garcia Hernández et al., 2009b). As a consequence, the aim of this study is to establish suitable and utilitarian procedures for improved prediction of catchment-scale precipitation volumes and temperature distributions to improve hydrological model performance with limited data available. Compared to previous studies, three major aspects characterize the novelty of this work: i) the comparison of time-varying and constant temperature lapse rates on an hourly scale for flood analysis in complex Alpine terrain; ii) the use of digital elevation data as well as numerical weather forecasts as sources of external information for KED; and iii) the hydrologically-oriented evaluation of the results in terms of their impact on the predictive capability of the RSII model.

3.2 Materials and methods

3.2.1 Study region and data

The analyses described herein refer to the Visp and Dranse catchments in the Valais region of Switzerland described in Chapter 2 Section 2.2. These catchments, the DTM, and the meteorological stations used in this analysis are depicted in Figure 3.1.

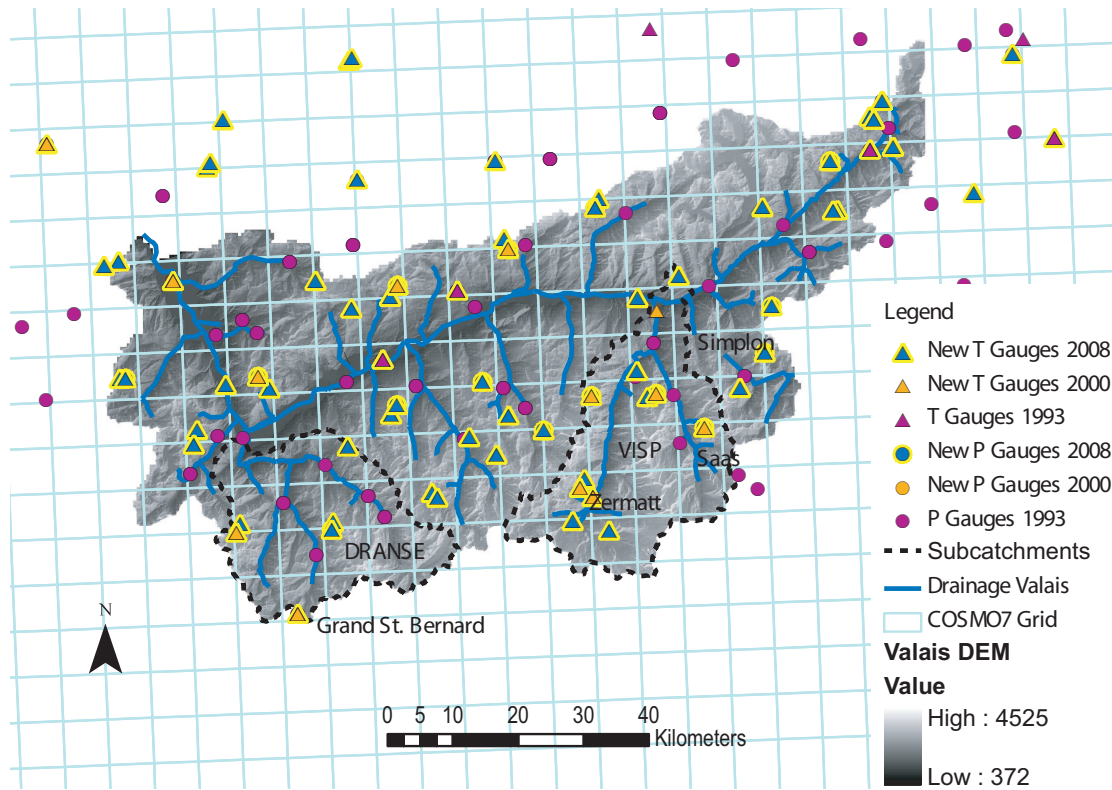


Figure 3.1: Map of Valais region indicating catchment delineations and locations of all temperature (T) and precipitation (P) gauges used. 'New gauges' refers to the additional gauges built after 1993. A background shaded DTM (elevation indicated by the grey-scale color bar) and the river network are also indicated. Source: (MeteoSwiss). The COSMO7 grid is also shown. Source: (COSMO, 2011).

Floods in the Valais are typically associated with storm patterns which originate from the south that are caused by a depression over central Europe (Roe, 2005). Prevailing wind directions during storms were evaluated through radio sounding data taken at 500 hPa from the stations in Payerne, Switzerland and Milan, Italy (DAS, 2009). These stations are situated to the west and to the southeast of the study region respectively. Two extreme flood events in the Valais are analyzed in this Chapter: 23 - 26 September 1993 (72 h); and 13 - 16 October 2000 (72 h); in addition to the most recent flood event, 24 May - 1 June 2008 (192 h). Measured discharges for these three flood events in the Visp are shown in Figure 3.2. Hourly precipitation and temperature records over the Valais collected by MeteoSwiss and WSL (the Swiss Federal

Table 3.1: Minimum, maximum and mean precipitation (mm/hr) and temperature (°C) statistics during the 1993, 2000, and 2008 flood events in the Valais.

Precipitation Statistics (mm h ⁻¹)			
	1993	2000	2008
Minimum	0.0	0.0	0.0
Maximum	50.0	29.3	21.2
Mean	1.4	1.9	1.1
Temperature Statistics °C			
	1993	2000	2008
Minimum	2	-3	-5
Maximum	26	19	24
Mean	12	5	6

Institute for Forest, Snow and Landscape Research) were used in this analysis after initial filtering of outliers (Figure 3.1). As an example, mean time series of measured rainfall rates and temperature from all station data within the Valais are shown in Figures 3.3a) and 3.3c) for the 1993 storm. Precipitation and temperature statistics for all events across the Valais are summarized in Table 3.1.

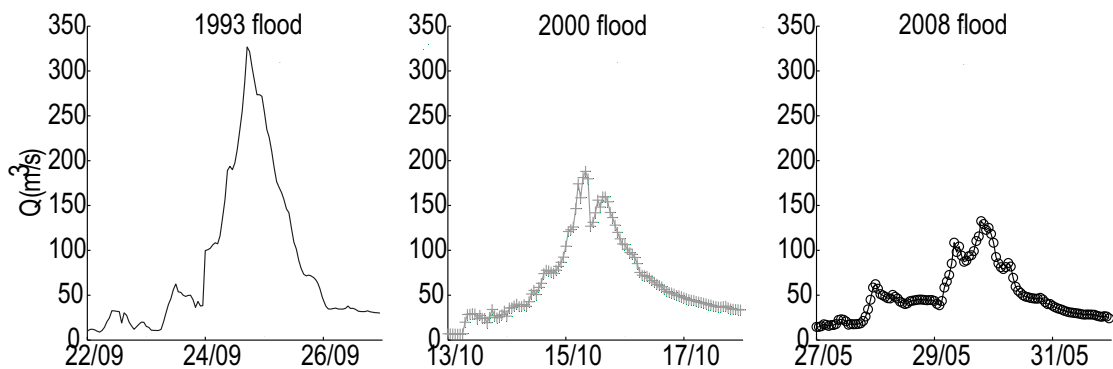


Figure 3.2: Measured discharge at the outlet of the Visp catchment during the three case study flood events. Source: (FOEN, 2008)

Numerical weather forecast reanalysis data from COSMO7 are used as an additional information source. The COSMO7 model is described in detail in Chapter 2 Section 2.3.2 of this thesis.

Composite COSMO7 data sets for this analysis were constructed by using the first 12 hours of each forecast after a six hour initialization period. The integration of the COSMO7 grid with the more detailed topography (upscaled to 500 m × 500 m resolution for computational needs) was performed according to procedures defined by MeteoSwiss (Kaufmann, 2008). Figures 3.3b) and 3.3c) show the histogram of COSMO7 mean rainfall rates and mean COSMO7 temperature over the Valais for the 1993 event respectively. The COSMO7 temperature profile

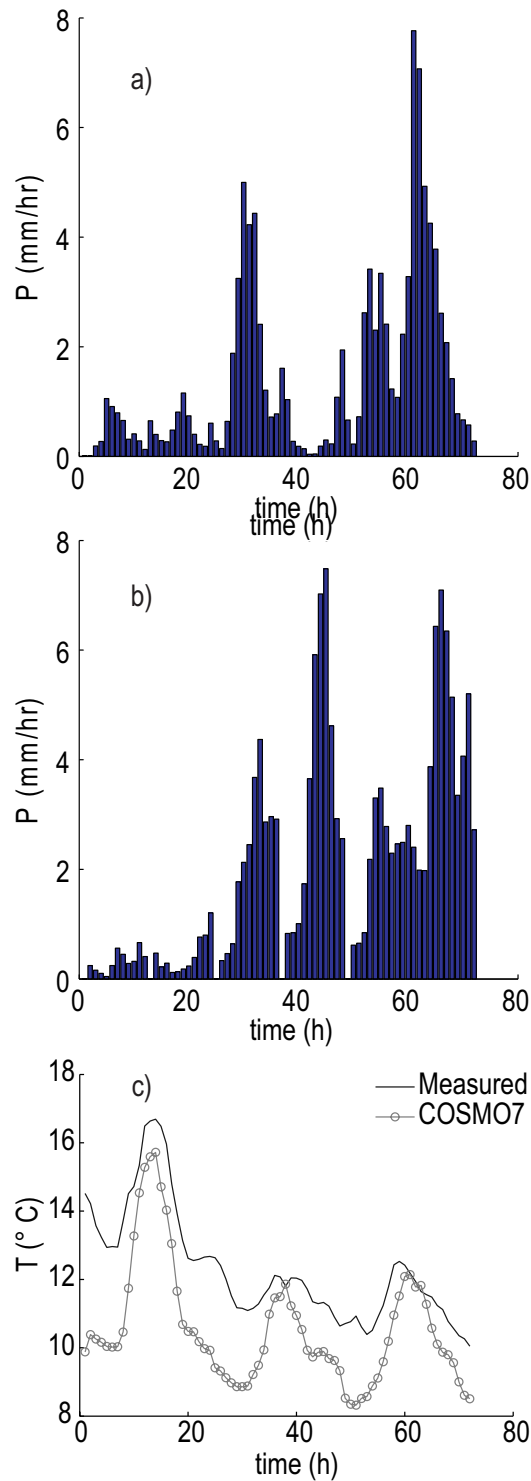


Figure 3.3: Mean precipitation or temperature across the Valais: a) 1993 mean measured precipitation intensity, b) 1993 mean precipitation intensity forecasted by COSMO7, c) 1993 mean measured and COSMO7 forecasted temperatures. Differences in temperatures are due to the fact that the average elevation of the COSMO7 grid points is located 400 m above the average measurement station elevation. Sources: COSMO2011, MeteoSwiss

differs from the measured by approximately 2 °C because the average elevation of the COSMO7 grid points of the virtual terrain which correspond to the temperature gauges is 400 m above the station elevations.

3.2.2 Spatial interpolation methods

The interpolation methods analyzed herein include Shepard's Inverse Distance Weighting (IDW), Ordinary Kriging (OK) and Kriging with External Drift (KED). IDW is a deterministic method which estimates the interpolated values by a weighted mean of the data where the weights are inversely proportional to the distance to a power (typically squared) between the interpolated value and each data point (Isaaks and Srivastava, 1989). In contrast, kriging methods consist of a family of least-square linear regression algorithms used to estimate a random field from which measured data are considered to be drawn as a sampling of a field realization (Goovaerts, 1997). Numerous versions of kriging exist which vary in the assumptions that define their relative system of equations (e.g. simple, ordinary, universal). All kriging methods represent optimal linear statistical estimators in that they are unbiased and minimize error variances (Goovaerts, 1997; Isaaks and Srivastava, 1989).

OK accounts for local fluctuations of the mean value of the random field at hand over a suitably defined moving window by assuming stationarity in each search neighborhood (Cressie, 1988). KED, on the other hand, performs the prediction of sparse variables or variables poorly correlated in space by considering that there is a local trend within the neighborhood; primary data is assumed to have a linear relation with the auxiliary information exhaustively sampled over the Valais (Ahmed and de Marsily, 1987; Goovaerts, 1997).

Also, particular to this analysis, kriging computations rely on an unbiased (i.e. free of systematic error) and robust (i.e. the estimator is stable with respect to the number of data points used for the analysis) semivariogram estimator to determine the spatial correlation structure of the forcing field (Li and Lake, 1994). This estimator has been proven to outperform other semivariogram estimators (e.g. Matheron's semivariogram (Matheron, 1970) and Cressie's estimator (Cressie, 1984)) and to be resistant to outliers and contaminated data (Li and Lake, 1994).

(Li and Lake, 1994) define their moving window semivariogram estimator as:

$$\gamma_{N2}(h) = \gamma_{N1}(h) + \frac{h}{d} \gamma'_{N1}(h) \quad (3.1)$$

where h is the lag distance, d is the dimension in Euclidean space and $\gamma'_{N1}(h)$ is the derivative of $\gamma_{N1}(h)$ with respect to h . Here the derivative is approximated with a forward difference method, although the choice of the numerical differentiation scheme is largely immaterial.

$\gamma_{N1}(h)$ is defined as:

$$\gamma_{N1}(h) = \frac{1}{n} \sum_{i=1}^n \frac{1}{2m} \sum_{j \in D_{i,h}} [Z(x_i) - Z(x_j)]^2 \quad (3.2)$$

where the first sum is extended over the number of data values in the entire field n . The second sum is extended over the set of data values $D_{i,h}$ in a moving window of size h centered at point i where m is the number of data values in $D_{i,h}$ including the points j and i located inside the window.

Figure 3.4 shows a comparison between the Matheron, Cressie and Li-Lake variograms. All estimators are unbiased whereas only the Cressie and Li-Lake variograms are considered robust. This plot shows that the main advantage of the new semivariogram estimator lies in its proven stability at higher lag distances compared to the other estimators. This is due to the fact that the new estimator uses the whole data set at every lag distance, providing in this way more robust statistics (Li and Lake, 1994). It has been noted however that the second term on the right-hand side of Eq. 3.1 introduces, for short lag-distances, a departure of the Li-Lake semivariogram estimator from the Matheron estimator. This departure is likely to be a consequence of the precision of the numerical derivative and further analyses will be needed to clarify this issue that remains behind the scope of the present paper. Suffice it here to notice that given the sparsity of the data points, semivariogram identification would not be possible if the variogram evaluation was performed with the Matheron estimator. The robustness and resilience properties allows the estimator to perform better in the presence of limited and irregularly distributed data points, which is the present case within the Valais region of the Swiss Alps.

The relatively invariant spatial structure of the sampled rainfall and temperature fields throughout the storm events at hand allows the use of the storm-averaged semivariogram to properly characterize spatial correlations (Haberlandt, 2007). All precipitation values are considered for variogram inference and kriging. Considering that only flood cases are analyzed in this study, areas without rain or with intermittent rainfall are very limited so that precipitation probability distributions are less positively skewed than those which can be obtained during less intense rainfall events.

3.2.3 Hydrological model

Hydrological computations are based on the RSII model described in Chapter 2 Section 2.4 of this thesis.

3.2.4 Interpolation details

Preliminary linear regression analyses showed a clear linear trend between elevation and precipitation in catchments as previously indicated by (Sevruk, 1997) and an even more

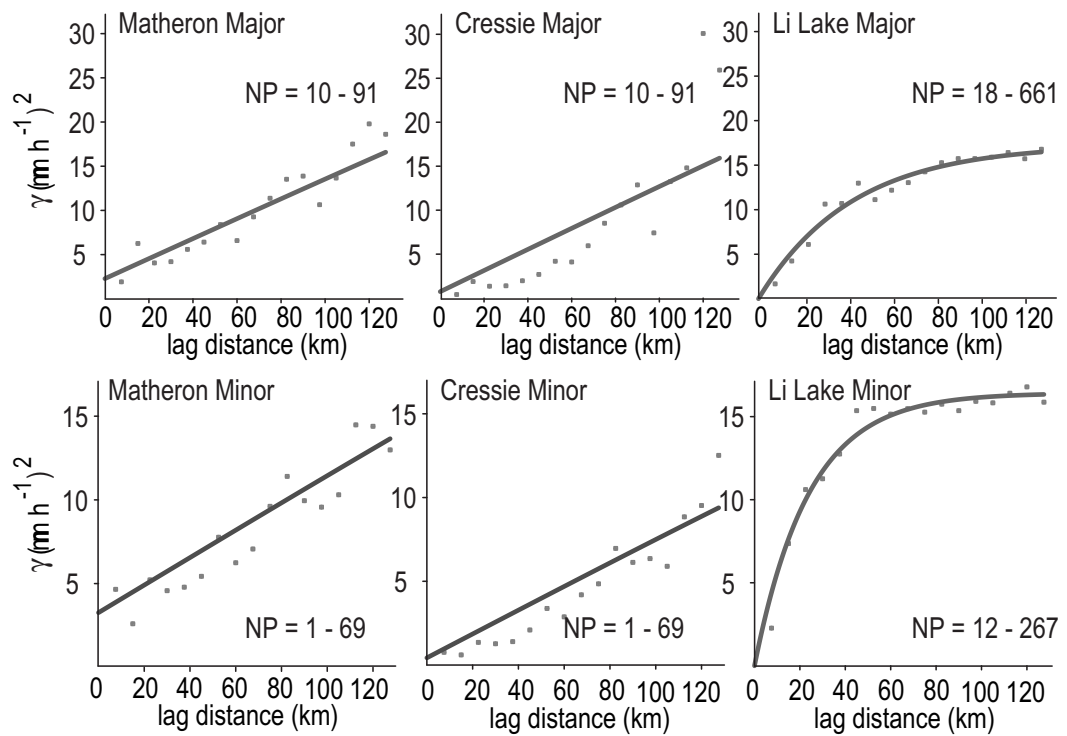


Figure 3.4: Comparison of variogram estimators for the 1993 flood event: Matheron versus Cressie and Li and Lake. Major (top) and minor (bottom) anisotropic variograms are shown along with the number of points pairs used in each estimate.

Chapter 3. Improved interpolation of meteorological forcings

apparent linear trend between elevation and temperature. Given the random field $Z(\mathbf{x})$ (hourly precipitation or temperature in the application at hand), with \mathbf{x} the vector representing the position in the 2D plane, the expectation (E) of the random variable is:

$$E[Z(\mathbf{x})] = \mathbf{a} + \mathbf{bS}(\mathbf{x}) \quad (3.3)$$

where $S(\mathbf{x})$ represents the local elevation at location \mathbf{x} . The residuals of this relation at the measurement stations are used to define the semivariograms in KED. Similar preliminary linear regression analyses showed that temperature measurements were found to be strongly correlated with the closest COSMO7 grid point at an hourly time step. In contrast, for precipitation, measurements and COSMO7 reanalyses showed the strongest linear correlation with cumulative data over the event. Thus, precipitation interpolation uses event averaged linear drift whereas hourly COSMO7 reanalyses are used as the external drift factor for temperature interpolations.

Interpolation computations and post-processing are conducted on a 500 m \times 500 m resolution grid with an hourly time-step using the R GSTAT geostatistical software (Pebesma, 2004). In all interpolation methods, the measurement errors at the meteorological stations are assumed to be negligible. This assumption does not consider that wind at high altitude regions greatly decreases the accuracy of snow accumulation in rain gauges. Sevruk (1985) has made estimates of the mean annual bias for rain-gauges in Switzerland. By such estimate, a systematic undercatch of 10% in the summer is common for rain gauges in Switzerland in wind-exposed sites, especially at high elevations. Correction of gauge measurements for systematic snowfall undercatch has not been performed and is beyond the scope of our analysis.

Interpolated fields are provided as inputs to the hydrological model by assigning to each subcatchment (within a proper size range) the precipitation time series estimated at its centroid. The temperature time series at the median of the elevation bands derived with KED are assigned to each elevation band within a subcatchment. In contrast, for temperature interpolations with OK and IDW, time-varying lapse rates are estimated from station data through linear regression. Hourly temperature data are subsequently de-trended to perform interpolations. Final temperature fields are ultimately calculated, for both IDW and OK by redistributing the interpolated fields according to local elevation and time-varying lapse rates derived from data.

The performance of the interpolation methods is analyzed via cross validation conducted using the GSTAT package (Pebesma, 2004). Two statistical measures of accuracy are used to validate the interpolation results: 1) Mean Bias and 2) Root Mean Square Error, RMSE. The Mean Bias is defined as the mean of the differences between predictions and observations. It defines the tendency of the method towards over or under-prediction. In addition, for kriging methods, standardized errors (i.e. the residuals of predictions and observations normalized by their respective variances) are compared.

To test the different interpolation methods from an hydrologically relevant viewpoint, the RSII model (described in Chapter 2 Section 2.4) was run with IDW and kriging rainfall and temperature estimations. The test was carried out on the 1993 flood event for which the model had been previously calibrated (Jordan, 2007; Jordan et al., 2008). All methods are compared relative to the current (base case) IDW method based on a constant lapse rate (i.e., the method used in calibration and in use currently for the operational version of the model). The calibrated model is assumed to well represent the actual functioning of the catchment, allowing the assessment on the different interpolation techniques. To focus on the impact of input fields, this study assumes that better reproduction of discharge volumes can be made by simply changing the spatial distribution of the hydro-meteorological interpolations. Therefore it is important to note that although this model was calibrated for input fields generated by IDW, it is assumed that further calibration with other input fields which provide more appropriate volumes would undoubtedly yield improved results.

3.3 Results and discussion

3.3.1 Variogram estimates

Experimental variograms are fitted with the exponential model as meteorological fields typically exhibit the type of short-range variability that can be best described by this model (Goovaerts, 1999). Variogram analysis (see Figure 3.5b as a representative example for the 2000 storm event) shows a clear identification of range and sill. Consistent anisotropy patterns are identified for all examined storm events, for both precipitation and temperature. Rainfall variograms exhibit a principal direction of anisotropy (south-east) that corresponds to the prevailing wind direction at 500 hPa detailed by the radio sounding data. Anisotropy is geometric (i.e. the sill remains relatively constant regardless of the direction), while no zonal anisotropy (i.e. different correlation structures in different directions) is detected. In contrast, spatial correlation structure of temperature data does not show significant anisotropy.

Rainfall fields obtained through anisotropic variograms have proven to well reproduce the spatial correlation structure of rainfall as shown by comparison with previous studies in the Swiss Alps (Petrascheck and Hegg, 2002). In contrast, isotropic variograms and relative interpolated rainfall fields (not shown here for brevity) did not confirm such detailed studies. Here, anisotropic variogram estimators are used in the present analysis.

3.3.2 Precipitation interpolation

The analysis of precipitation interpolations compares IDW with geostatistical methods (OK, KED with elevation as the external drift and KED with COSMO7 reanalyses as the drift). Figure 3.6 shows, for each interpolation method, the cumulative precipitation maps for the 2008 event (this event being representative of the general behavior during the other flood events examined). Visual inspection of Figure 3.6 chiefly stresses the advantages of geostatistical

Chapter 3. Improved interpolation of meteorological forcings

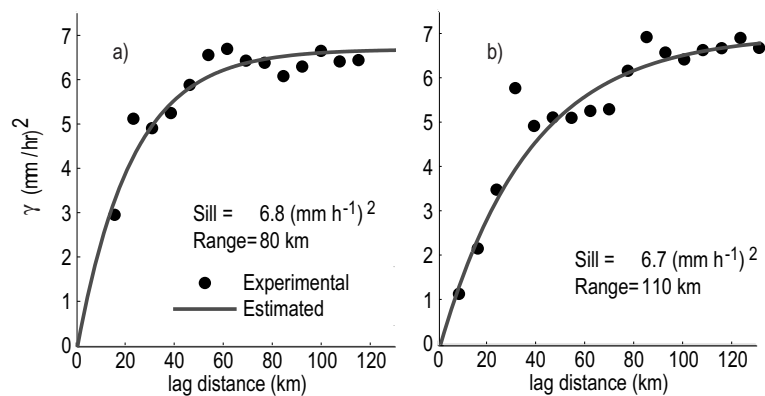


Figure 3.5: Average anisotropic variograms for precipitation during the 2000 event: a) minor axis at 70 degrees from north b) principal direction showing prevailing wind direction at 160 degrees from north. The anisotropy ratio was found to be 0.5.

methods (panels b-d) with respect to IDW (panel a). IDW interpolations suffer the appearance of the so called 'bull's eyes' effect around the measurement points. This effect could be reduced with a suitable exponent for the inverse of the distance between the estimation point and the measurement stations, a proxy for the correlation length of rainfall. Accounting for the spatial structure of rainfall, as estimated from available data, geostatistical methods partially avoid this problem. Maximum cumulative precipitation is recorded on the south-eastern boundary of the watershed (i.e. the Simplon alpine pass). Figure 3.6d shows that using COSMO7 reanalyses as the external drift factor produces pixels with higher precipitation volumes along this border of the watershed, as compared to other methods. In fact, some pixels show two times the cumulated precipitation recorded by stations within that pixel. Most notably, by using geostatistical methods, the anisotropic structure of the rainfall field in agreement with the predominant synoptic scale wind direction emerges from the geostatistical methods. The resulting spatial patterns of rainfall are compatible with more detailed studies carried out in the Swiss Alps (Petrascheck and Hegg, 2002), reinforcing the choice of anisotropic variograms for the description of the spatial correlation structure of rainfall in the study case at hand.

Daily mean precipitation values calculated by averaging the various predictions in the Visp and the Dranse catchments are shown in Table 3.2. Foremost, the results show that IDW interpolation produces the lowest mean precipitation values except in cases where the COSMO7 reanalyses seemingly under predict rainfall relative to the other methods based on ground measurements. As such, it is apparent that kriging with COSMO7 as an auxiliary variable is highly dependent upon the quality of the forecast. Furthermore, the mean precipitation intensities indicate that the volumes generated with OK and KED are consistently greater than IDW.

To further analyze the interpolation methods quantitatively, cross validation performances are compared in Figures 3.7 through 3.8 and in Table 3.3. As shown by sample histograms in Figure

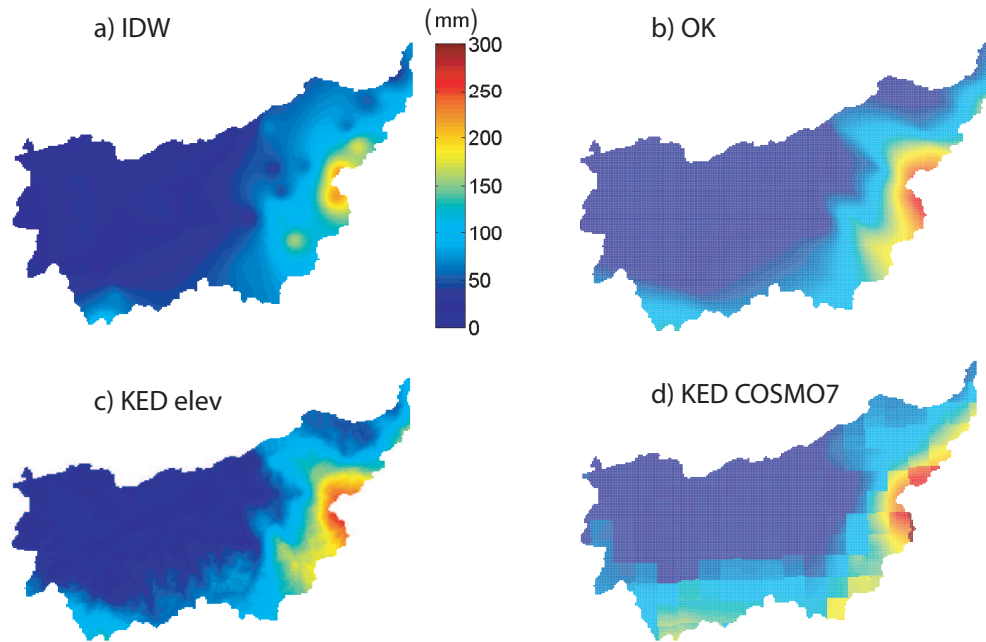


Figure 3.6: Cumulative precipitation (mm) over the 2008 event with the different interpolation methods: a) IDW b) OK c) KED with elevation and d) KED with COSMO7. Mean precipitation for OK, KED with elevation and KED with COSMO7 are respectively +9%, +16%, and +29% with respect to IDW mean precipitation predictions.

Table 3.2: Mean daily rain intensities (mm day^{-1}) during the 1993, 2000, and 2008 flood events in the Visp and the Dranse.

	Visp			Dranse		
	1993	2000	2008	1993	2000	2008
IDW	44.3	67.9	10.9	22.6	48.0	4.7
OK iso	45.1	72.8	12.9	23.9	50.4	5.4
OK aniso	49.6	74.4	13.0	23.9	53.0	5.6
KED elev	47.2	96.7	13.4	23.2	68.0	6.5
KED COSMO7	36.7	61.4	12.7	25.5	56.6	11.3

Chapter 3. Improved interpolation of meteorological forcings

3.7, the mean residuals for all methods are distributed symmetrically with a single peak. To indicate a good predictive model within the context of kriging, the cross-validation residuals should have a normal distribution (Isaaks and Srivastava, 1989). The following results thereby imply that the variogram models are relatively accurate for all kriging methods.

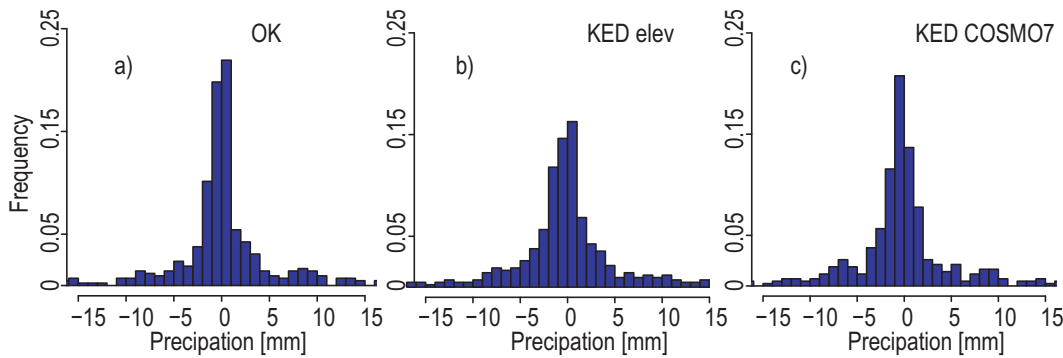


Figure 3.7: Histogram of residuals for all precipitation kriging methods for the 2008 event: a) OK b) KED with elevation c) KED with COSMO7. Residuals for the 1993 and 2000 events are similarly symmetric and single-peak.

Furthermore, cross validation results evaluated in Figure 3.8 compare the Mean Bias for all stations in the study area (Figure 3.8a) and for the stations located above 1500 m asl (Figure 3.8b). An analysis of interpolation validation at high elevations is important in order to investigate the performances of different methods in the presence of complex topography and at elevations at which most of the catchment is located. In fact, 83 and 90 % of the area within the Dranse and the Visp, respectively, is found to be above 1500 m asl. Figure 3.8a shows that, with a few exceptions, KED with elevation produces the least biased predictions of observed rainfall whereas IDW tends to overestimate precipitation, particularly for the 2008 event. The general overestimation of precipitation for stations above 1500 m for the 2008 event (Figure 3.8b, dark red bars) suggests some inadequacy of the rain gauge network active during this event in that portion of the catchment. Even in this latter case, however, KED with elevation as the external drift factor produces less biased estimates as compared to the other methods.

In contrast, the RMSE results (Table 3.3) are not as conclusive as the mean bias results. For all flood events, OK and KED had similar RMSE values. Overall, IDW produces the largest errors for all events.

Figure 3.9 details cross-validation results in terms of the distribution of standardized errors (SE) for geostatistical methods during the 2008 event. Median errors (indicated by the thick black line within the boxes) are negligible for all kriging methods. The spread above and below the median in each box shows the 25 and 75 % quantiles while the bottom and top whiskers indicate the 10 and 90 % quantiles respectively. Ordinary kriging shows the widest distribution and errors. Conversely, KED with elevation shows the smallest box spread while KED with COSMO7 shows the smallest error distribution range considering the 10 and 90 % quantiles.

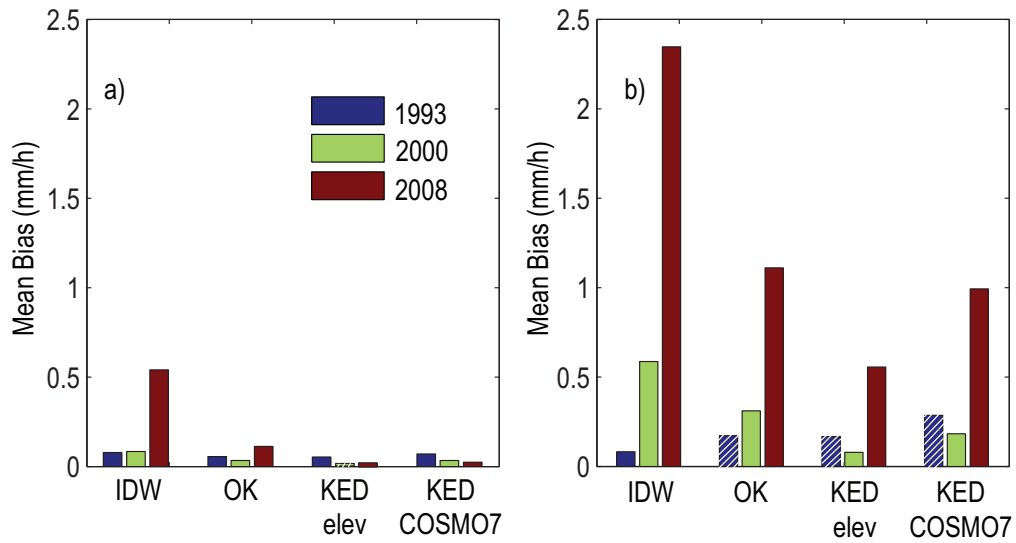


Figure 3.8: Mean Bias for all precipitation interpolation methods for all events (white diagonal patterns indicate negative biases): a) all stations b) stations above 1500 m asl.

Table 3.3: RMSE for all interpolation methods for all events (left) all stations (right) stations above 1500 m.

	RMSE All Stations			RMSE Stations > 1500m		
	1993	2000	2008	1993	2000	2008
IDW	2.3	2.0	2.1	2.4	2.4	2.3
OK aniso	2.2	1.9	2.2	2.1	2.0	2.1
KED elev	2.2	1.9	2.2	2.1	2.0	2.2
KED COSMO7	2.2	1.9	2.1	2.3	2.4	2.1

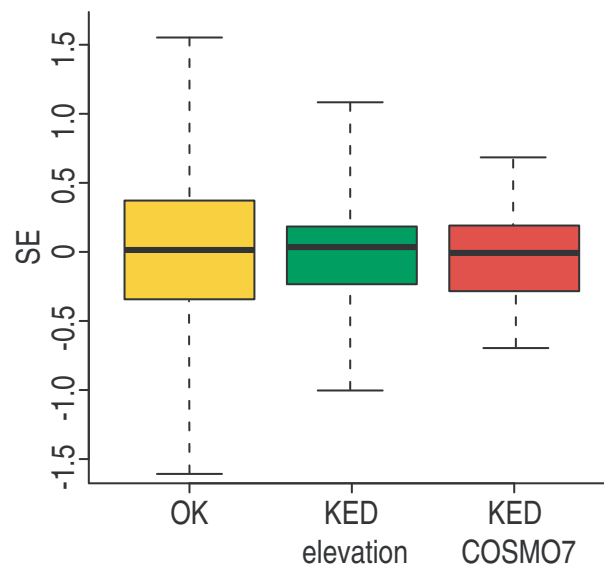


Figure 3.9: Standardized errors (SE) for the precipitation kriging methods during the 2008 event. The median of the distribution of the SEs for each method is shown by the black lines within the boxes while the upper and lower 25% quantiles are the top and bottom values of the boxes respectively. The whiskers extend above to the 90% quantile and below to the 10% quantile.

3.3.3 Temperature interpolation

Accurate mapping of temperatures is crucial to accurately describe snow/rainfall partitioning and melting processes and thus model hydrologic response in alpine watersheds. Figure 3.10 compares the different temperature interpolation techniques in terms of maps of mean temperature over the entire event for the 2008 case (used here as a representative example for the other studied events). Here, time-varying temperature lapse rates were directly derived from hourly ground measurements for IDW and OK interpolations (Figure 3.10a-b), while for elevation and COSMO7 driven KED (Figure 3.10c-d) the vertical dependence of temperature from topography is embedded in the method either directly (KED with elevation) or indirectly through the weather forecast model (KED with COSMO7). In the former case, temperature differences between valleys and hilltops appear to be stronger as compared to the latter case (KED interpolations). Also Figure 3.10d suggests that the coarse resolution of the weather forecast grid (6.6 km × 6.6 km) does not resolve the detailed features of this complex topography needed to represent temperature fields. An effective use of numerical temperature forecasts would thus require data downscaling techniques to reproduce the characteristic patterns better approximated by the other interpolation methods.

Statistically, the cross validation results for temperature show that kriging with elevation as the external drift provides the overall smallest bias and error in terms of the Mean Bias (Figures 3.11a and 3.11b) and RMSE (Figures 3.11c and 3.11d) for all events including stations above 1500 m (Figures 3.11b) and 3.11d) respectively. This ensemble of cross validation results

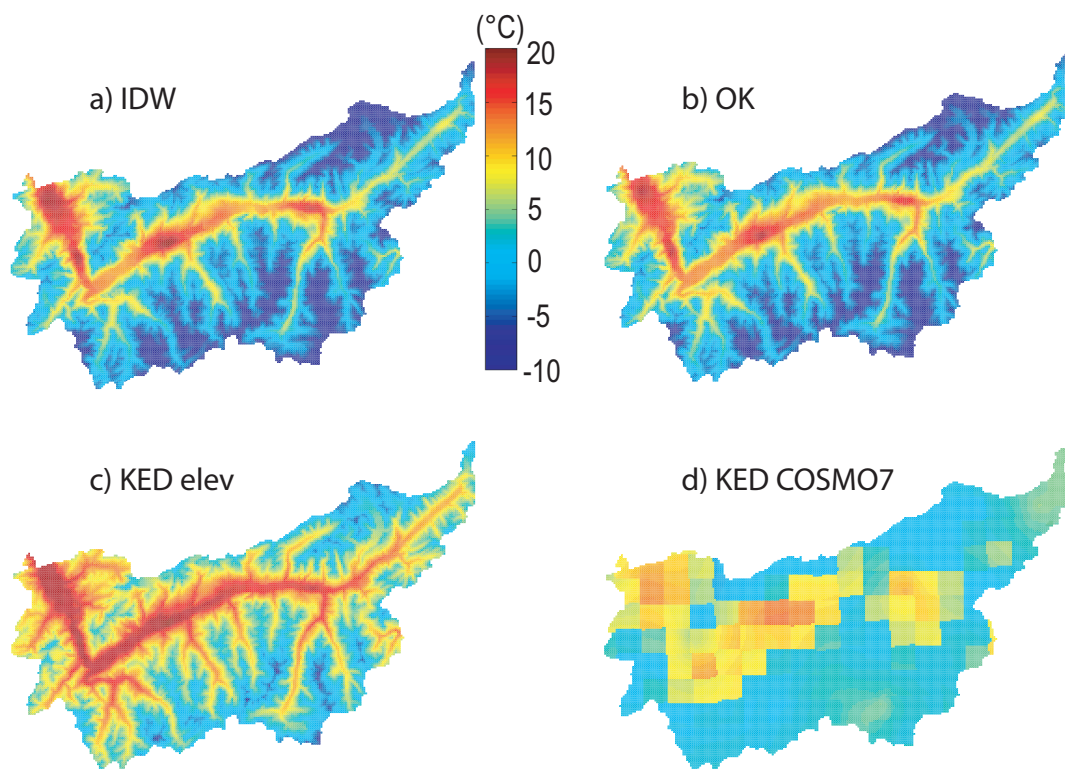


Figure 3.10: Mean temperatures over the 2008 event: a) IDW b) OK c) KED with elevation and d) KED with COSMO7. Differences in mean temperatures for OK, KED with elevation and KED with COSMO7 predictions are respectively +2%, +20%, and -22% relative to IDW.

Chapter 3. Improved interpolation of meteorological forcings

strongly suggests the need for temperature interpolation to include elevation as an auxiliary variable.

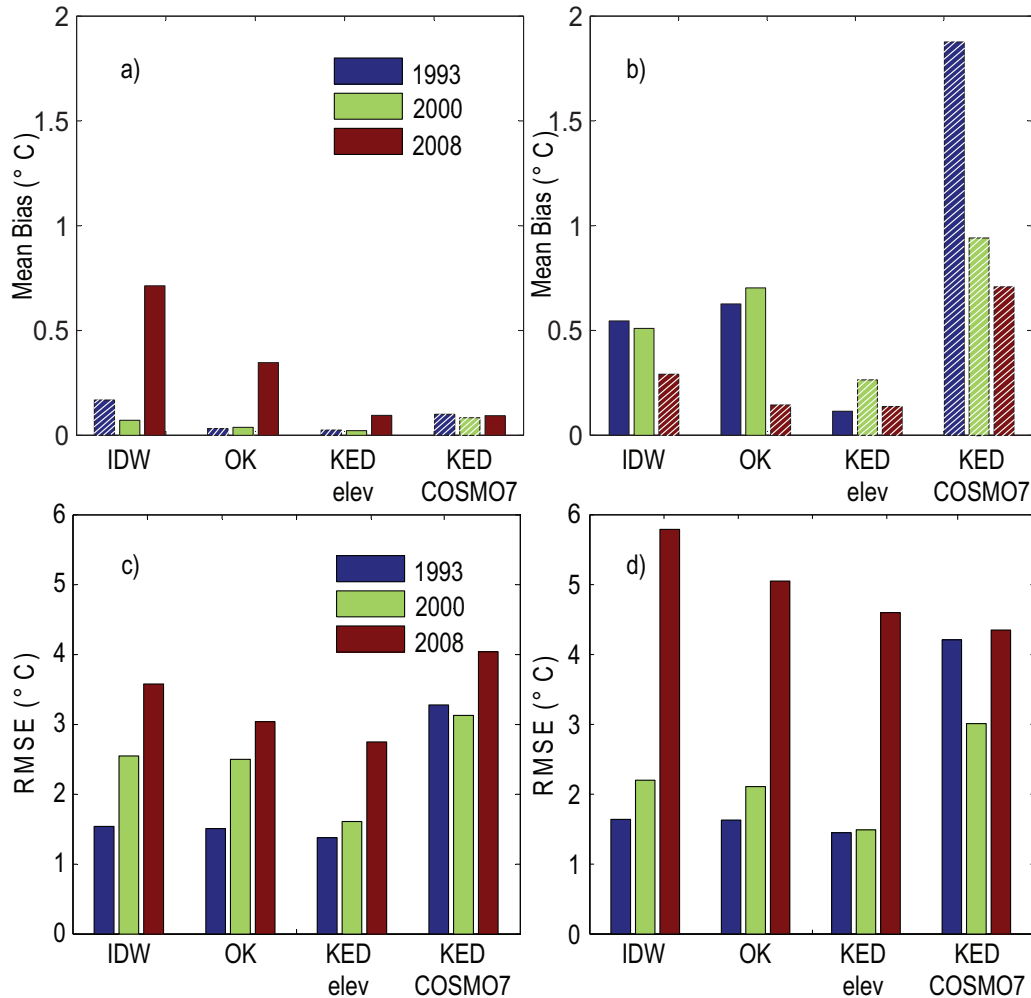


Figure 3.11: Mean Bias and errors of temperature predictions for all interpolation methods for all events: a) Mean Bias for all stations (white diagonal patterns indicate negative biases) b) Mean Bias for stations above 1500 m (white diagonal patterns indicate negative biases) c) RMSE for all stations d) RMSE for stations above 1500 m asl.

Mean interpolated temperature time series in the Visp are shown in Figures 3.12a and 3.12b for the 1993 and 2000 flood events respectively. In general, KED with elevation provides higher mean temperatures over the course of both storm events. Also, the KED time series for the 1993 flood event (Figure 3.12a) is in best agreement with the measured temperature time series for 1993 as shown in Figure 3.3c. The discrepancy in temperatures is explained by the fact that for this event, measurement stations did not extend above 2470 m asl, so the mean measured temperatures are much higher.

By comparing the mean interpolated temperature and mean measured precipitation time

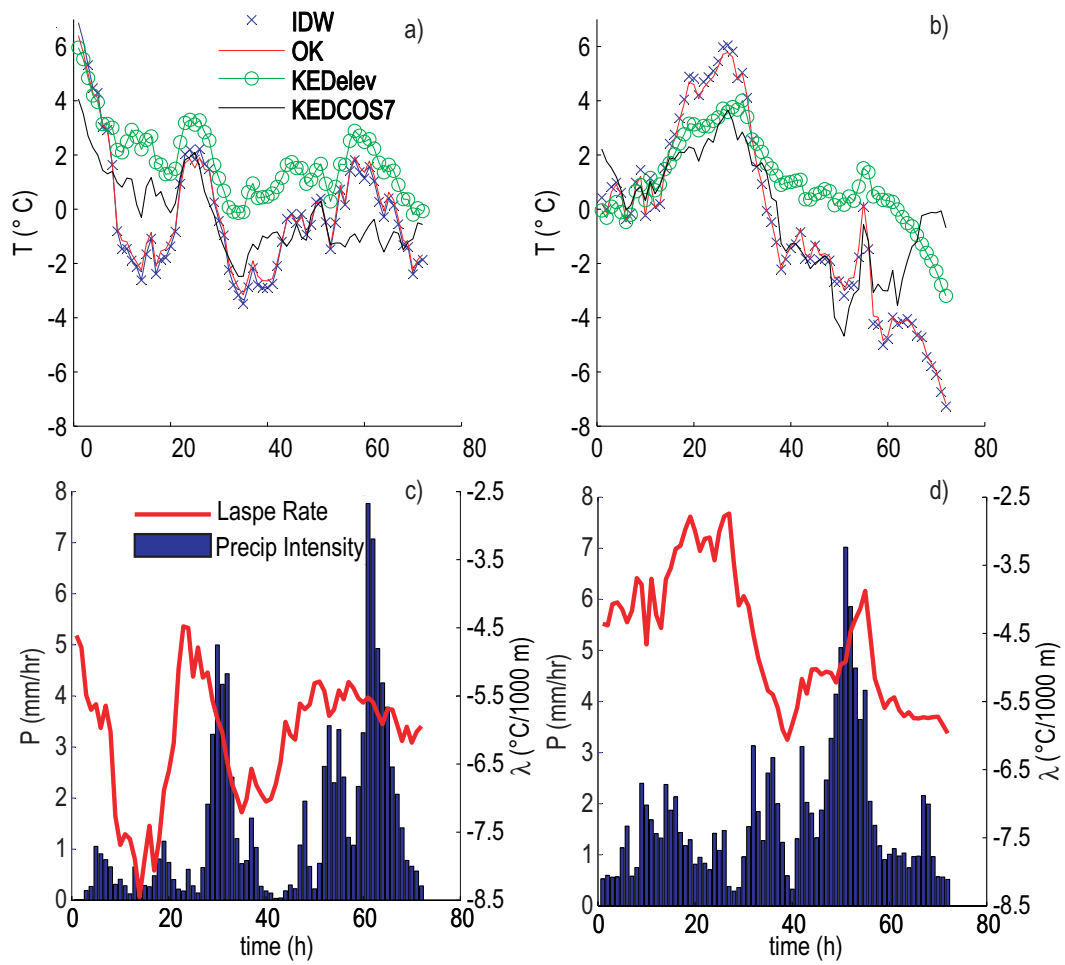


Figure 3.12: Comparison of precipitation and temperature time series with lapse rates derived from station data (λ): a) 1993 mean estimated temperature time series ($^{\circ}\text{C}$) in Visp b) 2000 mean estimated temperature time series ($^{\circ}\text{C}$) in Visp c) 1993 time series of mean precipitation (mm h^{-1}) in the Visp versus catchment-averaged temperature lapse rates evaluated from station data d) 2000 time series of mean precipitation (mm h^{-1}) in the Visp versus catchment-averaged temperature lapse rates evaluated from station data.

series profiles in the Visp catchment for 1993 (Figures 3.12a and 3.12c respectively), it is also clear that during periods of maximum precipitation intensity and an increase in temperature (seen at hour 60) there is no corresponding change in temperature found through KED with COSMO7 predictions. The COSMO7 reanalyses do not consistently correspond to meteorological trends presumably because they cannot resolve subgrid phenomena due to a relatively coarse resolution. In the case of the Swiss Alps, the effect of grid resolution can be quite dramatic. Indeed, a COSMO forecast model grid point that provides an areal average over a measurement station can differ by more than 1 km in elevation. Furthermore, the COSMO7 model is limited to interpolations up to 3200 m asl.

The time-variant lapse rates derived from data show gradients for the 2000 event (Figure 3.12d) in the Visp catchment that are never below $-6.5\text{ }^{\circ}\text{C} / 1000\text{ m}$ and range between -2.5 and $-6.0\text{ }^{\circ}\text{C} / 1000\text{ m}$. This provides evidence that, for flood modeling, even seasonally-derived constant lapse rates will be unable to capture the dynamics of temperature changes during an event. As the data suggests, lapse rates exhibit considerably large ranges in mountainous regions. Measured lapse rates in complex topography have been reported to range between -3 and $-7\text{ }^{\circ}\text{C} / 1000\text{ m}$ (Blandford et al., 2008). Also, $-6.5\text{ }^{\circ}\text{C} / 1000\text{ m}$, the constant lapse rate value noted in an observed standard atmospheric profile, has been refuted as inaccurate as a constant gradient in space and time in other complex terrain studies due to the effects of large scale advection and diurnal wind patterns (Rolland, 2003; Minder et al., 2010). In effect, typical constant lapse rates would undoubtedly generate inaccurate forcings for flood forecasting models.

3.3.4 Effect of interpolation techniques on runoff predictions

All interpolated fields have been incorporated into the RSII model (Chapter 2 Section 2.4) for the flood event of 1993 (one of the most severe flood events ever-recorded in the Visp catchment). Results of the hydrologic model are summarized in three experiments. In Experiment I, the temperature and precipitation fields are introduced so that the same interpolation method is used to generate both meteorological fields (Figure 3.13a). The IDW base case which uses a constant lapse rate is plotted in the first plot for comparison. In Experiment II, the IDW and kriged precipitation fields are introduced with the same temperature field generated by KED with elevation (as this method shows the best cross validation results) (Figure 3.13b). Similarly, in Experiment III the IDW and kriged temperature fields are introduced with the same precipitation field generated by KED with elevation (Figure 3.13c). In all cases, the original 1993 calibration parameters, obtained with the IDW base case inputs, are left untouched and initial conditions are unchanged.

Results from Experiment I indicate that KED with elevation clearly generates more volume during the event. IDW and OK with variable lapse rates also generate more volume. However, the IDW and OK volumes are not sufficient to capture the discharge peak. Most significantly, it is quite evident that the base case of using IDW with a constant lapse rate within the Visp does

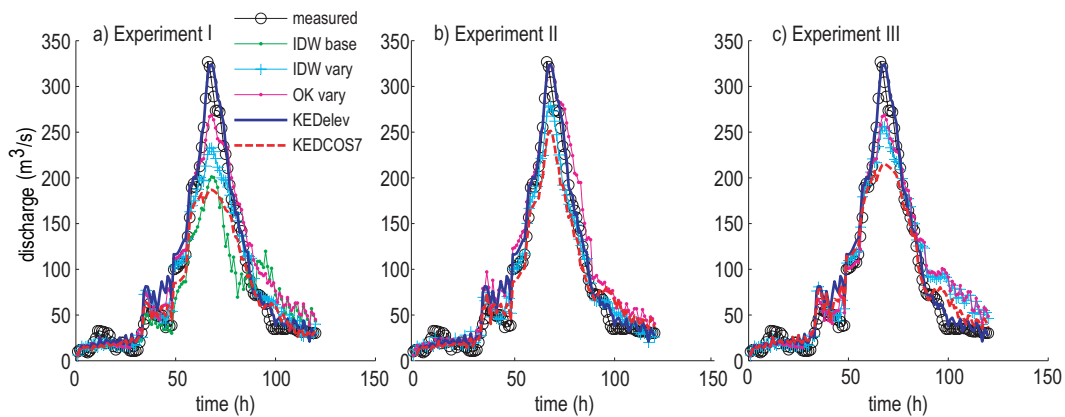


Figure 3.13: RSII discharges over the 1993 event: a) all precipitation and temperature interpolation methods versus measured and IDW base case, b) all precipitation interpolation methods with KED with elevation derived temperature, c) all temperature interpolation methods with KED with elevation derived precipitation.

not allow for sufficient volume to be generated (Figure 3.13a). Similarly, the precipitation and temperature fields found through KED with COSMO7 generate volumes and peaks in least agreement with measured discharge data.

In Experiment II, the effect of changing only the precipitation fields shows that the choice of the precipitation interpolation method has lesser impact. KED and OK for precipitation generate the volume and peak most similar to those of the measured discharge data. In contrast, precipitation fields generated by IDW or KED with COSMO7 are less in agreement with measured data. These results correspond with the daily precipitation intensities calculated in Table 3.3.

In Experiment III, the major effect induced by changing solely the temperature field is quite apparent. With the precipitation field generated by KED with elevation and the temperature predictions produced by IDW or kriging, the temperature fields provided by KED with elevation clearly capture the largest discharges at the peak of the storm. OK and IDW temperature fields show similar results where less volume is generated presumably due to the lower mean temperatures over the course of the event. Similarly, the temperature field generated by KED with COSMO7 does not provide sufficient volume such as in Experiment I.

The increase in volume can be explained by Figure 3.12 which shows that mean temperatures estimated by IDW, OK and particularly KED COS7 are below 2°C . In the RSII model, the critical temperature range is given between 0 and 2°C which defines that any precipitation above 2°C is definitively rain. In contrast, mean temperatures generated by KED with elevation are more frequently above or near 2°C prompting rainfall responses rather than snowfall accumulation.

To quantify the hydrologic effect of the different interpolation techniques, runoff volumes rather than measures of model performance based on local error such as the Nash-Sutcliffe

Chapter 3. Improved interpolation of meteorological forcings

Table 3.4: Specific runoff volumes (m) during the 1993 event at Visp: Measured and IDW base case volumes are first listed. Below, the left column refers to Experiment I, the center column refers to Experiment II and the right column refers to Experiment III.

Specific Runoff Volumes (m)			
Measured	5.5		
IDW (base case) ^a	4.6		
	Experiment I ^b	Experiment II ^c	Experiment III ^d
IDW	5.2	5.3	6.0
OK aniso	6.1	6.7	6.1
KED elev	6.0	6.0	6.0
KED COSMO7	4.6	5.1	5.4

^a IDW with constant lapse rate used for temperature interpolations

^b All temperature and all precipitation interpolation methods

^c Constant KED with elevation derived temperatures with all precipitation interpolation methods

^d Constant KED with elevation derived precipitation with all temperature interpolation methods

index (Nash and Sutcliffe, 1970) are used. Table 3.4 indicates that hydrologic simulations run with KED-interpolated input fields significantly improve results in terms of specific runoff volume; previous runoff underestimations are resolved by using inputs which can capture flood volumes and peaks. The fact that the hydrologic model was not calibrated for the KED with elevation input fields, which produce the best match with the measured data, reinforces the conclusion that detailed spatial interpolation tools are needed to catch the prominent characters of the hydrologic response.

3.4 Conclusions

Based on the results, kriging can be used effectively to estimate precipitation and temperature fields in complex, alpine topography during flood events. Conclusions from this study include the following:

- Variogram analysis shows that significant anisotropy (induced by dominant wind and orographic patterns) is detected in field data and its effect thus needs to be accounted for in spatial interpolation. Cross validation residuals for precipitation showing a symmetric, single-peak distribution suggest the reliability of the variogram and interpolation techniques;
- Comparative analyses of the different interpolation techniques suggest that geostatistical methods perform better than IDW. In particular, KED with elevation as auxiliary

information gives the overall best validation statistics for the considered set of events and, notably, it does so for the 2008 event which includes all stations within the current monitoring network. This conclusion is further strengthened by the definitive best performance results associated with KED with elevation for temperature interpolations. The comparison of data- versus KED- derived lapse rates shows that elevation as external drift is the determinant factor for improved snow/rainfall partitioning and melting over the study region, and possibly in general in Alpine contexts;

- The use of the improved rainfall and temperature fields as inputs to the operational RSII hydrological model provides evidence for increased accuracy in the prediction of discharge volumes and peaks. Placing meteorological fields into a hydrological model proved essential in confirming the suitability of the interpolation methods for generating reliable spatially distributed flood modeling inputs.

Chapter 4

Snowfall limits and hydrological modeling

The fact is the human race is not only slow about borrowing valuable ideas—it sometimes persists in not borrowing them at all.

Mark Twain

4.1 Introduction

It has long been recognized that Alpine precipitation is controlled by numerous meteorological factors. Most notably, the observed precipitation type is influenced by latent heat (Unterstrasser and Zaengl, 2006), thermal and moisture distributions, vertical atmospheric motion and ice nuclei distributions (Bourgouin, 2000). Relative humidity has been shown to highly impact the precipitation phase near the freezing point; Matsuo and Sasyo (1981) demonstrated snowfall with temperatures up to 4 °C when the air was relatively unsaturated. In general, the energy necessary for phase transformation (i.e., melting and evaporation) extracts latent heat from the atmosphere with limits depending on the relative humidity. The wet-bulb temperature gives an indication of the air humidity as it measures the lowest temperature that can be achieved by the evaporation of water from a parcel of moistened air. It is classically measured with a psychrometer whose bulb is moistened such that air near the wet bulb is cooled by the transfer of heat from the air required to evaporate the water. Together with the dry-bulb temperature, the wet bulb temperature determines saturation; the wet-bulb temperature is always lower than the dry-bulb temperature due to evaporative cooling until atmospheric saturation is achieved, where both temperatures are equal (Schneider et al., 2011).

The wet-bulb temperature of different atmospheric layers plays a significant role in the initiation, melting and freezing of hydrometeors, thereby acting as an influential factor in the prediction of the altitude where the transition from snow- to rainfall occurs, i.e., snowfall limit (SL). Accordingly, the wet-bulb temperature is used in different precipitation phase models for forecast purposes (Bourgouin, 2000; Graham and Evans, 2011). In contrast, computation of SLs within hydrological models is typically based on a spatial interpolation of dry ground temperatures with estimated lapse rates, neglecting both pressure and relative humidity (e.g. Hingray et al., 2010; Fundel and Zappa, 2011), although a limited amount of hydrological studies use the wet bulb temperature for SL calculations (Blöschl et al., 1991; Haiden et al., 2011). Because the phase of precipitation depends on the conditions in the location where it is formed as well as ground conditions, the typical dry temperature interpolation can provide considerably erroneous information, particularly if lapse rates are treated as constant in time (Tobin et al., 2011; Minder et al., 2010).

Current snow research for hydrological modeling purposes focuses on the prediction of snow water equivalent (Jonas et al., 2009) and snow-covered areas. Both predictions face two major challenges: full energy/mass balance approaches require a significant amount of measurement inputs such as radiation fluxes and water vapor pressure (Rohrer and Braun, 1994; Lehning et al., 2006) and typically there exist few point measurements available for generalized model calibration and validation. To address this last problem, numerous studies have focused on the use of remotely sensed snow-covered areas to improve snow simulation routines (Parajka and Blöschl, 2008; Finger et al., 2011). In the context of real-time flood forecasting, however, updating model states with remotely sensed snow cover information at different spatio-temporal resolutions is relatively complex (Dozier, 2011). Flood forecasting models are driven by Limited Area Models (LAMs) to provide predictions for meteorological variables. In this context, a straight-forward option to better define the snow component of hydrological models is to directly use SL output from LAMs as an input to hydrological modeling to improve the snow/rain delimitation.

LAM temperature and precipitation forecasts have previously been used to update hydrological models (Akhtar et al., 2008) and cross validation of LAMs with measured ground data has been used to compute snowfall accumulation forecasts (Haiden et al., 2011). It is well-understood that LAM output variables contain error (Pappenberger et al., 2011). However, to the authors' knowledge, SL output, specifically, has not yet been tested in terms of its viability for hydrological modeling. This study therefore attempts to use LAM SLs as hourly input to a catchment-scale hydrological model. The main goal for this study is to improve flood forecasting for the Visp catchment in the Swiss Alps characterized by strong topographic gradients where an incorrect snow/rainfall limit (on daily or sub-daily timescales) typically (Mezghani and Hingray, 2009) implies a significant over- (or under-)estimation of the source catchment areas contributing to runoff and infiltration, with a view to operational hydrology.

4.2 Materials and methods

4.2.1 Study site and meteorological data

The analyses described herein refer to the Visp catchment (see Chapter 2 Section 2.2 of this thesis for further details on this catchment). Dry-bulb temperature and precipitation measurements were obtained from the MeteoSwiss ANETZ meteorological network (Gutermann, 1986). The use of other Snow and Avalanche research institute (SLF) temperature stations was initially considered. However, these stations are installed in predominantly exposed areas for wind and snow observations (Lehning et al., 2002). Accordingly, they are not considered representative of average local temperature conditions and have not been used in this study. Rather, all MeteoSwiss stations indicated in Figure 4.1 are used as inputs to the hydrological model. These stations are located in or near the Valais region (indicated by the dark outline). The Valais region, corresponding to the catchment of the Rhone river, which receives the Vispa discharge, is relevant for the spatial interpolation of meteorological variables because it corresponds to the scale of typical weather phenomena in this area.

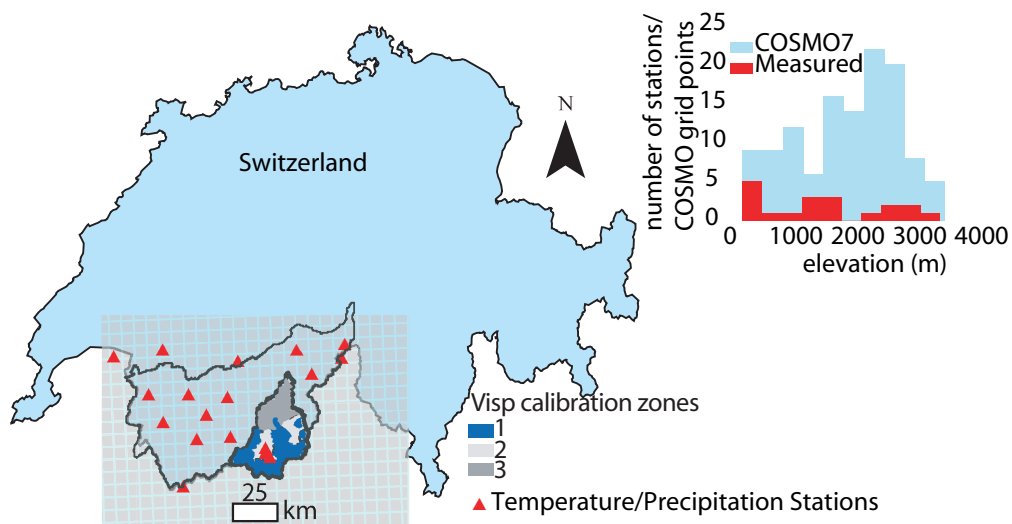


Figure 4.1: Location of the Visp in Switzerland with the COSMO7 grid, the hourly temperature and precipitation stations utilized, and the zones used for GLUE calibration. Only COSMO grid points located within the large black polygon line (indicating the Valais region) were used. Inset: Number of COSMO7 grid points and meteorological stations (with hourly data) versus their respective true ground elevations. Sources: (COSMO, 2011; MeteoSwiss)

4.2.2 COSMO models and output

Both the COSMO2 and COSMO7 forecast reanalyses are used in this study. Details of these forecast models are provided in Chapter 2 Section 2.3.2 of this thesis.

Twenty-four hour periods from the COSMO2 and COSMO7 models are analyzed. Because

the COSMO7 product provides 72 hour forecasts, the data is reconstructed by using the first 24 hours of each reanalysis forecast after a six hour initialization period. This process uses the most recent forecast information (i.e., the smallest lead time predicted) and reduces sensitivity to state variable initialization. Accordingly, COSMO7 model output is used from hour 6 through hour 30, omitting the forecast information predicting further into the future. COSMO7 data was available for 2008 and 2009, while COSMO2 was available for 2009.

The SLs used in these analyses are the output of COSMO. They are computed based on the wet bulb temperature at every point of the horizontal grid using an empirical method developed at MeteoSwiss (Häberli et al., 2008, Stoll Personal Communication). In this approach, SLs are calculated by using a loop from top to bottom over all model layers below 8000m searching for the first layer with a wet-bulb temperature ≥ 1.3 °C. The elevation corresponding to the 1.3°C isotherm is assumed to be the threshold for snowfall; above this temperature the precipitation falls as rain and vice versa. Model output of the SL is provided as an elevation (in m asl) for each COSMO (x,y) grid point. All COSMO grid points in the Valais are used to provide the SL input to the hydrological model (see Figure 4.1).

The empirical wet bulb temperature threshold of 1.3°C has been determined by MeteoSwiss based on their forecasters' experience (Häberli et al., 2008) and is also used by the German Meteo Service (DWD) (Schulz and Schattler, 2009). Other authors suggest different values; for example, Steinacker (1983) has proposed the threshold value to be close to 1.0°C. It should be noted that the meteorological services use the empirical wet-bulb based SL rather than directly characterizing the COSMO SL from the model's 3D rain and snow fields. The resulting predicted SL will be different from the actual SL since the estimation procedure neglects some (micro-) physical processes and in particular any local variations of hydrometeor melting conditions (related to vertical winds, hydrometeor size or fall speed). The simplified procedure is, however, preferred in operational forecasting environments due to its robustness and greater computational time efficiency (Häberli et al., 2008; Graham and Evans, 2011).

4.2.3 Hydrological model

Hydrological simulations are based on the RSII model described in Chapter 2 Section 2.4 of this thesis. An additional reservoir with a constant recharge has been implemented in order to simulate interflow, which provides a rapid, yet delayed flow contribution in the subsurface layer (Bergstrom, 1995). A time-variable lapse rate is also used with the IDW approach used to interpolate the temperature forcings in accordance with findings of Chapter 3 of this thesis and other studies (Tobin et al., 2011; Blandford et al., 2008; Minder et al., 2010).

4.2.4 Snowfall limit methods

The partitioning between rain- and snowfall is described in Chapter 2, Section 2.4.2 of this thesis. Briefly the approach is solely based on temperature using two critical temperatures to

delineate between snow and rain as shown below:

$$\alpha(z) = \begin{cases} 0 & T(z) < T_{c1} \\ \frac{T(z)-T_{c1}}{\Delta T_c} & T_{c1} \leq T(z) \leq T_{c2} \\ 1 & T(z) > T_{c2} \end{cases} \quad (4.1)$$

where α is the ratio of rainfall to total precipitation (-).

In accordance to observed snow/rain distributions (Rohrer and Braun, 1994), the critical temperatures are set to $T_{c1} = 0^\circ\text{C}$ and $T_{c2} = 2^\circ\text{C}$.

This approach shall hereafter be referred to as the Ground Method to indicate its use of dry-bulb ground temperatures alone for SL calculation.

To overcome the limitations of the Ground Method, a new method is proposed here, based on the snowfall limits H_{SL} predicted by COSMO, which we call the COSMO Method. The basic principle of a temperature range $\Delta T_c = 2^\circ\text{C}$ for which snowfall and rainfall occur simultaneously, is maintained. However, in the COSMO Method, the ratio α is estimated based on H_{SL} (m asl) in three steps:

1. The range of elevations over which snowfall and rainfall occur, ΔH , is computed as:

$$\Delta H = H_0 - H_1 = \frac{\Delta T_c}{\ell}, \quad (4.2)$$

where $\ell > 0$ is the time-variable lapse rate estimated from the COSMO temperature field.

It is assumed, as before, that α varies linearly in this range; for elevations $z > H_0$ no rainfall occurs ($\alpha = 0$) and for $z < H_1$ only rainfall occurs ($\alpha = 1$).

2. Assuming furthermore that at the elevation H_{SL} , 75% of the precipitation falls as snow, i.e. $\alpha(H_{SL}) = \alpha_{SL} = 0.25$, the elevations H_1, H_0 can be related to H_{SL} as follows:

$$\begin{aligned} H_1 &= H_{SL} - (1 - \alpha_{SL})\Delta H \\ H_0 &= H_{SL} + \alpha_{SL}\Delta H \end{aligned} \quad (4.3)$$

3. These elevations are then used to determine $\alpha(z)$ for a given elevation band:

$$\alpha(z) = \begin{cases} 0 & z > H_0 \\ \frac{z-H_1}{H_0-H_1} & H_0 \geq z \geq H_1 \\ 1 & z < H_1 \end{cases} \quad (4.4)$$

$$\alpha(z) = \begin{cases} 1 & z > H_0 \\ \frac{z-H_1}{H_0-H_1} & H_0 \geq z \geq H_1 \\ 0 & z < H_1 \end{cases} \quad (4.5)$$

Note that there is generally no clear definition of what the SL actually means (Steinacker, 1983); it represents the transition from liquid to solid precipitation, which we assume here to take place at 25% rainfall. For the Ground Method, this transition (25% rainfall) corresponds to the threshold of 0.5 °C (dry-bulb).

Both methods account for their own respective lapse rate in their calculations of the SL. A preliminary analysis of the lapse rates demonstrated that some values can be negative due to the presence of inversion layers in the Valais region. It is known that inversion layers can occur during the winter up to elevations of 1000 m in the European Alps (Agrawala et al., 2007). Mean negative lapse rates were noted for some periods on the order of days in 2008 and 2009 respectively. In order to compare the SL methods under typical meteorological conditions and for the sake of simplicity in this analysis, negative lapse rates were ignored. A positive lapse rate from the previous time step was maintained in the SL calculations.

4.2.5 Hydrological model calibration and validation

Two different hydrological models are set up by combining the snow/rainfall-runoff module with each of the above SL limit computation methods. Only COSMO7 model output is used as input to the model in order to have two years of input for calibration and validation. These two models are calibrated independently with measured discharge at the Visp catchment outlet using the Generalized Likelihood Uncertainty Estimation (GLUE) approach (Beven and Freer, 2001), which is a well-established Monte Carlo simulation method used to assess the plausibility of hydrological simulations (Pappenberger et al., 2007). This approach assumes that, given the modeler's imperfect knowledge of a system, there are many parameter sets that can be considered equally good simulators of the system. In the hydrologic literature, equally good parameter sets are termed equifinal, e.g. (Beven, 2004). As a result, instead of a single hydrological simulation corresponding to a single best parameter set, an ensemble of simulations corresponding to an ensemble of acceptable parameter sets is retained. These parameter sets are identified by generating a high number of random parameter sets drawn from a prior parameter range and by retaining those sets that have a model performance above a certain threshold criteria (see Table 4.1). For the calibration, the catchment is divided into 3 zones with similar physical characteristics (e.g., presence of glaciers) (see Figure 4.1). The model performance criteria are the Nash-Sutcliffe efficiency (Nash and Sutcliffe, 1970) and the mean absolute residual error, referred to as NSE and MARE respectively. The theoretical optimums are 1 for the NSE and 0 for the MARE criterion and their respective thresholds for acceptability are ≥ 0.8 and ≤ 0.3 . The best parameter sets under these two criteria were selected by taking the intersection of the parameter sets which satisfied both thresholds of acceptability.

These performance criteria are computed over only medium to high flow events in order to exclude the daily fluctuations during low flow situations caused by hydropower operations. Simulations herein could not incorporate these fluctuations because the reservoir storage and

Table 4.1: Prior parameter range for Monte Carlo simulations with and without the best performing parameter sets per zone for both the case of incorporating COSMO snowfall limits (COS) and using dry-bulb ground temperature derived snowfall limits (GND)

Parameter	Prior	Zone 1		Zone 2		Zone 3	
		COS	GND	COS	GND	COS	GND
Degree-day glacier [mm day ⁻¹ °C ⁻¹]	1-8	1.7	2.0	6.8	6.1	3.7	6.4
Degree-day snow [mm day ⁻¹ °C ⁻¹]	3-9	4.0	6.4	8.0	8.4	5.9	5.4
Interflow residence time [hr]	5-200	95	181	12	60	8	26
Subsurface residence time [days]	10-60	33	32	33	32	32	32
Recharge [mm d ⁻¹]	0.1-5	1.3	2.1	1.0	0.9	1.7	1.5
Strickler coefficient [m ^{1/3} s ⁻¹]	10-150	100	105	14	20	50	25

release mechanisms are not public information. The two models (one for each SL method) are calibrated independently to match the mean flow over the entire calibration period and the peak flows for the critical flow event at the end of May 2008. The May 2008 event was considered a high flow event, without, however, being an alert-level flood event (Garcia Hernández et al., 2009b). The model is validated on the discharge time series for the June 2008 and April 2009 events by performing a continuous simulation through 2008 and 2009. The range of prior parameter values was determined based on accepted values from literature and use of the model in the Valais since 2005. In order to hot start the model (i.e., assign a spin-up period that allows the choice of the initial parameter sets to be immaterial) and account for the beginning of the hydrological year, the initial conditions for October-December of 2007 were obtained by running the model with measured data only (since no COSMO data were available). One hundred acceptable parameter sets were selected based on the NSE and MARE criteria for the May 2008 event by retaining the parameter sets that adhered to both the MARE and NSE thresholds of acceptability (≥ 0.8 for NSE and ≤ 0.3 for MARE).

4.2.6 Snow cover validation

For additional validation purposes, a daily IMS snow coverage image (Interactive Multisensor Snow and Ice Mapping System) provided by the National Oceanographic and Atmospheric Administration (NOAA) National Ice Center (30 May 2008) and two daily National Snow and Ice Data Center (NSIDC) MODIS (Moderate Resolution Imaging Spectroradiometer) MOD10-L2 satellite images (1 July 2008 and 1 May 2009) was used to validate the snow coverage for the three events.

IMS images (4km x 4km resolution) are produced based on a composite of satellite images using visible, passive and microwave wavelengths (see NIC, 2008; Helfrich et al., 2007; Pullen et al., 2011, for details). A prime advantage of the microwave sensors is their ability to penetrate clouds. The IMS determination of ‘snow/no-snow coverage’ is indicated when at least 40 % of a grid cell is covered by snow of any depth.

MOD10-L2 images (500m x 500m resolution) are Terra satellites images of snow cover (see Hall et al., 2006, for details). The snow mapping algorithm classifies pixels as snow, snow-covered lake ice, cloud, water, land, or other based on the reflectance or radiance properties in each 500 m pixel using the Normalized Difference Snow Index (NDSI) ratio, i.e., the difference in reflectance of snow in the visible and near-infrared wavelengths (Hall et al., 2006). Fractional snow cover maps are based on the regression technique of Salomonson and Appel (2004). The MODIS products calculate the fractional area (in percent) of each pixel covered by snow for both land and inland water bodies not covered by clouds.

A comparison of MODIS and IMS snow coverage estimates on a daily basis with snow measurement stations (e.g., Snotel) indicated that the accuracy of IMS snow coverage increases with increasing snow cover and MODIS images tend to overestimate snow cover in the accumulation season (Brubaker et al., 2005). Most relevant to this analysis, Brubaker et al. (2005) demonstrated that IMS detected snow-free cells at a rate between 95 and 100 % in the spring season relative to measurement data. Similarly, snow-free cells as indicated by MODIS were confirmed 100 % by station data throughout the year 2000.

Both types of snow images provide a means to distinguish between snow-covered and snow-free areas. In this study, they are used to validate the simulated snow cover at the time of the calibration and validation events. Since the model yields snow heights (in terms of water equivalent) per elevation band rather than absence or presence of snow per pixel, this validation requires a post-treatment of the simulation results in two steps: i) the simulated mean snow-covered area of the catchment is computed and ii) the corresponding snow-covered pixels are estimated based on the hypsometric curve of the catchment. As both the model and the snow cover images integrate snow cover over the winter season, it is assumed here that this validation approach is suitable to confirm the results of this analysis.

It should be noted that this study attempted to validate all rain events with these MODIS images because they have the same resolution as the hydrological model input interpolations (i.e., 500 m). However, MODIS images can only be used on clear days immediately following rain events due to the inability of infrared to penetrate clouds. For the May 2008 event, a coarse 4 km resolution IMS satellite image was the only validation image available because small rain events followed the event and hindered visibility.

4.3 Results

4.3.1 COSMO and ground station data comparison

A comparison of ground station versus COSMO reanalysis temperatures demonstrates that both data sets show strongly time-varying lapse rates (Figure 4.2). The lapse rates might be biased for both data sources: For observed temperatures, this is primarily due to the concentration of hourly gauges within the elevation range of 500 - 1000 m asl (Frei and Schär, 1998)(Figure 4.1). For COSMO outputs, this can be related to the coarseness of the resolution

which prevents an accurate parameterization of a detailed heat balance (Leimer et al., 2011) and to the fact that a grid point cannot be identified with a real-world location due to the different model orography. Both of these factors also partly explain the difference between COSMO2 and COSMO7 predictions. In spite of the different sources of bias, these lapse rates can be considered reasonable; they show the same, expected, variation with consistently lower lapse rates in winter and steeper rates in spring, early summer (Rolland, 2003; Blandford et al., 2008; Minder et al., 2010).

By looking more in detail at the particular months of May 2008, July 2008 and April 2009 (Figure 4.2), (the two spring events and one summer flood event), differences emerge in the lapse rates estimated by the two data sources (COSMO and observed station data) through analysis of the mean lapse rates per month. In the months when the flood events occurred, the predicted mean hourly lapse rates are higher for the COSMO model output. With steeper lapse rates predicted by the COSMO stations, the SL can be predicted to be lower because lower temperatures are extrapolated to higher altitudes.

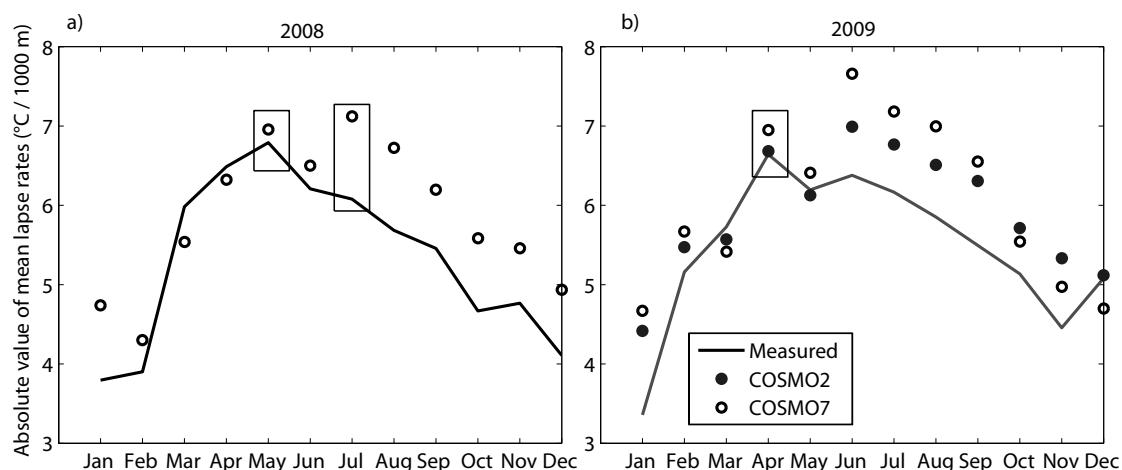


Figure 4.2: Comparison of the monthly mean of the absolute value of the variable lapse rates obtained from COSMO2 (2009 only) and COSMO7 temperatures and from measured hourly ground temperature data for a) 2008 and b) 2009. The rectangles over May 2008, July 2008 and April 2009 indicate the calibration ('C') and validation ('V') periods.

Similarly, a comparison of COSMO SLs with the 25% snowfall elevation obtained via the Ground Method shows that there is a difference in the SLs calculated for all event months (Figure 4.3). For the calibration and validation events, the mean of the monthly snow limits predicted by COSMO are lower. The wet-bulb threshold of 1.3 °C for 25% of rainfall was apparently lower than the corresponding threshold of the Ground Method, which is 0.5 °C (dry-bulb). For comparison purposes, we also computed the SL with COSMO dry-bulb temperatures and a snow/rain transition range of 0-2°C. Figure 4.3 shows that the SLs computed with COSMO dry temperatures do not correspond to the snowfall limits determined by the COSMO method (using wet-bulb temperatures). The differences between the SLs determined by the Ground Method and the COSMO Method are therefore due to a combined effect of contrasting lapse

rates and the incorporation of relative humidity information. Furthermore, the time-varying differences between the wet-bulb and dry-bulb derived SLs for COSMO2 and COSMO7 suggest that the wet-bulb temperature cannot easily be replaced by a dry-bulb temperature SL estimation routine; if the bias has been constant in time, one might have proposed to simply modify the snow/rain transition threshold for the dry temperature estimation, however this is not the current case.

4.3.2 Hydrological modeling

Before analyzing the simulation results of both SL methods, the plausibility of the calibrated parameter values should be analyzed. In fact, calibrating the rainfall-runoff transformation model combined with two different SL methods will necessarily lead to different parameter sets. However, it is expected that only the parameters directly related to fast runoff processes are very sensitive to the choice of the SL method and to the related timing and spatial distribution of water input during peak flow events. Slow runoff parameters should not vary significantly between the two model set-ups. This is confirmed by the two best parameter sets found for each of the methods (Table 4.1). As expected, the residence times of the slow subsurface stores and the recharge flux show similar values for the two methods. In contrast the fast runoff parameters (the Strickler coefficient and the interflow residence time) vary strongly between the two methods, except the former for the highest elevation zone (Zone 1, see Table 4.1), which has the highest glacier coverage (97%) and the smallest contribution to fast runoff processes. For this zone, the calibrated degree-day factor for snow also strongly

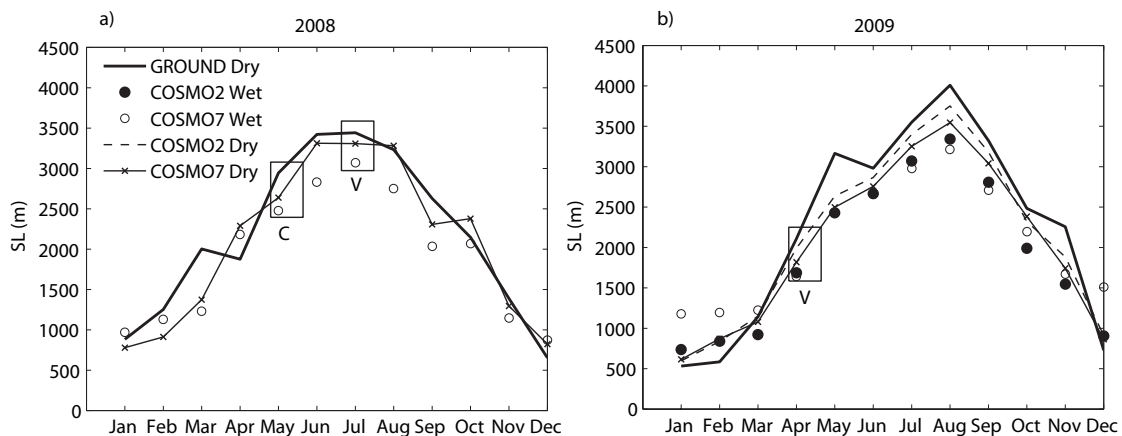


Figure 4.3: Comparison of the mean monthly snowfall limits calculated with the COSMO2 (for 2009 only) and COSMO7 model outputs by the COSMO (Wet) Method and with observed ground temperatures by the Ground (Dry) Method for a) 2008 and b) 2009. The mean monthly snow limits calculated according to the dry COSMO2 or COSMO7 temperatures is also indicated. The rectangles over May 2008, July 2008 and April 2009 snow limits indicate the calibration ('C') or validation ('V') periods.

varies between the methods. This might indicate an effect of compensation for imperfect liquid water input to the rainfall-runoff transformation module. A similar effect might be suspected for the strongly varying glacier degree-day factor for Zone 3 that has an extremely small glacier coverage (1%).

The 100 best discharge simulations identified with the calibration procedure outlined in Section 4.2.5 for each of two methods are compared to the observed discharge in Figure 4.4. Note that the sub-daily fluctuations around the base flow have been filtered from the observed discharge time series using the daily mean discharge. These fluctuations are in fact the result of unknown hydraulic regulations, which typically only take place during low and medium flow.

As shown in Figure 4.4, the Ground Method causes the non-flood event of May 2008 to be closer to the flood alarm level (Garcia Hernández et al., 2009b) with some acceptable simulations crossing this threshold and the mean of the acceptable simulations significantly exceeding the peak discharge.

With the COSMO Method, this non-flood peak is more accurately predicted (see the NSE and MARE values in Figure 4.4). Furthermore, the validation events also suggest that the COSMO Method provides a more accurate snow/rainfall partitioning as evidenced by a better reproduction of the peaks, particularly for the April 2009 validation event. Note that the peak in July 2008 is approximately the same for both methods in spite of the different lapse rates and predicted snow limits. This result indicates that the SL plays a minor role during this summer period.

In fact, reliable SLs are most critical in spring when the soil storage and the snow layer of significant parts of the catchment are close to their saturation thresholds. At this time, the SL highly influences the runoff contributing area. Simultaneously, dry air temperature interpolation leads to SLs at higher elevations, which potentially produces a considerable overestimation of rainfall-experiencing catchment areas and an underestimation of snow receiving areas. This is illustrated in Figure 4.5 showing a comparison of the SLs and the corresponding regions of the catchment receiving snow or rain for the day when the catchment received the most rainfall during the 2008 calibration event, (30 May 2008). The SL is significantly lower with the COSMO Method; the percentage of the catchment receiving snow is 51% and 36% for the COSMO and Ground Methods respectively.

A comparison of snow coverage for the last day of the 2008 calibration event in Figure 4.6 shows a similar difference. With the COSMO Method, the simulated snow covered area corresponds to 57% of the catchment area (Figure 4.6b). In contrast, the Ground Method generates 44% snow coverage (Figure 4.6a). The use of a 4 km resolution IMS satellite image (again, no finer, cloud-free resolution images were available) to validate the simulated snow covered area suggests a snow coverage for 66% of the catchment area (Figure 4.6c).

Similar results can be seen with a comparison of snow coverage for the two validation events

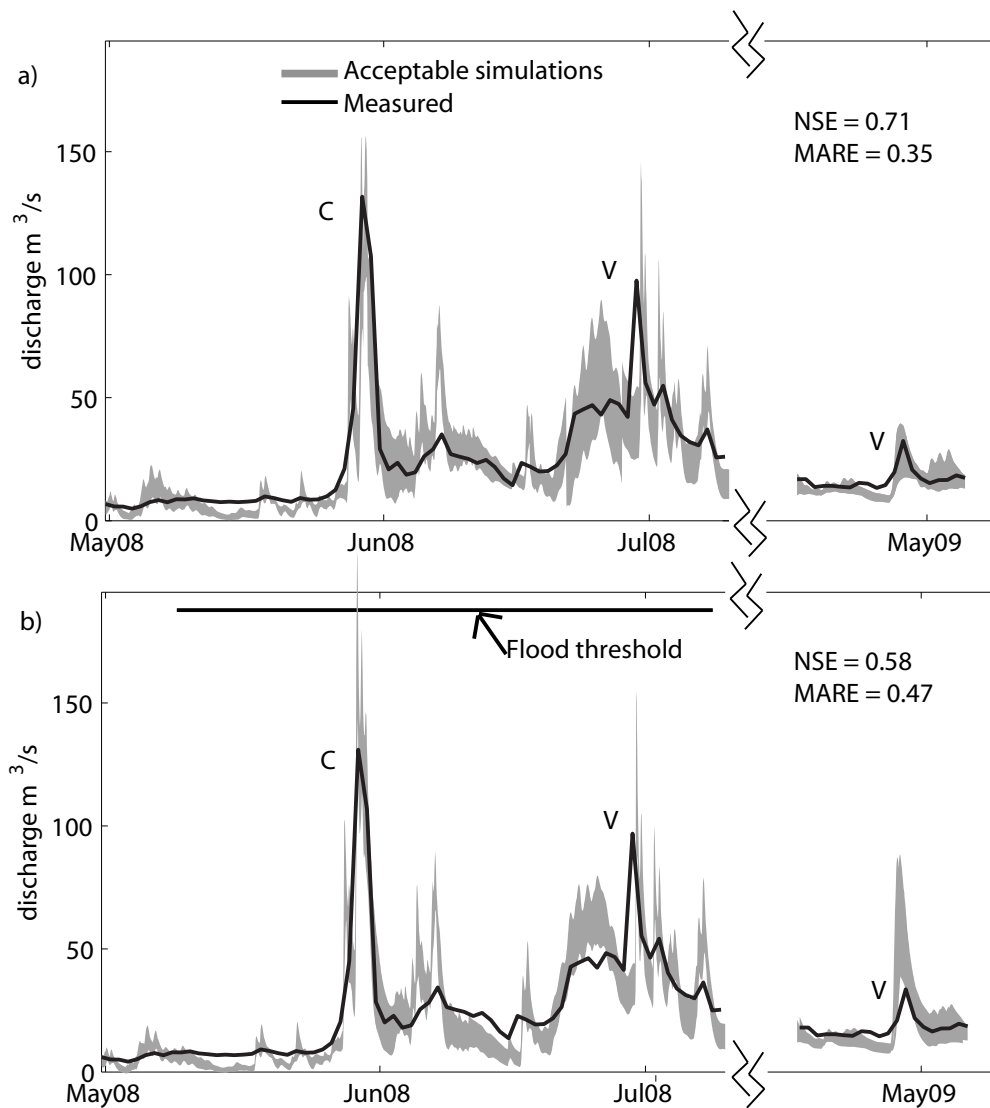


Figure 4.4: a) Discharge comparison for the calibration rain event in May 2008 and the validation events in July of 2008 and April of 2009 with the COSMO7 snowfall limit reanalysis forecasts (COSMO Method). b) Discharge comparison for the calibration rain event in May 2008 and the validation events in July of 2008 and April of 2009 with ground temperature based snowfall limit estimation (Ground Method). Mean NSE and MARE values over the three events are shown. The measured discharge has been filtered to smooth daily fluctuations outside of the peak events. The 'C' and 'V' labels indicate either calibration or validation event.

with MODIS (MOD10-L2) snow cover images at 500 m resolution. For both validation events the meteorological forcing interpolation resolution for the hydrological model and the satellite image resolution are the same.

In the case of the 2008 validation event, the snow coverage is very similar for the Ground and COSMO Methods (25% and 23% snow respectively) (Figures 4.7a and b) and close to that of the MODIS satellite image which shows 24 % snow coverage. This result is not unexpected in that the hydrographs are very similar for both methods.

In contrast, for the 2009 spring validation event, the snow coverage of the hydrological model output has a different spatial snow coverage than the satellite image along the valley branches (Figure 4.7). Quantitatively, with the COSMO Method, the simulated snow covered area is 89% of the catchment area and corresponds well to the image snow covered area at 91%. In

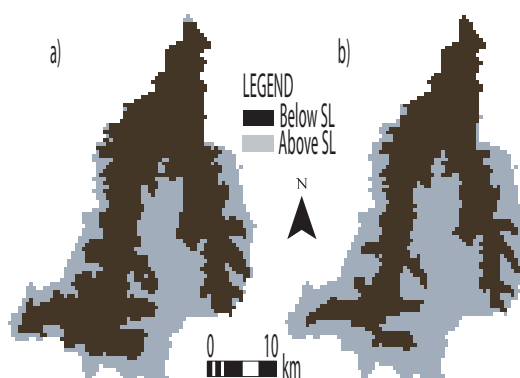


Figure 4.5: Snowfall limits (SL) for the 30 May 2008 (i.e., the day with highest rainfall during the calibration event) as derived by a) the Ground Method and b) the COSMO Method.

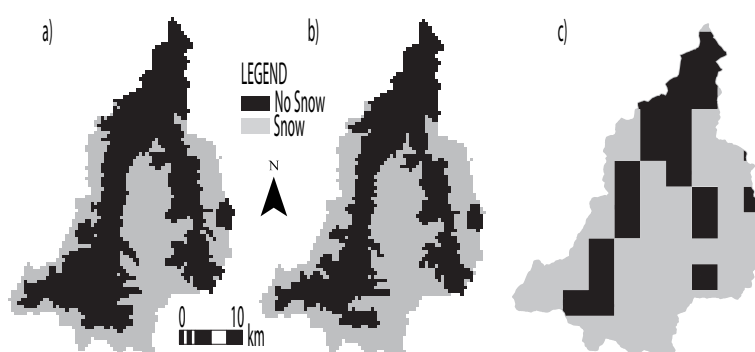


Figure 4.6: Snow coverage (30 May 2008, calibration event) simulated with a) hourly ground temperature stations (Ground Method) and b) COSMO7 snowfall limit forecasts (COSMO Method). c) Observed snow coverage (30 May 2008) based on an IMS snow coverage satellite image. The resolution for images a)-b) is 500 m and for c) is 4 km. Snow coverage percentages are a) 44%, b) 57% and c) 66% respectively.

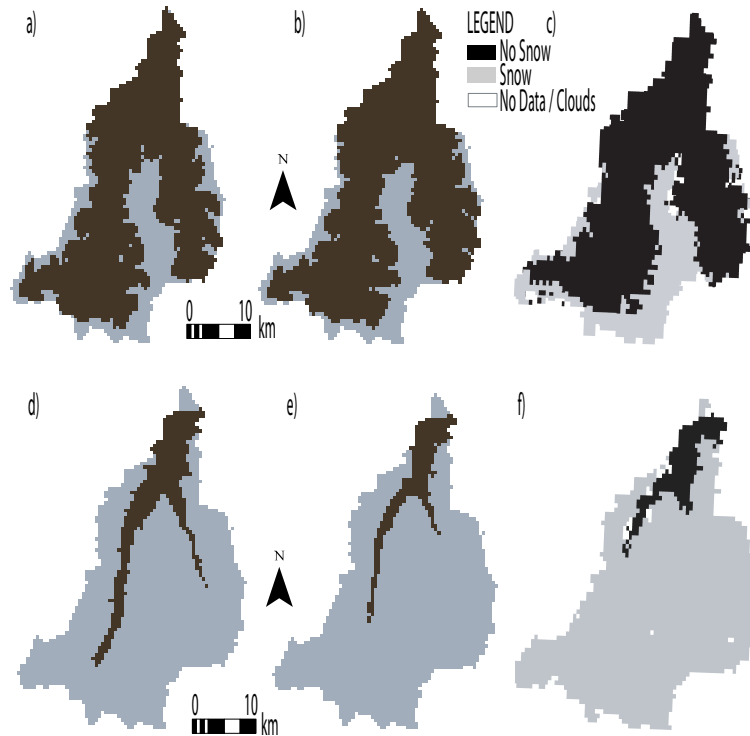


Figure 4.7: Snow coverage for validation events, July 2008 (top) and April 2009 (bottom), simulated with a,d) hourly ground temperature stations (Ground Method) and b,e) COSMO7 snow-fall limit forecasts (COSMO Method). Observed daily snow coverage from MODIS (MOD10-L2) satellites is shown in (c) for 1 July 2008 and f) for 1 May 2009 (1 day after late April event). The resolution for all images is 500 m. Snow coverage percentages are a) 25%, b) 23%, c) 24%, d) 83%, e) 89% and f) 91% respectively.

contrast, the Ground Method generates 83% snow coverage (Figure 4.7d).

These results suggest that the Ground Method underestimates the snow coverage for all three analyzed peak flow events. This could possibly explain why the interflow residence parameter of the corresponding calibrated model is much higher than for the COSMO Method (to obtain a similar hydrological response as the COSMO Method, the Ground Method model tries to retain the water longer in the considerably larger contributing, snow-free, catchment part).

In conclusion, the calibration and validation images indicate that the proposed SL calculation method based on COSMO output has the potential to provide a more accurate data source for locating the snow/rain transition during spring and that solely ground temperature measurements may be inadequate to provide SL information during this time of the year. Future hydrological analyses will be conducted with more reanalysis data to validate and define the limits of the new method.

4.4 Conclusions

Hydrological flood forecasting models commonly compute the snow/rain transition elevation (snowfall limit, SL) based on lapse rates derived from dry, ground temperature measurements. However, this study shows that such an approach can lead to significant inaccuracies in runoff computations due to the resulting erroneous spatial interpolations of the SLs. This is particularly critical in spring when (dry) air temperature-based SL estimation is highly likely to overestimate the SL elevation when a large part of the catchment is close to saturation. To overcome this problem, this study has proposed a new method to estimate snow/rain transition limits for hydrological models based on SL output from COSMO Limited Area Models that are calculated with humidity and wet bulb temperature information. Using a case study from the Swiss Alps, the new method is shown here to yield better estimates of contributing areas during spring peak flow events involving snowmelt. This, in turn, significantly improved runoff simulation. In conclusion, this work suggests that there exists a broad potential use for reanalysis datasets from Limited Area Models for hydrological modeling in Alpine regions.

Chapter 5

Improving the degree-day method for sub-daily melt simulations

Simplicity means the achievement of maximum effect with minimum means.

Dr. Koichi Kawana, Architect

5.1 Introduction

Hydrologic prediction in Alpine regions critically depends on the simulation of snowmelt processes, e.g. to predict discharge regimes for hydropower production (Schaefli et al., 2007) or for real-time flood forecasts where runoff volumes depend on total rainfall and meltwater input (Tobin et al., 2012). A range of snowmelt methods of different complexity and data requirements exists. If seasonal streamflow distributions are sought, however, the complexity of any snowmelt simulation method should be in balance with that of the hydrologic response model for which it is being developed.

The most detailed methods include distributed snowmelt and hydrological models which use a full energy balance approach (Lehning et al., 2006). Such approaches are demanding in terms of data collection and computations. For many real-world applications in sparsely gauged catchments (Rossa et al., 2010), however, detailed methods are not feasible and much simpler methods are required. A popular simple snowmelt simulation method for catchment-scale hydrological models is the temperature-index approach relating snowmelt rates directly to air temperature via a so-called degree-day factor (Hamlin et al., 1998; Dunn and Colohan, 1999; Schaefli et al., 2005; Bocchiola et al., 2010).

Chapter 5. Improving the degree-day method for sub-daily melt simulations

Whether full energy balance models outperform simpler temperature-index approaches in terms of simulating catchment-scale discharge or melt is currently an ongoing debate (Kustas et al., 1994; Zappa et al., 2003; Slater et al., 2007; Debele et al., 2010). Based on the work of Ohmura (2001), it is commonly accepted that the good performance of heuristic temperature-based methods can be explained based on physical reasons; temperature is a physical variable controlling the rates of longwave radiation and sensible heat flux and is highly correlated to the three most important energy sources which determine snowmelt: incoming longwave radiation, absorbed global radiation (shortwave) and sensible heat flux. However, using solely temperature as a proxy for snowmelt neglects vapor pressure, wind, and reflected radiation, quantities known to influence the energy balance and snowmelt processes (Kustas et al., 1994; Pellicciotti et al., 2005; Carenzo et al., 2009).

Accordingly, basic temperature-index models cannot account for the high natural variability of melt rates (Blöschl and Kirnbauer, 1992), a problem which is exacerbated if such melt models are combined with simplified, lumped rainfall-runoff schemes that further smooth the hydrologic response or if they are used for small time steps which need to capture diurnal cycles (e.g., hourly time steps are typically required for hydrologic applications).

In order to increase the physical basis and to emulate simplified energy balance models, there are many research efforts in progress to include more physical information in temperature-index models (i.e. extended approaches). The most straightforward extension is the incorporation of global radiation measurements which distribute melt in space according to local factors of exposition and account for varying solar position (Braun et al., 1994; Brubaker et al., 1996; Kustas et al., 1994; Cazorzi and DallaFontana, 1996; Klok et al., 2001; Hock, 2003; Debele et al., 2010; Jost et al., 2012). Further research has tried to include the evolution of snow density and snow cover albedo over the melt season (Blöschl, 1991; Pomeroy et al., 2003; Pellicciotti et al., 2005; Carenzo et al., 2009; Li and Williams, 2008; Hebel and Purves, 2008). This seasonality can also be emulated with time-varying snowmelt factors, e.g. as a function of snow density (Kuusisto, 1980).

The most widely used extended temperature-index approach was proposed by Hock (1999), accounting for incoming potential radiation of differently exposed (aspect, slope), regularly spaced grid cells (Huss et al., 2008; Kling and Gupta, 2009; Koboltschnig et al., 2009; Magnusson et al., 2011; Kobierska et al., 2011). This approach has been shown to give good results at the catchment scale, in particular for sub-daily and spatially distributed simulations of snowmelt (Hock, 1999; Jost et al., 2007; Konz et al., 2007).

This approach, which we call hereafter the “Hock method”, has, however, several shortcomings: First of all, studies have highlighted that it is oversensitive to temperature variations (Pellicciotti et al., 2005; Viviroli et al., 2009). Secondly, while being almost universally applicable given the wide-spread availability of digital terrain models (DEM), it does not account for actual incoming radiation, i.e. actual weather conditions. It might be argued that the method mimics diurnal melt cycles disconnected from real variations of the melt-temperature relation. Finally,

the melt method is solved on a finely discretized scale to account for the spatial heterogeneity of terrain slopes and aspects; the resulting snowmelt at a fine grid-scale is often averaged over some coarser areal units to provide melt input to (semi-)lumped hydrological models that are set up for practical applications (Viviroli et al., 2009). This “up-scaling” smoothes the simulated spatial variability of snowmelt and the net effect of including high spatial details in the snowmelt routine on the simulated catchment discharge is not trivial to quantify.

This work proposes a new, time-variable melt method based on the classical degree-day method to overcome these shortcomings. The new method uses observed or interpolated daily temperature extremes to impose a diurnal cycle on the melt rates at the scale of the precipitation-runoff transformation model (i.e. each subcatchment has its specific melt rates). To assess the performance of this new, time-variable degree-day method and to compare it to the classical degree-day method and the Hock method, analyses on three scales are conducted as listed below.

1. Initially, the classical degree-day (CD) and time-variable degree-day (TD) methods are compared on a point scale by comparing observed snowmelt lysimeter outflow and simulated snowpack outflow. This analysis provides a general idea of the performance of the TD method at a point location.
2. The CD, TD and Hock methods are subsequently tested with a distributed point dataset to compare the melt model performance in terms of melt simulated over a certain melt period. The purpose of the distributed point analysis is two-fold: a) to understand how well the widely-used Hock method ‘mimics’ the effect of real (and not potential) radiation on snowmelt and b) to test whether the models show a performance difference depending on the dominant aspect of the locations of temperature observations (which should help to elucidate the question whether the relationship between snowmelt and temperature is stronger for certain aspects).
3. Finally, the methods are compared on a catchment-scale analysis with the spatially-explicit model of the hydrologic response described in Chapter 2 Section 2.5 of this thesis. This analysis assesses the performances of the melt models in terms of catchment-scale hydrology, which is a commonly accepted method to evaluate the performance of snowmelt routines (see namely Brubaker et al., 1996; Hock, 1999, 2003).

The ultimate goal of the steps of this approach is to demonstrate the performance of the TD method, which has been developed to capture sub-daily melt fluctuations for a range of data-constrained, minimalist hydrological models which are typically used for real-world applications. This work has been prioritized due to the difficulty in quantifying the water stored in the snow layer or Snow Water Equivalent (SWE) for Alpine catchment modeling. In the particular case of the Swiss Alps, the average water stored in the form of snow in catchments is not easily related to SWE measurements. This is due to three factors: 1) Switzerland has limited monitoring infrastructure with regards to SWE sampling. A total of 42 stations measure

SWE every 14 days in Switzerland. 2) Snow cover distribution is temporally and spatially highly variable in Alpine regions. 3) Existing gridded SWE data over Europe, which uses SWE and snow depth measurements along with remotely sensed snow-cover area (SCA) data (Hüsler et al., 2012), is more representative of flatter terrain over Switzerland. In fact, it is quite difficult to regionalize SWE and to update the states of gridded SWE data when measurements are limiting. Due to these factors, a properly calibrated snowmelt scheme is assumed here to be the best approach to provide catchment-representative distributions of snowmelt contributions in this Alpine study region.

A review of the datasets in this study is provided in Section 5.2 of this Chapter while the modeling approaches and experimental set-up are detailed in Section 5.3 and 5.4 respectively. Results, in Section 5.5, compare the temperature-index approaches in terms of whether the methods properly reflect actual melt conditions. This Chapter concludes with a summary of the findings in Section 5.6.

5.2 Data and study catchment

5.2.1 Point scale analysis

The Cotton Creek Experimental Watershed (CCEW) catchment is a study site used to examine the impact of forest harvesting on peak flows in montane catchments. As spring snowmelt dominates the hydrology, frequent, distributed snow measurements have been collected in order to analyze the spatial and temporal variability of melt. Data for the point scale analysis were utilized from two sites in the CCEW. Hourly precipitation is from the Cotton Upper climate station (CIU, 1780 m a.s.l), and hourly air temperature and snowmelt lysimeter outflow are from a hillslope monitoring site (Site 6003, 1652 m a.s.l.) located approximately 1500 m north of CIU (Jost et al., 2012). Periodic snow depth measurements from the spring snowmelt seasons of 2007 and 2008 are used to calibrate and validate the melt model's snow height predictions, respectively. The hourly snowmelt lysimeter data permit testing of the sub-daily dynamics for the CD and TD melt methods. Further details of the dataset are available in Smith (2011) and in Jost et al. (2012).

5.2.2 Distributed point and catchment analysis

Data for the distributed and catchment-scale studies were obtained from a high resolution, wireless sensor network installed in June 2009 in the Dranse de Ferret catchment located in the Valais region. This catchment is part of the larger watershed, the Dranse, described in Section 2.2 of this thesis (Figure 5.1).

Data were collected at 1 min intervals between June and October 2009 and are accessible in real time on the internet (www.climaps.com). Prior to June, snow accumulations and the risk of avalanche made the transport and installation of the meteorological stations impossible. For

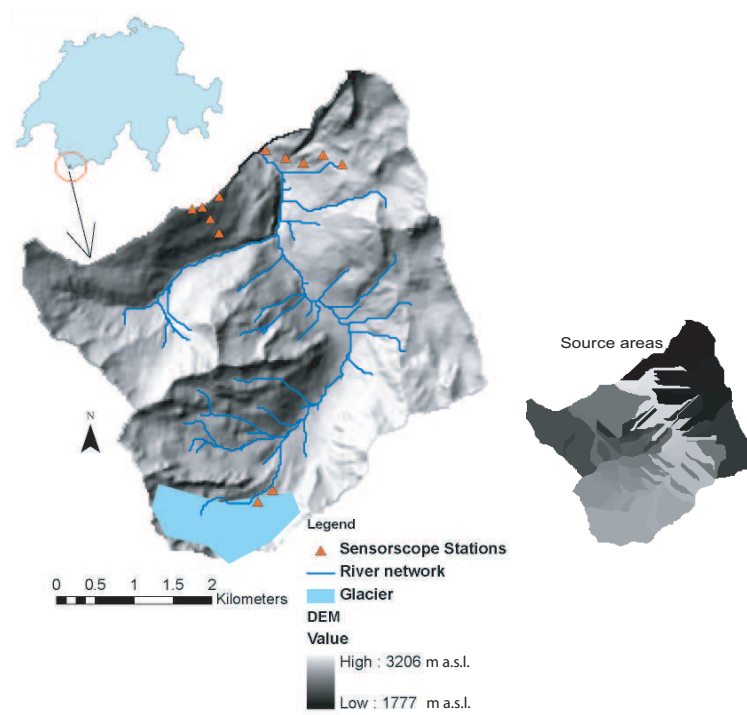


Figure 5.1: Map of the Dranse de Ferret catchment indicating locations of Sensorscope meteorological stations, the glacier, and the river network generated based on the digital elevation model (25 m resolution) indicated in gray shades. Top inset: location of this catchment within Switzerland; bottom inset: location of source areas.

Chapter 5. Improving the degree-day method for sub-daily melt simulations

the 2009 field campaign, the wireless sensor network consisted of 12 “Sensorscope” stations. Two of the 10 stations were located on the glacier (see Figure 5.1) which collected data between September and mid-October (due to installation challenges). For this analysis, the stations located on the glacier were not utilized due to the short time span of the data and since the data could not be obtained during the melting season (notably April through the beginning of July for this region).

The “Sensorscope” technology (Ingelrest et al., 2010) measures various meteorological data, including: air temperature at 1.5 m above ground, precipitation, incoming shortwave radiation, skin temperature, humidity, wind speed and wind direction as well as soil moisture, soil temperature and suction. Profiles of the temperature and radiation measured at one station can be seen in Figures 5.2. For further technical details on measuring devices used, please refer to (Nadeau et al., 2009; Simoni et al., 2011).

It should be noted that temperature measurements from passively ventilated sensors (such as those used in this wireless sensor network field campaign) have an inherent bias due to heating of the radiation shield (e.g. Huwald et al., 2009). However, in this study the temperatures could not be corrected as proposed in (Huwald et al., 2009) due to a lack of reflected shortwave radiation measurements and the wide range of albedo observed at the different stations.

For the distributed point data analysis, temperature, precipitation and radiation data are used from the 10 non-glacier stations located in two groups to test the performances of the CD, TD and Hock melt methods. Each group is composed of 5 stations and located on either the southeast or southwest face of the region. The stations are located at elevations ranging between 1780 and 2300 m on the southwest-facing slope and between 2160 and 2430 m on the southeast-facing slope. Compared to previous research conducted at the site scale (Kustas et al., 1994; Jost et al., 2007) with distributed measurements (Cazorzi and DallaFontana, 1996; Pellicciotti et al., 2005; Zappa et al., 2003; Bavay et al., 2009), the locations of the meteorological stations offer a unique opportunity to compare the melt method performances relative to temperature measurements from differing aspects.

The mean positioning of the groups is different where the southeast facing group is more south-facing than the southwest facing group (Simoni et al., 2011). In effect, incoming shortwave radiation values were recorded to be approximately 8 W m^{-2} higher for the southeast facing group throughout the 5 month field experiment and, the groups, separated by approximately 1 km, do not show well correlated temperature lapse rates. For the southeast facing stations, the mean hourly lapse rate over the experimental period was $-0.0075 \text{ }^{\circ}\text{C m}^{-1}$ whereas the mean hourly lapse rate for the southwest facing stations was $-0.0054 \text{ }^{\circ}\text{C m}^{-1}$. Within such an Alpine environment, the spatial distribution of surface temperatures is strongly influenced by the complex topography and related effects on the energy balance (e.g., local wind systems, differences in expositions and shading). These effects cannot be captured by a simple temperature lapse rate. For the purpose of this study, it is nevertheless assumed that the contrasting lapse rates between the two groups of measurement stations reflect differences

in the radiation balance that are likely to influence snowmelt rates.

For the catchment-scale analysis, the same meteorological variables from the 10 stations are used to test the performances of the three melt methods, however, these data were spatially distributed throughout the catchment using interpolation (see Experimental Set-up Section 5.4). The Dranse de Ferret catchment site has a total surface area of 21 km². The altitude ranges between 1775 m and 3206 m a.s.l. and the catchment is drained by the Dranse de Ferret river. The Dranse de Ferret catchment has steep slopes and is surrounded by high mountains (e.g. the nearby Grand St. Bernard pass, 2500 m a.s.l.). Approximately 5% of the catchment area is covered by glacier. Due to the high mountainous location of the catchment, the climatic regime is particular; annual rainfall in this region can locally exceed 2 m y⁻¹ and discharge peaks in the spring due to snowmelt.

Water level data are available from a flow meter constructed at the outlet of the catchment. The stage-discharge curve was obtained with the salt dilution method (Simoni et al., 2011). The resulting discharge profile can be seen in Figure 5.3. Analysis of the discharge from this dataset was originally conducted by Simoni et al. (2011), where the contributions of glacier melt, snowmelt, rainfall-runoff and baseflow to the discharge time series were detailed. Once the baseflow is subtracted, snowmelt composes approximately 85% of the remaining discharge volume, whereas glacier melt comprises less than 10%. Due to its small impact on the discharge signal, this study has neglected glacier melt in the calibration of the hydrological model.

5.3 Modeling approaches

Simulation of snowmelt-induced hydrologic processes requires a suite of modeling steps: i) characterization of solid and liquid water input to the system (rainfall, snowfall), ii) modeling of the snowpack evolution, its solid and liquid water content (resulting from rainfall, snowmelt and refreezing) and water outflow from the snowpack, in addition to iii) transformation of the so-called equivalent precipitation (total water outflow from the snowpack plus rainfall on snow-free ground) to river discharge. In the context of this paper, the focus is on the newly proposed snowmelt algorithm, the TD method; for all other modeling steps, only the essential details are presented.

5.3.1 Aggregation state of precipitation

The partitioning of precipitation into snow- and rainfall is described in Section 2.4.2 of this thesis.

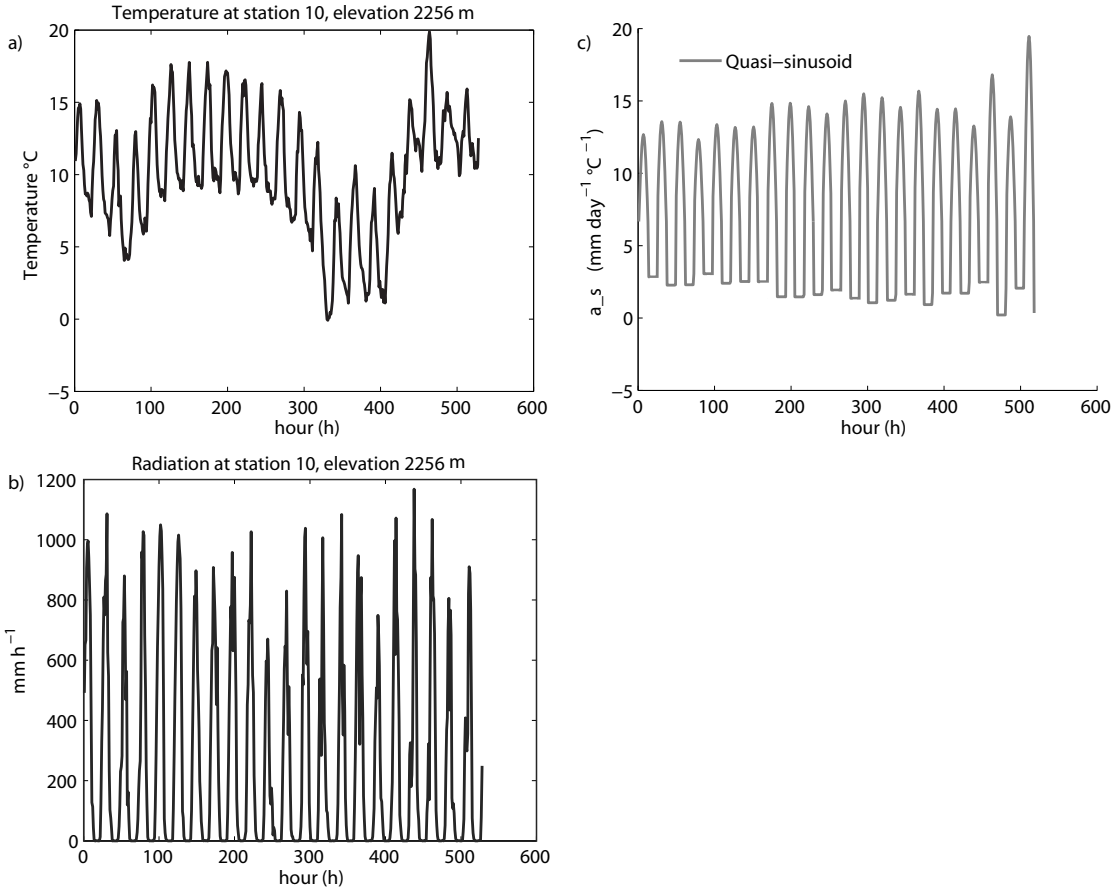


Figure 5.2: a) Measured temperature and b) measured radiation at station 10 (elevation 2256 m) during the simulation period used in the distributed point and catchment-scale analyses. c) a_s as a function of time, illustrating the quasi-sinusoidal function of Equation 5.3.

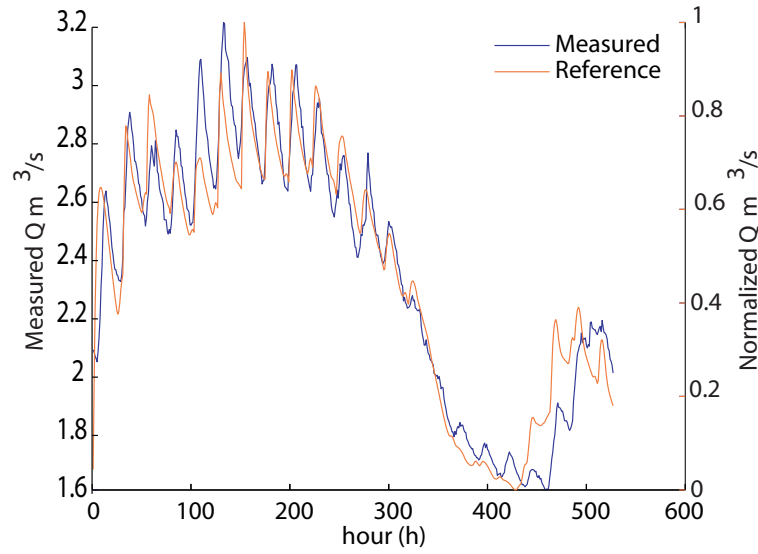


Figure 5.3: Catchment-scale analysis: left) measured discharge Q ($m^3 s^{-1}$), right) normalized measured and reference discharge Q ($m^3 s^{-1}$)

5.3.2 Snowmelt and refreezing

Three snowmelt methods, based on the temperature-index concept, are analyzed in this study: 1) the classical degree-day method with a constant degree-day factor (the CD method), 2) the well-known method proposed by Hock (1999), called the Hock method hereafter, and 3) the new approach with a degree-day factor that varies within the day (the TD method).

The constant degree-day method, the simplest temperature-index snowmelt method, is based on the assumption that melt rates depend solely on air temperature (Rango and Martinec, 1995). According to this formulation, the rate of snowmelt, at location \mathbf{x} and at time t , $M(\mathbf{x}, t)$, (mm h^{-1}) is given by:

$$M(\mathbf{x}, t) = \begin{cases} \frac{a_c(T(\mathbf{x}, t) - T_0)}{n} & T(\mathbf{x}, t) > T_0 \\ 0 & T(\mathbf{x}, t) \leq T_0 \end{cases} \quad (5.1)$$

where $T(\mathbf{x}, t)$ is the air temperature at a location \mathbf{x} at time t (h), T_0 is the constant threshold temperature above which melt occurs (here assumed to be 0°C), a_c ($\text{mm day}^{-1} \text{ }^\circ\text{C}^{-1}$) is the constant degree-day factor and $1/n$ is the time-step conversion factor with $n = 24$ (h/d). a_c represents the rate of snowmelt corresponding to one degree of positive temperature during one day.

In the Hock method, the above basic melt equation is modified to account for the local

estimate of potential (clear-sky) incoming solar radiation I_{pot} (W m^{-2}) in the form:

$$M(\mathbf{x}, t) = \begin{cases} \left(\frac{1}{n} a_i + \rho_i I_{pot}(\mathbf{x}, t)\right)(T(\mathbf{x}, t) - T_0) & T(\mathbf{x}, t) > T_0 \\ 0 & T(\mathbf{x}, t) \leq T_0 \end{cases} \quad (5.2)$$

where a_i is the melt factor ($\text{mm day}^{-1} \text{ } ^\circ\text{C}^{-1}$) and ρ_i is a radiation coefficient for snow ($\text{m}^2 \text{ W}^{-1} \text{ mm h}^{-1} \text{ } ^\circ\text{C}^{-1}$). Clear-sky incoming potential solar radiation (I_{pot}) is simply inferred from geographic location (latitude) and topography (shading, local slope, aspect and elevation). According to Hock (1999), the empirical snowmelt model parameter, ρ_i , has been fixed in this study to $0.6 \cdot 10^{-3}$ ($\text{m}^2 \text{ W}^{-1} \text{ mm h}^{-1} \text{ } ^\circ\text{C}^{-1}$). Note that a_i is usually called melt factor rather than degree-day factor to avoid confusion between the methods. In the remainder of this paper, the generic term degree-factor will be used for both a_c and a_i .

A modified version of the CD method is herein proposed. In this case the degree-day factor is allowed to vary throughout the day, to account for the actual distribution of snowmelt rates in time, which peaks at the hours of maximum incident radiation and falls to a minimum during the night. We, thus, assume that the snowmelt rate follows the typically sinusoidal variation of radiation during the day and that it is constant during the night, i.e. we impose a quasi-sinusoidal function (Figure 5.2c) of time-variability on the degree-day factor. The amplitude of the degree-day factor's daily cycle variability cannot be directly related to actual radiation because this variable is rarely measured. We, therefore, assume that the daily temperature amplitude (difference between daily maximum and daily minimum temperature) is a good proxy of the amplitude of the daily cycle of incoming radiation and that it can efficiently discriminate between days when there is a strong within-day variability of radiation (and thus of snowmelt rates) and days with a low variability.

This new time-variable degree-day factor a_s , which replaces the constant a_c in Eq. 5.1 can be written as:

$$a_s(t_d) = \begin{cases} a_c + \beta \Delta_T(d) \sin\left(\pi \frac{t_d - t_0}{t_1 - t_0}\right) & t_0 \leq t_d < t_1 \\ a_c - \beta \Delta_T Z & \text{otherwise} \end{cases} \quad (5.3)$$

where t_d (h) is the hour of the day d , t_0 (h) is the start time of daylight and t_1 (h) is the end of daylight on day d . a_c ($\text{mm day}^{-1} \text{ } ^\circ\text{C}^{-1}$) is the constant degree-day factor, $\Delta_T(d)$ ($^\circ\text{C}$) is the difference between the maximum and the minimum daily temperature on day d and β ($\text{mm day}^{-1} \text{ } ^\circ\text{C}^{-2}$) is a factor to convert the temperature amplitude into a degree-day factor amplitude which has to be calibrated (considering the constraint that a_s has to be positive for positive temperatures). Z (-) is a factor to ensure that the daily mean value of a_s equals a_c , i.e. that the integral of the sinusoidal function during the day time equals the integral of the constant value during the night, i.e.

$$Z = \frac{\int_{t_0}^{t_1} \sin\left(\pi \frac{t_d - t_0}{t_1 - t_0}\right) dt_d}{l_n} = 2 \frac{t_1 - t_0}{\pi l_n}, \quad (5.4)$$

where $l_n = 24 - t_1 + t_0$ (h) is the length of the night. Note that t_0 and t_1 could also be allowed to be a function of d rather than constant.

The snowmelt method resulting from applying Eq. 5.3 with a_s is called the time-variable degree-day method (TD). The resulting degree-day factor shows sub-daily fluctuations around a constant mean value; the amplitude of these fluctuations is proportional to the daily temperature amplitude, which accounts for cloudy or rainy days when incoming radiation decreases (Figure 5.4a and b). Note that there was a previous attempt to account for the within-day variability of temperature for snowmelt computation by Dunn and Colohan (1999), who considered only the fraction of the day when the temperature exceeded a critical threshold for melt rather than the mean daily temperature for daily melt computations.

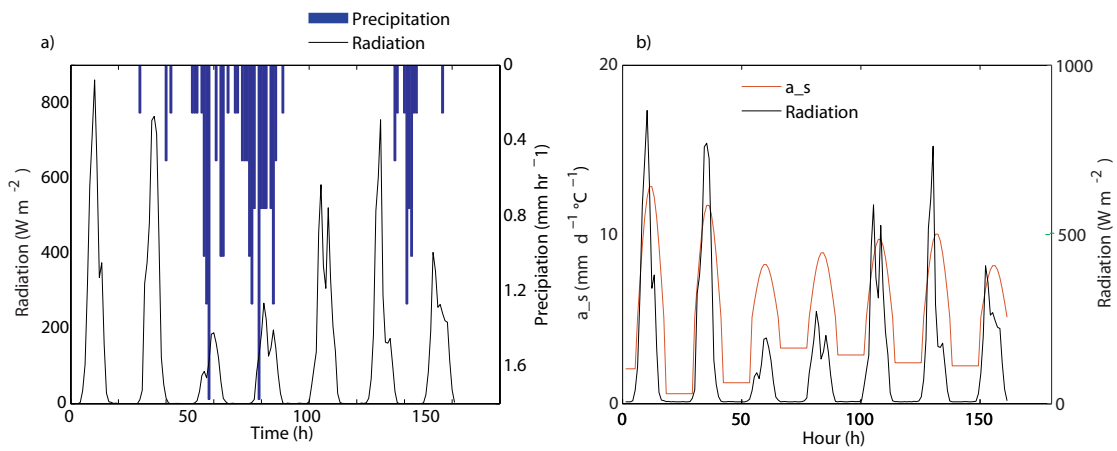


Figure 5.4: a) The measured radiation and precipitation time series averaged over all Sensescope stations during a rain event, b) the corresponding time series of the time-variable degree-day factor a_s

For hourly snowmelt simulations, refreezing during periods when the temperature drops below the critical threshold for melt has to be considered. For all melt methods analyzed, refreezing is calculated analog to melting:

$$F(\mathbf{x}, t) = \begin{cases} \frac{a_f(t)(T(\mathbf{x}, t) - T_0)}{n} & T(\mathbf{x}, t) \leq T_0 \\ 0 & T(\mathbf{x}, t) > T_0 \end{cases} \quad (5.5)$$

where a_f ($\text{mm day}^{-1} \text{ } ^\circ\text{C}^{-1}$) is the refreezing factor. This refreezing factor is often linearly related to the degree-day factor (Anderson, 1973) through a multiplicative factor a_r (–) to account for the fact that refreezing with negative temperatures is usually assumed to be lower than the corresponding melt rates with positive temperatures (but e.g. Bergstrom, 1975, assumes $a_r = 1$). Accordingly, $a_{f,x} = a_r a_x$ where $x = c, i, s$ stands for one of the three degree-day factors. The calibrated factor a_f is used in place of the degree-day factors when the temperatures fall below or equal to the threshold temperature T_0 . The melt equations defined by $M(\mathbf{x}, t)$ are replaced by the freezing equation $F(\mathbf{x}, t)$ in this case.

Melt generated by the TD method and the Hock method are distributed in space and time. (The CD method is assumed constant in time and space.) The Hock method is defined on a pixel basis due to its use of solar positioning data and a digital terrain model. Melt per pixel from the Hock method is summed on a subcatchment basis for use in the hydrological model. The TD method is distributed in time and space with the time-varying quasi-sinusoidal function defined by the temperature extremes in each subcatchment, thereby remaining constant in each subcatchment.

Snowpack evolution

The evolution of the solid and the liquid water content (in terms of snow water equivalent) of the snowpack is simulated separately with the same equations defined in Section 2.4.2 of this thesis. The solid store has as input snowfall and as output, snowmelt; the liquid store has as inputs, snowmelt and rainfall, and as outputs, snowpack outflow and refreezing (see Hingray et al., 2010); the routine is very similar to the snowmelt routine of the well-know HBV model, (Bergstrom, 1975).

5.3.3 Spatially-explicit hydrological model

For the catchment-scale analysis, the spatially-explicit hydrological model described in Section 2.5 of this thesis is used to integrate the melt methods. With this model, the snowpack outflow together with rainfall on snow-free catchment parts (the so-called equivalent precipitation) is transformed into river discharge, based on the formulation of transport by travel time distributions (Rodriguez-Iturbe and Valdés, 1979; Gupta et al., 1980; Rodriguez-Iturbe and Rinaldo, 1997).

In such a spatially-explicit model, the hydrologic response of a water input event (rainfall or water outflow from the snowpack) is determined by the set of flow paths that are activated by the spatial input pattern and by the volume of water traveling through the individual paths relative to the total water input to the catchment.

5.4 Experimental set-up

5.4.1 Point scale analysis

The performance of the proposed TD method is compared against the CD method for the point scale dataset from the CCEW CIU station (Jost et al., 2012). Both models are calibrated on the spring melt seasons so that the simulated snowpack outflow reproduces as closely as possible the observed snowmelt lysimeter outflow (the calibration criterion is the sum-of-squared-errors, SSE). The TD method has 4 parameters to calibrate (a_s , β , a_r , θ_{cr}) while the CD method has 3 parameters to calibrate (a_c , a_r , θ_{cr}). The Hock method will not be compared for the single point analysis because its performance has been demonstrated elsewhere (Kling

et al., 2006; Viviroli et al., 2009) and assessing its performance against the new TD method is relevant only for distributed melt simulations (for which the method has been developed). Data from the 2007 hydrological year (Nov 2007 to Oct 2008) are used for calibration and data from the 2008 hydrological year are used for validation.

5.4.2 Distributed point analysis

The objective of the distributed point analysis is to investigate how the CD, TD and Hock methods emulate the temporal evolution of available melt energy as a function of hourly temperature and, in the case of the Hock method, as a function of potential radiation and temperature. To assess the behavior of the three methods, the potential melt that would be obtained with each method if the available snow was not limiting, is compared against a reference potential melt series. This reference series is compiled by applying Eq. 5.2 with a_c equal to 3 (mm day⁻¹ °C⁻¹) (which is an average value for such environments, e.g. Hock, 2003; Pellicciotti et al., 2005) using actual observed radiation at all the meteorological stations. The reference melt is then averaged over the stations.

To investigate how the methods perform for different dominant expositions, three different experiments are conducted: Experiment 1 includes all meteorological stations; Experiment 2 includes only the southwest facing stations; and Experiment 3, only the southeast facing stations. Given that the CD, TD and the Hock methods do not consider actual radiation, they do not simulate the same amount of potential melt as the reference simulation if run with the same degree-day factor (3 mm day⁻¹ °C⁻¹). To obtain a meaningful comparison between the temporal evolution of the different potential melt simulations, the parameters of the CD, TD and Hock methods are, thus, calibrated such as to fit as closely as possible the reference simulation (the calibration criterion is the SSE). The CD method has 1 parameter to calibrate (a_c), the TD method has 2 parameters to calibrate (a_c , β) and the Hock method has 1 parameter to calibrate (a_i) (refreezing factors are not applicable due to the high temperatures during the simulation period). The performance of the three melt methods with respect to the reference simulation is evaluated, for each experiment, by comparing the simulated, potential cumulated snowmelt and the reference potential cumulated snowmelt.

5.4.3 Catchment-scale analysis

Input interpolation

Spatial interpolation of ground temperature and precipitation measurements is performed through kriging with external drift (KED) (using elevation as auxiliary information) (Goovaerts, 1997). Previous studies in similar environments have shown the adequacy of regression-based approaches (see Chapter 3 of this thesis), particularly when high-elevation station data are available to validate data (Goovaerts, 1999; Stahl et al., 2006; Tobin et al., 2011).

Data from the distributed meteorological stations in the two groups (southeast and southwest

Chapter 5. Improving the degree-day method for sub-daily melt simulations

facing) in the Dranse de Ferret catchment were initially analyzed to detect correlations between temperature and the measured meteorological variables between the groups. Temperature distributions along the vertical direction for each group are controlled solely by elevation gradients in the study period; after removing the elevation effect, all the stations show a mean temperature of 13 °C at the reference elevation of 1780 m a.s.l. In effect, the use of elevation as the external drift factor for the KED interpolation seems fully justified.

The radiation is spatially distributed as follows: first, the potential radiation for each DEM grid cell is computed according to the method proposed by Hock (1999), which is based on topography (local aspect and slope), solar positioning and geographic location; subsequently, these values are rescaled (at an hourly time step) to match the incoming shortwave radiation measured at the stations (see as an example, Figure 5.5). This rescaling procedure takes into account the effect of cloudiness (which decreases the incoming solar radiation) while preserving, however, the spatial structure of the incoming radiation field.

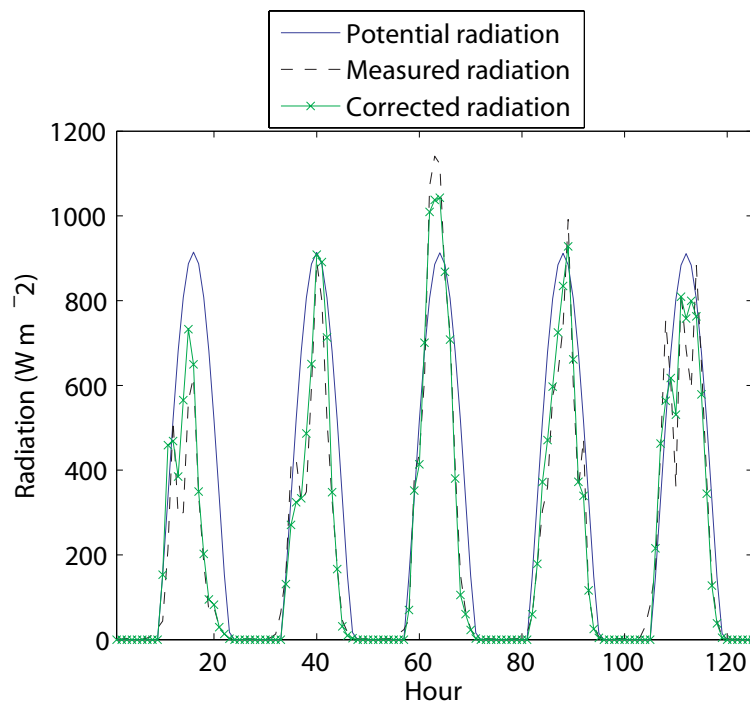


Figure 5.5: Mean measured, potential and corrected potential radiation for all 10 non-glacier Sensorscope stations.

Initial conditions

A distributed, initial snow height is determined based on a theoretical snowpack model that gives the annual evolution of the snowpack as a function of the mean annual values of temperature and precipitation and their seasonality and uses a CD snowmelt formulation (Woods, 2009). Such a simple model distributes the mean snow height for a given time of year

as a function of altitude (by simply distributing the mean annual temperature as a function of altitude). In the context of the present study that analyzes simplified snowmelt models, such a rough estimate of how snow height at the start of the modeling period (June) might vary with altitude is assumed to be sufficient. For more comprehensive methods to calculate the gradient of snow depth with elevation see (Gruenewald and Lehning, 2011; Lehning et al., 2011). The resulting initial snow heights have a minimum of 355 mm (water equivalent, w.e.) for the lowest source area at a mean altitude of 1,890 m asl and a maximum of 1.2 m w.e. for the highest source area at a mean altitude of 2,745 m asl.

This initial snowpack height is imposed in order to simulate an early stage of the melt period when there is still a significant influence of the snowpack contributing to runoff. This approach is used to demonstrate the evolution of the snowpack from the beginning of the spring melt season (rather than at the time of observations, June through October). The retained initial snow distribution can be assumed to reasonably reflect what could have prevailed earlier in the melt season; this assumption is supported by the findings of Simoni et al. (2011), which indicated that the snowmelt stemmed from well-distributed source areas and was a dominant discharge component.

5.4.4 Hydrological model set-up

A total of 89 source areas were identified for the Dranse de Ferret catchment (see inset of Figure 5.1). Based on the spatial input fields, each subcatchment was assigned an area-average precipitation time series and a temperature time series. To compare the performance of the melt methods at the catchment-scale, each of the methods were combined with the precipitation-runoff model described in Section 2.5 of this thesis. For each model, the parameters were calibrated such that the simulated discharge follows as closely as possible the reference discharge (see details hereafter).

The reference discharge series for such a calibration is usually observed discharge; for our particular case study, however, we could not use observed discharge directly because spring discharge measurements could not be collected given the risk of avalanche at the experimental catchment. We, thus, generated a reference discharge time series for comparison purposes as follows: The distributed temperatures and precipitation fields, the previously discussed initial snow heights and the distributed, corrected radiation field (see Section 5.4.3) were used as inputs. A parameter set was then selected (within a literature-based prior range, see Table 5.1) based on its ability to provide reasonable temporal discharge dynamics. The actual observed discharge, while being on a different scale due to lower initial snow heights, was assumed to accurately describe the actual dynamics of the discharge in terms of the coefficient of variation (CV) (hourly discharge variance divided by the hourly mean). Accordingly, the parameter set was chosen such that the CV of the simulated discharge was as close as possible to the CV of the observed discharge. The observed discharge CV is 0.6 and the selected parameter set (see Table 5.1 provides a discharge with a CV of 0.64 (-).

Chapter 5. Improving the degree-day method for sub-daily melt simulations

Table 5.1: Reference hydrological model parameters for Monte Carlo simulation. Note that for the catchment-scale analysis, all temperatures were always positive (i.e. no refreezing occurred)

Soil Model		
	<i>Value</i>	<i>unit</i>
Porosity, η	0.5	[-]
Active soil layer depth, Z_r	300	mm
Soil moisture threshold, s_*	0.3	[-]
Soil moisture at wilting point, s_w	0.05	[-]
Saturated hydraulic conductivity, k_{sat}	20	mm h ⁻¹
Clapp and Hornberger exponent, c	12.8	[-]
Initial soil moisture, s_o	0.45	[-]
Routing Model		
Surface discharge residence time	2	h
Subsurface discharge residence time	20	h
Wave celerity	1	m s ⁻¹
Dispersion coefficient	1000	m ² s ⁻¹

As shown in Figure 5.3, the corresponding reference simulation shows a dynamic very similar to the observed discharge, in terms of daily discharge cycles and a decreasing amplitude towards the end of the melt period, which is typical for high mountainous spring snow discharge (Herrmann and Rau, 1984). In addition to this reference simulation, we also retained a range of plausible simulations by using Monte Carlo analysis to randomly generate a high number of parameter sets from a uniform distribution spanning the prior parameter range. These additional plausible simulations were selected by retaining the 50 simulations that most closely match the reference series (based on the SSE). These simulations show a range of possible discharge behaviors around the reference discharge time series (see light red shaded regions around the reference series in Figure 5.6).

Once this reference series was established, we calibrated the parameters of the three models (i.e., the combination of CD, TD and Hock melt methods with the precipitation-runoff model) on the reference series using again a Monte Carlo analysis. The resulting discharge profiles were compared to the reference time series. Acceptable simulations were chosen based on two performance indicators: 1) the Nash-Sutcliffe efficiency, NSE, (Nash and Sutcliffe, 1970) and 2) the percentage of time steps, %TimeBound where the simulated discharge falls into the range of plausible reference simulations (see performance indicators in Figures 5.6 and 5.7). Again, rather than retaining a single best parameter set, we retained 50 sets that have a $NSE \geq 0.7$ and $\%TimeBound \geq 80\%$. This provided a range of behavior for the discharge simulation (see Figure 5.6). Through this Monte Carlo calibration procedure, we ensure that the melt methods work with an ensemble of parameter sets which yield reasonable sub-daily discharge variability.

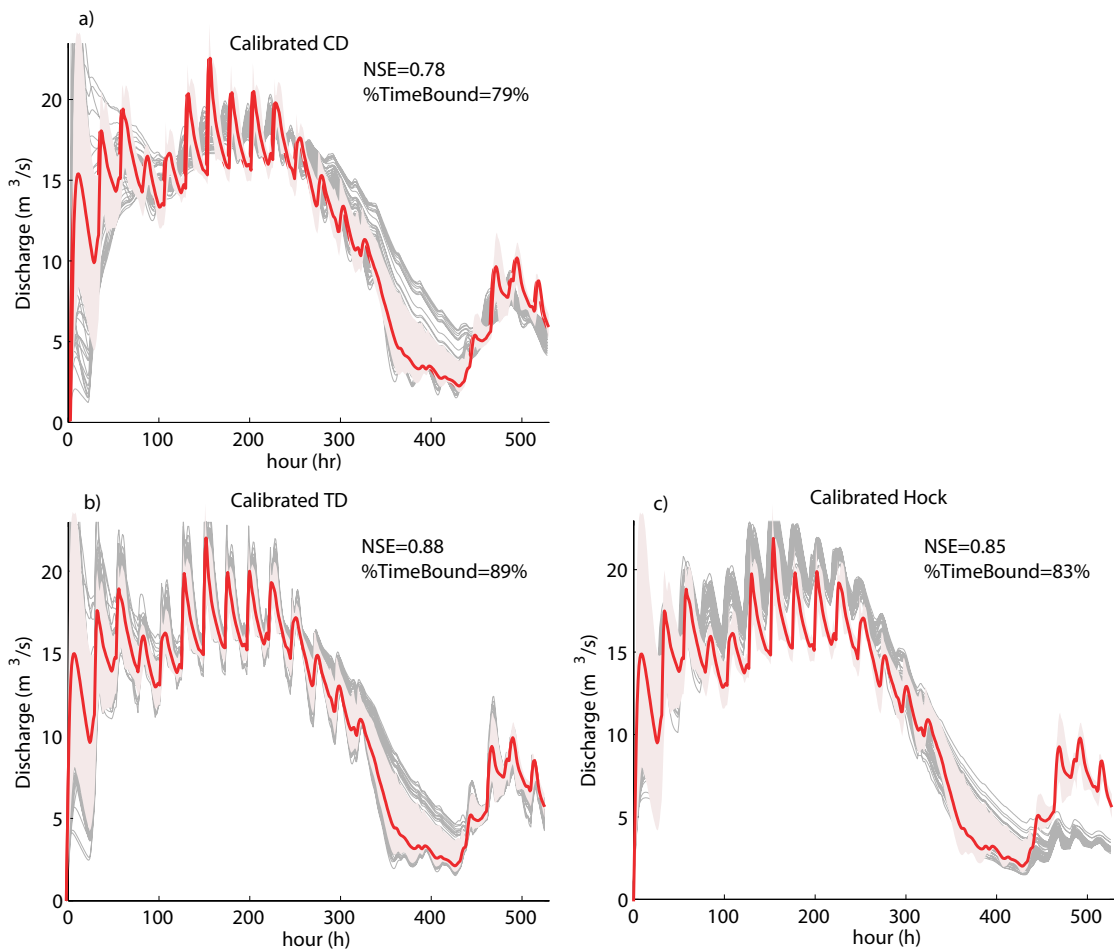


Figure 5.6: Catchment scale analysis: The reference (red) with plausibility range (rose) and simulated discharges (grey) for case study 1 (all 10 stations) for a) the calibrated CD method, b) the calibrated TD method and c) the calibrated Hock method. Discharge time series that have a $\text{NSE} \geq 0.7$ and $\geq 80\%$ of time steps which fall into the range of plausible reference simulations (except for a) are shown. Best parameter sets gave the following NSE and %TimeBound respectively: a) 0.78, 79% a) 0.88, 89% and b) 0.85, 83%.

Chapter 5. Improving the degree-day method for sub-daily melt simulations

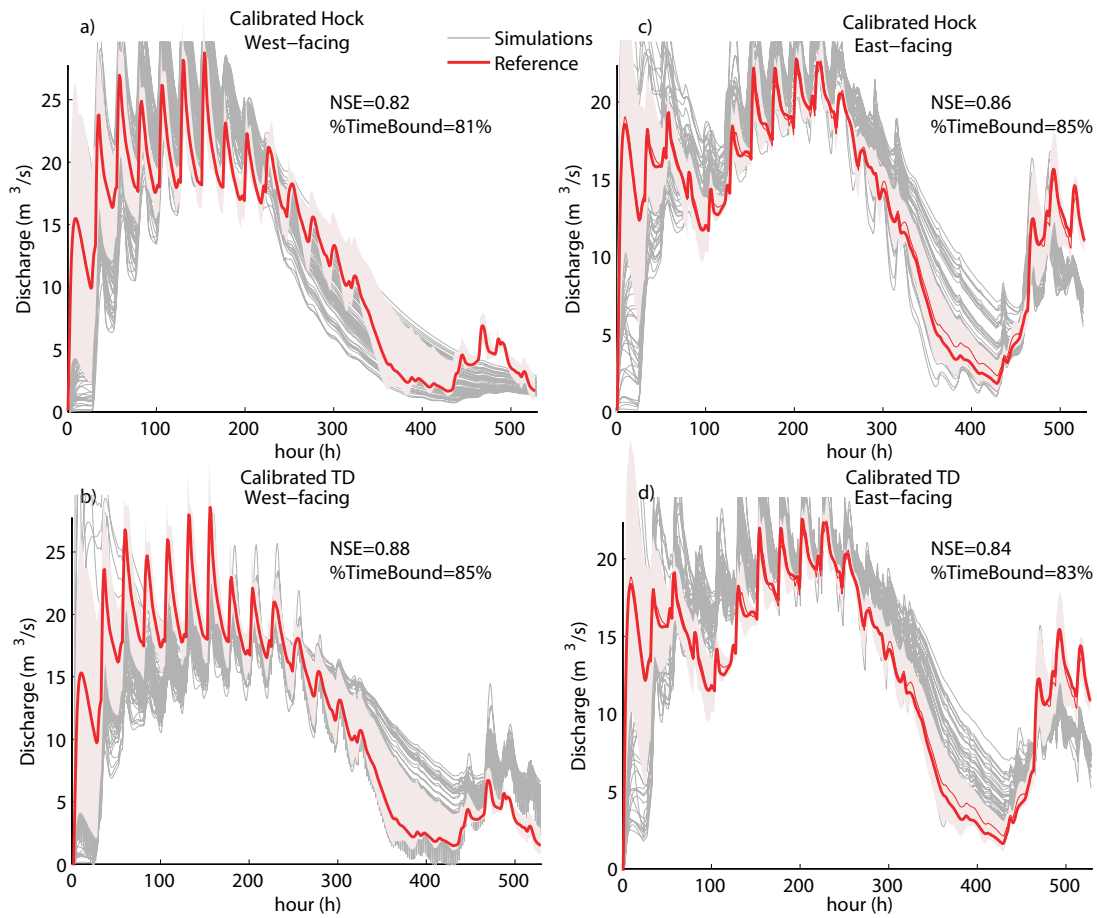


Figure 5.7: Catchment scale analysis: The reference (red) with plausibility range (rose) and simulated discharges (grey) for case studies 2 and 3 (5 stations in either group): a) the calibrated Hock method for west-facing stations, b) the calibrated TD method for west-facing stations, c) the calibrated Hock method for east-facing stations and d) the calibrated TD method for east-facing stations. Simulated discharge time series that have a NSE index ≥ 0.7 and $\geq 80\%$ percent of time steps which fall into the range of plausible reference simulations are shown. Best parameter sets gave the following NSE indices and percentage of time steps respectively: a) 0.82, 81% b) 0.88, 85% c) 0.86, 85% and d) 0.84, 83%.

Similar to the distributed point analysis (comparing potential melt), the above procedure is repeated with three numerical experiments to assess the impact of temperature distributions on the ability of the different snowmelt methods to approximate the reference discharge time series. Each of the experiments corresponds to a different scenario of measured temperature inputs: Experiment 1) the whole dataset; Experiment 2) only stations belonging to the south-west facing group; and Experiment 3) only southeast facing stations. The reference series generation procedure and the ensuing model calibration process yield for each experiment, i) a reference series and its plausible range and ii) 3 ensembles of acceptable simulations corresponding to each of the 3 precipitation-discharge models.

5.5 Results and discussion

5.5.1 Point analysis of melt methods

The calibrated parameter values for the CD method are $a_c=3 \text{ mm day}^{-1} \text{ }^\circ\text{C}^{-1}$, $a_r=0.8$ (-) and $\theta_{cr}=0.025$ (-). For the TD method, the degree-day and refreezing factors are the same while $\theta_{cr}=0.015$ (-) and the calibrated amplitude factor β equals 0.18 (-). Figure 5.8 shows that the CD method cannot capture the strong, diurnal melt variations for either the calibration or validation case. The TD method performs slightly better for the 2007 event and significantly better for the 2008 validation event where most of the peaks are captured. If viewed alongside the temperature time series it is evident that the TD method is the most effective when there is a significant range in the daily maximum and minimum temperatures such as during the 2008 spring event. This result implies that when the temperature differences are greatest, the amplitudes imposed in the TD method are better able to mimic the effect of incoming radiation on snowmelt.

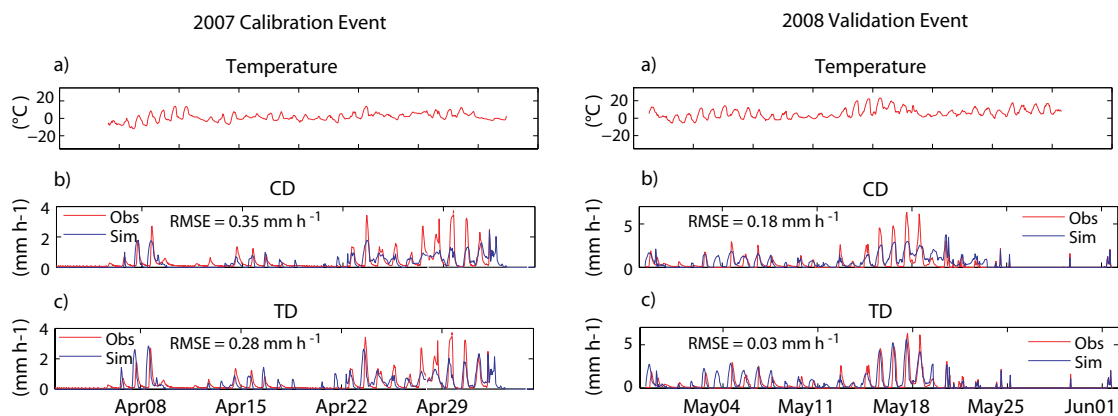


Figure 5.8: Point scale analysis (Cotton Creek): a) Temperature time series for the 2007 calibration event (left) and the 2008 validation event (right). Simulated versus measured snowpack outflow for b) the CD method and c) the TD method.

An important point to note for this analysis includes that the temperature drops frequently below zero (unlike the Dranse de Ferret catchment-scale analysis), so it was necessary to have

a proper calibration of the refreezing factor a_r . Overall, the point scale experiment shows that the proposed TD method represents a considerable improvement over the CD method without using any additional data, only at the cost of one additional calibration parameter.

Furthermore, using the CCEW dataset, a temperature sensitivity analysis was conducted to demonstrate the impact of non-ventilated temperature sensors on the TD and CD methods. Huwald et al. (2009) demonstrated a systematic bias with some temperature sensors due to trapping of heat in the temperature shield. The temperature error is proportional to the incoming shortwave radiation times albedo or the outgoing shortwave radiation. It is inversely proportional to the wind speed. The analysis demonstrated that a 2 °C bias in maximum daily temperatures on dry days impacts both the CD and TD methods by overestimating melt rates each time step where the temperature error has a stronger impact on the TD method. It is therefore recommended to use the TD method with ventilated temperature sensors, such as those used with standard meteorological service stations.

5.5.2 Distributed point melt analysis

Potential snowmelt is compared for the three different experiments of temperature distributions (Section 5.4.2). As previously mentioned, the 'reference' snowmelt is the melt that can be potentially produced with Eq. 5.2 with measured incoming radiation (instead of potential) at the given stations. In Experiment 1, using temperature observations from all stations, the potential melt for the CD, TD and Hock methods are compared with the reference melt series. If the degree-day factors are not calibrated, the Hock method clearly models the reference melt more accurately, as illustrated in Figure 5.9a showing the cumulated melt for all methods over the entire simulation period. This shows that overall, the Hock method simulates the potential melt that would be obtained with observed radiation quite well; in other words, the fact that the Hock method uses potential radiation does, for this experiment, not lead to large deviations from the reference.

Subsequently, the degree-day factors of all three methods are calibrated such as to produce exactly the same amount of potential melt as the reference series at the end of the entire observation period (Figure 5.9b). The potential melt generated by the calibrated Hock method is still closest to the reference series where the potential melt generated with the CD and the TD methods seems unable to follow the reference series. This result is due to the length of the observation period, including the very warm conditions in early summer. If only the early part of the observation period, which is effectively relevant for snowmelt, is considered (around 22 days), the CD and TD methods are able to reproduce the reference series as well as the Hock method (see the inset on Figure 5.9b). The coefficients of determination (R^2 values) of the potential melt generated by the Hock, the TD and the CD methods versus the reference melt are 0.9, 0.9 and 0.8 (-) respectively.

The results are similar for Experiments 2 and 3 (Figure 5.10) but with one important difference between the methods: for the CD and the TD method, the calibrated value of a_c remains

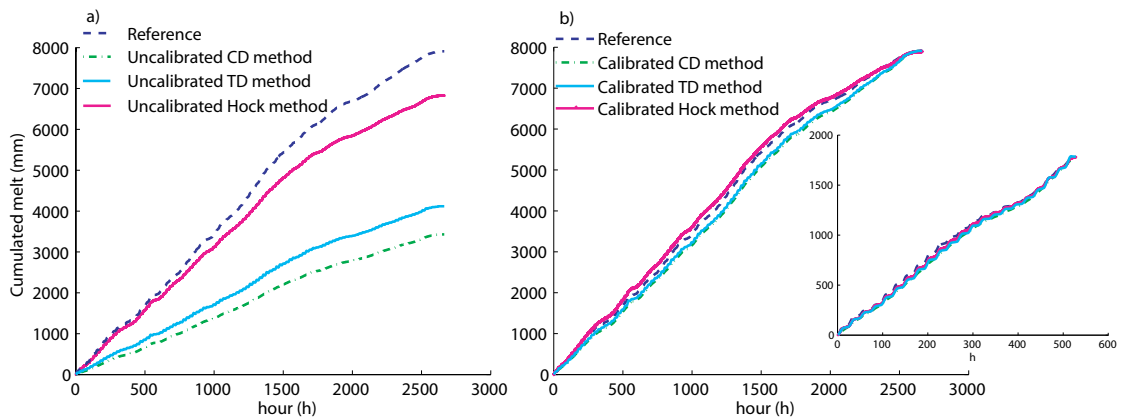


Figure 5.9: Distributed point analysis: a) The reference potential cumulated melt, the melt calculated by the uncalibrated CD, TD and Hock methods. b) Calibration of the CD, TD and Hock methods in terms of matching the reference potential melt series (cumulated over the entire observation period, 111 days). The inset shows the same result for calibration over the first 22 days.

constant throughout all experiments (at $6.9 \text{ (mm day}^{-1} \text{ }^{\circ}\text{C}^{-1})$) whereas for the Hock method, the calibrated degree-day factors are 7, 6.8 and 7.2 for Experiments 1, 2 and 3 respectively. The CD and TD methods are thereby more robust with a consistent degree-day factor for all temperature distributions. Conversely, the Hock method is highly sensitive to the dominant aspect of the meteorological observations since it requires different degree-day factors to reproduce the reference potential melt series from different station groups.

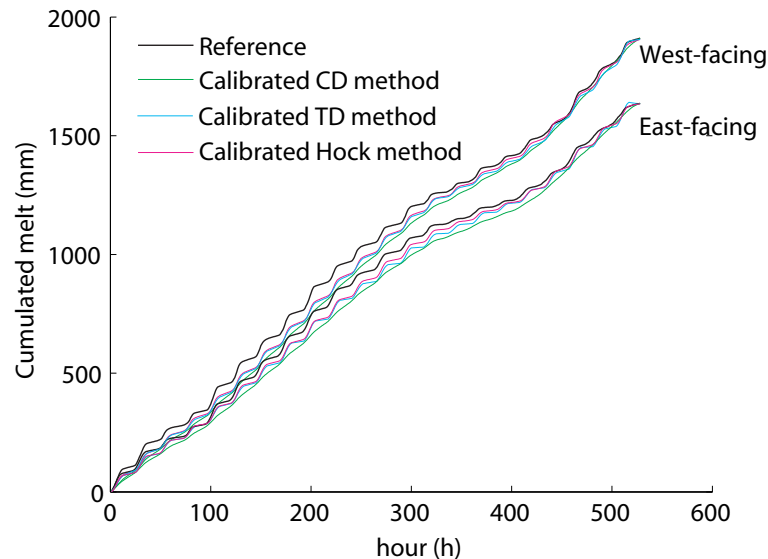


Figure 5.10: Distributed point analysis: Potential melt for either the southeast or southwest facing group simulated with the 3 methods and the reference series, cumulated over the first 22 days of the observation period.

Chapter 5. Improving the degree-day method for sub-daily melt simulations

Furthermore, for Experiments 2 and 3, the calibrated CD, TD and Hock methods demonstrate that there is a clear difference in potential melt when either station group is considered (i.e., southeast versus southwest). This result underlines the importance of having good estimates of spatial temperature variability (and namely of lapse rates) to produce good results with degree-day-based melt methods.

The sub-daily variability in simulated melt rates for all three methods is compared in Figure 5.11a, which shows for each day of the simulation period and for all methods, the daily mean melt and the maximum and minimum values (for Experiment 1). It can be seen that the daily mean values are quite close to the reference series for all three methods. The daily amplitude, however, is strongly underestimated by the CD method, which confirms the results of the single point analysis. Experiments 2 and 3 show similar results (not shown).

Figure 5.11b shows a comparison of the daily minimum and maximum melt for the TD method and the reference potential melt. The diurnal, time-varying degree-day factor of the TD method provides an improved means to capture the daily minimum and maximum values of the reference melt. Most significantly, this figure as well as the inset in Figure 5.9b showing cumulated melt over the 22-day measured melt period, demonstrate that imposing this variability causes the TD method to have a better fit to the reference melt in terms of diurnal pattern. RMSE (root mean square error) values are reduced by moving from the CD method to the TD method; the error for the daily maximum melt over the time series relative to the reference melt is reduced from 2.2 to 0.7 mm h⁻¹. Similarly, the RMSE for the minimum melt is reduced from 6.8 to 0.9 mm h⁻¹.

5.5.3 Catchment-scale analysis

Preliminary path probability analysis

To illustrate the effect of the source area delineation within the hydrological model, probabilities of flow paths from selected source areas generated by the reference simulation (see Section 5.4.4) were analyzed. Figure 5.12 depicts four examples of source areas with contrasting mean slopes, areas, elevations and aspects and their corresponding 'path probability', i.e. the probability that this source area is activated (through snowpack outflow and rainfall) as a function of time.

It can be seen that the path probability is influenced by the area, elevation, slope and aspect of the source area. Intuitively, the greater the source area is in size (Figures 5.12a and 5.12c), the longer this area has an impact on the equivalent precipitation (snowpack outflow and rainfall). Source areas at higher altitudes (Figure 5.12c) have a higher path probability later in the melt period, i.e. they have a higher probability to be activated later in the season, which simply results from the deeper snowpack at higher elevations. Similarly, melt from north-facing areas (Figures 5.12b) is activated later than melt in south-facing areas (Figures 5.12d) due to less frequent exposure to incoming radiation.

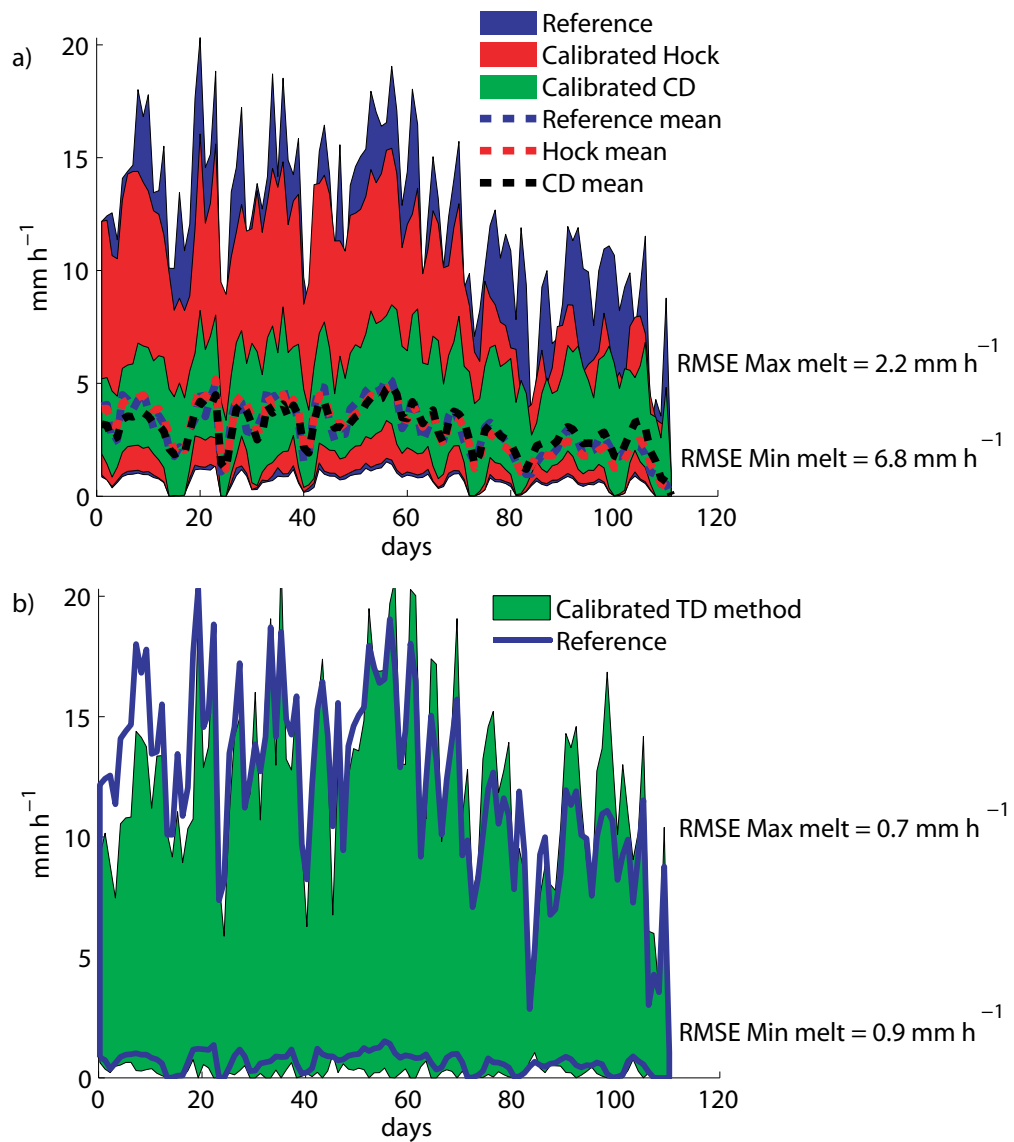


Figure 5.11: Distributed point analysis: a) Potential daily melt variability for the reference melt, the calibrated CD method and the calibrated Hock method. RMSE values compare the minimum and maximum daily melt between the CD and reference cases. Daily mean melt is indicated by the dashed lines. b) Ranges of daily minimum and maximum melt for the reference melt (blue line) and the calibrated TD method melt (shown in green). RMSE values compare the daily minimum and maximum melt between the TD and reference cases.

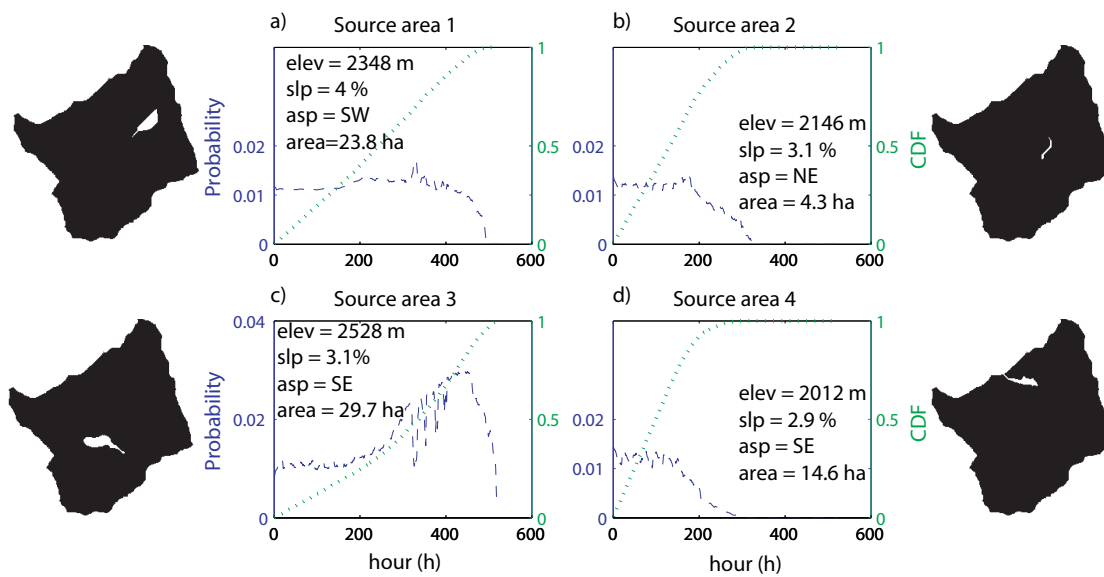


Figure 5.12: Time changing path probabilities, (i.e., the probability that the source area is activated through snowpack outflow and rainfall as a function of time) for specific source areas for the melt period considered. The locations of these source areas; their mean elevation (elev), slope (slp), area and aspect (asp) are given as insets. The cumulated distribution function is shown on the right y-axis.

Comparison of the melt methods

For the catchment-scale analysis, each of the three melt methods is used to generate the equivalent precipitation used in the hydrological model with either all meteorological stations (Experiment 1) or either the southeast or southwest facing groups as input data (Experiments 2 and 3 respectively). Hereafter, we first present an analysis of the spatial results, followed by an analysis of the discharge time series.

The differences in spatial melt are analyzed for the melt methods using a uniform snowpack input for visualization purposes for Experiment 1, after calibrating all parameters according to the method described in Section 5.4.4. Figure 5.13 shows all methods' distribution of snow heights after 200 hours of simulation and the snow height remaining after 200 hours as produced by the measured radiation (the reference melt series). It can be seen that, spatially, the CD and TD methods better capture the reference melt. The Hock method predicts more extreme melt rates throughout the catchment, which can be explained by this model's proven sensitivity to temperature extremes (Pellicciotti et al, 2005), which is evident on a pixel basis.

As already demonstrated in all previous analyses, the CD method cannot be calibrated such as to capture the sub-daily melt amplitudes of the reference discharge. The catchment-scale analysis confirms these results as depicted in Figure 5.6a where the CD simulated discharge times series appears to be smoother than the reference discharge (red solid line) and its plausibility range (light red shaded region). In contrast, with the calibrated TD method as well

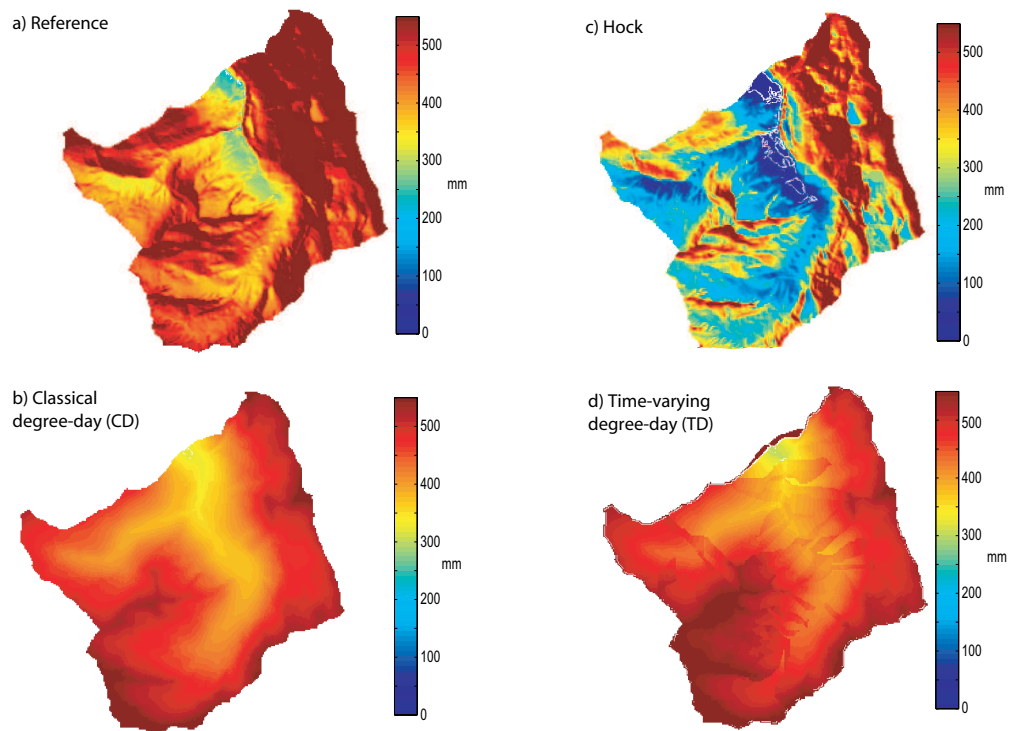


Figure 5.13: Distributed point analysis: distribution of snow heights (mm) from a uniform snowpack initialization after 200 hours of simulation for: a) the reference melt case, b) the calibrated CD method, c) the calibrated Hock method and d) the calibrated TD method.

as the calibrated Hock method, the reference series is very well captured (Figure 5.6b, c).

Overall, both the TD and Hock methods perform comparably well even if local differences are visible (e.g. the Hock method performs less well for the late rise of discharge but in exchange it captures better earlier peaks). However, in absolute terms, the TD method shows better Nash-Sutcliffe indices with respect to the reference discharge and a greater percentage of discharge simulations which fall into the range of plausible reference simulations (see performance indicators in Figure 5.6). It is important to note that the size of the Dranse de Ferret catchment is critical to note the strong diurnal fluctuations visible in Figure 5.3. If a larger catchment had been studied, this variability would most likely have been smoothed out (Beven and Wood, 1993).

Moreover, it should be recognized that the reference discharge series might be biased towards one or the other of the studied methods. On one hand, the reference series lends itself to be similar to the TD method discharge because both methods consider the actual, physical conditions, and incoming radiation and temperature have a close relationship as noted by Ohmura (2001). The TD method is also more coherent with the well-known physical relations between minimum and maximum temperature, radiation and melt (Walter et al., 2005). On the other hand, the method proposed by Hock is used to distribute the measured radiation across the catchment and in effect, the reference discharge can also be seen to be biased towards the Hock method in the distributed case. In spite of the possible biases towards the reference case, the comparison of the calibrated TD and Hock method for Experiment 1 leads to the conclusion that considering all temperature observations, both methods perform equally well.

Clear differences between the two methods become visible in Experiments 2 and 3 (Figure 5.7). If the temperature distribution data come from only the southwesterly facing group, the discharges are initially higher for the Hock method. A distribution of high mean temperatures attributed to the shallower lapse rates seems to be biasing the Hock melt method. Consequently, the Hock method provides an over-estimation of melt in the main peak hours (hours 75-250) and an underestimation in the lower peak (hours 450-525) without being able to capture the variability in the recession part of the discharge curve.

In contrast, for Experiment 3, the east-facing case, the results for both methods are comparable qualitatively even if the Hock method outperforms the TD method in terms of having a greater percentage of simulations which fall into the range of plausible reference simulations and the Nash index (See performance indicators in Figure 5.7). It is interesting to note that the reference discharge generated by using only the east-facing stations as input contrasts significantly from the reference discharge for the case of using all ten stations. Such a contrasting behavior indicates that the steep, mean lapse rate for the group of east-facing stations generates more variable mean temperatures and makes the discharge behavior quite different. In conclusion, results from Experiments 2 and 3 confirm the sensitivity of both melt methods to the spatial distribution of temperature, but the TD method appears, once again, to be more robust.

In terms of applicability of these melt methods, the Hock method has the major advantage that high resolution digital terrain models are now almost universally available; however, there are some open questions with regard to the performance of this method as a function of available temperature observations. Regarding the performance of the proposed TD method, it obviously depends on the quality of spatially distributed estimates of daily minimum and maximum temperature. Fortunately, minimum and maximum temperature observations can be quite wide-spread. For example, in the United States maximum and minimum thermometers have been widely installed due to their low cost and reliability (Quayle et al., 1991). Accordingly, both methods have their specific utility for different types of applications.

Finally, it should also be emphasized that the sub-daily degree-day factor variability could also be obtained by directly relating the daytime degree-day factor to the daytime hourly temperature and by imposing a constant mean value during nighttime. Such an approach would present two main differences with the proposed TD method: the resulting degree-day factor would have significantly less smooth sub-daily variability and its daily mean would fluctuate. Overall, this might result in too strong a variability of the simulated melt. Additionally, if this methodology is applied to hydrological models already using the classical degree-day approach, replacing the calibrated (constant) degree-day factor with a factor having a fluctuating daily mean value might lead to unforeseen effects on the model performance. As the goal of the proposed method is to impose physically-based variability around calibrated degree-day factors, the development and performance assessment of such a direct-temperature approach is left for future research.

5.6 Conclusions

The proposed quasi-sinusoidal function for the sub-daily variation of the degree-day factor requires only observed daily minimum and maximum temperatures as input, which are widely available. The main findings of the presented model performance comparisons are summarized hereafter:

- The point analysis at the Cotton Creek Experimental Watershed (CCEW) (Canada) demonstrates that the proposed quasi-sinusoidal function for the degree-day factor captures the sub-daily melt variability significantly better than a constant degree-day factor as in the classical degree-day (CD) method.
- The distributed point analyses at the Dranse de Ferret experimental catchment (in the Dranse catchment) indicate that, at the point scale, the proposed time-variable (TD) method and the Hock method have relatively equal performances in terms of generating potential melt, i.e. both methods capture the temporal distribution of available melt energy in a very similar way. The performance of the potential radiation-based Hock method demonstrates that this method clearly adds variability. However, the corresponding variability imposed by the TD method is more physically-based and appears

Chapter 5. Improving the degree-day method for sub-daily melt simulations

to be less sensitive to temperature distributions. These results suggest that additional analyses with distributed meteorological observations can help to further understand how well the snowmelt methods perform as a function of exposition.

- Furthermore, the distributed point data analyses underline that degree-day snowmelt models, which strongly rely on temperature information, require a good representation of the spatial variability of temperature (realistic lapse rates) to correctly model the spatial variability of snowmelt.
- In terms of catchment-scale discharge simulation, the presented results for the Dranse de Ferret catchment suggest that the TD method might outperform the potential radiation-based Hock method in terms of spatial variability of hourly snowmelt. Given that the TD method assigns degree-day factors directly at the subcatchment scale rather than at the grid-scale (Hock method), the TD method has, in particular, the advantage of maintaining realistic diurnal melt variations at the scale of an entire hydrological system, which smoothes out, to some degree, small scale variabilities.

Overall, the TD method, based solely on daily maximum and minimum temperature data, proves to be a robust, minimalist approach to provide a suitably accurate snowmelt response for spatially-explicit hydrological models with different degrees of spatial lumping. It, thus, represents a valuable approach for a wide range of hydrological modeling applications in high mountainous environments which are limited in data and require sub-daily snowmelt computations.

Chapter 6

A fit-for-purpose uncertainty approach for Alpine hydrological model calibration

Skepticism should be embraced – not ridiculed. There is much about the climate yet to be revealed, and science unexposed to intense challenge is unreliable.

William Stewart, Author 'Climate of Uncertainty'

6.1 Introduction

The role of environmental models is to break down natural, physical processes into a system of equations which can provide verifiable predictions about hypotheses. However, it has long been recognized that there is an inherent amount of uncertainty associated with environmental processes (Chamberlin, 1890). Uncertainty and imperfect representations of environmental, physical systems generally stems from limited knowledge on physical processes (i.e., epistemic uncertainty) and/or from natural variability (some processes such as the weather or subsurface flow paths have random characteristics) (Montanari, 2011). Input data uncertainty (such as the interpolation of precipitation and temperature) is also a large source of hydrological modeling error (Hrachowitz and Weiler, 2011; Hudson and Wackernagel, 1994; Kavetski et al., 2006). Similarly, model parameter uncertainty is common due to the difficulty in measuring some parameters values in the field or laboratory (Fleming et al., 2010). An

Chapter 6. A fit-for-purpose uncertainty approach for Alpine hydrological model calibration

equally significant source of error is operational uncertainty (Bérod, 2009; Montanari, 2011). In the case of flood forecasting, interpretation of output ensembles is a challenge with Numerical Weather Prediction ensembles (Cloke and Pappenberger, 2009). Operators need to understand that ensemble outputs must be flexible according to new observations, climate evolution, and socio-economical modifications (Bérod, 2009). Only by having adaptable, yet reliable hydrological predictions can operators effectively and confidently interpret result ensembles for decision-making.

6.1.1 Background: Uncertainty approaches

Research on how to quantify uncertainties in the environmental field has existed for more than three decades (Spear and Hornberger, 1980). In the particular field of hydrological modeling, in spite of years of trial and experience, an on-going debate exists regarding what constitutes an appropriate representation of uncertainty. The general disagreement stems from whether a proper statistical context is necessary to summarize parameter and predictive distributions.

There are two broad views on using statistics or probability theory for representing uncertainty: the frequentist or Bayesian view. Frequentists maintain that the primary cause for uncertainty is randomness so that probabilities represent the likelihood of outcomes that could happen if it is possible to take a large number of samples over all possible outcomes. The relative occurrence of any particular event, i.e. its relative frequency, converges to a limit as the number of repetitions of the experiment increases.

In contrast, Bayesians relax this assumption by recognizing that prior estimates of probabilities can be used as an input to estimating probabilities. Based on the formal likelihood framework theorem originally proposed by Bayes (1763), probabilities of an event can be introduced as a measure of the degree of belief that the subject has in the truth of the statement. In practical terms, the idea is to assign a probability to any event on the basis of the current state of knowledge and to update prior probabilities in light of new information. Effectively, Bayes Theorem states that given a set of feasible models M and observations O , the probability of any models M given observations O is:

$$P(M|O) = P(M)P(O|M) \setminus C \quad (6.1)$$

where $P(O|M)$ is the likelihood of simulating the observations given the model, $P(M)$ is a prior probability for all feasible models and C is a scaling constant used to ensure that the cumulative of the posterior probability density $P(M|O)$ is unity. Bayes theorem uses the prior probability density to calculate the posterior density by incorporating new evidence with each time step (Beven, 2009). In this approach, the likelihood is directly connected to the prior probability density of the observations, conditional on the knowledge of the parameters that identify a specific model (Mantovan and Todini, 2006).

Unlike statistically-based methods, uncertainty in hydrological modeling is also commonly

treated with fuzzy approaches when assuming uncertainty is non-random and can either be attributed to a lack of information or conflicting information (Beven, 2009). Fuzzy sets, introduced by Zadeh (1965), define a set of objects without clear boundaries or precisely defined characteristics to estimate the possibilities of potential outcomes (rather than probabilities). A fuzzy set application is considered a complement to statistical methods when considering expert knowledge, 'soft' information or qualitative measures of performance (Bárdossy, 2005). A classic example of a fuzzy set could be the number of days with 'heavy rain' where 'heavy' is based on human judgement rather than a precise, quantitative threshold. In fuzzy theory, ranges rather than thresholds are provided to define 'best' estimates. For example, a triangular fuzzy number is commonly applied in hydrological modeling contexts where a membership value of one is assigned to the most likely value, zero to the lowest and highest possible values and a linear membership function is assumed between these values.

6.1.2 Formal Bayesian methods

The fundamental advantage of Bayesian, formal methods is that with a proper probability density function and reliable information content, a predictive distribution of the hydrological response can be generated and used for accurate uncertainty estimation. Furthermore, formal methods provide a means to quantify the various error sources associated within hydrological modeling systematically (Vrugt et al., 2009). Attempting to separate and quantify individual error sources can be necessary for improving specific aspects of hydrological models.

Examples of well-known formal approaches in the field of hydrology include the BATEA approach, the Bayesian Forecasting System (BFS), the Meta-Gaussian approach and the DREAM method. The BATEA (Kavetski et al., 2006) method explicitly accounts for input uncertainty associated with poor precipitation forcings. Precipitation errors are assumed to take a multiplicative Gaussian form and a rainfall multiplier approach is used to adjust the precipitation depths. Similarly, the BFS approach, developed by Krzysztofowicz (1999), assumes that input precipitation is the largest component of uncertainty and additionally assumes that hydrological modeling uncertainty is the aggregation of all other uncertainties. The method produces probabilistic river stage forecasts through probabilistic precipitation forecasts by using input and process uncertainty processors. A technique which was adopted by BFS is the Meta-Gaussian approach (Montanari and Brath, 2004) which uses statistical inference in the Gaussian domain by using the Normal Quantile Transform (NQT). This approach estimates the probability distributions of runoff simulation errors conditioned by the value of flow by assuming the forecast error is a stationary and ergodic stochastic process (i.e., it has statistical properties that can be deduced from a long sample of the process) (Hostache et al., 2010). Another approach is the DREAM method (Vrugt et al., 2009). This method is based on the well known Shuffled Evolution Metropolis (SCEM-UA) global optimization algorithm and uses a Monte Carlo Markov Chain (MCMC) scheme to provide a Bayesian estimate of global uncertainty on the hydrograph output of hydrological models.

Chapter 6. A fit-for-purpose uncertainty approach for Alpine hydrological model calibration

The MCMC technique is a common method to randomly sample the feasible parameter space with Monte Carlo (MC) simulations for hydrological modeling. MC simulation is a method of exploring the response surface in a high-dimensional model space (i.e., for models with multiple parameters) as an alternative to discrete sampling. Common to all formal methods is that each likelihood function (or objective function to be minimized or maximized) forms a response surface when enough Monte Carlo simulations are performed. The MCMC technique involves concentrating sampling around high likelihood (or well-performing) regions of the likelihood surface. This form of intelligent sampling ensures greater efficiency than a random search and ensures that the likelihood response surface is well-represented. Most importantly, the method produces a posterior distribution of predictions associated with the likelihood surface.

Disadvantages of formal Bayesian methods include that many of the simplest and most straight-forward approaches assume that the measurement errors are mutually independent (uncorrelated). However, in hydrologic modeling, errors are often non-stationary and show autocorrelation (Vrugt et al., 2009). More complex models such as those using autoregressive schemes are able to account for heteroscedasticity (i.e., changing variance) or correlation in errors (Schaeffli et al., 2007; Yang et al., 2007; Vrugt et al., 2008), however, these methods are not trivial to implement in data sparse contexts or operational environments. Additionally, in practice it is quite difficult to identify and quantify individual error sources because input, parameter and structural error typically interact strongly through model processing (Beven, 2009; Montanari, 2011). Finally, from a philosophical standpoint, formal methods assume that epistemic uncertainties can be represented as if they were random in nature (Beven et al., 2012), so that the sources of error for data are limited to random error. This is often not the case when observable measurements are scarce in complex systems such as mountainous regions because error directly stems from a lack of verifiable data.

6.1.3 Informal methods

In contrast to formal statistical methods, informal methods do not require a full treatment of uncertainties and detailed data validation to define prior probability distributions. Informal likelihood measures, which are based on hydrological modeling experience, are generally used so that model properties are not falsely assumed (e.g., linear relationships approximated with nonlinear ones and vice versa) (Gupta et al., 1998) and to not overestimate information content in error residuals that may not have a consistent stationary structure due to the many sources of uncertainty (Beven, 2009).

The most applied, informal likelihood method to assess parameter uncertainty and numerically estimate hydrologic prediction uncertainty is the Generalized Likelihood Uncertainty Estimation (GLUE) approach (Beven and Binley, 1992). GLUE is based on the set of acceptable or 'behavioral' models, weighted by a measure of probability (likelihood), which reflects the performance of each model in the set during calibration. An assessment of uncertainty

arising from parameter uncertainty is provided by the probability distribution of all likelihood-weighted model outputs (Hostache et al., 2010). The probability distribution enables an implicit handling of residuals, and an appropriate hydrologically reasoned likelihood is used in testing hypotheses.

As in the case of GLUE and other non-probabilistic methods, multiple simulations facilitate local and global sensitivity analyses that can be used to determine the most important parameters in controlling uncertainty in model output. Ranges in sensitivity are provided by sampling the response surface and conditioning the model to find behavioral models.

Contrary to the concept of finding an optimal model, the GLUE approach accepts the idea of equifinality; model users have an imperfect knowledge of a system, so an ensemble of models, parameters and variables are considered equal or almost equal simulators of the system. This idea is in direct contrast with optimization schemes because a global maximum (or minimum) is not sought. Rather, the likelihood surface is assumed to have multiple minima or maxima. As Fleming et al. (2010) states, "the error landscape is not a well-defined and localized crater, but instead a field of craters of approximately equal depth." Such a landscape, characteristic of hydrological modeling output, does not make finding a global optimum robust to the impact of factors such as the choice of likelihood, the realization of errors or the period of calibration data.

A primary advantage of the GLUE method is that it can be easily used with sparse data sets. Furthermore, it has been found to be easy to implement and use while providing good estimates of total streamflow uncertainty relative to statistical methods such as the formal MCMC DREAM method (Vrugt et al., 2009). The GLUE method also considers epistemic uncertainty in addition to aleatory uncertainty to provide a range of plausibility for discharge simulations.

Disadvantages of the GLUE method include the subjectivity in deciding which given set of parameters is acceptable ('behavioral') based on subjective thresholds assigned to likelihood measures. Using less formal likelihood measures in GLUE prevents the formulation of precise distributions (limited by computation time) of the observable variables (i.e., the method is not probabilistic in the sense of providing $P(O|M)$ as in Equation 6.1). Not explicitly accounting for the errors can make the learning process to condition the model to which parameter sets are behavioral less efficient. Another disadvantage is that without a formal representation of the structure of errors as a component of the model, it is not possible to distinguish the different components of the total error (Vrugt et al., 2009).

6.1.4 Likelihood measures and multi-criteria performances

To reduce the subjectivity of informal likelihood measures, studies have tried to quantify limits of acceptability based on observations; By defining limits of acceptability based on discharge observation errors, Liu et al. (2009) account for input error implicitly, most notably uncertainty

Chapter 6. A fit-for-purpose uncertainty approach for Alpine hydrological model calibration

in the rating curve. Others have included 'soft' data such as monthly water balances (Seibert and McDonnell, 2002; Winsemius et al., 2009) to define quasi-objective limits of acceptability. Additional information has also been used to more accurately describe fuzzy performance measures in terms of effective water table dynamics and flood inundation predictions (Freer et al., 2004; Pappenberger et al., 2007) respectively.

The choice of likelihood measure is also under debate, particularly with informal methods of uncertainty analysis. In the presence of an imperfect model, a calibrated model will tend to best match the hydrograph behavior it is calibrated to fit (such as the peak). However, the calibration of rainfall-runoff models is inherently a multi-objective problem (Gupta et al., 1998) because different parameter sets may capture the best performances for contrasting hydrograph dynamics such as base flow, time to peak, and discharge recession. However, there is no consensus amongst uncertainty experts whether a particular combined criterion exploits all the necessary information provided by individual criterion.

Numerous codes exist to use multiple criteria and choose a Pareto optimal parameter front which attempts to exploit the information provided by all criteria and limit a trade-off among performance measures (Gupta et al., 1998; Yapo et al., 1998; Vrugt et al., 2003). The issue with Pareto optimal search is that an improvement in one likelihood measure can lead to a poor performance with another likelihood. Also, in spite of Pareto optimization providing a frontier of acceptability where none of the performance measures can be further improved, as with optimizing single criterion, acceptable models on the Pareto front can change when calibrating with a different event or using different forcing inputs (Beven, 2009). As a result, Pareto optimization can lead to the faulty rejection of good performing models just behind the Pareto front which are more robust to changing inputs.

6.1.5 Uncertainty estimation technique and tool

In the present case, due to inherent errors associated with sparse measured inputs and simplified hydrologic processes as a result of operational constraints, an informal method has been adopted. Using an informal likelihood approach prevents the misrepresentation of model sources of uncertainty by avoiding the need to be explicit in error estimation. Also, this procedure accounts for potential errors most certainly associated with area-averaged or interpolated meteorological inputs (Hingray et al., 2010; Tobin et al., 2011).

In light of the progress in the uncertainty assessment techniques aforementioned, the goals of this work are three-fold;

The first goal is to propose a 'fit for purpose' (Beven et al., 2012) uncertainty estimation procedure using the assumption of multiple working hypotheses to provide a plausible range of simulations which captures the hydrologic dynamics of catchments, focusing on flood events.

The second goal is to constrain the uncertainty of hydrological model inputs and processes by

incorporating variable temperature gradients and diurnal snowmelt variations to help in the prediction of snow or rain and the resulting runoff (Tobin et al., 2011).

The third goal is to establish a semi-automatic calibration procedure and visualization tool to limit operational uncertainty on the possible range of good performing models. This is accomplished by constraining parameter ranges and exploiting all hydrograph behavior information available according to single and combined criteria.

The automatic part of the proposed uncertainty assessment technique is necessary to provide a relatively easy means for model operators (i.e., calibrators or users) to calibrate catchments modeled by the flood forecasting model utilized herein. Calibrating the hydrological model to provide an ensemble of good-performing, multiple working hypotheses is important to assure the model is more robust to forecast biases (Pappenberger et al., 2007), changing or unknown hydropower operations (Hingray et al., 2010), and climate change impacts such as snowmelt regime shifts (Horton et al., 2006). Furthermore, the aim of the visualization tool is to convey the ambiguity and imprecision of the hydrological model to the users so that they can be empowered to make decisions knowing the limitations of certainty. In this sense, the calibration procedure is not entirely automatic because there is a need for some subjective judgement on the user's part as to which performance criteria is most important for certain hydrological behavior at specific times. The multi-criteria visualization interface offers a unique tool for users to choose the most relevant likelihood measure or combined likelihood measure to provide a well-performing ensemble of plausible model outputs.

6.2 Materials and methods

This study concerns the Visp and Dranse catchments described in Section 2.2 of this thesis. Uncertainty analysis and calibration is performed with the RSII hydrological model, described in Section 2.4. A previous manual calibration of the RSII model was conducted in previous studies (Jordan, 2007; Garcia Hernández et al., 2009b). This work applies a new semi-automatic calibration approach which will also provide uncertainty estimations on the flood responses.

The proposed informal method for uncertainty estimation is based on the GLUE methodology (Beven, 2006) and multi-criteria performance measures (Gupta et al., 1998). The methodology can be summarized as follows:

1. Zones are determined based on physical characteristics to be able to better explore the parameter space in each zone;
2. Hydrograph recession limbs are evaluated for all previous flood events to have a general idea of recession behavior and to constrain the range of recession constants;
3. A first round of MC simulations is run with and without the input improvements (lapse rates) and process improvements (snowmelt);

Chapter 6. A fit-for-purpose uncertainty approach for Alpine hydrological model calibration

4. A second round of Monte Carlo (MC) simulations is run with improvements to inputs and processes and a broad range of acceptability in order to conduct a sensitivity analysis. Parameter values per zone are constrained based on performances given for each likelihood measure;
5. A visualization tool is used to view the 50 best parameter sets per zone to see zone-specific performance and possible model characterization deficiencies;
6. A third round of MC simulations is run with a) improvements to inputs and processes b) constrained parameter ranges per zone and c) a customized weighted likelihood measures to get the overall best 100 parameter sets per zone.

Details of each step of the methodology are provided below.

6.2.1 Zones for parameter space exploration

The Visp and Dranse catchments are separated into calibration zones based upon the outlet points, the Swiss hydrological atlas (Weingartner, 2009), the locations of glaciers and the vegetation line. Zones for the catchments can be seen in Figure 6.1.

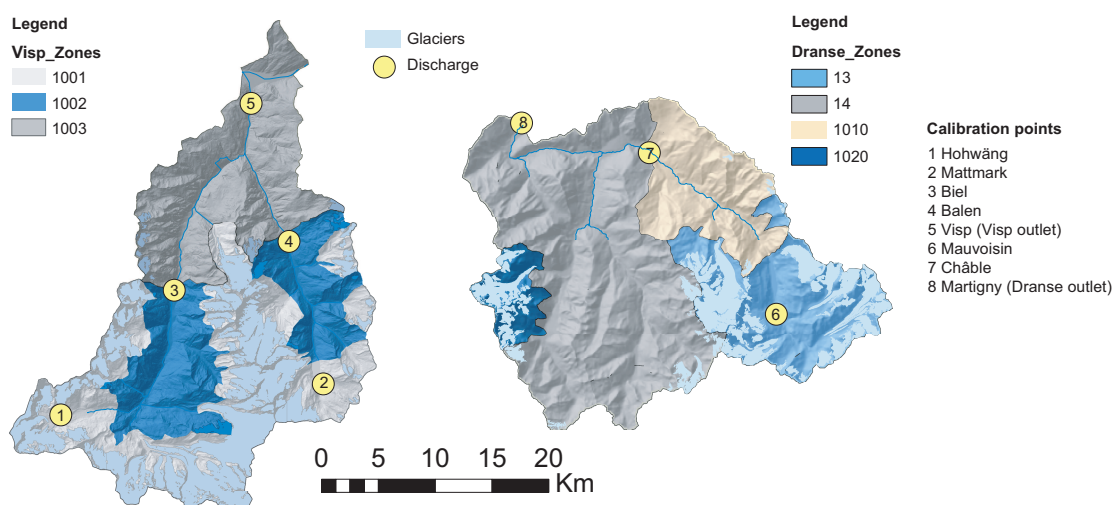


Figure 6.1: Calibration zones in the Visp and Dranse catchments used to explore the parameter space.

The zones enable a better look at systematic errors within regions such as poor antecedent soil moisture conditions or overestimation of recession periods. They provide a means to see which regions of the study catchments are not well represented by the hydrological model.

Transferring parameter vectors between zones with similar physical properties (e.g., glaciers) for easier calibration such as in the work of (Bárdossy, 2007) was not feasible in this work;

although other zones could be assumed to provide good water balances, the variability of the daily discharge is highly impacted by hydropower operations which differ from zone to zone.

6.2.2 Constraining prior parameter ranges

If the initial parameter range is well-defined within feasible, physically-based limits, it is more likely for an uncertainty estimation method to find good performing models with MC simulations. Here the goal is to constrain the parameter range for the release coefficient of the groundwater reservoir (i.e., baseflow) and the Strickler routing parameter (see Table 6.1) based on hydrograph recession limbs detailing slow and fast rates respectively.

Recession curve analysis

Representing base flow as an exponential decay function has long been an accepted methodology (Barnes, 1939). The theory maintains that, after surface runoff and interflow are depleted, the recession of flow versus time plot consists typically only of groundwater drainage, i.e. base flow. The recession hydrograph can be assumed to be an exponential decay process and that the decrease in flow rate from anytime t to any time $t + 1$ is constant. In exponential form, the flow rate Q and constant K , representing a characteristic storage delay in the watershed, can be written as (Brutsaert and J., 1977):

$$Q(t) = Q_0 e^{-t/K} \quad (6.2)$$

where t is the time (hours) and Q_0 is the flow rate ($\text{m}^3 \text{s}^{-1}$) at $t=0$. Such an approach has been successful in separating baseflow from the total runoff during storm events (Szilagyi and Parlange, 1998; Szilagyi et al., 1998).

To quantify mean characteristic storage delays in the watershed based on analyzing recession curves, Brutsaert (2005) describe in detail two methodologies which assume that the time dependence of the flow rate in a river can be characterized by an exponential decay process. The first method uses a semi-logarithmic plot of Q versus t to identify the base flow recession graphically as the 'straight' lower envelope of a number of tail end sections of low flow recession hydrographs. By shifting the slopes horizontally until the best coincidence is obtained, the value of $-K^{-1}$, or the average base flow residence time is obtained.

Based on this method, the fast and slow recession constants were analyzed for all flood hydrographs between 1984 and 2008 (which includes 6 large flood events) in each zone. Two typical examples are represented here. Figure 6.2 shows the log transform of the discharge for the Biel stream gauge during the 1993 flood and the Visp gauge for the flood event in 2000. (The diurnal pumping cycles and daily melting cycles are also recaptured in the system.)

Chapter 6. A fit-for-purpose uncertainty approach for Alpine hydrological model calibration

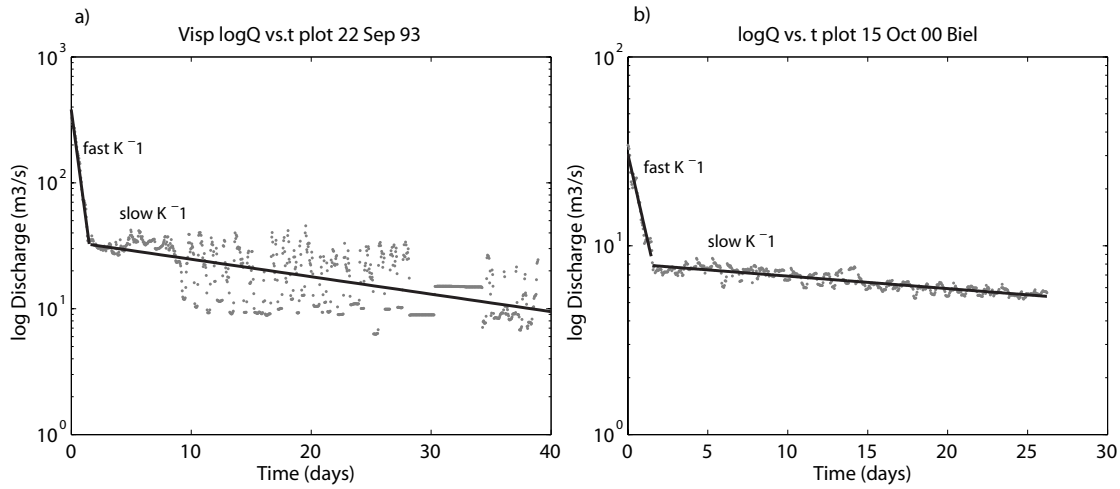


Figure 6.2: log dQ vs. t plots for a) 1993 flood at the Visp outlet b) 2000 flood at Biel calibration point. Both the slow and fast responses are visible in the semilog plot.

The second approach used to characterize the catchment residence times utilizes plots of Q_i versus Q_{i+1} where the exponential outflow function, Q_n , is represented by the following form:

$$Q_n = Q_0 K_r^n \quad (6.3)$$

in which $K_r = Q_i / Q_{i-1}$ is the depletion ratio, $n = t / \Delta t$ is the number of time intervals of duration Δt from the beginning of the recession, when t is assumed to be zero and Q_i is the rate of flow at the i th time interval.

Once again, all flood hydrographs were analyzed between 1984 and 2008 to determine a range in the K_r values. Figure 6.3 shows the 1993 flood case at the Visp gauge. The value of K_r , the rate of groundwater storage depletion, is obtained from the slope of the lower envelope. This K_r factor can be expected to depend on the same soil, aquifer and basin characteristics as K from Equation 6.2.

Analysis of the recession curves for the flood events in the Visp and Dranse basin (not shown here for the sake of brevity) demonstrated that the Dranse basin has a similar fast-slow response as the Visp. Both have linear base flow recessions when evaluated in exponential form supporting the use of a linear relation in the RSII groundwater model. However, the K values are different between the catchments and between the zones within the catchments due to contrasting physical characteristics such as slope, aquifer thickness, hydraulic conductivity and soil porosity. Moreover, the K values are not only catchment and sub-catchment dependent but are influenced by seasons (including diurnal glacial melt) and extractions due to hydropower use.

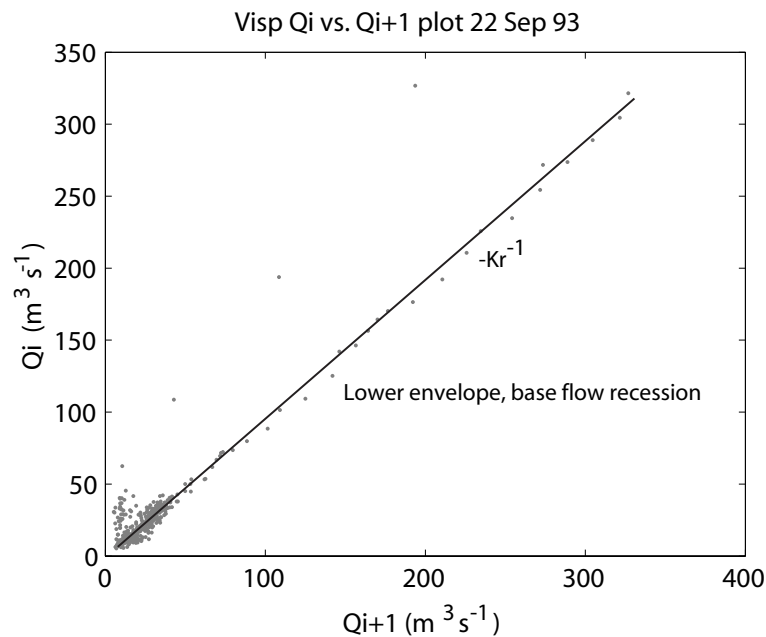


Figure 6.3: Q_i vs. Q_{i+1} ($\text{m}^3 \text{s}^{-1}$) plot for 1993 flood in the Visp watershed showing K_r , the rate of groundwater storage depletion

It should be noted that flood events for the Visp and the Dranse catchments have occurred in the spring through autumn seasons. To date, six significant flood events have been recorded in both catchments. The discharge signal of other strong precipitation events was often not visible due to hydropower operations. With such a limited event database, it was not possible to perform a statistical analysis on the K values on a seasonal basis or lumped or to create a reliable master recession curve (Lamb and Beven, 1997). As a result, the extremes of the K values after an analysis of all recession hydrographs during the flood events were used to set the initial parameter ranges per zone for the fast and slow responses in the groundwater model (see Table 6.1).

Of the parameter ranges listed in Table 6.1, it should be noted that the groundwater and Strickler coefficients are not entirely physically-based. Many state variables of similar semi-lumped models do not exactly represent any physical quantity and are used rather to describe model states (HBV). In the case of the RSII model, the Strickler coefficient range is broad and cannot be related directly to channel roughness and sinuosity properties (i.e., the inverse of published Manning values). Accordingly, this parameter is used more for tuning the runoff reservoir such as to minimize the differences between simulated and observed discharges. Overall, for real-world systems in hydrological modeling, only the observed discharge can be used to estimate the states of a large set of parameters due to a lack of verifiable data and the difficulty of measuring the parameter values in the field on a catchment-scale. Fortunately, if parameter values are calibrated such that the entire hydrological year, the somewhat heuristic choice of parameter values begins to have a more consistent basis from one hydrological year

Chapter 6. A fit-for-purpose uncertainty approach for Alpine hydrological model calibration

Table 6.1: Reference hydrological model parameters for Monte Carlo simulation (LB and UB are lower and upper bounds)

Snow model			
Parameter (unit)	LB	UB	Source
Snow degree-day factor ($\text{mm day}^{-1} \text{ } ^\circ\text{C}^{-1}$)	1.3	11.6	Sigh et al. 2000; Hock, 2003
Infiltration model			
Release coefficient of groundwater reservoir (hr)	0.1	500	Recession curve analysis
Maximum height of groundwater reservoir (m)	0.5	2	
Glacier model			
Coefficient of linear snow reservoir (hr)	4	18	Klok et al. 2001
Coefficient of linear glacier reservoir (hr)	0.2	15	Baker et al. 2002
Glacier degree day factor ($\text{mm day}^{-1} \text{ } ^\circ\text{C}^{-1}$)	5	20	Rango and Martinec, 1995
Overland flow model			
Strickler coefficient ($\text{m}^{1/3}\text{s}^{-1}$)	0.1	75	Recession curve analysis

to the next.

In the case of the Swiss Alps, calibration must initialize states in September in order to properly account for the parameters influenced by the initialization of snow water equivalent. Unlike in rainfall-dominated basins, where discrete precipitation events must be captured, the snowpack integrates individual precipitation events throughout the winter season. As a result, accurate calibration of snowmelt-dominated catchments such as the Visp and Dranse must include properly accounting for total snowpack and melt processes (which are largely influenced by maximum temperatures) (Hay and Clark, 2003).

Performance and likelihood measures

To reduce the subjectivity of likelihood measures in the GLUE methodology, five performance measures are evaluated independently and combined after rescaling to analyze hydrograph behavior such as base flow and time to peak (see Table 6.2). The multiple performance measures have been chosen based on the work of Reusser et al. (2009) who demonstrated that multiple measures provide a better characterization of the temporal dynamics of hydrographs and can provide a clearer picture of structural model deficiencies. In this approach, individual performance measures are used to provide an idea of specific hydrograph behavior demonstrating where the model is not well-defined in preliminary simulations.

Table 6.2: Performance Measures (LB and UB are lower and upper bounds)

Performance Measures		
	<i>LB</i>	<i>UB</i>
Absolute value of peak, APK (%)	0	± 10
Nash-Sutcliffe efficiency, NSE (-)	$-\infty$	1
NSE log of discharge, NSEL (-)	$-\infty$	1
Mean absolute relative error, MARE(-)	0	$+\infty$
Absolute value of volume, AVL (%)	0	± 10

The most important goal for flood forecasting is to predict the timing and amplitude of the extreme event peak. The absolute value of the peak (APK) performance measure has been developed so that simulations are accepted only within a window of ± 6 hours of the measured peak. Such an approach emphasizes the importance of having the peak within a precise limit of acceptability for flood alert forecasting and hydropower decision-making. Furthermore, in the context of flood forecasting, it is critical to adhere to this performance measure because global performance measures are much less meaningful when lead times to flood events are short.

In addition to the peak criterion, the Nash-Sutcliffe efficiency of the log of the discharge is used to emphasize matching base flows (referred to hereafter as NSEL). The Nash-Sutcliffe efficiency criterion (NSE) is also used directly on the discharge to determine coincidence with peak flows. The NSE criterion based on squared errors is useful in mountainous terrain which have flashy hydrologic responses and can be subject to large rainfall and rain-on-snow events (Fleming et al., 2010). However, as the NSE includes the squared error, this criterion can be quite sensitive to outliers. Furthermore, as demonstrated by Schaefli and Gupta (2007), the use of the mean observed discharge value as the benchmark in the NSE criterion can be a poor predictor in the case of strongly seasonal time series. This can be considered the case for both the Visp and Dranse upper subcatchments which are highly impacted by snow and glacier melt during the spring and summer seasons. As a result, to limit the bias of outliers and the mean observed discharge, the Mean Absolute Relative Error (MARE) is also used to measure the overall model performance. Furthermore, a ratio of the absolute value of the measured to simulated volume (AVL) is used as an overall performance measure where ± 10 -20 % from the measured volume is the range for the limits of acceptability.

Particular to this hydrological model, there are zones within the complex, alpine catchments which have been proven to be poorly represented by the model due to aleatory and epistemic uncertainty associated with a) unknown reservoir operations, b) pumping and re-distribution of water between zones and c) non-linearities of the basin. As a result, by solely setting fixed thresholds for the 4 performance measures other than the strict Peak criterion (i.e., the NSEL, NSE, MARE and AVL measures), it was recognized that it was not possible to find acceptable simulations in poorly modeled calibration zones for certain performance measures

Chapter 6. A fit-for-purpose uncertainty approach for Alpine hydrological model calibration

(or conversely too many acceptable simulations were found with too low a threshold in well modeled zones).

Effectively, a customized weighted likelihood measure was developed to consider all 4 measures without rejecting potential solutions if they do not adhere to one or more of the criteria, similar to the work of Seibert and McDonnell (2002); Beven (2004). In this approach, each of the 4 performance criteria were rescaled between 0 and 1 (0 being the worst and 1 the best) to define a likelihood measure. Likelihood measures enable a probabilistic analysis of the hydrograph behavior. The MARE criterion is also transformed to (1-MARE) to coincide with the 0(worst) and 1(best) limits. The AVL criterion $\pm 10-20\%$ is transformed to be one minus the absolute value of the volume difference normalized by the measured volume so that it can be rescaled as a probability between 0 and 1. All 4 criteria are weighted according to the weighted criterion (WC), Equation 6.4. These weights have been determined based on giving preference to high flow criteria, namely the NSE and AVL criteria (again, the MARE is focused on long-term performance and the NSEL criterion is geared towards analyzing low-flow performance). Cumulatively, the WC criterion has a score between 0 and 1 (again 0 being the worst and 1, the best):

$$WC = 0.3(NSE) + 0.2(1 - MARE) + 0.3\left(1 - \frac{AVL}{(\text{Measured Volume})}\right) + 0.2(NSEL) \quad (6.4)$$

The best parameter sets are then determined moving from upstream to downstream zones by first choosing those sets which adhere to the limits of acceptability of the Peak, APK, criterion. Subsequently, the scores of the WC measure are stored per zone and sorted. The 100 best parameter sets for the most upstream zone with the highest scores are saved for analysis with the downstream zones. In effect, this technique exploits all the criteria information and considers the performances in zones independently to adapt to the reality that the model is able to better predict hydrological processes in certain zones versus others.

6.2.3 Inputs and processes

To address high input uncertainty associated with the sparsely gauged catchments considered (most notably at upper elevations), input temperatures are interpolated by using a temporally variable temperature gradient. Linear regression of the meteorological service station temperature measurements with elevation in the Valais indicate that the lapse rates change seasonally and they are based on wet and dry periods. Wet versus dry was determined by taking a moving average over a week-long period for the precipitation time series. Only windows with mean precipitation intensity over 0.2 mm/h were taken as wet periods. See Table 6.3.

In spite of these general trends, the high variability of the lapse rates between years and seasons indicates that in this complex alpine region they cannot be generalized as constant. Supporting the results of Chapter 3 in this thesis and previous studies (Blandford et al., 2008; Minder et al., 2010), variable lapse rates on an hourly scale are necessary for accurately

Table 6.3: Lapse rates for all MeteoSwiss ANETZ meteorological stations in the Valais ($^{\circ}\text{C m}^{-1}/1000$)

	Annual		Autumn		Winter		Spring		Summer	
	Dry	Wet	Dry	Wet	Dry	Wet	Dry	Wet	Dry	Wet
1987	-4.7	-5.5	-4.2	-5.4	-3.1	-4.9	-6.1	-6.1	-5.8	-6.2
1993	-5.0	-5.7	-4.9	-5.6	-3.4	-5.3	-6.7	-6.1	-6.0	-6.2
1994	-5.3	-5.7	-4.7	-5.8	-4.7	-5.2	-6.4	-6.4	-5.9	-5.3
2000	-5.1	-5.7	-4.7	-5.4	-3.7	-5.5	-6.1	-6.0	-6.0	-6.2

detailing temperature gradients to better characterize the transition from rain to snow in alpine environments. Due to the difficulty in defining variograms with highly skewed distributions (i.e., precipitation intensities of 0 mm h^{-1} for extended periods of time) and computational time constraints including long run-times, it was not feasible to apply the kriging with external drift methodology of Chapter 3 for the hydrological year analyses of this study. Based on previous analyses, linear regression is considered to be a robust minimalist approach to ensure the dependency of temperature on altitude (Hudson and Wackernagel, 1994).

To address endemic structural error (Beven, 2009) the new snow melt method proposed in Chapter 5 of this thesis has been incorporated into the hydrological model. This method provides diurnal variations of the calibrated degree-day factors for the calibration zones of the catchments (see Figure 6.1). It has been well-established that temperature is a physical variable controlling the rates of longwave radiation and sensible heat flux and is highly correlated to the three most important energy sources which determine snowmelt (incoming longwave radiation, absorbed global radiation (shortwave) and sensible heat flux) (Hock, Ohmura, Rango and Martinec). As shown by radiation measurements taken in the Dranse catchment, a diurnal cycle given by a quasi-sinusoid function is able to mimic the radiation as shown in Figure 6.4. The mean of this function is preserved as the calibrated degree-day factor for each zone. See more details of this method including mathematical formulations in Chapter 5 of this thesis.

Monte Carlo simulation framework

A sampling tool called RSPilot was created to automatically perform a random search on feasible parameter sets from a prior uniform distribution within the ranges defined in Table 6.1. Two thousand MC simulations were conducted in the first round of simulation for three cases (with and without model input and process improvements) while 5,000 MC realizations of the model were conducted in the 2nd and 3rd rounds. For the three rounds of simulations, the parameter sets are varied to enable the creation of a response surface. A uniform random sampling strategy is initially used due to a lack of knowledge on prior probability distributions for effective values of parameters and their covariations. It is assumed here that there is not

Chapter 6. A fit-for-purpose uncertainty approach for Alpine hydrological model calibration

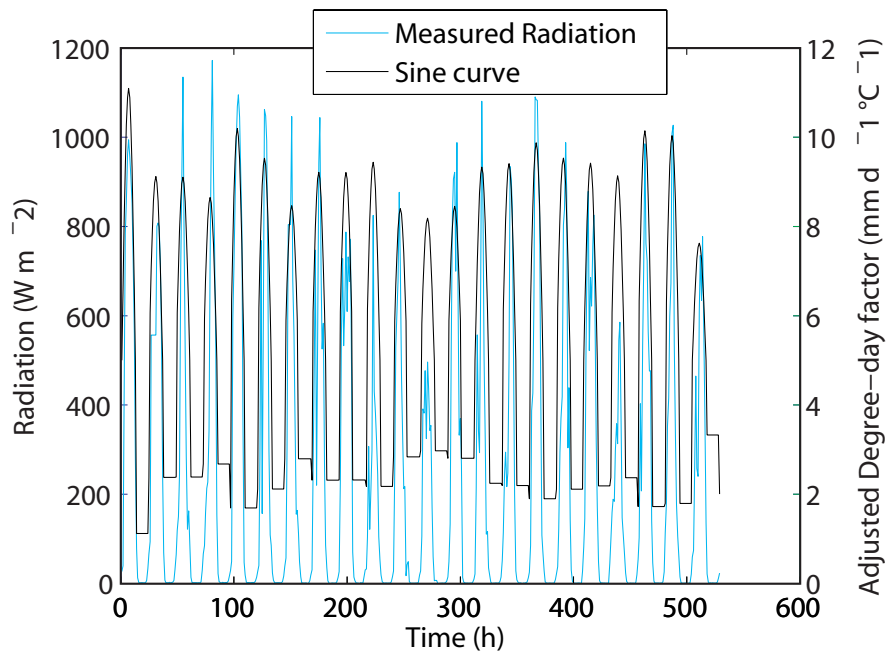


Figure 6.4: Radiation with overlaying quasi-sinusoid function used to impose diurnal variability for the snow degree-day factor with the mean of the function preserved as the calibrated value of the degree-day factor.

enough information to define informative priors from which to sample, so a uniform random sampling strategy plus a multi-criteria approach is effective at identifying scattered regions of behavioral simulations on the response surface of a complex model space.

For the first round of simulations, the original model performance (case 1) is compared with the performance with the proposed input improvement (i.e., variable lapse rates) (case 2) and the proposed process improvement (i.e., imposed diurnal melt variability) (case 3). Effectively, 2000 simulations are run for each case. All parameter values are selected from the limits defined in Table 6.1.

Similar to the work of Winsemius et al. (2009), the second round of MC simulations is conducted for a hydrological year as a learning tool. However, the second round of MC simulations is used to constrain the parameter limits on the basis of the sensitivity analysis, rather than the limits of acceptability as in Winsemius et al. (2009). A broad acceptability range (0 to 1 in the cases of MARE, NSE, NSEL and $\pm 20\%$ in the case of the AVL and APK criteria) is used so that the sensitivity analysis can demonstrate the possible range of performance for a parameter relative to the parameter set to which it belongs. The broad range is necessary for flood calibration because there is a limited number of events available to estimate the variability of parameters.

The sensitivity analysis enables an investigation of the reaction of the model (in terms of discharge) to changes in parameters. Dotty plots are used to show projections of points on a

likelihood surface onto a single parameter axis (Beven, 2004). Histograms are used to show marginal distributions of the best performing parameter sets relative to a specific parameter. Analysis with both these methods shows which parameters are more sensitive, on a relative basis.

The third round of MC simulations is used to apply the customized WC criterion to find the best 100 parameter sets. The constrained parameter value limits and the input/process improvements are incorporated into this final round of analysis.

Interactive visualization

The visualization tool integrated into the operational version of the RSII flood forecasting model enables acceptable simulations to be viewed relative to the measured discharge immediately following the MC simulations (Figure 6.5). This tool enables one to look at the performance based on criteria individually, similar to looking outside the Pareto optimal surface to find other acceptable working hypotheses. Specific hydrograph behavior can subsequently be addressed; for instance, if the APK and AVL likelihood measures do not show many acceptable simulations, the range for the maximum height of the groundwater reservoir is adjusted to obtain better volumes. Moreover, if during spring melt simulations, the NSEL measure does not show many acceptable simulations, the range for the melt coefficients is altered accordingly.

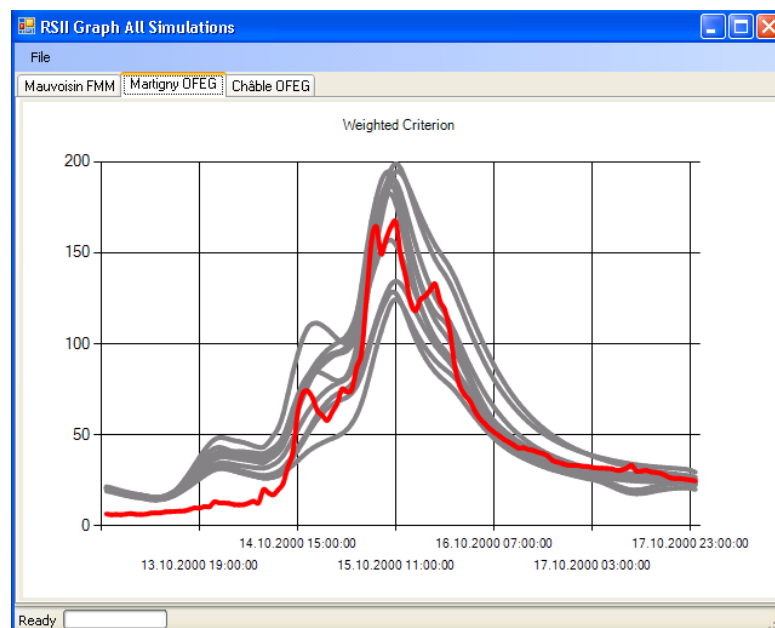


Figure 6.5: Example of visualization interface showing the customized weighted criterion per calibration zone in the Dranse catchment.

In addition to demonstrating performances based on individual likelihood measures, this tool shows a comparative analysis between two of the simplest means of combining multiple

Chapter 6. A fit-for-purpose uncertainty approach for Alpine hydrological model calibration

likelihood measures, the fuzzy union and intersection (Beven, 2004). A fuzzy union emphasizes the best performance of each model over all the measures considered. The fuzzy intersection shows the worst performance which adheres to all likelihood criteria. The intersection exploits more of the information from each criteria, however, if any of the measures are zero, taking a fuzzy intersection leads to rejection of the model. Both are simple concepts which are useful to communicate if the model produces all-around good hydrograph behavior. However, the union and intersection can be seen to be too optimistic or pessimistic respectively where neither fully utilizes the information provided by multi-criteria in all cases.

With such a broad extent of adaptability in measuring performance, the validation tool is the novelty of this work because it enables a means to compare individual and combined likelihood measures. To the author's knowledge, such a tool which can easily be adapted to the specific modeling needs (e.g. prediction of spring floods dominated by snowmelt) has not yet been developed.

To facilitate the use of this tool for operators, the tool includes an interactive interface where the mouse can be used to choose among the simulations. Users can choose the simulations which provide the best responses visually such as capturing peak flows. Although this functionality adds a layer of subjectivity, it enables the user to place emphasis on the parts of the hydrograph behavior which are most critical to match. In addition, the mouse click provides a unique identifier for the parameter set used to generate a specific simulation so that it can be used for quick validation with other event databases (since acceptable parameter sets are automatically saved).

6.3 Results

6.3.1 Round 1 MC simulations: Input and process improvement analysis

Variable lapse rates

By enabling the lapse rates to vary in time, it is possible to capture a much greater quantity of acceptable parameter sets for the calibration zones. In Figure 6.6, it can be seen that in the Dranse catchment at least two times more parameter sets have acceptable performances. Comparison statistics are found in Figure 6.6. Furthermore, of the parameter sets, the highest performances are achieved in each calibration zone using variable lapse rates, with a particularly evident improvement for the Châble calibration point. Such results indicate that a constant lapse rate (the standard, $-0.0065 \text{ }^{\circ}\text{C m}^{-1}$ for an atmospheric profile) is not representative of the dynamics of temperatures in the catchments (similar results are seen with the Visp catchment). Improper temperature interpolations highly impact the rain/snow delineation and the resulting runoff. These results confirm the findings in Chapter 3 of this thesis.

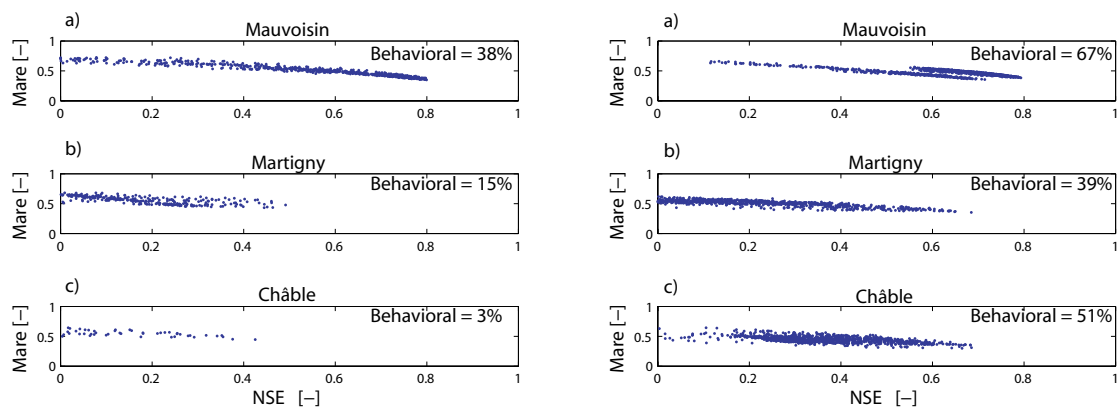


Figure 6.6: Performance comparison for the 2000 calibration event in the Dranse catchment, (MARE versus NSE) at calibration points a) Mauvoisin, b) outlet of Dranse catchment at Martigny and c) Châble. Left and right indicate hydrological model performance with a constant lapse rate and with variable lapse rates respectively.

Diurnal snowmelt

Snowmelt process characterization was tested using the original classical degree-day (CD) method and the proposed, time-variable degree-day (TD) method proposed in Chapter 5 of this thesis. Calibration of the TD method involves calibrating the refreezing factor, a_r , the amplitude factor β , and the degree-day factor for snow a_s while calibration of the CD method involves calibrating the refreezing factor, a_r , and the degree-day factor a_c . In this preliminary analysis, 2000 simulations were run for a fixed parameter set, varying only the 2 or 3 parameters of the melt methods. As demonstrated in Figure 6.7, the diurnal variability is much better represented by the TD method at the Visp outlet during August and September 2000, two months that are significantly affected by snowmelt in their upper catchments. The coefficients of determination (R^2 values) for the discharge from the CD and TD methods with respect to the measured discharge are 0.4 and 0.7 (-) respectively. Fluctuations in the data are due to a combined effect of hydropower pumping schemes and the diurnal cycle of snow and glacier melt. This is why the CD method can capture some diurnal fluctuations in spite of its constant value within each zone. By analyzing the mean daily temperature difference along with the diurnal variations, it is clear that the TD method has an apparent advantage, particularly when the daily temperature difference is large. These results support the findings in Chapter 5 of this thesis.

Based on these results, both the input and process improvements were fully integrated into the hydrological model and used in the subsequent analyses to calibrate the hydrological model and find an ensemble of plausible model outputs.

Chapter 6. A fit-for-purpose uncertainty approach for Alpine hydrological model calibration

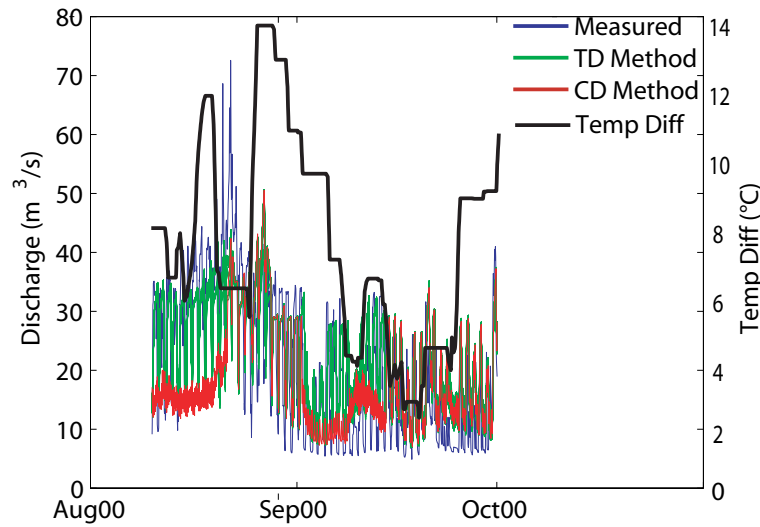


Figure 6.7: Spring diurnal variations at Visp, 2000 showing improved variability using TD method in RSII hydrological model.

6.3.2 Round 2 MC simulations: Sensitivity analysis

A sensitivity analysis was conducted to investigate the reaction of the model (in terms of discharge) to changes in parameters. In Figures 6.8a-d, each point corresponds to an entire parameter set. In Figures 6.8a and b, it can be seen that for both the 2000 calibration event and the 1993 validation event, the glacier degree-day coefficient has a much better performance in terms of the MARE likelihood measure between the ranges of 2 and 7 $\text{mm day}^{-1} \text{ } ^\circ\text{C}^{-1}$ with slight variations depending on the calibration zone. Effectively, the parameter ranges are reduced during the third round of Monte Carlo simulations.

A generalized histogram for all the zones in the Visp catchment in Figure 6.9 shows the marginal distributions for the maximum height for the groundwater reservoir relative to the NSE criterion. Similar to the glacier degree-day coefficient, the parameter can be limited in order to achieve the best performance.

Effectively, both the degree-day factor for glacier and the maximum groundwater height appear to be the most important parameters controlling uncertainty in the model output. Their respective parameter ranges have been constrained as indicated in Table 6.4. Confining the parameter range can be considered a risk with few simulations (relative to the millions that have been typically generated with the GLUE methodology for simpler hydrological models (Iorgulescu et al., 2005)). However, due to the fact that zero, or practically no good-performing parameter sets are found with higher degree-day coefficients, it is assumed that there is a very low chance in finding good parameter sets outside of the range.

Furthermore, by looking at the cumulative distribution functions (cdf), Figures 6.10a and b shows that the snow degree-day factor is sensitive, particularly for the 2000 event. In

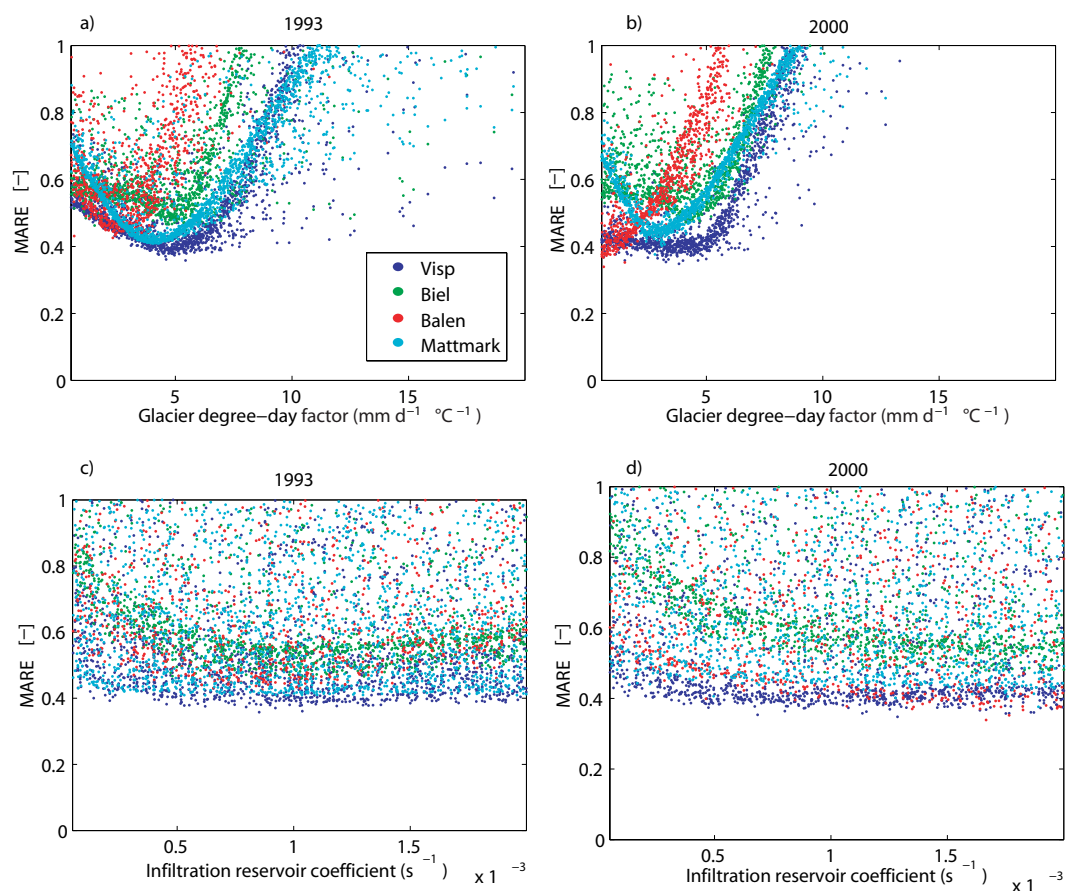


Figure 6.8: Dotty plots for glacier degree-day factor versus the MARE criterion for a) 1993 and b) 2000 in the Visp. Dotty plots for the release coefficient of groundwater reservoir versus the MARE criterion for c) 1993 and d) 2000 in the Visp.

Table 6.4: Constrained hydrological model parameters for Monte Carlo simulation (LB and UB are lower and upper bounds)

Snow model		
Parameter (unit)	LB	UB
Snow degree-day factor (mm day ⁻¹ °C ⁻¹)	2	10
Infiltration model		
Maximum height of groundwater reservoir (m)	0.1	1.2
Glacier model		
Glacier degree-day factor (mm day ⁻¹ °C ⁻¹)	2	7

Figures 6.8c and d, it can be also seen that better performances can be achieved with higher groundwater infiltration coefficients, although the difference is slight. The most noteworthy finding in Figures 6.8c and d is that performance, as suggested previously, is highly dependent

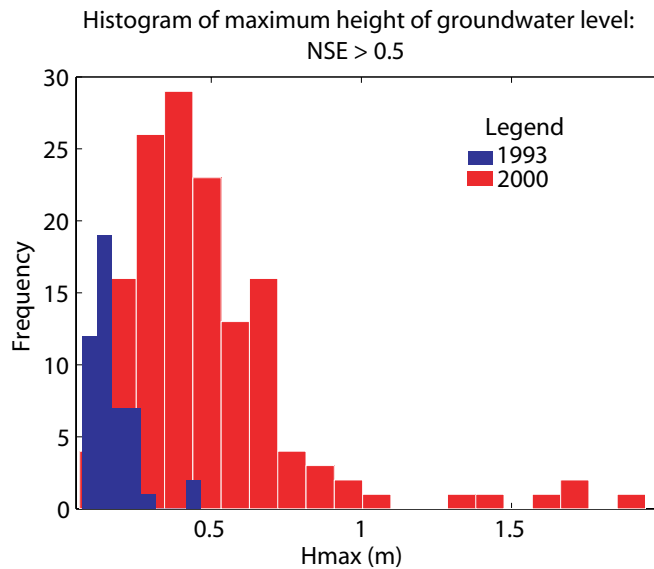


Figure 6.9: Marginal distributions for the maximum height for the groundwater reservoir relative to the NSE criterion (≥ 0.5) in the Visp catchment.

on the calibration zone.

In contrast, poor identifiability and high uncertainty are associated with the residence time parameter for the base flow in spite of the restricted, physically-based parameter range determined through recession analysis (Figure 6.10c and d). In this case, the model output is not sensitive to variations in parameter values because the parameter distribution remains uniform; one can select any value for this parameter within the given range to obtain an optimal performance. This parameter is not constrained any more than the recession analysis suggested as a result.

Interestingly, the different performances within each zone support the original notion that some zones are better described by the hydrological model versus others. This highlights the usefulness of the customized weighted likelihood measure developed in this study to rank the performances rather than rejecting potentially good parameter sets based on subjective threshold limits.

6.3.3 Visualization Tool

Results with the visualization tool emphasize the need for a weighted measure to choose the correct criteria. In Figure 6.11, it can be seen that using solely an intersection (bottom right of Figure) gives a false impression of the best performance. The intersection misses all parameter sets that might be just below the Pareto optimal surface for one certain criteria, however, it is shown here that some parameter sets clearly capture the peak and volume of the flood events.

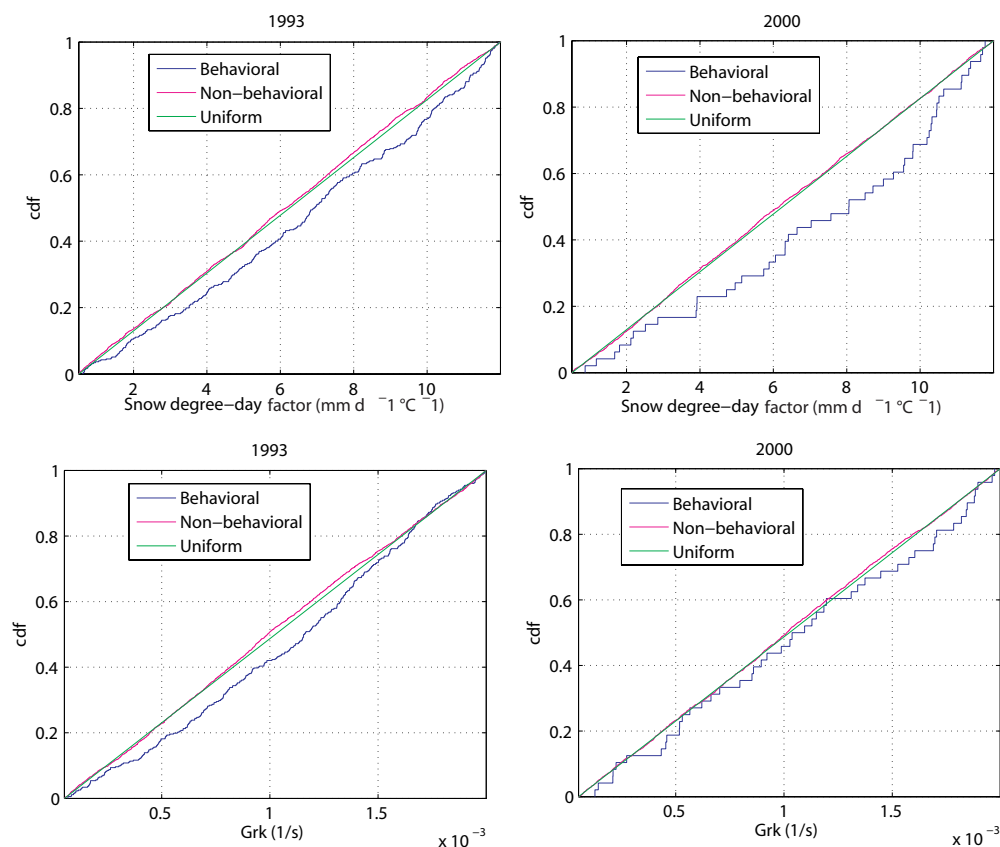


Figure 6.10: Cumulative distribution function (cdf) after MC simulations for the a) snow degree-day factor 1993, b) snow degree-day factor 2000, c) release coefficient of groundwater reservoir 1993 and d) release coefficient of groundwater reservoir 2000 in the Visp. Behavioral refers to values of parameters for accepted simulations and non-behavioral refers to values of parameters for unacceptable simulations based on the NSE criterion $\geq 0.5(-)$. All random parameter values are taken from a uniform distribution.

6.3.4 Round 3 MC simulations: Application of weighted criterion

Based on the constrained parameters determined in the sensitivity analysis, a third round of Monte Carlo simulations was performed. Results indicate that the semi-automated uncertainty analysis provides better performing parameter sets for each zone within the Dranse and the Visp for both the calibration and validation event, which in most cases captures the flood peak. This can be attributed to using the strict limits of acceptability with the peak criterion. Overall, as compared to results from a previous manual calibration (Jordan, 2007), higher NSE and APK measures for all catchments are achieved for the calibration and validation events with this customized uncertainty estimation technique (Table 6.5).

It should be noted that the 1993 validation event in the Visp catchment demonstrated poor performance in terms of volume and peak. Figure 6.13 indicates that there is not enough input volume within the hydrological model for this event. This is most likely attributed to the lack

Chapter 6. A fit-for-purpose uncertainty approach for Alpine hydrological model calibration

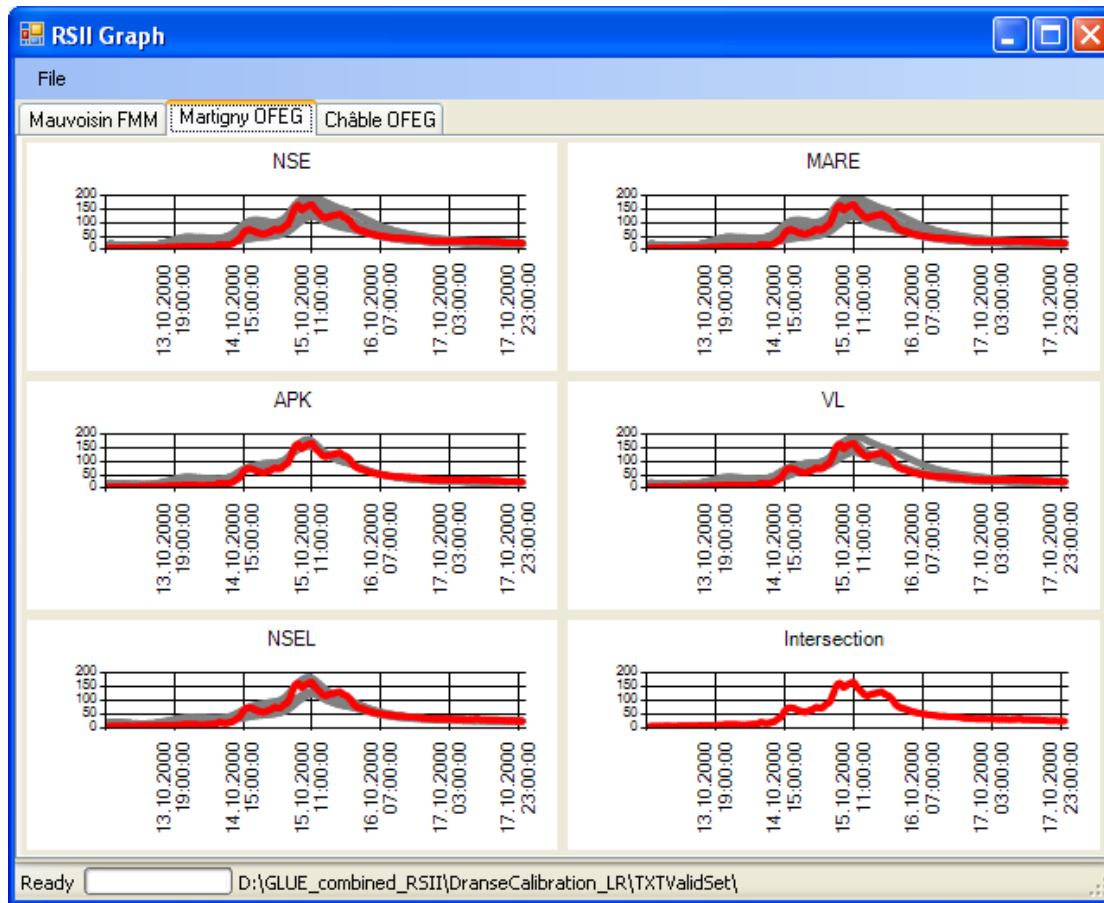


Figure 6.11: Visual interface showing individual likelihood measures and a combined measure for each calibration zone within the Dranse catchment.

of input data at this time indicating this calibration method cannot fully account for epistemic errors, particularly in the high elevation regions where sparse measurements are available. Furthermore, Chapter 3 of this thesis demonstrates that the IDW interpolation approach for precipitation is insufficient to produce appropriate runoff volumes whereas, over a flood event, given a robust variogram and including anisotropy, the kriging with external drift methodology can significantly improve the hydrograph response in terms of peak and volume. As previously explained in Section 6.2.3, generating variograms prior to flood events prohibits the use of this kriging method operationally, at the moment, because zero precipitation is frequent making residual distributions highly skewed. Testing the recommended kriging method of Chapter 3 by transforming precipitation residuals into the Gaussian domain and updating the robust variogram real-time when precipitation events occur is therefore left for future work.

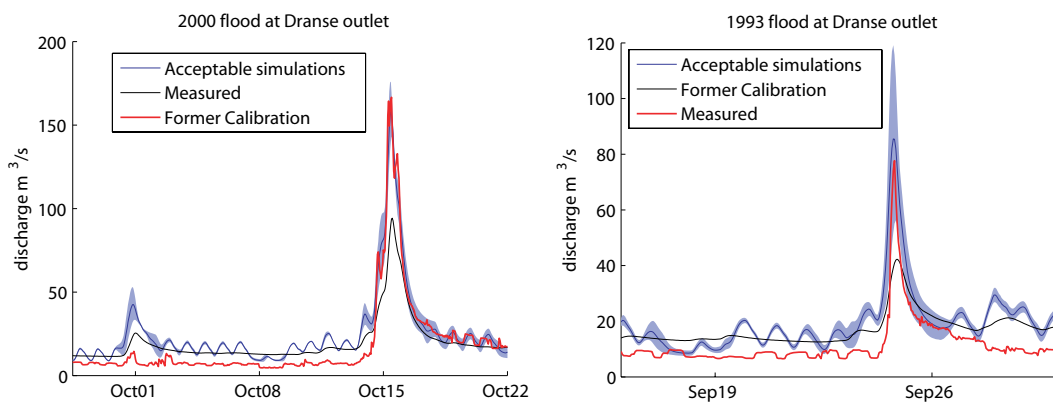


Figure 6.12: Calibration and validation at the Dranse outlet, a) 2000 flood event and b) 1993 flood event respectively. Source measured data: (FOEN, 2008)

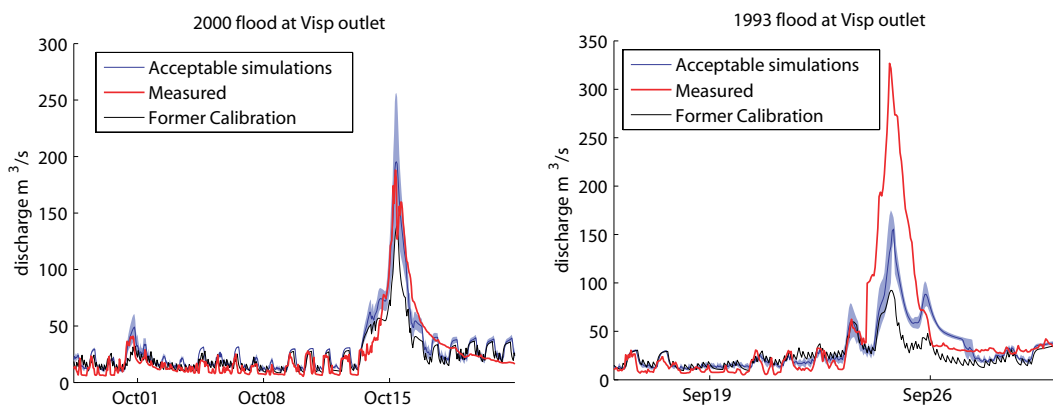


Figure 6.13: Calibration and validation at the Visp outlet, a) 2000 flood event and b) 1993 flood event respectively. Source measured data: (FOEN, 2008)

Chapter 6. A fit-for-purpose uncertainty approach for Alpine hydrological model calibration

Table 6.5: Final performances with respect to the APK (Peak) and NSE (Nash-Sutcliffe efficiency) likelihood measures for Manual Calibration (MC) and Customized Calibration (CC). NA indicates the discharge gauge was damaged during the flood event, so peak values are unknown while the NSE criterion is calculated over the remainder of the hydrological year.

	Dranse							
	APK				NSE			
	2000		1993		2000		1993	
	MC	CC	MC	CC	MC	CC	MC	CC
Châble	- 47%	- 10%	- 22%	- 8%	0.3	0.6	0.0	0.51
Dranse	- 44%	+ 5%	- 47%	- 10%	0.4	0.77	0.0	0.6
Mauvoisin	- 62%	- 9%	- 54%	+ 5%	0.75	0.77	0.8	0.83
	Visp							
	APK				NSE			
	2000		1993		2000		1993	
	MC	CC	MC	CC	MC	CC	MC	CC
Visp	- 27%	- 9%	- 72%	-55%	0.36	0.74	0.45	0.48
Biel	- 44%	- 8%	+ 7%	- 9%	0.29	0.62	0.4	0.55
Balen	NA	NA	NA	NA	0.5	0.7	0.59	0.61
Mattmark	+ 10%	- 10%	- 59%	- 8%	0.71	0.73	0.59	0.62

6.4 Conclusions

This research demonstrates a semi-automatic uncertainty estimation method and visualization tool for the calibration of a hydrological model used in operational flood forecasting in the Swiss Alps. Due to inherent errors in hydrological modeling input and model structure, this tool emphasizes the concept of multiple working hypotheses where a range of plausible model outputs based on equally performing parameter sets are provided. This tool enables the exploration of parameter model spaces and it provides users a means to gain more certainty on the choices of parameters which produce good model performances. Sensitivity analyses enabled the parameter ranges to be constrained. Hydrograph behavior was evaluated based on analyzing individual likelihood measures and using a visualization tool. Best method performances were evaluated based on using a customized weighted likelihood measure to rank performances per calibration zone. Results indicate that temporally variable lapse rates provide a greater number of good performing parameter sets, and diurnal variability of discharge is better achieved with a time variable degree-day factor for snow. Also, the weighted criterion measure is effective in detailing parameter sets that perform well.

Overall, in each calibration zone, better performances are achieved relative to manual calibration. The improvements can be attributed to the use of multi-criteria and a unique visualization tool which enables the analysis of plausible model ensembles. Further testing of these tools is required to ensure that they are reliable and can effectively reduce uncertainty for water resource managers. Due to the random search method utilized which was slow to sample parameter sets because of long computational times, it is recommended to integrate more efficient sampling procedures in the future. Also, more 'soft' data and fuzzy performance measures can be used to incorporate expert knowledge or data of different timescales. Furthermore, it is recommended to integrate geostatistical methods to interpolate forcings in an operational environment so that runoff volume generation can be improved.

Conclusions and Perspectives

A primary challenge for flood forecasting in complex, mountainous terrain is reducing prediction uncertainty. This research has addressed this issue by improving the hydrological modeling component of the RSII flood forecasting model used in the Swiss Alps and associating plausibility ranges to model predictions. The chapters of this thesis have discussed methodologies adapted specifically to mountainous regions to better define the distribution of inputs, the description of snowmelt processes and the reduction of output uncertainty. All chapters deal with the common difficulty of characterizing complex, hydro-meteorological processes when limited measurements are available for validation.

Chapter 3 of this thesis demonstrates that hydrological model uncertainty can be reduced by improving the spatial interpolation of inputs to obtain correct flood volumes. Kriging with external drift is demonstrated to be an effective geostatistical method to estimate precipitation and temperature fields for Alpine terrain. Results indicate foremost that this method enables highly accurate predictions of discharge volumes and peaks during flood events. Elevation as external drift is also shown to be the determinant factor for improving snow/rainfall partitioning and melt estimations over the study region. Particular to this study is the use of a non-standard variogram which proves to be a robust means to detect correlations between the limited meteorological forcing measurements (classical variograms failed in this respect). Variogram analysis shows that significant anisotropy (induced by dominant wind and orographic patterns) is detected in field data and its effect thus needs to be accounted for in spatial interpolation.

It is recommended that the interpolation methodology of Chapter 3 be fully integrated into the real-time RSII operational flood forecasts. This method also has the potential to provide better input estimations for other ensemble hydrological models used in Alpine contexts, most notably those used in the Common Information Platform for Natural Hazards in Switzerland (OFEV, 2010). With a better distribution of input data in the future, particularly in Switzerland

(Romang et al., 2011), the ability to generate reliable variograms and the accuracy of this method will undoubtedly improve. A key component to the success of this interpolation method is the chosen variogram. As limited studies have used this variogram, it is recommended to continue geostatistical analyses to further understand the potential and limitations of this variogram. Furthermore, it was a deliberate decision to use this geostatistical method because other studies have demonstrated good performances with this method when using radar as an external drift factor (Krajewski, 1987; Haberlandt, 2007; Velasco-Forero et al., 2008). It is expected that once a radar is installed in the Valais region, better performances will be achieved with this method.

The inputs to the hydrological model are further improved in Chapter 4 of this thesis. Prior to this improvement, the hydrological model used the common approach of utilizing dry, ground temperature measurements to calculate the snowfall limit. However, this research has demonstrated that accounting for the wet bulb temperature is critical to accurately define the snow/rain transition. COSMO reanalyses, which considers the wet bulb temperature in their snowfall limit calculations, is used as input to the hydrological model. Results indicate that the proposed method to integrate COSMO reanalyses significantly improves runoff simulations during the spring, which is a critical time for flood development when most Alpine catchments are close to saturation.

Although COSMO output has previously been integrated into hydrological models to provide a grid of meteorological forcings, the study in Chapter 4 was novel in its attempt to transfer meteorological knowledge on wet bulb information from COSMO reanalyses into hydrology. Further tests are therefore required to test the rigor of this method and the viability of using COSMO reanalyses (or forecasts in an operational context), particularly as the resolution of COSMO models becomes finer in the future. Most importantly, extremely limited hydrological studies have tested the use of wet bulb temperature measurements in determining lapse rates. Such an approach could be a simple means to improve hydrological predictions in mountainous terrain where an inaccurate temperature lapse rate has significant consequences on defining runoff contributing areas.

Chapter 5 of this thesis demonstrates the potential of a new minimalist snowmelt formulation. This method uses a quasi-sinusoid function to enable daily minimum and maximum temperature data to mimic diurnal radiation cycles. This approach is compared with the commonly used potential radiation-based Hock approach (Hock, 1999) which has successfully modeled sub-daily snowmelt in numerous previous studies. The robustness of these methods is validated on a unique wireless, distributed dataset (Ingelrest et al., 2010), which enables a comparison of the approaches based on different temperature distributions. Results indicate that both methods are comparable in terms of generating potential melt. However, the performances of the methods can depend on the dominant exposition of the dataset. In effect, this study has brought to light that snowmelt methods require a good representation of the spatial variability of temperature (i.e., realistic lapse rates) to correctly model the spatial variability of snowmelt.

It is recommended to conduct future analyses with distributed meteorological observations during the spring snowmelt season. Additional field campaigns can help elucidate how well the snowmelt methods perform as a function of exposition. Furthermore, as the minimalist, proposed melt method has only been tested in these limited cases (yet has potential to be applied in high mountainous environments which are limited in data), it is recommended to further examine the method's robustness with hourly snowmelt databases extending over several melt seasons.

The application of a spatially-explicit hydrological model used to test the snowmelt method performances has been found to be an integral part of the analysis of Chapter 5 (Rinaldo et al., 1995). It is recommended to continue to exploit such an approach due to its physical description of water particle travel times in channeled and hillslope states, where hillslope processes are particularly dominant in complex morphology such as the Swiss Alps. Furthermore, this spatially-explicit approach is a good reference for a wide range of hydrological modeling applications from lumped to semi-distributed because source areas are defined based on homogeneous snowmelt or rainfall contributing areas; as long as the correlation scales of rainfall events or snowmelt contributions over source areas are larger than the area of the subcatchments themselves, the model enables any snowmelt or rainfall pattern to be routed to the outlet. By explicitly describing path probabilities, this approach also allows the catchment to gauge only certain hydrologic pathways as time elapses. The time evolution of the path probability, and hence of the selected pathways, is dictated by the relative inflow distribution through rain and melt (related to altitude, exposure and other factors). For instance, if no snowmelt at all occurs in a given source area of the catchment at a given time, its morphology goes unseen by the response at the same time. In contrast, when a sizable proportion of inflow characterizes the source area, its contribution and the related shape of the basin can be detected.

Future work should explore the idea of inverse modeling the discharge signal to determine which source areas are activated over time. Such a study can be useful to determine which regions influence the fluctuations of saturated antecedent soil moisture conditions and hydrograph behavior as well as answer when specific source areas contribute to dynamic flood responses. A deconvolution of the discharge with the total melt signal can be used to show the individual contributions of each source area. Deconvolution with the GLUE approach exercised in this thesis could be used to determine weights which scale the source area melt to elucidate its contribution to the output discharge. Such an analysis would depend on properly sizing source areas for a reasonably-sized catchment; source areas must not be too finely discretized to be able to distinguish between different source area signals, and the catchment must not be so large that diurnal snowmelt cycles are dampened.

Furthermore, by predicting maximum saturation conditions and identifying flow directions for synoptic scale precipitation events that are aligned with the main axes of catchments, it can be possible to define the most damaging flood conditions or impacts from 'the perfect storm' for catchments in the Valais with the use of the spatially-explicit model. By simulating

Chapter 7. Conclusions and Perspectives

peak rainfall impulses which are aligned with the advection of peak flood responses, it can be possible to demonstrate the worst possible hydrological conditions which can occur in Alpine regions assuming a saturated snowpack and rain-on-snow conditions. Preventive scenario analysis can then be performed with the RSII model such as by adjusting reservoir levels to determine how to best mitigate potential flood damage.

The final chapter of this thesis demonstrates the performance of a customized uncertainty estimation technique and software tool used to assign plausibility ranges to flood predictions. The technique utilizes a visualization interface to display model ensembles and multi-criteria performance measures for the calibration of the hydrological model. Results indicate that by integrating the input and process improvements from Chapters 3-5 of this thesis into this method, the hydrological modeling output error is reduced and calibration achieves a better range of plausible model outputs.

Further tests with this uncertainty estimation technique and calibration tool are required to test the rigor of the approach, particularly the inherent subjectivity of the visualization interface. The visualization tool of this research is key because it enables a means to communicate the inherent uncertainty of hydrological modeling to water resources managers particularly the idea that uncertainty highly depends on the performance measure utilized. Future work could also incorporate the use of 'soft' data such as monthly reservoir water balances (Winsemius et al., 2009) to reduce the sensitivity of all the aforementioned methods to the impact of limited station data available. Point measurements which contain extractable information for model calibration should also be considered (Schaefli, 2011) and perhaps in a fuzzy context (Bárdossy, 2005).

Most importantly, future research lanes with the calibration tools developed herein must include better quantification of the uncertainty cascade (Pappenberger et al., 2005) produced when the hydrological model, calibrated with measured data, begins to use Limited Area Model probabilistic forecasts as inputs. Although research has shown promising results in using statistically downscaled Limited Area Model output, it will most likely be necessary to use correction biases such as magnitude correction factors to obtain better temperature, precipitation and resulting runoff time series (Hay and Clark, 2003). Fortunately, advances in data assimilation have demonstrated sophisticated developments such as extended Kalman filtering which can address state and error updating (Liu et al., 2012). However, few studies have quantified the efficacy of data assimilation real-time. Furthermore, studies must be conducted on the impact of merging uncertainty ranges from forecasting inputs and hydrological model ensembles. It will undoubtedly be critical to test the best means to validate combined uncertainty ranges when the flood forecasting model becomes fully operational.

Bibliography

- Addor, N., Juan, S., Fundel, F., Zappa, M., 2011. An operational hydrological ensemble prediction system for the city of Zurich (Switzerland): skill, case studies and scenarios. *Hydrol. Earth Syst. Sc.* 15, 2327–2347.
- Agrawala, S., Abegg, B., Jette-Nantel, S., Crick, F., de Montfalcon, A., 2007. Climate Change in the European Alps, Adapting Winter Tourism and Natural Hazards Management. OECD.
- Ahmed, T., de Marsily, G., 1987. Comparison of geostatistical methods for estimating transmissivity using data transmissivity and specific capacity. *Water Resour. Res.* 23, 1717–1737.
- Ajami, N., Qingyun, D., Soroosh, S., 2007. An integrated hydrologic Bayesian multimodel combination framework: Confronting input, parameter, and model structural uncertainty in hydrologic prediction. *Water Resour. Res.* 43, W01403.
- Akhtar, M., Ahmad, N., Booij, M., 2008. Use of regional climate model simulations as input for hydrological models for the Hindukush-Karakorum-Himalaya region. *Hydrol. Earth Syst. Sc.* 13, 1075–1089.
- Alfieri, L., Smith, P., Thielen-delPozo, J., Beven, K., 2011. A staggered approach to flash flood forecasting, case study in the Cévennes region. *Adv. Geosci.* 29, 13–20.
- Allamano, P., Claps, P., Laio, F., 2009. Global warming increases flood risk in mountainous areas. *Geophys. Res. Lett.* 36, 1–5.
- Ament, F., Weusthoff, T., Arpagaus, M., 2011. Evaluation of MAP D-PHASE heavy precipitation alerts in Switzerland during summer 2007. *Atmos. Res.* 100, 178–189.
- Anderson, E., 1973. National Weather Service River Forecast System—Snow Accumulation and Ablation Model. Technical Memorandum NWS HYDRO-17. NOAA. U.S. Department of Commerce, Silver Spring, MD. 217pp.
- Anderton, S., White, S., Alvera, B., 2002. Micro-scale spatial variability and the timing of snow melt runoff in a high mountain catchment. *J. Hydrol.* 268, 158–176.

Bibliography

- Attinger, S., Fallot, J.M., 2003. Fréquence des intempéries et des précipitations abondantes en Valais (Alpes Suisses Occidentales) durant le 20ème siècle. *Association Int. de Climatol.* 15, 253–259.
- Bárdossy, A., 2005. *Encyclopedia of Hydrological Sciences*. Wiley Publishing. volume 130. chapter Fuzzy Sets in Rainfall/Runoff Modeling. pp. 1–8.
- Bárdossy, A., 2007. Calibration of hydrological model parameters for ungauged catchments. *Hydrol. Earth Syst. Sc.* 11, 703–710.
- Barnes, B., 1939. Consistency in unit graphs. *J. Hydraul. Div. Proc.* 85, 39–61.
- Bauer, H., Weusthoff, T., Dorninger, M., Wulfmeyer, V., Schwitalla, T., Gorgas, T., Arpagaus, M., Warrach-Sagi, K., 2011. Predictive skill of a subset of models participating in D-PHASE in the COPS region. *Q. J. Roy. Meteor. Soc.* 137, 287–305.
- Bavay, M., Lehning, M., Jonas, T., Lowe, H., 2009. Simulations of future snow cover and discharge in alpine headwater catchments. *Hydrol. Process.* 23, 95–108.
- Bayes, T., 1763. On essay towards solving a problem in the doctrine of chances. *Phil. Trans. R. Soc. Lond.* 53, 370–418.
- Benestad, R., Haugen, J., 2007. On complex extremes: flood hazards and combined high spring-time precipitation and temperature in Norway. *Clim. Change* 85, 381–406.
- Bergstrom, S., 1975. Development of a snow routine for the HBV-2 model. *Nord. Hydrol.* 6, 73–92.
- Bergstrom, S., 1995. *Computer Models of Watershed Hydrology*. Water Resource Publications, Littleton, Colorado. chapter The HBV model. b edition. pp. 443–476.
- Berne, A., Delrieu, G., Andrieu, H., Creutin, J.D., 2004. Influence of the vertical profile of reflectivity on radar-estimated rain rates at short time steps. *J. Hydrometeorol.* 5, 296–310.
- Bérod, D., 2009. Uncertainties for the hydrologist : paranoia treated by schizophrenia. *Houille Blanche* , 77–81.
- Bérod, D., Singh, V., Devrad, D., Musy, A., 1995. A geomorphologic non-linear cascade (GNC) model for estimation of floods from small Alpine watersheds. *J. Hydrol.* 166, 147–170.
- Beven, K., 2004. *Rainfall Runoff Modelling - The Primer*. Wiley Publishing, New York.
- Beven, K., 2005. On the concept of model structural error. *Water Sc. Techno.* 52, 165–175.
- Beven, K., 2006. A manifesto for the equifinality thesis. *J. Hydrol.* 320, 18–36.
- Beven, K., 2009. *Environmental Modeling: An Uncertain Future?* Routedledge, New York.
- Beven, K., Binley, A., 1992. The future of distributed models: Model calibration and uncertainty prediction. *Hydrol. Process.* 6, 279–298.

- Beven, K., Buytaert, W., Smith, L., 2012. On virtual observatories and modelled realities (or why discharge must be treated as a virtual variable). *Hydrol. Process.* 10.
- Beven, K., Freer, J., 2001. Equifinality, data assimilation, and uncertainty estimation in mechanistic modelling of complex environmental systems using the GLUE methodology. *J. Hydrol.* 249, 11–29.
- Beven, K., Smith, P., Wood, A., 2011. On the colour and spin of epistemic error (and what we might do about it). *Hydrol. Earth Syst. Sc.* 15, 3123–3133.
- Beven, K., Westerberg, I., 2011. On red herrings and real herrings: disinformation and information in hydrological inference. *Hydrol. Process.* 25, 1676–1680.
- Beven, K., Wood, E., 1993. *Channel Network Hydrology*. Wiley Publishing. chapter Flow routing and the hydrological response of channel networks. pp. 99–128.
- Blandford, T., Humes, K., Harshburger, B., Moore, B., Walden, V., 2008. Seasonal and synoptic variations in near-surface air temperature lapse rates in a mountainous basin. *J. Appl. Meteorol. and Climatol.* 47, 249–261.
- Blöschl, G., 1991. The influence of uncertainty in air temperature and albedo on snowmelt. *Nord. Hydrol.* 22, 95–108.
- Blöschl, G., Kirnbauer, R., 1992. An analysis of snow cover patterns in a small Alpine catchment. *Hydrol. Proc.* 6, 99–109.
- Blöschl, G., Kirnbauer, R., Gutknecht, D., 1991. Distributed snowmelt simulations in an Alpine catchment. 1. model evaluation on the basis of snow cover patterns. *Water Resour. Res.* 27, 3171–3179.
- Blöschl, G., Montanari, A., 2010. Climate change impacts - throwing the dice? *Hydrol. Process.* 24, 374–381.
- Bocchiola, D., Mihalcea, C., Diolaiuti, G., Mosconi, B., Smiraglia, C., Rosso, R., 2010. Flow prediction in high altitude ungauged catchments: A case study in the Italian Alps (Pantano Basin, Adamello Group). *Adv. Water Resour.* 33, 1224–1234.
- Botter, G., Bertuzzo, E., A, R., 2010. Transport in the hydrologic response: travel time distributions, soil moisture dynamics and the old water paradox. *Water Resour. Res.* 46, W03514.
- Botter, G., Bertuzzo, E., Bellin, A., Rinaldo, A., 2005. On the lagrangian formulations of reactive solute transport in the hydrologic response. *Water Resour. Res.* 41, 4008–4016.
- Botter, G., Rinaldo, A., 2003. Scale effect of geomorphologic and kinematic dispersion. *Water Resour. Res.* 39, 1286.
- Bourgouin, P., 2000. A method to determine precipitation types. *Weather Forecast.* , 583–592.

Bibliography

- Braithwaite, R., 1995. Positive degree-day factors for ablation on the Greenland ice sheet studied by energy-balance modelling. *J. Glaciol.* 41, 153–160.
- Braithwaite, R., 2008. Temperature and precipitation climate at the equilibrium-line altitude of glaciers expressed by the degree-day factor for melting snow. *J. Glaciol.* 54, 437–444.
- Brath, A., Montanari, A., Toth, E., 2004. Analysis of the effects of different scenarios of historical data availability on the calibration of a spatially-distributed hydrological model. *J. Hydrol.* 291, 232–253.
- Braun, L., Brun, E., Durand, Y., Martin, E., Tourasse, P., 1994. Simulation of discharge using different methods of meteorological data distribution, basin discretization and snow modelling. *Nord. Hydrol.* 25, 129–144.
- Brubaker, K., Pinker, R., Deviatova, E., 2005. Evaluation and comparison of MODIS and IMS snow-cover estimates for the continental United States using station data. *J. Hydrometeorol.* 6, 1002–1017.
- Brubaker, K., Rango, A., Kustas, W., 1996. Incorporating radiation inputs into the snowmelt runoff model. *Hydrol. Process.* 10, 1329–1343.
- Brutsaert, W., 2005. *Hydrology. An Introduction.* Cambridge Univ. Press, New York.
- Brutsaert, W., J., N., 1977. Regionalized drought flow hydrographs from a mature glaciated plateau. *Water Resour. Res.* 13, 637–643.
- Buizza, R., Miller, M., Palmer, T., 1999. Stochastic representation of model uncertainties in the ECMWF ensemble prediction system. *Q. J. Roy. Meteor. Soc.* 125, 2887–2908.
- Buytaert, W., Celleri, R., Willems, P., 2006. Spatial and temporal rainfall variability in mountainous areas: A case study from the south Ecuadorian Andes. *J. Hydrol.* 329, 413–421.
- Carenzo, M., Pellicciotti, F., Rimkus, S., Burlando, P., 2009. Assessing the transferability and robustness of an enhanced temperature-index glacier-melt model. *J. Glaciol.* 55, 258–274.
- Cazorzi, F., DallaFontana, G., 1996. Snowmelt modelling by combining air temperature and a distributed radiation index. *J. Hydrol.* 181, 169–187.
- Chamberlin, T., 1890. The method of multiple working hypotheses. *Science* 15.
- Chanson, H., 2004. *The Hydraulics of Open Channel Flow.* Butterworth-Heinemann, Oxford, UK. 2nd edition.
- Cloke, H., Pappenberger, F., 2009. Ensemble flood forecasting: A review. *J. Hydrol.* 375, 613–626.
- COSMO, 2011. Consortium for Small-scale Modeling. Technical Report. <http://www.cosmo-model.org>.

- Cressie, N., 1984. Geostatistics for Natural Resources Characterization. D. Reidel, Norwell, MA. chapter Towards resistant geostatistics. 1, pp. 21–44.
- Cressie, N., 1988. Spatial prediction and ordinary kriging. *Math. Geol.* 20, 405–421.
- Cvetkovic, V., Dagan, G., 1994. Transport of kinetically sorbing solute by steady random velocity in heterogeneous porous formations. *J. Fluid Mech.* 265, 189–215.
- Cvetkovic, V., Dagan, G., 1996. Reactive transport and immiscible flow in geological media. I. General theory. *Proc. R. Soc. Lond.* A452, 303–328.
- Dagan, G., 1989. Flow and transport in porous formations. Springer-Verlag, Berlin-Heidelberg.
- Daly, C., 2006. Guidelines for assessing the suitability of spatial climate data sets. *Int. J. Hydrol.* 26, 707–721.
- DAS, 2009. Department of Atmospheric Science, University of Wyoming, World radiosounding data. <http://weather.uwyo.edu/upperair/sounding.html>.
- Debele, B., Srinivasan, R., Gosain, A., 2010. Comparison of process-based and temperature-index snowmelt modeling in SWAT. *Water Resour. Manag.* 24, 1065–1088.
- Dozier, J., 2011. Mountain hydrology, snow color, and the fourth paradigm. *EOS* 92, 373–374.
- Dubois, G., 1997. A geostatistical autopsy of the Austrian indoor radon survey (1992-2002). *Sci. of the Total Env.* 377, 378–395.
- Dunn, S., Colohan, R., 1999. Developing the snow component of a distributed hydrological model: a step-wise approach based on multi-objective analysis. *J. Hydrol.* 223, 1–16.
- Dunne, T., 1978. *Hillslope Hydrology*. Wiley Interscience. chapter Field studies of hillslope flow processes. pp. 227–293.
- Finger, D., Pellicciotti, F., Konz, M., Rimkus, S., Burlando, P., 2011. The value of glacier mass balance, satellite snow cover images, and hourly discharge for improving the performance of a physically based distributed hydrological model. *Water Resour. Res.* 47, W07519.
- Finsterwalder, S., Schunk, H., 1887. *Der suldenferner*. zeitschrift des Deutschen und Oesterreichischen Alpenvereins 18, 72–89.
- Fleming, S., Weber, F., Weston, S., 2010. Multi-objective, manifoldly constrained Monte Carlo optimization and uncertainty estimation for an operational hydrologic forecast model, in: AMS (Ed.), 24th Conference on Hydrology, AMS, Washington, DC.
- FOEN, 2008. *The Hydrological Yearbook of Switzerland*, Swiss Federal Office for the Environment. <http://www.bafu.admin.ch/publikationen/publikation/01062/index.html?lang=de>.
- Freer, J., McMillan, H., McDonnell, J., Beven, K., 2004. Constraining dynamic topmodel responses for imprecise water table information using fuzzy rule based performance measures. *J. Hydrol.* 3-4, 254–277.

Bibliography

- Frei, C., Schär, C., 1998. A precipitation climatology of the Alps from high-resolution rain-gauge observations. *Int. J. of Climatol.* 18, 873–900.
- Fundel, F., Zappa, M., 2011. Hydrological ensemble forecasting in mesoscale catchments: Sensitivity to initial conditions and value of reforecasts. *Water Resour. Res.* 47, W09520.
- Garcia Hernández, J., Boillat, J.L., Jordan, E., Hingray, B., 2009a. Hydrometeorological forecast on the Rhone River Catchment upstream of Lake Geneva. *Houille Blanche* 5, 61–70.
- Garcia Hernández, J., Brauchli, T., Boillat, J.L., Schleiss, A., 2011. Flood management in the Upper Rhone River basin: from forecast to decision. *Houille Blanche* 2, 69–75.
- Garcia Hernández, J., Horton, P., Tobin, C., Boillat, J.L., 2009b. Prévision hydrométéorologique et gestion de crues sur le Rhône alpin. *Eau énergie air* 4, 297–302.
- Garcia Hernández, J., Jordan, E., Dubois, J., Boillat, J.L., 2007. Flow modelling in hydraulic systems. Communication 32. Laboratory of Hydraulic Construction, EPFL.
- Germann, U., Galli, G., Boscacci, M., Bolliger, M., 2006. Radar precipitation measurement in a mountainous region. *Q. J. Roy. Meteor. Soc.* 132, 1669–1692.
- Goovaerts, P., 1997. *Geostatistics for Natural Resources Evaluation*. Oxford University Press, New York.
- Goovaerts, P., 1999. Using elevation to aid the geostatistical mapping of rainfall erosivity. *CATENA* 34, 227–242.
- Goovaerts, P., 2000. Geostatistical approaches for incorporating elevation into the spatial interpolation of rainfall. *J. Hydrol.* 228, 113–129.
- Graham, R., Evans, M., 2011. Strength and weaknesses of P-type algorithms, in: NOAA Warning Decision Training, NOAA. [Http://www.wdtb.noaa.gov/courses/winterawoc/documents](http://www.wdtb.noaa.gov/courses/winterawoc/documents).
- Griffiths, G., McSaveny, M., 1983. Distribution of mean annual precipitation across some stepland regions of New Zealand. *N.Z. J. Sci.* 26, 197–209.
- Groisman, P., Legates, D., 1994. The accuracy of United States precipitation data. *B. Am. Meteorol. Soc.* 75, 215–227.
- Gruenewald, T., Lehning, M., 2011. Altitudinal dependency of snow amounts in two small alpine catchments: can catchment-wide snow amounts be estimated via single snow or precipitation stations? *Ann. Glaciol.* 52, 153–158.
- Guan, H., Wilson, J., Makhnin, O., 2005. Geostatistical mapping of mountain precipitation incorporating autosearched effects of terrain and climatic characteristics. *J. Hydrometeorol.* 6, 1018–1031.
- Gupta, H., Beven, K., Wagener, T., 2005. *Encyclopedia of Hydrological Sciences*. Wiley Publishing, volume 142. chapter Model calibration and uncertainty estimation. pp. 1–18.

- Gupta, H., Sorooshian, S., Yapo, P., 1998. Toward improved calibration of hydrological models: Multiple and noncommensurable measures of information. *Water Resour. Res.* 34, 751–763.
- Gupta, V., Waymire, E., Wang, E., 1980. A representation of the instantaneous unit hydrograph from geomorphology. *Water Resour. Res.* 16, 855–862.
- Gutermann, T., 1986. Das automatische Wetterbeobachtungsnetz der Schweiz (ANETZ). *MeteoSwiss*. CH-8044 Zurich, Switzerland. sma, bericht edition. 17 pp.
- Haberlandt, U., 2007. Geostatistical interpolation of hourly precipitation from rain gauges and radar for a large-scale extreme rainfall event. *J. Hydrol.* 332, 144–157.
- Häberli, C., Mettler, J., Mühlhäuser, C., Musa, M., Oswald, M., Perl, M., Rohrer, M., Steinegger, U., Suter, S., Dürr, B., 2008. Functions for the Calculation of meteorological and climatological quantities used at the Swiss Meteorological Institute, Version 4.3. Technical Report.
- Hagedorn, R., Hamill, T., Whitaker, J., 2007. Probabilistic forecast calibration using ECMWF and GFS ensemble forecasts. part I: 2-meter temperature. *Mon. Weather Rev.* 136, 2608–2619.
- Haiden, T., Kann, A., Wittmann, C., Pistotnik, G., Bica, B., Gruber, C., 2011. The Integrated Nowcasting through Comprehensive Analysis (INCA) system and its validation over the eastern Alpine region. *Weather Forecast* 26, 166–183.
- Hall, D., Riggs, G., Salomonson, V., 2006. updated daily. MODIS/Terra snow cover 5-min L2 swath 500m V005, chapter 1 July 2008, 1 May 2009, Digital media.
- Hamdi, Y., Hingray, B., Musy, A., 2005. Un modèle de prévision hydro-météorologique pour les crues du Rhône supérieur en Suisse. *Eau énergie air* 1, 325–332.
- Hamlin, L., Pietroniro, A., Prowse, T., Soulis, R., Kouwen, N., 1998. Application of indexed snowmelt algorithms in a northern wetland regime. *Hydrol. Process.* 12, 1641–1657.
- Hancock, P., Hutchinson, M., 2006. Spatial interpolation of large climate data sets using bivariate thin plate smoothing splines. *Environ. Modell. Softw.* 21, 1684–1694.
- Hay, L., Clark, M., 2003. Use of statistically and dynamically downscaled atmospheric model output for hydrologic simulations in three mountainous basins in the western United States. *J. Hydrol.* 282, 56–75.
- Hebeler, F., Purves, R., 2008. The influence of resolution and topographic uncertainty on melt modelling using hypsometric sub-grid parameterization. *Hydrol. Process.* 22, 3965–3979.
- Heilig, A., Eisen, O., Schneebeli, M., 2010. Temporal observations of a seasonal snowpack using upward-looking GPR. *Hydrol. Process.* 24, 3133–3145.
- Helfrich, S.R., McNamara, D., Ramsay, B.H., Baldwin, T., Kasheta, T., 2007. Enhancements to, and forthcoming developments in the Interactive Multisensor Snow and Ice Mapping System (IMS). *Hydrol. Process.* 21, 1576–1586.

Bibliography

- Herrmann, A., Rau, R., 1984. Snow cover stores and winter runoff behavior of a small basin in the German highlands, in: *Snow Hydrologic Research in Central Europe: Proc. Hann. Munden Meeting, DVWK-Mitteilungen 7 Bonn*. pp. 449–472.
- Hingray, B., Mezghani, A., Schaepli, B., Niggli, M., Faivre, G., Guex, G., Hamdi, Y., Musy, A., 2006. Estimation des débits de crue du Rhône à Porte du Scex et autres points amont caractéristiques. *Projet CONSECRU 2. Rapport final. Laboratoire Hydrologie et Aménagements, EPFL*.
- Hingray, B., Schaepli, B., Mezghani, A., Y. Hamdi, 2010. Signature-based model calibration for hydrological prediction in mesoscale Alpine catchments. *Hydrol. Sci. J.* 55, 1002–1016.
- Hock, R., 1999. A distributed temperature-index ice- and snowmelt model including potential direct solar radiation. *J. Glaciol.* 45, 101–111.
- Hock, R., 2003. Temperature index melt modelling in mountain areas. *J. Hydrol.* 282, 104–115.
- Hoeting, J., Madigan, D., Raftery, A., Volinsky, C., 1999. Bayesian model averaging: A tutorial. *Stat. Sci.* 14, 382–417.
- Horton, P., Schaepli, B., Mezghani, A., Hingray, B., Musy, A., 2006. Assessment of climate-change impacts on Alpine discharge regimes with climate model uncertainty. *Hydrol. Process.* 20, 2091–2109.
- Hostache, R., Matgen, P., Montanari, A., Montanari, M., Hoffman, L., Pfister, L., 2010. Propagation of uncertainties in coupled hydro-meteorological forecasting systems: A stochastic approach for the assessment of the total predictive uncertainty. *Atmos. Res.* 100, 263–274.
- Hrachowitz, M., Weiler, M., 2011. Uncertainty of precipitation estimates caused by sparse gauging networks in a small, mountainous watershed. *J. Hydrol. Eng.* 16, 460–471.
- Hudson, G., Wackernagel, H., 1994. Mapping temperature using kriging with external drift - theory and an example from Scotland. *Int. J. Climatol.* 14, 77–91.
- Hüsler, E., Jonas, T., Wunderle, S., Albrecht, S., 2012. Validation of a modified snow cover retrieval algorithm from historical 1-km AVHRR data over the European Alps. *Remote Sens. Environ.* 121, 497–515.
- Huss, M., 2011. Present and future contribution of glacier storage change to runoff from macroscale drainage basins in Europe. *Water Resour. Res.* 47, W07511.
- Huss, M., Farinotti, D., Bauder, A., Funk, M., 2008. Modelling runoff from highly glacierized alpine drainage basins in a changing climate. *Hydrol. Process. - Sp. Iss.* 22, 3888–3902.
- Huwald, H., Higgins, C., Boldi, M.O., Bou-Zeid, E., Lehning, M., Parlange, M., 2009. Albedo effect on radiative errors in air temperature measurements. *Water Resour. Res.* 45, W08431.

- Ingelrest, F., Barrenetxea, G., Schaefer, G., Vetterli, M., Couach, O., Parlange, M., 2010. Sensorscope: Application-specific sensor network for environmental monitoring. *ACM Transactions on Sensor Networks* 6.
- Iorgulescu, I., Beven, K., Musy, A., 2005. Data-based modelling of runoff and chemical tracer concentrations in the Haute-Mentue research catchment (Switzerland). *Hydrol. Process.* 19, 2557–2573.
- Isaaks, E., Srivastava, R., 1989. *Applied Geostatistics*. Oxford University Press, New York.
- Jasper, K., Gurtz, J., Lang, H., 2002. Advanced flood forecasting in Alpine watersheds by coupling meteorological observations and forecasts with a distributed hydrological model. *J. Hydrol.* 267, 40–52.
- Jonas, T., Marty, C., Magnusson, J., 2009. Estimating the snow water equivalent from snow depth measurements in the Swiss Alps. *J. Hydrol.* 378, 161–167.
- de Jong, C., Collins, D., Ranzi, R., 2005. *Climate and Hydrology in Mountain Areas*. Wiley publishing, England.
- Jordan, F., 2007. *Modèle de prévision et de gestion des crues : optimisation des opérations des aménagements hydroélectriques à accumulation pour la réduction des débits de crue*. Ph.D. thesis. École Polytechnique Fédérale de Lausanne.
- Jordan, F., Hernández, J.G., Boillat, J.L., Schleiss, A., 2008. Flood forecast and flood management model: Optimization of the operation of storage power plants for flood routing, in: 11th International Interpraevent 2008 Conference Proceedings, Dornbirn, Austria.
- Joss, J., Schadler, B., Galli, G., Cavalli, R., Boscacci, M., Held, E., Bruna, G., Kappenberger, G., Nespor, V., Spiess, R., 1997. Operational use of radar for precipitation measurements in Switzerland. *MeteoSwiss*. Locarno, Switzerland.
- Jost, G., Moore, R.D., Smith, R., Gluns, D., 2012. Distributed temperature-index snowmelt modelling for forested catchments. *J. Hydrol.* 420-421, 87–101.
- Jost, G., Weiler, M., Gluns, D., Alila, Y., 2007. The influence of forest and topography on snow accumulation and melt at the watershed-scale. *J. Hydrol.* 347, 101–115.
- Juan, S., Ahrens, B., Walser, A., Ewen, T., Schar, C., 2008. Aprobabilistic view on the August 2005 floods in the upper Rhine catchment. *Nat. Hazard. Earth Sys.* 8, 281–291.
- Katzfey, J., 1995. Simulation of extreme New Zealand precipitation events. Part II. Mechanisms of precipitation development. *Mon. Weather Rev.* 123, 737–754.
- Kaufmann, P., 2008. Association of surface stations to NWP model grid points. *COSMO Newsletter* 9 DWD, Offenbach, Germany , 54–55.

Bibliography

- Kavetski, D., Kuczera, G., Franks, S., 2006. Bayesian analysis of input uncertainty in hydrological modeling: 2. application. *Water Resour. Res.* 42, W03408.
- Kienzle, S., 2008. A new temperature based method to separate rain and snow. *Hydrol. Process.* 22, 5067–5085.
- Kling, H., Furst, J., Nachtnebel, H., 2006. Seasonal, spatially distributed modelling of accumulation and melting of snow for computing runoff in a long-term large-basin water balance model. *Hydrol. Process.* 20, 2141–2156.
- Kling, H., Gupta, H., 2009. On the development of regionalization relationships for lumped watershed models: The impact of ignoring sub-basin scale variability. *J. Hydrol.* 373, 337–351.
- Klok, E., Jasper, K., Roelofsma, K., Gurtz, J., Badoux, A., 2001. Distributed hydrological modelling of a heavily glaciated Alpine river basin. *Hydrol. Sci. J.* 46, 553–570.
- Kobierska, F., Jonas, T., Magnusson, J., Zappa, M., Bavay, M., Bosshard, T., Paul, F., Bernasconi, S., 2011. Climate change effects on snowmelt and discharge of a partly glacierized watershed in central switzerland (SoilTrec Critical Zone Observatory). *Appl. Geochem.* 26, S60–S62.
- Koboltschnig, G., Schoner, W., Holzman, H., Zappa, M., 2009. Glaciers melt of a small basin contributing to runoff under the extreme climate conditions in the summer of 2003. *Hydrol. Process.* 23, 1010–1018.
- Konz, M., Uhlenbrook, S., Braun, L., Shrestha, A., Demuth, S., 2007. Implementation of a process-based catchment model in a poorly gauged, highly glacierized Himalayan headwater. *Hydrol. Earth Syst. Sc.* 11, 1323–1339.
- Krajewski, W., 1987. Cokriging radar-rainfall and rain gage data. *J. Geophys. Res.* 92, 9571–9580.
- Kravchenko, A., 1996. Estimation of mean annual precipitation in Wyoming using geostatistical analysis, AGU 16th Annual Hydrology Days, Fort Collins, Colorado. pp. 271–282.
- Krzysztofowicz, R., 1999. A simple energy budget algorithm for the snowmelt runoff model. *Water Resour. Res.* 35, 2739–2750.
- Kurtzman, D., Kadmon, R., 1999. Mapping of temperature variables in Israel: a comparison of different interpolation methods. *Clim. Res.* 13, 33–43.
- Kustas, W., Rango, A., Uijlenhoet, R., 1994. A simple energy budget algorithm for the snowmelt runoff model. *Water Resour. Res.* 30, 1515–1527.
- Kuusisto, E., 1980. On the values and variability of degree-day melting factor in Finland. *Nord. Hydrol.* 34, 235–242.
- Laio, F., Porporato, A., Ridolfi, L., Rodriguez-Iturbe, I., 2001. Plants in water-controlled ecosystems: active role in hydrologic processes and response to water stress: II. Probabilistic soil moisture dynamics. *Adv. Water Res.* 24, 707 – 723.

- Lamb, R., Beven, K., 1997. Using interactive recession curve analysis to specify a general catchment storage model. *Hydrol. Earth Syst. Sc.* 1, 101–113.
- Lehning, M., Bartelta, P., Brown, B., Fierza, C., 2002. A physical SNOWPACK model for the Swiss avalanche warning: Part III: meteorological forcing, thin layer formation and evaluation. *Cold Reg Sci Technol* 35, 169–184.
- Lehning, M., Gruenewald, T., Schirmer, M., 2011. Mountain snow distribution governed by an altitudinal gradient and terrain roughness. *Geophys. Res. Lett.* 38.
- Lehning, M., Volksch, I., Gustafsson, D., Nguyen, T., Stahli, M., Zappa, M., 2006. ALPINE3D: a detailed model of mountain surface processes and its application to snow hydrology. *Hydrol. Process.* 20, 2111–2128.
- Leimer, S., Thorsten, P., Pfahl, S., Wilcke, W., 2011. Towards a new generation of high-resolution meteorological input data for small-scale hydrological modeling. *J. Hydrol.* 402, 317–332.
- Li, D., Lake, L., 1994. A moving window semivariance estimator. *Water Resour. Res.* 30, 1479–1489.
- Li, X., Williams, M., 2008. Snowmelt runoff modelling in an arid mountain watershed, Tarim Basin, China. *Hydrol. Process.* 22, 3931–3940.
- Liu, Y., Freer, J., Beven, K., Matgen, P., 2009. Towards a limits of acceptability approach to the calibration of hydrological models: Extending observation error. *J. Hydrol.* 367, 93–103.
- Liu, Y., Weerts, A., Clark, M., Franssen, H.H., Kumar, S., Moradkhani, H., Seo, D., Schwanenberg, D., Smith, P., van Dijk, A., van Velzen, N., He, M., Lee, H., Noh, S., Rakovec, O., Restrepo, P., 2012. Advancing data assimilation in operational hydrologic forecasting: progresses, challenges and emerging opportunities. *Hydrol. Earth Syst. Sc.* 9, 3415–3472.
- Loffler, J., Rossler, O., 2005. *Climate and Hydrology in Mountain Areas*. Wiley Publishing, chapter Climatologic and Hydrologic Coupling in the Ecology of Norwegian High Mountain Catchments. 13, pp. 185–214.
- Magnusson, J., Farinotti, D., Jonas, T., Bavay, M., 2011. Quantitative evaluation of different hydrological modelling approaches in a partly glacierized Swiss watershed. *Hydrol. Process.* 25, 2071–2084.
- Maidment, D., 1993. *Handbook of hydrology*. McGraw-Hill, New York.
- Mandapaka, P., Krajewski, W., Mantilla, R., 2009. Dissecting the effect of rainfall variability on the statistical structure of peak flows. *Adv. Water Res.* 32, 1508–1525.
- Mantovan, P., Todini, E., 2006. Hydrological forecasting uncertainty assessment: Incoherence of the GLUE methodology. *J. Hydrol.* 330, 368–381.

Bibliography

- Matheron, G., 1970. La Théorie des Variables Régionalisées et ses Applications. Fascicule 5, Les Cahiers du Centre de Morphologie Mathématique, École des Mines de Paris, Fontainebleau.
- Matsuo, T., Sasyo, Y., 1981. Non-melting phenomena of snowflakes observed in sub saturated air below freezing level. *J. Meteorol. Soc. Jpn.* 59, 26–32.
- Merz, R., Blöschl, G., 2003. A process typology of regional floods. *Water Resour. Res.* 39, 1340.
- Messerli, B., Viviroli, D., Weingartner, R., 2004. Mountains of the world: Vulnerable water towers for the 21(st) century. *Ambio* 13, 29–34.
- MeteoSwiss, . Swiss Meteorological Service. Technical Report. <http://www.meteoswiss.admin.ch/web/en.html>.
- Mezghani, A., Hingray, B., 2009. A combined downscaling-disaggregation weather generator for stochastic generation of multisite hourly weather variables over complex terrain: Development and multi-scale validation for the Upper Rhone River basin. *J. Hydrol.* 377, 245–260.
- Minder, J., Mote, P., Lundquist, J., 2010. Surface temperature lapse rates over complex terrain: Lessons from the Cascade Mountains. *J. Geophys. Res.* 115, 1–13.
- Molini, L., Parodi, A., Rebora, N., Craig, G., 2011. Classifying severe rainfall events over Italy by hydrometeorological and dynamical criteria. *Q. J. Roy. Meteor. Soc.* 137, 148–154.
- Montanari, A., 2005. Large sample behaviors of the Generalized Likelihood Uncertainty Estimation (GLUE) in assessing the uncertainty of rainfall-runoff simulations. *Water Resour. Res.* 41, W08406.
- Montanari, A., 2007. What do we mean by ‘uncertainty’? The need for a consistent wording about uncertainty assessment in hydrology. *Hydrol. Process.* 21, 841–845.
- Montanari, A., 2011. *Treatise on Water Science*. Oxford: Academic Press, Elsevier Ltd.. volume 2. chapter Uncertainty of Hydrologic Predictions. pp. 459–478.
- Montanari, A., Brath, A., 2004. A stochastic approach for assessing the uncertainty of rainfall-runoff. *Water Resour. Res.* 40, W01106.
- Nadeau, D., Brutsaert, W., Parlange, M., Bou-Zeid, E., Barrenetxea, G., Couach, O., Boldi, M.O., Selker, J., Vetterli, M., 2009. Estimation of urban sensible heat flux using a dense wireless network of observations. *Environ. Fluid Mech.* 9, 635–653.
- Nash, J., Sutcliffe, J., 1970. River flow forecasting through conceptual models, Part i — a: Discussion of principles. *J. Hydrol.* 3, 282–290.
- NIC, 2008. IMS daily northern hemisphere snow and ice analysis at 4 km and 24 km resolution. updated daily, National Ice Center, NOAA USA. Image from 30 May 2008.

- Nicótina, L., Celegon, E.A., Rinaldo, A., Marani, M., 2008. On the impact of rainfall patterns on the hydrologic response. *Water Resour. Res.* 44, W12401.
- Nicótina, L., Schaefli, B., Tarboton, D., Rinaldo, A., 2011. Model coupling instead of calibration: what can a catchment model learn from landscape evolution?, in: EGU (Ed.), *Geophys. Res. Abstracts*, EGU General Assembly 2011. pp. EGU2011–10099.
- Obled, C., Wendling, J., Beven, K., 1994. The sensitivity of hydrological models to spatial rainfall patterns - an evaluation using observed data. *J. Hydrol.* 159, 305–333.
- OFEN, 2012. Swiss Federal Office of Energy. Technical Report. <http://www.bfe.admin.ch>.
- OFEV, 2010. Swiss Federal Office on the Environment Project GIN: Common Information Platform for Natural Hazards. www.gin-info.ch.
- Ohmura, A., 2001. Physical basis for the temperature-based melt-index method. *J. Appl. Meteorol.* 40, 753–761.
- Pappenberger, F., Beven, K., Frodsham, K., Romanowicz, R., Patrick, M., 2007. Grasping the unavoidable subjectivity in calibration of flood inundation models: A vulnerability weighted approach. *J. Hydrol.* 333, 275–287.
- Pappenberger, F., Beven, K., Hunter, N., Bates, P., Gouweleeuw, B., Thielen, J., de Roo, A., 2005. Cascading model uncertainty from medium range weather forecasts (10 days) through a rainfall-runoff model to flood inundation predictions within the European Flood Forecasting System, EFFS. *Hydrol. Earth Syst. Sc.* 9, 381–393.
- Pappenberger, F., Cloke, H., Persson, A., Demeritt, D., 2011. On forecast (in)consistency in a hydro-meteorological chain: curse or blessing? *Hydrol. Earth Syst. Sc.* 15, 2391–2400.
- Parajka, J., Blöschl, G., 2008. The value of MODIS snow cover data in validating and calibrating conceptual hydrologic models. *J. Hydrol.* 358, 240–258.
- Pebesma, A., 2004. Multivariable geostatistics in S: the gstat package. *Comput. Geosci.* 30, 683–691.
- Pellicciotti, F., Brock, B., Strasser, U., Burlando, P., Funk, M., Corripio, J., 2005. An enhanced temperature-index glacier melt model including the shortwave radiation balance: development and testing for Haut Glacier d’Arolla, Switzerland. *J. Glaciol.* 51, 573–587.
- Pepin, N., 2000. Twentieth century change in the Front Range climate record. *Arct. Antarct. Alp. Res.* 32, 135–146.
- Pepin, N., Benham, D., Taylor, K., 1999. Modeling lapse rates in the maritime uplands of northern England: Implications for climate change. *Arct. Antarct. Alp. Res.* 31, 151–164.
- Petrascheck, A., 1996. Hochwasserschutz in der schweiz: Probleme, anforderungen, massnahmen. *Zeitschrift fur Kulturtechnik und Landesentwicklung* 37, 134–137.

Bibliography

- Petrascheck, A., Hegg, C., 2002. Hochwasser 2000, Les crues 2000: analyse des événements. Rapport de l'OFEV, WSL, Série Eaux, Berne.
- Pomeroy, J., Toth, B., Granger, R., Hedstrom, N., Essery, R., 2003. Variation in surface energetics during snowmelt in a subarctic mountain catchment. *J. Hydrometeorol.* 4, 702–719.
- Priestley, C., Taylor, R., 1972. On the assessment of surface heat flux and evaporation using large scale parameters. *Mon. Weather Rev.* 100, 81–92.
- Prudhomme, C., Reed, D., 1999. Mapping extreme rainfall in a mountainous region using geostatistical techniques: A case study in Scotland. *Int. J. Climatol.* 19, 1337–1356.
- Pullen, S., Jones, C., Rooney, G., 2011. Using satellite-derived snow cover data to implement a snow analysis in the Met Office Global NWP Model. *J. Appl. Meteorol. Clim.* 50, 958–973.
- Quayle, R., Easterling, D., Karl, T., Hughes, P., 1991. Effects of recent thermometer changes in the cooperative station network. *B. Am. Meteorol. Soc.* 72, 1718–1723.
- Rango, A., Martinec, J., 1995. Revisiting the degree-day method for snowmelt computations. *Water Resour. Bul.* 31, 657–669.
- Reusser, D., Blume, T., Schaefli, B., Zehe, E., 2009. Analysing the temporal dynamics of model performance for hydrological models. *Hydrol. Earth Syst. Sc.* 13, 999–1018.
- Rinaldo, A., Bellin, A., Marani, A., 1989. On mass response functions. *Water Resour. Res.* 25, 1603–1617.
- Rinaldo, A., Beven, K., Bertuzzo, E., Nicotina, L., Davies, J., Fiori, A., Russo, D., Botter, G., 2011. Catchment travel time distributions and water flow in soils. *Water Resour. Res.* 47, W07537.
- Rinaldo, A., Botter, G., Bertuzzo, E., Settin, T., Uccelli, A., Marani, M., 2006a. Transport at basin-scales, 1. Theoretical framework. *Hydrol. Earth Syst. Sc.* 10, 19–26.
- Rinaldo, A., Botter, G., Bertuzzo, E., Settin, T., Uccelli, A., Marani, M., 2006b. Transport at basin-scales, 2. Applications. *Hydrol. Earth Syst. Sc.* 10, 31–48.
- Rinaldo, A., Marani, A., 1987. Basin scale model of solute transport. *Water Resour. Res.* 23, 2107–2118.
- Rinaldo, A., Rigon, R., Marani, A., 1991. Geomorphological dispersion. *Water Resour. Res.* 28, 513–525.
- Rinaldo, A., Rodriguez-Iturbe, I., 1996. Geomorphological theory of the hydrologic response. *Hydrol. Process.* 10, 803–844.
- Rinaldo, A., Vogel, G., Rigon, R., Rodriguez-Iturbe, I., 1995. Can one gauge the shape of a basin? *Water Resour. Res.* 31, 1119–1128.

- Rodriguez-Iturbe, I., Mejia, J., 1998. Design of rainfall networks in time and space. *Water Resour. Res.* 10, 713–728.
- Rodriguez-Iturbe, I., Porporato, A., 2004. *Ecohydrology of water-controlled ecosystems*. Cambridge University Press.
- Rodriguez-Iturbe, I., Porporato, A., Laio, F., Ridolfi, L., 2001. Plants in water-controlled ecosystems: active role in hydrologic processes and response to water stress: I. scope and general outline. *Adv. Water Res.* 24, 695–705.
- Rodriguez-Iturbe, I., Rinaldo, A., 1997. *Fractal river basins: Chance and self-organization*. Cambridge University Press.
- Rodriguez-Iturbe, I., Valdés, J., 1979. The geomorphologic structure of hydrologic response. *Water Resour. Res.* 15, 1409–1420.
- Roe, G., 2005. Orographic precipitation. *Annu. Rev. Earth Pl. Sc.* 33, 645–671.
- Rohrer, M., Braun, L., 1994. Long-term records of snow cover water equivalent in the Swiss Alps 2. simulation. *Nord. Hydrol.* 25, 65–78.
- Rolland, C., 2003. Spatial and seasonal variations of air temperature lapse rates in Alpine regions. *J. Clim.* 16, 1032–1046.
- Romang, H., Zappa, M., Hilker, N., Gerber, M., Dufour, F., Frede, V., Béroed, D., Oplatka, M., Hegg, C., Rhyner, J., 2011. IFKIS-Hydro: an early warning and information system for floods and debris flows. *Nat. Hazards* 56, 509–527.
- Rossa, A., Liechti, K., Zappa, M., Bruen, M., Germann, U., Hasse, G., Keil, C., Krahe, P., 2010. The COST 731 action: A review on uncertainty propagation in advanced hydro-meteorological forecast systems. *Atmos. Res.* 100, 150–167.
- Salomonson, V., Appel, I., 2004. Estimating fractional snow cover from Modis using the Normalized Difference Snow Index (NDSI). *Remote Sens. Environ.* 89, 351–360.
- Sangati, M., Borga, M., Rabuffetti, D., Bechini, R., 2009. Influence of rainfall and soil properties spatial aggregation on extreme flash flood response modelling: An evaluation based on the Sesia river basin, North Western Italy. *Adv. Water Res.* 32, 1090–1106.
- Schaefli, B., Gupta, H., 2007. Do Nash values have value? *Hydrol. Process.* 21, 2075–2080.
- Schaefli, B., Hingray, B., Musy, A., 2007. Climate change and hydropower production in the Swiss Alps: quantification of potential impacts and related modelling uncertainties. *Hydrol. Earth Syst. Sc.* 11, 1191–1205.
- Schaefli, B., Hingray, B., Niggli, M., Musy, A., 2005. A conceptual glacio-hydrological model for high mountainous catchments. *Hydrol. Earth Syst. Sc.* 9, 95–109.

Bibliography

- Schaefli, B.M.H., 2011. Integrating point glacier mass balance observations into hydrologic model identification. *Hydrol. Earth Syst. Sc.* 15, 1227–1241.
- Schneider, S., Mastrandrea, M., Root, T., 2011. *Encyclopedia of Climate and Weather*. Oxford University Press, New York. 2nd edition edition.
- Schulz, J., Schattler, U., 2009. Kurze Beschreibung des Lokal-Modells Europa COSMO-EU (LME) und seiner Datenbanken auf dem Datenserver des DWD. German Meteorological Service (DWD). Offenbach, Germany.
- Seibert, J., McDonnell, J., 2002. On the dialog between experimentalist and modeler in catchment hydrology: Use of soft data for multicriteria model calibration. *Water Resour. Res.* 38, 1241.
- Sevruk, B., 1997. Regional dependency of precipitation-altitude relationship in the Swiss Alps. *Clim. Change* 36, 355–369.
- Sicart, J., Hock, R., Six, D., 2008. Glacier melt, air temperature, and energy balance in different climates: The Bolivian Tropics, the French Alps, and northern Sweden. *J. Geophys. Res.* 113, D24113.
- Simoni, S., Padoan, S., Nadeau, D., Diebold, M., Porporato, A., Barrenetxea, G., Ingelrest, F., Vetterli, M., Parlange, M., 2011. Hydrologic response of an alpine watershed: Application of a meteorological wireless sensor network. *Water Resour. Res.* 47.
- Sinclair, M., Wratt, D., Henderson, R., Gray, W., 1997. Factors affecting the distribution and spillover of precipitation in the Southern Alps of New Zealand - a case study. *J. Appl. Meteorol.* 36, 428–442.
- Skoien, J., Bloschl, G., 2008. Topological kriging of runoff. *Geoenv VI - Geostatistics for Environmental Applications, Proceedings* 15, 222–231.
- Slater, A., Bohn, T., McCreight, J., Serreze, M., M.C., Lettenmaier, D., 2007. A multimodel simulation of pan-Arctic hydrology. *J. Geophys. Res. - Biogeosciences* 112, 1–17.
- Smith, M., Koren, V., Zhang, Z., Reed, S., Pan, J., Moreda, F., 2004. Runoff response to spatial variability in precipitation: An analysis of observed data. *J. Hydrol.* 298, 267–286.
- Smith, R., 2011. Space-time dynamics of runoff generation in a snowmelt-dominated montane catchment. Ph.D. thesis. Univ British Columbia, Vancouver. Department of Geography.
- Spear, R., Hornberger, G., 1980. Eutrophication in Peel Inlet. II. identification of critical uncertainties via generalized sensitivity analysis. *Water Resour. Res.* 14, 43–49.
- Stahl, K., Moore, R., Floyer, J., Asplin, M., McKendry, I., 2006. Comparison of approaches for spatial interpolation of daily air temperature in a large region with complex topography and highly variable station density. *Agr. Forest Meteorol.* 139, 224–236.

- Steinacker, R., 1983. Diagnose und prognose der schneefallgrenze. *Wetter und Leben* 35, 81–90.
- Sui, J., Koehler, G., 2001. Rain-on-snow induced flood events in Southern Germany. *J. Hydrol.* 252, 205–220.
- Szilagyi, J., Parlange, M., 1998. Baseflow separation based on analytical solutions of the Boussinesq equation. *J. Hydrol.* 204, 251–260.
- Szilagyi, J., Parlange, M., Albertson, J., 1998. Recession flow analysis for aquifer parameter determination. *Water Resour. Res.* 34, 1851–1857.
- Tarboton, D., 1997. A new method for the determination of flow directions and upslope areas in grid digital elevation models. *Water Resour. Res.* 33, 309–320.
- Taylor, G., 1921. Diffusion by continuous movements. *Proc. London Math. Soc. Ser. A* 20, 196–211.
- Tiedtke, A., 1989. A comprehensive mass flux scheme for cumulus parameterization in large-scale models. *Mon. Weather Rev.* 117, 1779–1799.
- Tobin, C., Nicotina, L., Parlange, M., Berne, A., Rinaldo, A., 2011. Improved interpolation of meteorological forcings for hydrologic applications in a Swiss Alpine region. *J. Hydrol.* 401, 77–89.
- Tobin, C., Rinaldo, A., Schaeffli, B., 2012. Snowfall limit forecasts and hydrological modeling. *J. Hydrometeorol.* in press.
- Unterstrasser, S., Zaengl, G., 2006. Cooling by melting precipitation in Alpine valleys: An idealized numerical modelling study. *Q. J. Roy. Meteor. Soc.* 132, 1489–1508.
- Van Genuchten, M.T., 1981. Analytical solution for chemical transport with simultaneous adsorption, zero-order production and first-order decay. *J. Hydrol.* 49, 213–233.
- Velasco-Forero, C., Sempere-Torres, D., Cassirage, E., Gomez-Hernandez, J., 2008. A non-parametric automatic blending methodology to estimate rainfall fields from rain gauge and radar data. *Adv. Water Res.* 32, 986–1002.
- Viviroli, D., H.H. Durr, H., Messerli, B., Meybeck, M., Weingartner, R., 2007. Mountains of the world, water towers for humanity: Typology, mapping, and global significance. *Water Resour. Res.* 43, W07447.
- Viviroli, D., Zappa, M., Gurtz, J., Weingartner, R., 2009. An introduction to the hydrological modelling system PREVAH and its pre- and post-processing tools. *Environ. Modell. Softw.* 24, 1209–1222.
- Vrugt, J., ter Braak, C., Gupta, H., Robinson, B., 2009. Equifinality of formal DREAM and informal GLUE Bayesian approaches in hydrologic modeling? *Stoch. Env. Res. Risk A.* 23, 1011–1026.

Bibliography

- Vrugt, J., Gupta, H., Bastidas, L., Bouten, W., Sorooshian, S., 2003. Effective and efficient algorithm for multiobjective optimization of hydrologic models. *Water Resour. Res.* 39, 1214.
- Vrugt, J., Gupta, H., Bastidas, L., Bouten, W., Sorooshian, S., 2008. Treatment of input uncertainty in hydrologic modeling: Doing hydrology backward with Markov Chain Monte Carlo simulation. *Water Resour. Res.* 44, W00B09.
- Walter, M., Brooks, E., McCool, D., King, L., Molnau, M., Boll, J., 2005. Process-based snowmelt modeling: Does it require more input data than temperature-index modeling? *J. Hydrol.* 300, 65–75.
- Webster, R., Oliver, M., 2001. *Geostatistics for Environmental Scientists*. Wiley Publishing, New York.
- Weingartner, R., 2009. *Hydrological Atlas of Switzerland*. 67, Publikation Gewässerkunde, Bern.
- Weingartner, R., Barben, M., Spreafico, M., 2003. Floods in mountain areas - an overview based on examples from Switzerland. *J. Hydrol.* 282, 10–24.
- Weingartner, R., Pearson, C., 1999. A comparison of the hydrology of the Swiss Alps and the Southern Alps of New Zealand. *Mt. Res. Dev.* 21, 370–381.
- Weusthoff, T., Ament, F., Arpagaus, M., Rotach, M., 2010. Assessing the benefits of convection-permitting models by neighborhood verification: Examples from MAP D-PHASE. *Mon. Weather Rev.* 138, 3418–3433.
- Winsemius, H., Schaefli, B., Montanari, A., Savenije, H., 2009. On the calibration of hydrological models in ungauged basins: A framework for integrating hard and soft hydrological information. *Water Resour. Res.* 45.
- WMO, 1986. Results of an intercomparison of models of snowmelt runoff, in: IAHS (Ed.), *Modelling Snowmelt-Induced Processes: Proceedings of the Budapest Symposium*, World Meteorological Organization, Geneva, Switzerland. pp. 103–112.
- Woods, R., 2009. Analytical model of seasonal climate impacts on snow hydrology: Continuous snowpacks. *Adv. Water Resour.* 32, 1465–1481.
- Woods, R., Sivapalan, M., 1999. A synthesis of space-time variability in storm response: rainfall, runoff generation, and routing. *Water Resour. Res.* 35, 2469–2485.
- Wratt, D., Revell, M., Sinclair, M., Gray, W., Henderson, R., Chater, A., 2000. Relationships between air mass properties and mesoscale rainfall in New Zealand's Southern Alps. *Atmos. Res.* 52, 261–282.
- Wratt, D., Ridley, R., Sinclair, M., Larson, H., Thompson, S., 1996. The New Zealand Southern Alps experiment. *B. Am. Meteorol. Soc.* 77, 683–692.

- Yang, J., Reichert, P., Abbaspour, K., 2007. Hydrological modelling of the Chaohe basin in China: Statistical model formulation and Bayesian inference. *J. Hydrol.* 340, 167–182.
- Yapo, P., Gupta, H., Sorooshian, S., 1998. Multi-objective global optimization for hydrologic models. *J. Hydrol.* 204, 83–97.
- Zadeh, L., 1965. Fuzzy Sets. *Control* 8, 338–353.
- Zappa, M., Pos, F., Strasser, U., Warmerdam, P., Gurtz, J., 2003. Seasonal water balance of an Alpine catchment as evaluated by different methods for spatially distributed snowmelt modelling. *Nord. Hydrol.* 34, 179–202.
- Zappa, M., Rotach, M., Arpagaus, M., Dorninger, M., Hegg, C., Montani, A., Ranzi, R., Ament, F., Germann, U., G. Grossi, G., Jaun, S., Rossa, A., Vogt, S., Walser, A., Wehrhan, J., Wunram, C., 2008. MAP D-PHASE: real-time demonstration of hydrological ensemble prediction systems. *Atmos. Sci. Lett.* 9, 80–87.

Cara C. Tobin, P.E.

Av Louis Ruchonnet 15,
1003, Lausanne, Switzerland,
+41 78 664 2272,
ctobin@stanfordalumni.org



EXPERIENCE

ASIAN DEVELOPMENT BANK

Environmental, Social Safeguards and Resettlement Specialist

- Environmental and social safeguards specialist for 157M\$ water and wastewater development projects serving 80,000 people in 6 Azerbaijani villages
- Environmental and resettlement specialist for 45M\$ water development project serving 19,000 people in 5 Armenian villages
- Preparation of all environmental assessment, resettlement and gender action reports

Yerevan, Armenia
Baku, Azerbaijan
Jan 2008 – April 2008

CH2M Hill

Environmental Engineering Consultant

- Project leader for ammonia toxicity river discharge study
- Provided technical internal training on thermal desalination to company engineers

Philadelphia, USA
Oct 2004 - June 2006

MWH Ltd.,

Environmental Engineer

- Lead hydraulic engineer for a \$150 million wastewater /desalination project
- Head modeler for 9 water and groundwater supply projects

Brisbane, Australia
Feb 2004 - Sep 2005
Christchurch, NZ
Feb 2003 - Feb 2004

KENNEDY JENKS

Civil Engineer

- Managed Drinking Water Source Assessments and water quality sampling programs
- Designed over \$300,000 in hydraulics upgrades for water and wastewater treatment systems

San Francisco, USA
Aug 2001 - Jan 2003

EDUCATION

SWISS FEDERAL INSTITUTE OF TECHNOLOGY

Ph.D. in Environmental Engineering

- Fulbright Fellowship (July 2006 – Dec 2007) and Swiss Confederation Grant for PhD (May 2008 – present)
- Doctoral research on improving a hydrological model and reducing flood forecasting uncertainty in the Swiss Alps

Lausanne, Switzerland
2012

STANFORD UNIVERSITY

Master's of Science in Environmental Engineering

- Specialization in Environmental Fluid Mechanics and Hydrology, National Science Foundation full scholarship

Stanford, USA
June 2001

GEORGIA INSTITUTE OF TECHNOLOGY

Bachelor's in Civil and Environmental Engineering

- Civil Engineering Valedictorian (3.94 GPA), National Science Foundation Fellowship

Atlanta, USA
June 1999

PUBLICATIONS

- C. Tobin, A. Rinaldo, and B. Schaepli. Snowfall limit forecasts and hydrological modeling. **JOURNAL OF HYDROMETEOROLOGY**, in press, 2012.
- C. Tobin, L. Nicotina, M. Parlange, A. Berne, and A. Rinaldo. Improved interpolation of meteorological forcings and hydrologic implications for a Swiss alpine region. **JOURNAL OF HYDROLOGY**, 401(1-2):77-89, 2011.
- J. McDonnell, K. Mcguire, P. et al.,. How old is streamwater? Open questions in catchment transit time conceptualization, modelling and analysis. **HYDROLOGICAL PROCESSES**, 24(12):1745-1754, 2010.
- J. García Hernández, P. Horton, C. Tobin, and J. Boillat. MINERVE 2010 : Prévission hydrométéorologique et gestion des crues sur le Rhône alpin. **WASSER, ENERGIE, LUFT**, (n°4):297-302, 2009.

EXPERTISE

HYDROLOGICAL PROCESS CHARACTERIZATION AND FLOOD PREDICTION UNCERTAINTY

- Provided Swiss cantons with an improved hydraulic-hydrological model including ameliorations to temperature / precipitation interpolation methods and snow/rainfall partitioning.
- Developed a minimalist snowmelt methodology applicable to data-limited, mountainous regions
- Designed and developed a VB.net visualization tool and software program to reduce parameter and model output uncertainty and to provide a range of plausibility for flood modeling outputs.

WATER TREATMENT / DESALINATION

- Recruited to provide hydraulic design expertise on a \$150 million fast-track wastewater and desalination treatment plan upgrade project with the Brisbane Water Enviro Alliance.
- Designed an oxidation pond, wetland and land disposal systems for a small island community with limited budget and aboriginal restrictions on land-use.
- Completed a detailed design for a chlorine dosing system and managed the tender process.
- Upgraded five water treatment plants by designing membrane treatment systems. Also designed spent ozone recycling for a lake oxygenation system to improve influent water quality.

WATER / WASTEWATER INFRASTRUCTURE DESIGN AND MODELING

- Designed trunk mains and laterals to divert catchments, prevent overflows, and provide storage for several municipalities. Staged upgrade works over ten years to optimize capital budget savings.
- Utilized MOUSE and GIS to model wastewater networks and pump stations in a context of aggressive growth (4 x current population). Developed options to support growth and staging of pipe/pump upgrades.
- Modeled rural and city water supplies with H2OMap and GIS to satisfy future irrigation and fireflow.
- Designed partially submerged discharge pipeline including conducting geotechnical investigations.

HYDROGEOLOGY

- Designed rapid-infiltration basins and generated pipework layout and basin rotation/operation plan. Measured percolation and wetland effluent rates on site.
- Created MODFLOW groundwater models to delineate Nitrate-N and faecal coliform plumes from septic systems. Estimated zones of influence around existing and proposed pumping wells.
- Developed a 3D MODFLOW groundwater model to depict the fate of a Light Nonaqueous Phase Liquid plume through varied lithology for litigation purposes.

WATER QUALITY

- Reviewed water quality contaminant papers for the U.S. EPA Detailed Water Contaminant Database.
- Performed Drinking Water Source Assessment Programs by analyzing potential contaminating activities and delineating zones of influence for 60% of the San Francisco Bay sources (by area).
- Managed and developed lead service line replacement programs and Total Coliform and Lead & Copper sampling / monitoring plans for the San Francisco Regional Water system.

ADDITIONAL INFORMATION

- **Languages:** Fluent in English (mother tongue) and French, Spanish (highly proficient)
- **Citizenship/Civil Status:** US Citizen, Irish Citizen, Swiss resident (Permit B until 2015)
- **Special Skills:** Professional Engineer, USA (PE072050)
- **Specialized Software:** ArcGIS, Visual Basic, Modflow, MOUSE, H2OMap, IDRISI, MS Office, Fortran, Matlab, R
- **Interests:** running, soccer, biking, saxophone, swing dancing